OFDM for Wireless Multimedia Communications

For a listing of recent titles in the *Artech House Universal Personal Communications Series,* turn to the back of this book.

OFDM for Wireless Multimedia Communications

Richard van Nee
Ramjee Prasad

Artech House
Boston • London

Library of Congress Cataloging-in-Publication Data
van Nee, Richard.
OFDM for wireless multimedia communications / Richard van Nee, Ramjee Prasad.
p. cm. — (Artech House universal personal communications library)
Includes bibliographical references and index.
ISBN 0-89006-530-6 (alk. paper)
1. Wireless communication systems. 2. Multimedia systems. 3. Multiplexing.
I. Prasad, Ramjee. II. Title. III. Series.

TK5103.2.N44 2000 99-052312
621.3845—dc21 CIP

British Library Cataloguing in Publication Data
van Nee, Richard
OFDM for wireless multimedia communications. — (Artech House
universal personal communications library)
1.Wireless communication systems 2. Multimedia systems
I. Title II. Prasad, Ramjee
621.3'82

ISBN 0-89006-530-6

Cover design by Igor Valdman

International Standard Book Number: 0-89006-530-6
Library of Congress Catalog Card Number: 99-052312

10 9 8 7 6 5 4 3 2

To my wife Iris, to our son Floris, to our daughters Roselinde and Mirrelijn, and to our newly born baby
—Richard van Nee

To my wife Jyoti, to our daughter Neeli, and to our sons Anand and Rajeev
—Ramjee Prasad

Contents

Preface

सर्वद्वारेषु देहेऽस्मिन् प्रकाश उपजायते ।
ज्ञानं यदा तदा विद्याद् विवृद्धं सत्त्वमित्युत

sarva-dvāreṣu dehe 'smin
prakāśa upajāyate
jñānaṁ yadā tadā vidyād
vivṛddhaṁ sattvam ity uta

The manifestations of the mode of goodness can be experienced when all the gates of the body are illuminated by knowledge

The Bhagavad Gita (14.11)

During the joint supervision of a Master's thesis "The Peak-to-Average Power Ratio of OFDM," of Arnout de Wild from Delft University of Technology, The Netherlands, we realized that there was a shortage of technical information on orthogonal frequency division multiplexing (OFDM) in a single reference. Therefore, we decided to write a comprehensive introduction to OFDM. This is the first book to give a broad treatment to OFDM for mobile multimedia communications. Until now, no such book was available in the market. We have attempted to fill this gap in the literature.

Currently, OFDM is of great interest by the researchers in the Universities and research laboratories all over the world. OFDM has already been accepted for the new wireless local area network standards from IEEE 802.11, High Performance Local Area Network type 2 (HIPERLAN/2) and Mobile Multimedia Access Communication (MMAC) Systems. Also, it is expected to be used for the wireless broadband multimedia communications.

OFDM for Wireless Multimedia Communications is the first book to take a comprehensive look at OFDM, providing the design guidelines one needs to maximize benefits from this important new technology. The book gives engineers a solid base for assessing the performance of wireless OFDM systems. It describes the new OFDM-based wireless LAN standards; examines the basics of direct-sequence and frequency-hopping CDMA, helpful in understanding combinations of OFDM and CDMA. It also looks at applications of OFDM, including digital audio and video broadcasting, and wireless ATM. Loaded with essential figures and equations, it is a must-have for practicing communications engineers, researchers, academics, and students of communications technology.

Chapter 1 presents a general introduction to wireless broadband multimedia communication systems (WBMCS), multipath propagation, and the history of OFDM. A part of this chapter is based on the contributions of Luis Correia from the Technical University of Lisbon, Portugal, Anand Raghawa Prasad from Lucent Technologies, and Hiroshi Harada from the Communications Research Laboratory, Ministry of Posts and Telecommunications, Yokosuka, Japan.

Chapters 2 to 5 deal with the basic knowledge of OFDM including modulation and coding, synchronization, and channel estimation, that every post-graduate student as well as practicing engineers must learn. Chapter 2 contains contributions of Rob Kopmeiners from Lucent Technologies on the FFT design.

Chapter 6 describes the peak-to-average power problem, as well as several solutions to it. It is partly based on the contribution of Arnout de Wild.

Basic principles of CDMA are discussed in Chapter 7 to understand multi carrier CDMA and frequency-hopping OFDMA, which are described in Chapters 8 and 9. Chapter 8 is based on the research contributions from Shinsuke Hara from the University of Osaka, Japan, a postdoctoral student at Delft University of Technology during 1995–96. Chapter 9 is based on a UMTS proposal, with main contributions of Ralf Böhnke from Sony, Germany, David Bhatoolaul and Magnus Sandell from Lucent Technologies, Matthias Wahlquist from Telia Research, Sweden, and Jan-Jaap van de Beek from Lulea University, Sweden.

Chapter 10 was witten from the viewpoint of top technocrats from industries, government departments, and policy-making bodies. It describes several applications of OFDM, with the main focus on wireless ATM in the Magic WAND project, and the new wireless LAN standards for the 5 GHz band from IEEE 802.11, HIPERLAN/2 and MMAC. It is partly based on contributions from Geert Awater from Lucent Technologies, and Masahiro Morikura and Hitoshi Takanashi from NTT in Japan and California, respectively.

We have tried our best to make each chapter quite complete in itself. This book will help generate many new research problems and solutions for future mobile multimedia communications. We cannot claim that this book is errorless. Any remarks to improve the text and correct any errors would be highly appreciated.

Acknowledgments

The material in this book originates from several projects at Lucent Technologies and research activities at Delft University of Technology, The Netherlands. A great deal of OFDM-knowledge was acquired during the Magic WAND project, in which several companies jointly managed to build a wireless ATM network demonstrator based on OFDM. We wish to thank all Magic WAND members who were involved in the design of the OFDM modem, in particular Geert Awater, James Hopper, Rob Kopmeiners, Erik Busking, Han Schmitz, Theo Kleijne, Martin Janssen, Jan Kruys, Urs Bernhard, Urs Lott, Alex Grant, James Aldis, Thomas Mark, Rodolfo Mannpelz, and Ari Vaisanen. Another fruitful source of information was the OFDM-based proposal for UMTS, with main contributions coming from Ralf Böhnke, David Bhatoolaul, Magnus Sandell, and Jan-Jaap van de Beek.

Richard wishes to thank Masahiro Morikura and Hitoshi Takanashi for all their contributions and the pleasant cooperation on the joint OFDM proposal for the IEEE 802.11 wireless LAN standard. All members of IEEE 802.11 and HiperLAN/2 are thanked for numerous contributions, that greatly improved the quality of the final standards and helped to gain more insight in various OFDM techniques.

Geert Awater and Rob Kopmeiners made contributions and corrected numerous mistakes. Neeli Rashmi Prasad helped to prepare the complete manuscript, freeing us from the enormous burden of editorial requirements. Shinsuke Hara from the University of Osaka, Japan, Hiroshi Harada from the Communications Research Laboratory, Ministry of Posts and Telecommunications, Yokosuka, Japan, Luis Correia from the Technical University of Lisbon, Portugal, Anand Raghawa Prasad from Lucent Technologies, and Arnout de Wild from Siemens, The Netherlands, are deeply acknowledged for their valuable contributions.

After the Magic WAND project, we studied several OFDM options for new high-rate wireless LAN products. A circle was completed by the selection of OFDM for the high rate extension of the IEEE 802.11 wireless LAN standard in July 1998. We hope this book will help to gain insight in the principles and design of OFDM-based systems, in particular the new OFDM-based wireless LAN standards.

Richard van Nee
Ramjee Prasad
October 1999

Chapter 1

Introduction

The spectacular growth of video, voice, and data communication over the Internet, and the equally rapid pervasion of mobile telephony, justify great expectations for mobile multimedia. Research and development are taking place all over the world to define the next generation of wireless broadband multimedia communications systems (WBMCS) that may create the "global information village." Figure 1.1 illustrates the basic concept of the global information village, which consists of various components at different scales ranging from global to picocellular size. As we know, the demand for wireless (mobile) communications and Internet/multimedia communications is growing exponentially. Therefore, it is imperative that both wireless and Internet/multimedia should be brought together. Thus, in the near future, wireless Internet Protocol (IP) and wireless asynchronous transfer mode (ATM) will play an important role in the development of WBMCS.

While present communications systems are primarily designed for one specific application, such as speech on a mobile telephone or high-rate data in a wireless local area network (LAN), the next generation of WBMCS will integrate various functions and applications. WBMCS is expected to provide its users with customer premises services that have information rates exceeding 2 Mbps. Supporting such large data rates with sufficient robustness to radio channel impairments, requires careful choosing of modulation technique. The most suitable modulation choice seems to be orthogonal frequency division multiplexing (OFDM). Before going into the details of OFDM, however, first we give some background information on the systems that will be using it.

The theme of WBMCS is to provide its users a means of radio access to broadband services supported on customer premises networks or offered directly by public fixed networks. WBMCS will provide a mobile/movable wireless extension to

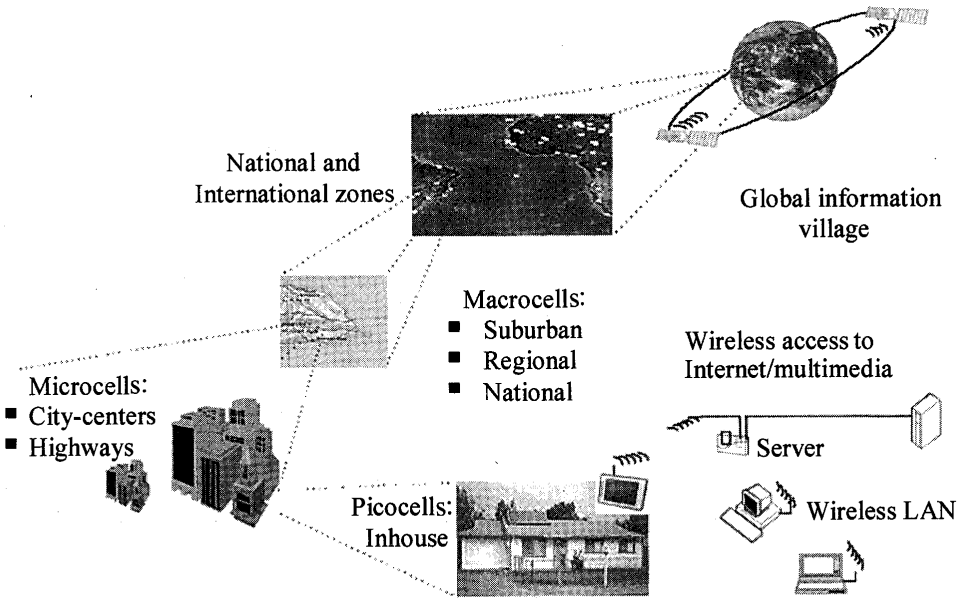

Figure 1.1 Global information village.

WBMCS is under investigation in North America, Europe, and Japan in the microwave and millimeter-wave bands to accommodate the necessary bandwidth. The research in the field of WBMCS has drawn much attention because of the increasing role of multimedia and computer applications in communications. There is a major thrust in three research areas: (1) microwave and millimeter-wave bands for fixed access in outdoor, public commercial networks, (2) evolution of WLAN for inbuilding systems, and (3) use of LAN technology outdoors rather than indoors. In short, WBMCS will provide novel multimedia and video mobile communications services, also related to wireless customer premises network (WCPN) and wireless local loop (WLL).

To implement the wireless broadband communication systems, the following challenges must be considered:

- Frequency allocation and selection;
- Channel characterization;
- Application and environment recognition, including health hazard issues;
- Technology development;
- Air interface multiple access techniques;
- Protocols and networks; and
- Systems development with efficient modulation, coding, and smart antenna techniques.

- Protocols and networks; and
- Systems development with efficient modulation, coding, and smart antenna techniques.

A significant number of research and development (R&D) projects are set up in the area of WBMCS. Within the European Advanced Communication Technologies and Services (ACTS) program are four European Union-funded R&D projects, namely Magic Wand (Wireless ATM Network Demonstrator), ATM Wireless Access Communication System (AWACS), System for Advanced Mobile Broadband Applications (SAMBA), and wireless broadband CPN/LAN for professional and residential multimedia applications (MEDIAN) [1–17]. Table 1.1 summarizes the European projects [11].

In the United States, seamless wireless network (SWAN) and broadband adaptive homing ATM architecture (BAHAMA), as well as two major projects in Bell Laboratories and a wireless ATM network (WATMnet), are being developed in the computer and communications (C&C) research laboratories of Nippon Electric Company (NEC) in the United States [2–6].

In Japan, Communication Research Laboratory (CRL) is working on several R&D projects, such as a broadband mobile communication system in the super high frequency (SHF) band (from 3 to 10 GHz) with a channel bit rate up to 10 Mbps and an indoor high speed WLAN in SHF band with a target bit rate of up to 155 Mbps [12].

In the Netherlands, Delft University of Technology has been busy with a multidisciplinary research project, "Mobile Multimedia Communication (MMC)," since April 1996. The team consists of experts from the telecommunications and traffic control and information theory groups of the department of Electrical Engineering, the Product Ergonomics group of the department of Industrial Design Engineering, and the Organizational Psychology group of the department of Technology and Society.

The MMC has the following objectives to achieve at 60 GHz:

- Wireless access of 155 Mbps using OFDM;
- Both indoor and outdoor use;
- Less complex, inexpensive mobile stations by moving most functionality to the access points;
- Modified OFDM; and
- Constant bit rate (CBR), variable bit rate (VBR), and available bit rate (ABR) services.

Table 1.1
Summary of European ACTS Projects.

ACTS project / Parameter	WAND	AWACS	SAMBA	MEDIAN
Frequency	5 GHz	19 GHz	40 GHz	61.2 GHz
Data rate	20 Mbps	70 Mbps	34 Mbps	155 Mbps
Modulation	OFDM, 16 subcarriers with 8-PSK (phase shift keying)	offset quadrature PSK (OQPSK)	OQPSK	OFDM, 512 carriers, differential QPSK (DQPSK)
Cell radius	20–50m (omnidirectional antennas)	50–100m (directional antennas, line-of-sight only)	10-50m (directional antennas at access point)	10m (directional antennas)
Radio access	time division multiple access/ time division duplex (TDMA/TDD)	TDMA/TDD	time division multiple access /frequency division duplex (TDMA/FDD)	TDMA/TDD

1.1 STANDARDIZATION AND FREQUENCY BANDS

There are three main forums for the standardization of wireless broadband communication systems; namely, IEEE 802.11 [18], European Telecommunication Standards Institute Broadband Radio Access Networks (ETSI BRAN) [19], and Multimedia Mobile Access Communications (MMAC) [20]. IEEE 802.11 made the first WLAN standard for the 2.4-GHz Industrial, Scientific, and Medical band (ISM). It specifies the medium access control and three different physical layers—direct-sequence spread spectrum, frequency hopping, and infrared—which give a data rate of 2 Mbps. Products based on this standard became available in 1998. Figure 1.2 shows an example of an IEEE 802.11 modem in a PCMCIA card. Following the initial 1- and 2-Mbps standard, IEEE 802.11 developed two new physical layer standards. One delivers data rates of up to 11 Mbps in the 2.4-GHz band, using complementary code keying [21,22]. Products based on this standard—with the old 1 and 2 Mbps as fallback rates—are available since mid 1999. An industry alliance called the Wireless Ethernet Compatibility Alliance (WECA) has been established to promote the high rate IEEE

available since mid 1999. An industry alliance called the Wireless Ethernet Compatibility Alliance (WECA) has been established to promote the high rate IEEE 802.11 technology and to certify interoperability of products from different vendors [23]. The second IEEE 802.11 standard extension targets a range of data rates from 6 up to 54 Mbps using OFDM in the 5-GHz band [24]. The OFDM standard was developed jointly with ETSI BRAN and MMAC, making OFDM effectively a worldwide standard for the 5-GHz band.

Table 1.2 lists the main characteristics of the IEEE 802.11 and the ETSI High Performance Local Area Network type 2 (HIPERLAN/2) standards. More details about these standards can be found in Chapter 10.

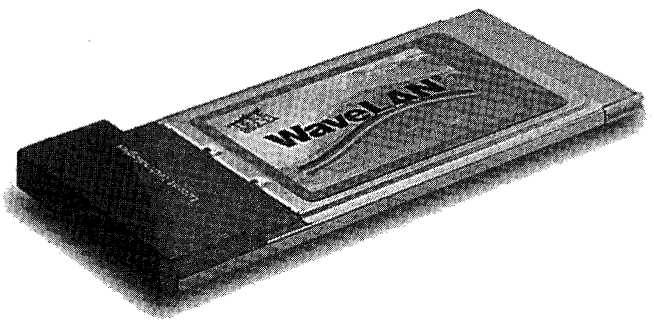

Figure 1.2 IEEE 802.11 modem for the 2.4-GHz band (WaveLAN™ from Lucent Technologies [25]).

Figure 1.3 shows that 2-, 5- and 60-GHz are the commercially important frequency bands because of geographically wide spectrum allocations in Europe, the United States (U.S.), and Japan for the wireless broadband multimedia communications networks. The 2.4-GHz band is an ISM band, which can be used for many types of transmission systems as long as they obey certain power, spectral density, and spreading gain requirements. The 5-GHz band is designated specifically for WBMCS. In Europe, only HIPERLAN devices are currently allowed in this band. HIPERLAN actually consists of a family of standards, one of which is an OFDM-based standard that is very similar to the IEEE 802.11 5-GHz standard. In Japan, MMAC supports both the IEEE 802.11 and the HIPERLAN standards. Notice that Japan only has 100 MHz available in the 5-GHz band, while the United States and Europe provide 300 and 455 MHz, repectively. In Europe, extra spectrum for HIPERLAN is available in the 17-GHz band, while Japan has allocated spectrum from 10- to 16-GHz to mobile broadband systems (MBS). An analysis of the propagation aspects at the bands foreseen for WBMCS microwaves, millimeterwaves, and infrared is presented in [26–31].

Table 1.2
Comparison of IEEE and HIPERLAN standards.

Parameter	IEEE 802.11 2 GHz	IEEE 802.11 5 GHz	HIPERLAN/2
Configurations	Centralized system with access points connected to wired network, or peer-to-peer networking	Centralized system with access points connected to wired network, or peer-to-peer networking	Centralized system with access points connected to wired network
Range	Up to 60m at 11 Mbps and up to 100m at 2 Mbps with omnidirectional antennas	Up to 30m at 24 Mbps and up to 60m at 6 Mbps with omnidirectional antennas	Up to 30m at 24 Mbps and up to 60m at 6 Mbps with omnidirectional antennas
Channel access	CSMA/CA, variable size data packets (up to 8192 bytes)	CSMA/CA, variable size data packets (up to 8192 bytes)	Reservation based access, scheduled by access point. Contention slots for making slot reservations
Frequency bands	2.4-2.4835 GHz	5.150–5.350 GHz; 5.725–5.825 GHz	5.150–5.350 GHz; 5.470–5.725 GHz;
Duplexing	TDD	TDD	TDD
Data rate	1, 2 Mbps (BPSK/QPSK) 5.5, 11 Mbps (CCK)	6, 9 Mbps (BPSK) 12, 18 Mbps (QPSK) 24, 36 Mbps (16-QAM) 54 Mbps (64-QAM)	6, 9 Mbps (BPSK) 12, 18 Mbps (QPSK) 24, 36 Mbps (16-QAM) 54 Mbps (64-QAM)

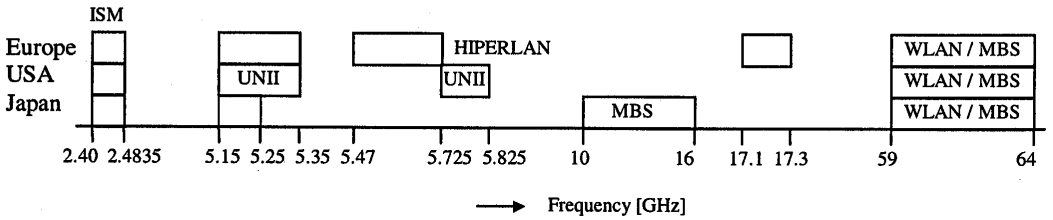

Figure 1.3 Frequency band for wireless broadband communications.

1.2 MULTIMEDIA COMMUNICATIONS

Multimedia and computer communications are playing an increasing role in today's society, creating new challenges to those working in the development of telecommunications systems. Besides that, telecommunications is increasingly relying upon wireless links. Thus, the pressure for wireless systems to cope with increasing data rates is enormous, and WBMCSs with data rates higher than 2 Mbps are emerging rapidly, even if at this moment applications for very high transmission rates do not exist.

Several WBMCSs are being considered for different users with different needs. They may accommodate data rates ranging between 2 and 155 Mbps; terminals can be mobile (moving while communicating) or portable (static while communicating); moving speeds can be as high as that of a fast train; users may or may not be allowed to use more than one channel if their application requires so; the system bandwidth may be fixed, or dynamically allocated according to the user's needs; communication between terminals may be direct or must go through a base station; possible ATM technology use; and so on. Many other cases can be listed as making the difference between various perspectives of a WBMCS, but two major approaches are emerging: WLANs directed to communication among computers, from which IEEE 802.11 [16, 18] and HIPERLAN [19, 20] are examples, with MBS [17] intended as a cellular system providing full mobility to B-ISDN users.

The different requirements imposed by the various approaches to WBMCSs have consequences on system design and development. The tradeoffs between maximum flexibility on one hand and complexity and cost on the other are always difficult to decide, as they have an impact not only on the deployment of a system, but also on its future evolution and market acceptance. GSM is a good example of a system foreseen to accommodate additional services and capacities to those initially offered, and the fact that operators are already implementing phase 2+ is proof of that.

This means that many decisions must be made on the several WBMCSs that will appear on the market. For IEEE 802.11, for example, those decisions have already been made, as the system will be commercialized in the very near future, but for other systems there are still many undecided aspects. Of course this depends on what are the applications intended to be supported by the systems, and whether these applications are targeted to the mass market or only to some niches. The former (from which mobile telephones are a good example) will certainly include WLANs, because the expansion of personal computers will dictate this application as a great success in WBMCSs; the latter will possibly have television broadcasters among their users (to establish links between HDTV cameras and the central control room).

Not only are market aspects at stake in the development and deployment of WBMCSs, but many technical challenges are posed as well. The transmission of such high data rates over radio in a mobile environment creates additional difficulties,

compared with that of existing systems; these difficulties are augmented by the fact that frequencies higher than UHF are needed to support the corresponding bandwidths, thus pushing mobile technology challenges (size and weight among other things) to frequencies where these aspects were not much considered until now. However, additional challenges are posed to those involved in WBMCSs development: in today's world, where consumers are in the habit of using a communications system that is available in different places (e.g., GSM roaming capability, because users can make and receive telephone calls in an increasing number of countries worldwide), or being able to exchange information among different systems (e.g., the exchange of files between different computer applications and systems), for future use it does not make sense to consider systems that offer a high data rate but do not support these capabilities to some extent.

1.2.1 Need for High Data Rates

Data rate is really what broadband is about. For example, the new IEEE and HIPERLAN standards specify bit rates of up to 54 Mbps, although 24 Mbps will be the typical rate used in most applications. Such high data rates impose large bandwidths, thus pushing carrier frequencies for values higher than the UHF band: HIPERLAN has frequencies allocated in the 5- and 17-GHz bands; MBS will occupy the 40- and 60-GHz bands; and even the infrared band is being considered for broadband WLANs. Many people argue whether there is a need for such high-capacity systems, however, bearing in mind all the compression algorithms developed and the type of applications that do require tens of megabits per second. We can examine this issue from another perspective.

The need for high-capacity systems is recognized by the "Visionary Group" [32], put together by the European Commission, to give a perspective of what should be the hot topics in the telecommunications for research in the next European programs (following R&D in Advanced Communications Technologies for Europe (RACE) and ACTS). In this visionary perspective, to meet the needs of society in the years to come as far as communications is concerned, capacity is one of the major issues to be developed because of the foreseen increase in demand for new services (especially those based on multimedia). Along with this, mobility will impose new challenges to the development of new personal and mobile communications systems.

We can conclude the following: even if at a certain point it may look academic to develop a system for a capacity much higher than what seems reasonable (in the sense that there are no applications requiring such high capacity), it is worthwhile to do so, as almost certainly in the future (which may be not very far off) applications will need those capacities and even more. The story of fiber optics is an example.

1.2.2 Services and Applications

The system concept of a WLAN such as IEEE 802.11 and of a mobile broadband cellular system such as MBS is totally different: each is directed to services and applications that differ in many aspects. A comparison of several systems, based on two of the key features (mobility and data rate), is shown in Figure 1.4 [33], where it is clear that no competition exists between the different approaches.

The applications and services of the various systems are also different. IEEE 802.11 is mainly intended for communications between computers (thus being an extension of wired LANS); nevertheless, it can support real-time voice and image signals, and users are allowed some mobility and can have access to public networks.

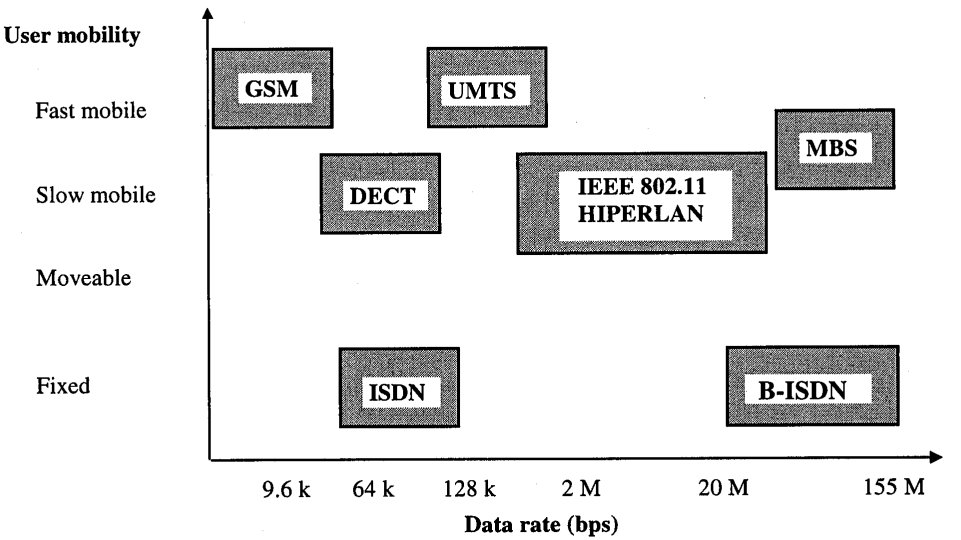

Figure 1.4 Comparison of mobility and data rates for several systems.

1.2.3 Antennas and Batteries

Antennas and batteries play a key role in wireless systems. With the advent of microelectronics and signal processing, antennas and batteries tend to impose the size and weight of mobile terminals. Of course, the higher one goes in frequency, the less developed the technology, and many problems are still found in size and weight at the millimeter-wave band. Power consumption is one example. Though these are likely to be solved in the near future. The number of hours battery-powered equipment can work or operate on stand by, and the percentage of its weight corresponding to the battery, is

not a specific problem of WBMCS. Laptop computers and cellular telephones are the most common terminals relying on batteries these days. This technology continues to demand huge R&D, to extend working time and reduce weight. Although a 100g mobile telephone battery corresponding to several hours of continuous work and a few days on standby is already on the market, users still want more. Mobile multimedia terminals, certainly those to be used in some applications of WBMCSs, will be an extension of the current cellular telephones. Therefore, we foresee that the current problems associated with batteries will be transposed on WBMCS terminals; the same applies to laptops.

Antennas (size, type, technology, etc.) are not a specific problem of WBMCSs as well, but again they are very much related to the type of systems that will be made available for users. It does not make sense to impose restrictions (e.g., pointing in a certain direction or avoiding someone to pass in between) on the type of mobility a mobile terminal can have. Even for portable terminals (e.g., computers), these restrictions make no sense. Hence, there are only two options as far as antennas are concerned: either an omnidirectional antenna (dipole type) or an adaptive array antenna is used. Either way, patch antennas seem a very promising solution for general use in WBMCS. For the frequency bands we consider, isolated patches or adaptive arrays (with many elements) can be made with a small size (e.g., a credit card), thus enabling the terminal not to be limited in size by the antenna system.

The role of antenna radiation patterns is not negligible when discussing system performance, nor is their influence on parameters associated with wave propagation. Although the tradeoff between an omnidirectional and a narrowbeam antenna is not particular of WBMCS, it assumes particular importance at microwave and millimeter waves because of the characteristics of wave propagation at these bands. Using an omnidirectional antenna means a lower gain, but also the possibility of receiving signals from various directions, without the requirement for knowing where the base station is, and allowing the received rays coming from reflections on the propagation scenario. On the other hand, the use of a very directive antenna provides a higher gain, but it must be pointed at the base station and does not receive reflected waves coming from directions very different from the one to which it is pointed. The need for pointing it can be very discouraging, if not a drawback, when a line of sight does not exist. On the other hand, omnidirectional antennas lead to high values of delay spread, but they may ensure that the link still exists, relying on reflections if the line of sight is lost.

1.2.4 Safety Considerations

Until a few years ago, the analysis of possible harmful effects of electromagnetic radiation on people was devoted mainly to power lines and radars, because of the huge power levels involved in those systems. Even when mobile telephone systems appeared, there was no major concern, as the antennas were installed on the roofs of cars. With

the development of personal communication systems, in which users carry mobile telephones inside their coat pockets, and the antenna radiates a few centimeters from the head, safety issues gained great importance and a new perspective. Much research in the literature focuses not only on the absorption of power inside the head, but also on the influence of the head on the antenna's radiation pattern and input impedance. However, these works have addressed only the frequency bands used in today's systems; that is, up to 2-GHz (mainly on the 900- and 1,800-MHz bands), and only very few references are made to systems working at higher frequencies, as it is in the case of WBMCSs.

The problems associated with infrared are different from those posed by microwaves and millimeter waves. Eye safety, rather than power absorption inside the head, is the issue here, because the eye acts as a filter to the electromagnetic radiation, allowing only light and near-frequency radiation to enter into it, and the amount of power absorption inside the human body is negligible. Exposure of the eye to high levels of infrared radiation may cause cataractlike diseases, and the maximum allowed transmitter power seems to limit the range to a few meters [31]. If this is the case, safety restrictions will pose severe limitations to the use of infrared in WBMCSs, as far as general applications are concerned. The question in this case is not that there are always problems during system operation (e.g., mobile telephones), but the damage that may be caused if someone looks at the transmitter during operation.

Microwaves and millimeter waves have no special effect on eyes, other than power absorption. In WLANs, antennas do not radiate very near (1 or 2 cm) to the user as in the mobile telephone case, thus enabling power limitations to be less restrictive; also if mobile multimedia terminals are used as they are in PDAs. But if terminals are used in the same form as mobile telephones, then maximum transmitter powers have to be established, similar to those for the current personal communication systems. The standards for safety levels have already been set in the United States and Europe, as the ones used for UHF extend up to 300 MHz (IEEE/ANSI and CENELEC recommendations are the references). Thus, it is left to researchers in this area to extend their work to higher frequencies, by evaluating SAR (the amount of power dissipated per unit of mass) levels inside the head (or other parts of the human body very near the radiating system), from which maximum transmitter powers will be established. This may not be as straightforward as it seems, however, because the calculation of SAR is usually done by solving integral or differential equations using numerical methods (method of moments or finite difference), which require models of the head made of small elements (e.g., cubes) with dimensions of the order of a tenth of the wavelength. This already requires powerful computer resources (in memory and CPU time) for frequencies in the high UHF band, and may limit the possibility of analyzing frequencies much higher than UHF. On the other hand, the higher the frequency, the smaller the penetration of radio waves into the human body, hence making it possible to have models of only some centimeters deep. This is an area for further research.

1.2.5 ATM-Based Wireless (Mobile) Broadband Multimedia Systems

Recent study of MBS, ATM, and ATM-oriented MBS has drawn the attention of several researchers [34–44]. With enormous complexity of managing and operating the many different types of networks now in use, the door is open for finding a common platform—a network on which all established services can be supported and which will allow new services to be introduced without needing new networks on which to run them. The answer seems to be ATM. This is the technology being defined and standardized for B-ISDN. Thus, ATM, when adequately modified, is also an answer for the future mobile wireless broadband multimedia systems.

ATM is a packet-oriented transmission scheme. The transmission path of the packets of constant length, the so-called ATM cells, is established during connection setup between the two endpoints by assigning a virtual channel. At this time, the necessary resources are provided and the logical channels are assigned. All packets of a virtual channel are carried over the same path. The transmission capacity of the virtual channel is characterized by the parameters, mean bit rate and peak bit rate during connection setup. ATM cells are generated according to the need of the data source. Thus, ATM is a very good method to meet the dynamic requirements of connections with variable data rates.

MBS is the interface between the fixed ATM net at the base station side and mobile ATM net at the mobile station side. Normally, the ATM net at the mobile station side only consists of one end system. For every end station, it is possible to operate several virtual channels with different data rates at the same time.

A conceptual view of the ATM-type broadband communications network is shown in Figure 1.5. The most important benefit of ATM is its flexibility; it is used for the new high bit rate services, which are either VBR or burst traffic. Several factors that tend to favor the use of ATM cell transport in MBS are as follows:

- Flexible bandwidth allocation and service-type selection for a range of applications;
- Efficient multiplexing of traffic from bursty data and multimedia sources;
- End-to-end provisioning of broadband services over wired and wireless networks;
- Suitability of available ATM switching for intercell switching;
- Improved service reliability with packet-switching techniques; and
- Ease of interfacing with wired B-ISDN systems.

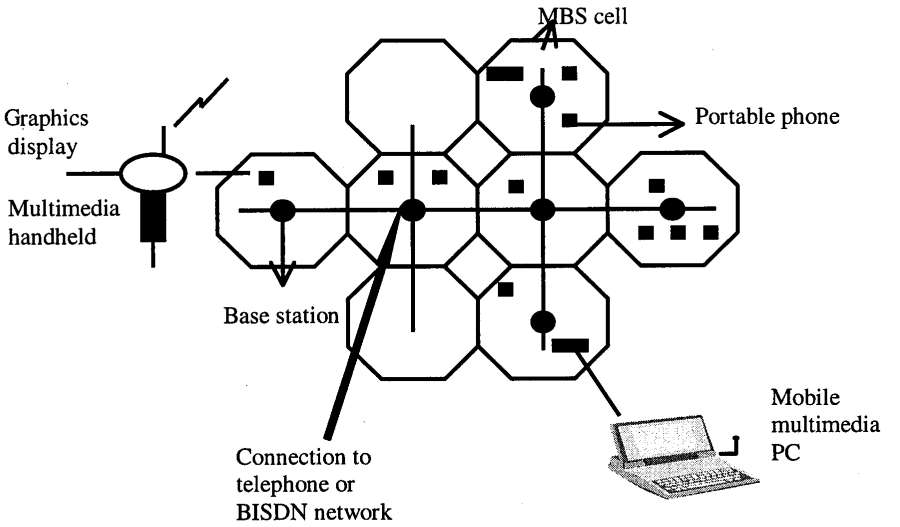

Figure 1.5 Conceptual view of MBS.

Taking the above points into consideration, adoption of ATM-compatible, fixed-length, cell-relay format for MBS is recommended. A possible ATM-compatible MBS approach is shown in Figure 1.6. With this approach, the 48-byte ATM cell payload becomes the basic unit of data within the MBS network. Within MBS, specific protocol layers (e.g., data link and medium-access control layer) are added to the ATM payload as required, and replaced by ATM headers before entering the fixed network [41]. The use of ATM switching for intercell traffic also avoids the crucial problem of developing a new backbone network with sufficient throughput to support intercommunication among large numbers of small cells. ATM multiplexers are used to combine traffic from several base stations into a single ATM port.

For a seamless internetworking mechanism with the wired broadband network, it is vital to have the MBS protocol layering harmonized with the ATM stack. Figure 1.7 shows a protocol reference model. In this approach, new wireless channel-specific physical, medium-access control, and data link layers are added below the ATM network layer. This means that regular network layer and control services such as call setup, virtual channel identifier/virtual path identifier (VCI/VPI) addressing, cell prioritization, and flow-control indication will continue to be used by mobile services. The baseline ATM network and signaling protocol are specified to particular mobility-related functions, such as address registration (roaming), broadcasting, handoff, and so forth.

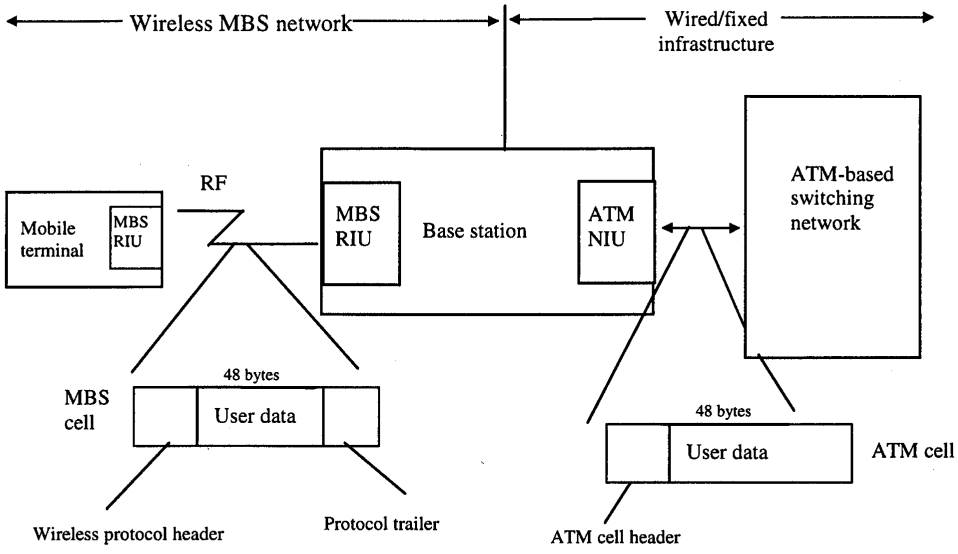

Figure 1.6 ATM-compatible MBS approach. Terms: radio interface unit (RIU); network interface unit (NIU).

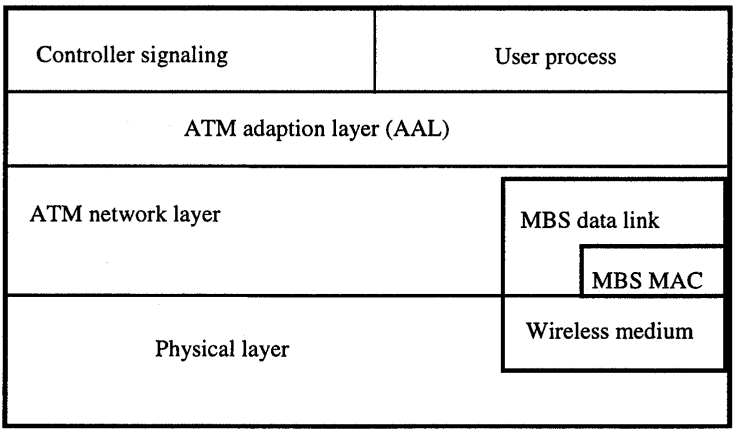

Figure 1.7 Relation of wireless network protocol layers.

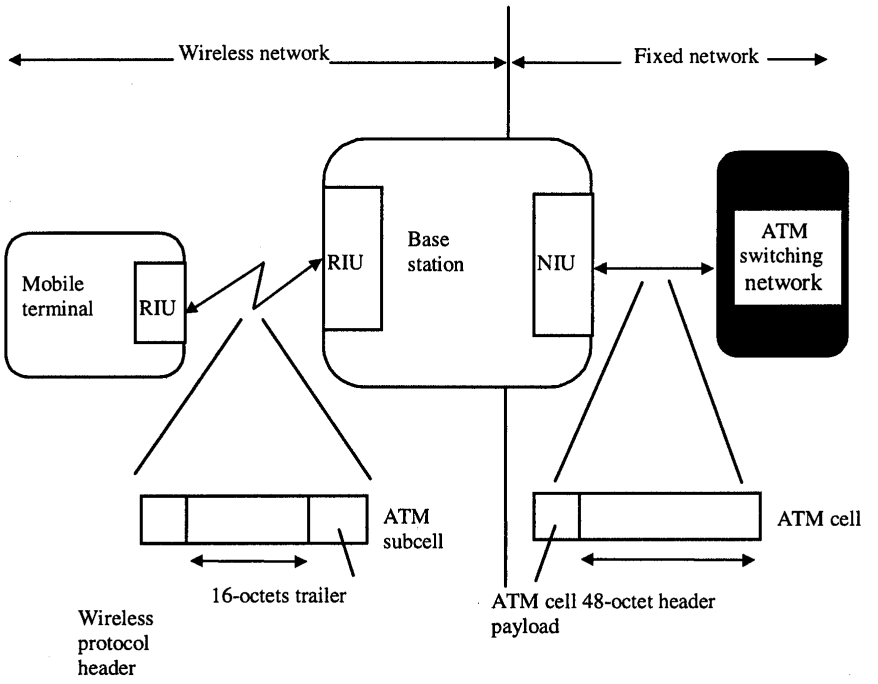

Figure 1.8 Conceptual view of an ATM-compatible air interface.

The payload of an ATM cell consists of 48 octets, meaning that without any segmentation, packet lengths of 384 bits would have to be transmitted over the mobile radio channel. Higher throughput levels over a fading mobile radio channel are achieved when using a packet of smaller lengths. So a suitable integer submultiple of a cell is chosen as the basic unit of data over the wireless radio medium. Based on the system parameters, a submultiple cell size of 16 octets or 128 bits is used as an appropriate value.

The air interface is terminated directly at the base station, as illustrated in Figure 1.8. Also shown is the segmentation of an ATM cell into its three subcells and the addition of an extra wireless ATM header.

1.3 MULTIPATH PROPAGATION

One of the basic reasons to use OFDM is the efficient way it can handle multipath propagation. To understand the effects of multipath fading, this section contains an overview of the most relevant parameters and models.

1.3.1 Multipath Channel Models

Fundamental work on modeling of the indoor radio channel is published in [45, 46]. One of the results of this work, which is also supported by many other measurements reported in the literature, is that the average received multipath power is an exponentially decaying function of the excess delay. Further, the amplitudes of individual multipath components are Rayleigh distributed. This observation has led to simplified channel models as used in [47, 48]. These models assume a fixed number of paths with equidistant delays. The path amplitudes are independent Rayleigh variables, while the path phases are uniformly distributed. Figure 1.9 shows an example of an average and an instantaneous power delay profile that were generated using this approach.

Compared to the more extensive models in [45, 46], the simplified model of [47, 48] may give somewhat optimistic results because the number of multipath components is fixed to the maximum possible amount. In the models of [45, 46], the number of paths is random. Paths arrive in clusters with Poisson distributed arrival times. Within a cluster, the path amplitudes are independent Rayleigh variables. The average power delay profile, averaged over a large number of channels, is an exponentially decaying function, just as for the models in [47, 48]. Thus, the only difference between the models is that the instantaneous power delay profiles have a slightly different shape, and channels generated by the method of [47, 48] generally show more multipath components than channels generated according to [45, 46]. This may give a somewhat optimistic diversity effect, because diversity is proportional to the number of paths. It probably does not make a difference when the models are used to determine the delay spread tolerance of a particular transmission system, however, because that is not depending on the number of paths, but rather on the amount of power in paths exceeding a certain excess delay. So, the channel models of [47, 48] seem a good basis to determine the delay spread tolerance of different modulation schemes. An additional advantage is that the simulation complexity is much lower than that of the models of [45, 46].

One of the key parameters in the design of a transmission system is the maximum delay spread value that it has to tolerate. For an idea of what typical delay spread figures are, the next section presents some measurement results obtained from the literature [49- 63].

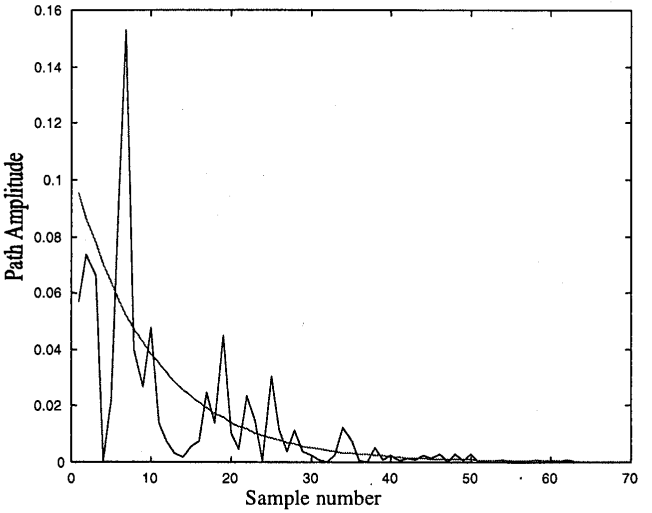

Figure 1.9 Example of generated average and instantaneous power delay profiles for a delay spread of 10 sampling intervals.

1.3.2 Delay Spread Values

Tables 1.3 to 1.5 summarize some delay spread results obtained from literature for frequencies from 800 MHz to 6 GHz. Two delay spread values are given; the *median* delay spread is the 50% value, meaning that 50% of all channels has a delay spread that is lower than the median value. Clearly, the median value is not so interesting for designing a wireless link, because there you want to guarantee that the link works for at least 90% or 99% of all channels. Therefore, the second column gives the measured *maximum* delay spread values. The reason to use maximum delay spread instead of a 90% or 99% value is that many papers only mention the maximum value. From the papers that do present cumulative distribution functions of their measured delay spreads, we can deduce that the 99% value is only a few percent smaller than the maximum measured delay spread.

Table 1.3
Measured delay spreads in frequency range of 800 MHz to 1.5 GHz.

Median delay spread [ns]	Maximum delay spread [ns]	Reference	Remarks
25	50	[46]	Office building
30	56	[58]	Office building
27	43	[59]	Office building
11	58	[60]	Office building
35	80	[61]	Office building
40	90		Shopping center
80	120		Airport
120	180		Factory
50	129	[62]	Warehouse
120	300		Factory

Table 1.4
Measured delay spreads in frequency range of 1.8 to 2.4 GHz

Median delay spread [ns]	Maximum delay spread [ns]	Reference	Remarks
40	120	[49]	Large building (New York stock exchange)
40	95	[50]	Office building
40	150	[51]	Office building
60	200	[54]	Shopping center
106	270		Laboratory
19	30	[55]	Office building: single room only
20	65	[56]	Office building
30	75		Cafeteria
105	170		Shopping center
30	56	[58]	Office building
25	30	[63]	Office building: single room only

Table 1.5
Measured delay spreads in frequency range of 4 to 6 GHz

Median delay spread [ns]	Maximum delay spread [ns]	Reference	Remarks
40	120	[49]	Large building (e.g., Stock Exchange)
50 35 10	60 55 35	[52]	Office building Meeting room (5m x 5m) with metal walls Single room with stone walls
40	130	[51]	Office building
40 65 25	120 125 65	[53]	Indoor sports arena Factory Office building
20	30	[63]	Office building: single room only

Interesting results that can be derived from the reported measurements are:

- Measurements done simultaneously on different frequencies show that there is no significant difference in delay spread in the frequency range of 800 MHz to 6 GHz.
- The delay spread is related to the building size; largest delay spreads (up to 270 ns) were measured in large buildings like shopping centers and factories. The reason for this phenomenon is that reflections can have larger delays if the distances between transmitter and reflectors (walls or other objects) are larger.
- For most office buildings, the maximum delay spread is in the range of 40 to 70 ns. Smaller delay spreads around 30 ns occur when both transmitter and receiver are within the same room. Delay spreads of 100 ns or more are seen only in office buildings with large rooms that are some tens of meters in diameter.
- Even small rooms (5m by 5m) can give significant delay spreads around 50 ns when there are metal walls [52]. The reason for this is that reflections from a metal wall only experience a small attenuation, so multiple reflections with significant delays still have considerable power, which increases the delay spread.

1.4 TIME VARIATION OF THE CHANNEL

To classify the time characteristics of the channel [1], the coherence time and Doppler spread are important parameters. The coherence time is the duration over which the channel characteristics do not change significantly. The time variations of the channel are evidenced as a Doppler spread in the frequency domain, which is determined as the width of the spectrum when a single sinusoid (constant envelope) is transmitted. Both

the time correlation function $\varphi_c(\Delta t)$ and the Doppler power spectrum $S_c(f)$ can be related to each other by applying the Fourier transform.

The range of values of the frequency f over which $S_c(f)$ is essentially nonzero is called the Doppler spread B_d of the channel. Because $S_c(f)$ is related to $\varphi_c(\Delta t)$ by the Fourier transform, the reciprocal of B_d is a measure of the coherence time $(\Delta t)_c$ of the channel; that is, $1/B_d$.

The coherence time $(\Delta t)_c$ is a measure of the width of the time correlation function. Clearly, a slow-changing channel has a large coherence time, or equivalently, a small Doppler spread. The rapidity of the fading can now be determined either from the correlation function $\varphi_c(\Delta t)$ or from the Doppler power spectrum $S_c(f)$. This implies that either the channel parameters $(\Delta t)_c$ or B_d can be used to characterize the rapidity of the fading. If the bit time T_b is large compared with the coherence time, then the channel is subject to fast fading. When selecting a bit duration that is smaller than the coherence time of the channel, the channel attenuation and phase shift are essentially fixed for the duration of at least one signaling interval. In this case, the channel is slowly fading or quasistatic. Like coherence bandwidth, there is no exact relationship between coherence time and Doppler spread. If the coherence time $(\Delta t)_c$ is defined as the time over which the time correlation function is above 0.5, $(\Delta t)_c$ is approximately given by $9/(16\pi B_d)$ [79, 80].

Doppler spread is caused by the differences in Doppler shifts of different components of the received signal, if either the transmitter or receiver is in motion. The frequency shift is related to the spatial angle between the direction of arrival of that component and the direction of vehicular motion. If a vehicle is moving at a constant speed V along the X axis, the Doppler shift f_m of the mth plane-wave component is given by $f_m = (V/\lambda)\cos(\alpha_m)$ [81], where α_m is the arrival angle of the mth plane-wave component relative to the direction of movement of the vehicle. It is worth noting here that waves arriving from ahead of the vehicle experience a positive Doppler shift, while those arriving from behind the vehicle have a negative shift. The maximum Doppler shift occurs at $\alpha_m = 0$, assuming $T_b >> (\Delta t)_c$ for fast-fading channel and $T_b << (\Delta t)_c$ for slow-fading channel.

Indoor measurements [82] show that in any fixed location, temporal variations in the received signal envelope caused by movement of personnel and machinery are slow, having a maximum Doppler spread of about 6 Hz.

1.5 HISTORY OF OFDM

OFDM is a special case of multicarrier transmission, where a single datastream is transmitted over a number of lower rate subcarriers. It is worth mentioning here that OFDM can be seen as either a modulation technique or a multiplexing technique. One

of the main reasons to use OFDM is to increase the robustness against frequency selective fading or narrowband interference. In a single carrier system, a single fade or interferer can cause the entire link to fail, but in a multicarrier system, only a small percentage of the subcarriers will be affected. Error correction coding can then be used to correct for the few erroneous subcarriers. The concept of using parallel data transmission and frequency division multiplexing was published in the mid-1960s [64, 65]. Some early development is traced back to the 1950s [66]. A U.S. patent was filed and issued in January, 1970 [67].

In a classical parallel data system, the total signal frequency band is divided into N nonoverlapping frequency subchannels. Each subchannel is modulated with a separate symbol and then the N subchannels are frequency-multiplexed. It seems good to avoid spectral overlap of channels to eliminate interchannel interference. However, this leads to inefficient use of the available spectrum. To cope with the inefficiency, the ideas proposed from the mid-1960s were to use (parallel data) and FDM with overlapping subchannels, in which each carrying a signaling rate b is spaced b apart in frequency to avoid the use of high-speed equalization and to combat impulsive noise and multipath distortion, as well as to fully use the available bandwidth.

Figure 1.10 illustrates the difference between the conventional nonoverlapping multicarrier technique and the overlapping multicarrier modulation technique. As shown in Figure 1.10, by using the overlapping multicarrier modulation technique, we save almost 50% of bandwidth. To realize the overlapping multicarrier technique, however we need to reduce crosstalk between subcarriers, which means that we want orthogonality between the different modulated carriers.

The word orthogonal indicates that there is a precise mathematical relationship between the frequencies of the carriers in the system. In a normal frequency-division multiplex system, many carriers are spaced apart in such a way that the signals can be received using conventional filters and demodulators. In such receivers, guard bands are introduced between the different carriers and in the frequency domain which results in a lowering of spectrum efficiency.

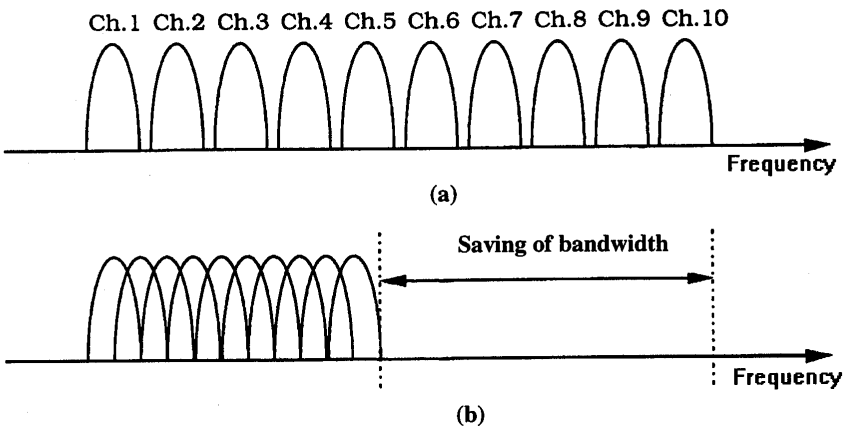

Figure 1.10 Concept of OFDM signal: (a) Conventional multicarrier technique, and (b) orthogonal multicarrier modulation technique.

It is possible, however, to arrange the carriers in an OFDM signal so that the sidebands of the individual carriers overlap and the signals are still received without adjacent carrier interference. To do this the carriers must be mathematically orthogonal. The receiver acts as a bank of demodulators, translating each carrier down to DC, with the resulting signal integrated over a symbol period to recover the raw data. If the other carriers all beat down the frequencies that, in the time domain, have a whole number of cycles in the symbol period T, then the integration process results in zero contribution from all these other carriers. Thus, the carriers are linearly independent (i.e., orthogonal) if the carrier spacing is a multiple of $1/T$. Chapter 2 presents in detail the basic principle of OFDM.

Much of the research focuses on the high efficient multicarrier transmission scheme based on "orthogonal frequency" carriers. In 1971, Weinstein and Ebert [68] applied the discrete Fourier transform (DFT) to parallel data transmission systems as part of the modulation and demodulation process. Figure 1.11 (a) shows the spectrum of the individual data of the subchannel. The OFDM signal, multiplexed in the individual spectra with a frequency spacing b equal to the transmission speed of each subcarrier, is shown in Figure 1.11(b). Figure 1.11 shows that at the center frequency of each subcarrier, there is no crosstalks from other channels. Therefore, if we use DFT at the receiver and calculate correlation values with the center of frequency of each subcarrier, we recover the transmitted data with no crosstalk. In addition, using the DFT-based multicarrier technique, frequency-division multiplex is achieved not by bandpass filtering but by baseband processing.

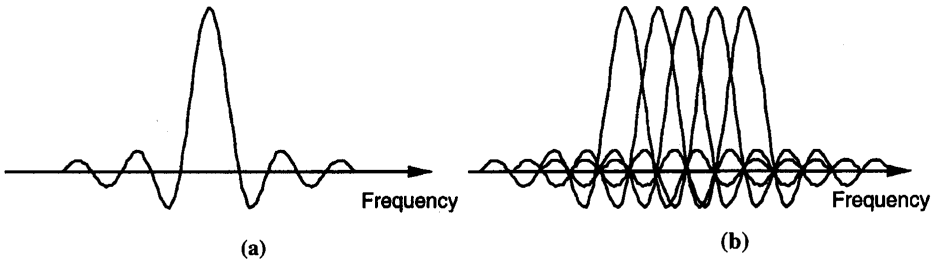

Figure 1.11 Spectra of (a) an OFDM subchannel and (b) an OFDM signal.

Moreover, to eliminate the banks of subcarrier oscillators and coherent demodulators required by frequency-division multiplex, completely digital implementations could be built around special-purpose hardware performing the fast Fourier transform (FFT), which is an efficient implementation of the DFT. Recent advances in very-large-scale integration (VLSI) technology make high-speed, large-size FFT chips commercially affordable. Using this method, both transmitter and receiver are implemented using efficient FFT techniques that reduce the number of operations from N^2 in DFT down to $N\log N$ [69].

In the 1960s, the OFDM technique was used in several high-frequency military systems such as KINEPLEX [66], ANDEFT [70], and KATHRYN [71]. For example, the variable-rate data modem in KATHRYN was built for the high-frequency band. It used up to 34 parallel low-rate phase-modulated channels with a spacing of 82 Hz.

In the 1980s, OFDM was studied for high-speed modems, digital mobile communications, and high-density recording. One of the systems realized the OFDM techniques for multiplexed QAM using DFT [72], and by using pilot tone, stabilizing carrier and clock frequency control and implementing trellis coding are also implemented [73]. Moreover, various-speed modems were developed for telephone networks [74].

In the 1990s, OFDM was exploited for wideband data communications over mobile radio FM channels, high-bit-rate digital subscriber lines (HDSL; 1.6 Mbps), asymmetric digital subscriber lines (ADSL; up to 6 Mbps), very-high-speed digital subscriber lines (VDSL; 100 Mbps), digital audio broadcasting (DAB), and high-definition television (HDTV) terrestrial broadcasting [75–80].

The OFDM transmission scheme has the following key advantages:

- OFDM is an efficient way to deal with multipath; for a given delay spread, the implementation complexity is significantly lower than that of a single carrier system with an equalizer.
- In relatively slow time-varying channels, it is possible to significantly enhance the capacity by adapting the data rate per subcarrier according to the signal-to-noise ratio of that particular subcarrier.

- OFDM is robust against narrowband interference, because such interference affects only a small percentage of the subcarriers.
- OFDM makes single-frequency networks possible, which is especially attractive for broadcasting applications.

On the other hand, OFDM also has some drawbacks compared with single-carrier modulation:

- OFDM is more sensitive to frequency offset and phase noise.
- OFDM has a relatively large peak-to-average power ratio, which tends to reduce the power efficiency of the RF amplifier.

1.6 PREVIEW OF THE BOOK

This book consists of 10 chapters. It covers all the necessary elements to achieve the OFDM-based WBMCS. In Chapter 2, the basics of OFDM are presented. It is explained how an OFDM signal is formed using the inverse fast Fourier transform, how the cyclic extension helps to mitigate the effects of multipath, and how windowing can limit the out-of-band radiation. Basic design rules are given how to choose the OFDM parameters, given a required bandwidth, multipath delay spread, and maximum Doppler spread.

In Chapter 3, we explain how coding and interleaving can be used to mitigate the effects of frequency-selective fading channels. *Quadrature amplitude modulation* is introduced as an appropriate modulation technique for the OFDM subcarriers.

Synchronization of the symbol clock and carrier frequency is the subject of Chapter 4. First, we discuss the sensitivity of OFDM to synchronization errors. Then, we describe different sychronization techniques. Special attention is given to packet transmission, which requires rapid synchronization at the beginning of each packet with a minimum of training overhead.

Chapter 5 describes channel estimation; that is, estimating the reference phases and amplitudes of all subcarriers. Various coherent and differential techniques are explained in conjunction with their relative merits on signal-to-noise ratio performance, overhead, and buffering delay.

The relatively large peak-to-average power (PAP) ratio of OFDM is the subject of Chapter 6. The distribution of the PAP ratio is shown, and various methods to reduce the PAP ratio are explained. This chapter demonstrates that for an arbitrary number of subcarriers, the PAP ratio can be reduced to about 5 dB without a significant loss in performance. This means that the required backoff—and hence the efficiency—of an RF power amplifier for an OFDM system is not much different from that for a single-carrier QPSK system.

In Chapter 7, we explain the basics of direct-sequence and frequency-hopping CDMA, which is especially helpful in understanding the following chapters on combinations of OFDM and CDMA.

Chapter 8 describes multicarrier CDMA. Different techniques with their transmitter and receiver architectures are introduced. Advantages and disadvantages compared with other CDMA techniques are discussed.

Orthogonal FDMA and frequency-hopping CDMA are the subjects of Chapter 9. It shows how OFDM and frequency hopping can be combined to get a multiple-access system with similar advantages as direct-sequence CDMA.

Finally, some applications of OFDM systems are described in Chapter 10: digital audio broadcasting, digital video broadcasting, wireless ATM in the Magic WAND project, and the new IEEE 802.11 and ETSI BRAN OFDM standards.

REFERENCES

[1] Prasad, R., *Universal Wireless Personal Communications*, Norwood, MA: Artech House, 1998.

[2] Prasad, R., "Wireless Broadband Communication Systems," *IEEE Comm. Mag.*, Vol. 35, p. 18, Jan. 1997.

[3] Honcharenko, W., J. P. Kruys, D. Y. Lee, and N.J. Shah, "Broadband Wireless Access," *IEEE Comm. Mag.*, Vol. 35, pp. 20–26, Jan. 1997.

[4] Correia, L. M., and R. Prasad, "An Overview of Wireless Broadband Communications," *IEEE Comm. Mag.*, Vol. 35, pp. 28–33, Jan. 1997.

[5] Morinaga, M., M. Nakagawa, and R. Kohno, "New Concepts and Technologies for achieving Highly Reliable and High Capacity Multimedia Wireless Communications System," *IEEE Comm. Mag.* Vol. 35, pp. 34–40, Jan. 1997.

[6] Da Silva, J. S., B. Arroyo-Fernandez, B. Barani, J. Pereira, and D. Ikonomou, "Mobile and Personal Communications: ACTS and Beyond," *Proc. PIMRC'97,* Helsinki, Finland, Sep. 1997.

[7] Prisoli, F. D., and R. Velt, "Design of Medium Access Control and Logical Link Control Functions for ATM Support in the MEDIAN System," *Proc. ACTS Mobile Comm. Summit'97,* pp. 734–744, Aalborg, Denmark, Oct. 1997.

[8] Rheinschmitt, R., A. de Haz, and M. Umehinc, "AWACS MAC and LLC Functionality," *Proc. ACTS Mobile Comm. Summit'97,* pp. 745–750, Aalborg, Denmark, Oct. 1997.

[9] van Nee, R., "An OFDM Modem for Wireless ATM," *Proceedings of IEEE 4th Symposium on Communications and Vehicular Technology in the Benelux*, Gent, Belgium, pp. 36-41, Oct. 7-8, 1996.

[10] Aldis, J., E. Busking, T. Kleijne, R. Kopmeiners, and R. van Nee, "Magic Into Reality, Building the WAND Modem," *Proc. ACTS Mobile Comm. Summit'97*, pp. 734–744, Aalborg, Denmark, Oct. 1997.

[11] Mikkonen, J., C. Corrado, C. Erci, and M. Progler, "Emerging Wireless Broadband Networks," *IEEE Comm. Mag.*, Feb. 1988.

[12] Wu, G., Y. Hase, K. Taira, and K. Iwasak, "Emerging Wireless ATM Oriented MAC Protocol for High-Speed Wireless LAN," Proc. PIMRC'97, pp. 198-203, Helsinki, Finland, Sep. 1997.

[13] Prasad, R., and L. M. Correia, "Wireless Broadband Multimedia Communications," *International Wireless and Telecommunications Symposium*, Shah Alam, Malaysia, Vol. 2, pp. 55–70 May 14–16,1997.

[14] Prasad, R., and L. M. Correia, "An Overview of Wireless Broadband Multimedia Communications," *Proc. MoMuC'97*, Seoul, Korea, pp. 17–31, Sep.-Oct. 1997.

[15] Chelouche, M., S. Hethuin, and L. Ramel, "Digital Wireless Broadband Corporate and Private Networks: RNET Concepts and Applications," *IEEE Comm. Mag.*, Vol. 35, pp. 42–51, Jan. 1997.

[16] IEEE 802.11, *IEEE Standard for Wireless LAN Medium Access Control and Physical Layer Specifications*, Nov. 1997.

[17] Fernandes, L., "R2067 MBS - Mobile Broadband System," in *Proc. ICUPC'93 — 2nd IEEE International Conference on Universal Personal Communications*, Ottawa, Canada, Oct.,1993.

[18] IEEE 802.11 Web URL: http://grouper.ieee.org/groups/802/11/.

[19] ETSI home page: http://www.etsi.org/.

[20] Kruys, J., "Standardization of Wireless High Speed Premises Data Networks," *Wireless ATM Workshop*, Espoo, Finland, Sep. 1996.

[21] van Nee, R., G. Awater, M. Morikura, H. Takanashi, M. Webster, and K. Halford, "New High Rate Wireless LAN Standards," *IEEE Communications Magazine*, Dec. 1999.

[22] IEEE, "Supplement to Standard for Telecommunications and Information Exchange Between Systems—LAN/MAN Specific Requirements—Part 11: Wireless MAC and PHY Specifications: Higher Speed Physical Layer Extension in the 2.4-GHz Band," P802.11b/D7.0, July 1999.

[23] WECA home page: http://www.wirelessethernet.com.

[24] IEEE, "Supplement to Standard for Telecommunications and Information Exchange Between Systems—LAN/MAN Specific Requirements—Part 11: Wireless MAC and PHY Specifications: High Speed Physical Layer in the 5-GHz Band," P802.11a/D7.0, July 1999.

[25] WaveLAN home page: http://www.wavelan.com.

[26] Prasad, R., "Research Challenges in Future Wireless Personal Communications: Microwave Perspective," *Proc. 25th European Microwave Conference* (Keynote opening address), Bologna, Italy, pp. 4–11, Sept. 4–7, 1995.

[27] Prasad, R., "Overview of Wireless Personal Communications: Microwave Perspectives," *IEEE Comm. Mag.*, Vol. 35, pp. 104–108, April 1997.

[28] Smulders, P. F. M., "Broadband Wireless LANs: a feasibility study," *Ph.D. Thesis*, Eindhoven Univ. of Technology, Eindhoven, The Netherlands, Dec. 1995.

[29] Correia, L. M., and P. O. Frances, "A Propagation Model for the Estimation of the Average Received Power in an Outdoor Environment at the Millimeter Wave Band," *Proc. VTC'94 — IEEE VTS 44th Vehicular Technology Conference*, Stockholm, Sweden, pp. 1785–1788, July 1994.

[30] Lovnes, G., J. J. Reis, and R. H. Raekken, "Channel Sounding Measurements at 59 GHz in City Streets," *Proc. PIMRC'94 — 5th IEEE International Symposium on Personal, Indoor; and Mobile Radio Communications*, The Hague, The Netherlands, pp. 496–500, Sep. 1994.

[31] Fernandes, J. J., P. A. Watson, and J. C. Neves, "Wireless LANs: Physical Properties of Infrared Systems versus mmWave Systems," *IEEE Comm. Mag.*, Vol. 32, No.8, pp. 68–73, Aug. 1994.

[32] European Commission, "Communications for Society Visionary Research," European Commission, DG XIII/B, Brussels, Belgium, Feb. 1997.

[33] Rokitansky, C. –H., and M. Scheibenbogen (eds.), "Updated Version of System Description Document," *RACE Deliverable R2067/UA/WP215/DS/P/068.b1*, RACE Central Office, European Commission, Brussels, Belgium, Dec. 1995.

[34] Prasad, A. R., "Asynchronous Transfer Mode Based Mobile Broadband System," *Proc. IEEE 3rd Symposium on Comm. & Vech. Technology in Benelux*, Eindhoven, The Netherlands, pp. 143–148, Oct. 1995.

[35] Prasad, R., and L. Vandendorpe, "An Overview of Millimeter Wave Indoor Wireless Communication System," *Proc. 2nd Int. Conf. on Universal Personal Communications*, pp. 885–889, Ottawa, Canada, 1993.

[36] Prasad, R., and L. Vandendorpe, "Cost 231 Project: Performance Evaluation of a Millimetric-Wave Indoor Wireless Communications System," *RACE Mobile Telecommunications Workshop*, Metz, France, pp. 137–144, June 16–18, 1993.

[37] Zauner, K., "On the ATM Road to Broadband," *Telecom Report International*, No.3, pp. 26–29, 1993.

[38] Tubtiang, H.I. Kwon and O. Pujolle, "A Simple ATM Switching Architecture for Broadband-ISDN and Its Performance," *Modeling and Performance Evaluation of ATM Technology (C-I5)*, pp. 361–367, IFIP 1993.

[39] Stallings, W., *Advances in ISDN and Broadband ISDN*, IEEE Computer Society Press, 1992.

[40] Leslie, I. M., D. R. McAuley, and D. L. Tennenhouse, "ATM Everywhere?" *IEEE Network*, pp. 40–46, March 1993.

[41] McTiffin, M. J., A. P. Hulbert, T. J. Ketseoglou, W. Heimsch, and O. Crisp, "Mobile access to an ATM Network Using A CDMA Air Interface," *IEEE J. Selected Areas in Comm.*, Vol. 12, No. 5, pp. 900–908, June 1994.

[42] Raychaudhri, D., "ATM-based Transport Architecture for Multiservices Wireless Personal Communication Networks," *IEEE J. Selected Areas in Comm.*, Vol.12, No. 8, pp. 1401–1414, Oct. 1994.

[43] Geij, R. R., "Mobile Multimedia Scenario using ATM and Microcellular Technologies," *Vehicular Technology*, Vol. 43, No. 3, pp. 699–703, Aug. 1994.

[44] Bakker, J. D., and R. Prasad, "Wireless Multimedia Communications Using a CDMA-based ATM Air Interface," *Proc. IEEE ISSSTA'96*, Mainz, Germany, pp. 1128–1132, Sept. 1996.

[45] Hashemi, H., "The Indoor Radio Propagation Channel," *Proceedings of the IEEE*, Vol. 81, no. 7, pp. 943-968, July 1993.

[46] Saleh, A. A. M., and R. A. Valenzuela, "A Statistical Model for Indoor Multipath Propagation," *IEEE Journal on Selected Areas in Communications*, vol. SAC-5, no. 2, pp. 128-137, Feb. 1987.

[47] Halls, G., "HIPERLAN Radio Channel Models and Simulation Results," RES10TTG 93/58.

[48] Chayat, N., "Tentative Criteria for Comparison of Modulation Methods," IEEE P802.11-97/96.

[49] Devasirvatham, D. M. J., "Multi-Frequency Propagation Measurements and Models in a Large Metropolitan Commercial Building for Personal Communications," *IEEE PIMRC '91*, pp. 98-103, London, UK, Sept. 23-25, 1991.

[50] Devasirvatham, D. M. J., "Time Delay Spread Measurements at 850 MHz and 1.7 GHz inside a Metropolitan Office Building," *Electronics Letters*, pp. 194–196, Feb. 2, 1989.

[51] Devasirvatham, D. M. J., M. J. Krain and D. A. Rappaport, "Radio Propagation Measurements at 850 MHz, 1.7 GHz and 4 GHz Inside Two Dissimilar Office buildings," *Electronics Letters*, Vol. 26, No. 7, pp. 445-447, March 29, 1990.

[52] Hafesi, P., D. Wedge, M. Beach, M. Lawton, "Propagation Measurements at 5.2 GHz in Commercial and Domestic Environments," *IEEE PIMRC '97*, Helsinki, pp. 509-513, Sept. 1-4, 1997.

[53] Hawbaker, D. A., and T. S. Rappaport, "Indoor Wideband Radiowave Propagation Measurements at 1.3 GHz and 4.0 GHz," *Electronics Letters*, vol. 26, no. 21, pp. 1800-1802, Oct. 11, 1990.

[54] Johnson, I. T., and E. Gurdenelli, "Measurements of Wideband Channel Characteristics in Cells Within Man Made Structures of Area Less Than 0.2 km^2," COST 231 TD(90)083.

[55] Lahteenmaki, J., "Indoor Measurements and Simulation of Propagation at 1.7 GHz," COST 231 TD(90)084.

[56] Anderson, P. C., O. J. M. Houen, K. Kladakis, K. T. Peterson, H. Fredskild and I. Zarnoczay, "Delay Spread Measurements at 2 GHz," COST 231 TD(91)029.

[57] Bultitude, R. J. C., et al., "The Dependance of Indoor Radio Channel Multipath Characteristics on Transmit/Receive Ranges," *IEEE Journal on Selected Areas in Communications*, Vol. 11, No. 7, pp. 979 - 990, Sep. 1993.

[58] Bultitude, R. J. C., S. A. Mahmoud and W. A. Sullivan, "A Comparison of Indoor Radio Propagation Characteristics at 910 MHz and 1.75 GHz," *IEEE Journal on Selected Areas in Communications*, Vol. 7, No. 1, pp. 20-30, Jan. 1989.

[59] Pahlavan, K., and S. J. Howard, "Frequency Domain Measurements of Indoor Radio Channels," *Electronics Letters*, vol. 25, no. 24, pp. 1645 - 1647, Nov. 23, 1989.

[60] Davies, R., and J. P. McGeehan, "Propagation Measurements at 1.7 GHz for Microcellular Urban Communications," *Electronics Letters*, vol. 26, no. 14, pp. 1053-1055, July 5, 1990.

[61] Zollinger, E., and A. Radovic, "Measured Time Variant Characteristics of Radio Channels in the Indoor Environment," COST 231 TD(91)089.

[62] Rappaport, T. S., and C. D. McGillem, "Characterization of UHF Multipath Radio Channels in Factory Buildings," *IEEE Transactions on Antennas and Propagation*, Vol. 37, No. 8, pp. 1058-1069, Aug. 1989.

[63] Nobles, P., and F. Halsall, "Delay Spread and Received Power Measurements Within a Building at 2 GHz, 5 GHz, and 17 GHz', *IEE Tenth International Conference on Antennas and Propagation*, Edinburgh, UK, April 14-17, 1997.

[64] R. W. Chang, "Synthesis of Band Limited Orthogonal Signals for Multichannel Data Transmission," *Bell Syst. Tech. J.,* Vol. 45, pp. 1775–1796, Dec. 1996.

[65] Salzberg, B. R., "Performance of an efficient parallel data transmission system," *IEEE Trans. Comm.,* Vol. COM-15, pp. 805 – 813, Dec. 1967.

[66] Mosier, R. R., and R.G. Clabaugh, "Kineplex, a Bandwidth Efficient Binary Transmission System," *AIEE Trans.,* Vol. 76, pp. 723 – 728, Jan. 1958.

[67] "Orthogonal Frequency Division Multiplexing," U.S. Patent No. 3, 488,4555, filed November 14, 1966, issued Jan. 6, 1970.

[68] Weinstein, S. B., and P .M. Ebert, "Data Transmission by Frequency Division Multiplexing Using the Discrete Fourier Transform," *IEEE Trans. Comm.,* Vol. COM-19, pp. 628 – 634, Oct. 1971.

[69] Zou, W. Y., and Y. Wu, "COFDM: an overview," *IEEE Trans. Broadc.,* Vol. 41, No. 1, pp. 1 – 8, March 1995.

[70] Porter, G. C., "Error Distribution and Diversity Performance of a Frequency Differential PSK HF modem," *IEEE Trans. Comm.,* Vol., COM-16, pp. 567–575, Aug. 1968.

[71] Zimmerman, M. S., and A. L. Kirsch, "The AN/GSC-10 (KATHRYN) variable rate data modem for HF radio," *IEEE Trans. Comm.,* Vol., COM-15, pp. 197 – 205, April 1967.

[72] Hirosaki, B., "An Orthogonally Multiplexed QAM system Using the Discrete Fourier Transform," *IEEE Trans. Comm.,* Vol., COM-29, pp. 982 – 989, July 1981.

[73] Hirosaki, B., "A 19.2 kbits Voice Band Data Modem Based on Orthogonality Multiplexed QAM Techniques," *Proc. of IEEE ICC'85,* pp. 21.1.1 – 5, 1985.

[74] Keasler, W. E., and D. L. Bitzer, "High speed modem suitable for operating with a switched network," U.S. Patent No. 4,206,320, June 1980.

[75] Chow, P. S., J. C. Tu and J. M. Cioffi, "Performance Evaluation of a Multichannel Transceiver System for ADSL and VHDSL services," *IEEE J. Selected Area,* Vol., SAC-9, No. 6, pp. 909 – 919, Aug. 1991.

[76] Chow, P. S., J. C. Tu, and J. M. Cioffi, "A Discrete Multitone Transceiver System for HDSL Applications," *IEEE J. Selected Areas in Comm.,* Vol. SAC-9, No. 6, pp. 909 – 919, Aug. 1991.

[77] Paiement, R. V., "Evaluation of Single Carrier and Multicarrier Modulation Techniques for Digital ATV Terrestrial Broadcasting," *CRC Report,* No. CRC-RP-004, Ottawa, Canada, Dec. 1994.

[78] Sari, H., G. Karma, and I. Jeanclaude, "Transmission Techniques for Digital Terrestrial TV Broadcasting," *IEEE Comm. Mag.*, Vol.33, pp. 100–109, Feb. 1995.

[79] Oppenheim, A.V., and R.W. Schaffer, *Discrete-time Signal Processing*, Prentice-Hall International, ISBN 0-13-216771-9, 1989.

[80] Hara, S., M. Mouri, M. Okada, and N. Morinaga, "Transmission Performance Analysis of Multi-Carrier Modulation in Frequency Selective Fast Rayleigh Fading Channel," in *Wireless Personal Communications*, Kluwer Academic Publishers, Vol.2, pp. 335 – 356, 1996.

[79] Rappaport, T. S., *Wireless Communication Principles & Practice*, Prentice-Hall PTR, New Jersey, 1996.

[80] Steel, R., (ed.), *Mobile Radio Communications*, IEEE Press, 1994.

[81] Macrario, R. C. V., (ed.), "Personal & Mobile Communications," Peter Peregrinus Ltd., 1991.

[82] Howard, S. J., and K. Rappaport, "Performance of a DFE Modem Evaluted From Measured Indoor Radio Multipath Profiles," Proc. ICC'90, Vol. 4, pp. 335.2.1 – 335.2.5, April 1990.

Chapter 2

OFDM Basics

2.1 INTRODUCTION

The basic principle of OFDM is to split a high-rate datastream into a number of lower rate streams that are transmitted simultaneously over a number of subcarriers. Because the symbol duration increases for the lower rate parallel subcarriers, the relative amount of dispersion in time caused by multipath delay spread is decreased. Intersymbol interference is eliminated almost completely by introducing a guard time in every OFDM symbol. In the guard time, the OFDM symbol is cyclically extended to avoid intercarrier interference. This whole process of generating an OFDM signal and the reasoning behind it are described in detail in sections 2.2 to 2.4.

In OFDM system design, a number of parameters are up for consideration, such as the number of subcarriers, guard time, symbol duration, subcarrier spacing, modulation type per subcarrier, and the type of forward error correction coding. The choice of parameters is influenced by system requirements such as available bandwidth, required bit rate, tolerable delay spread, and Doppler values. Some requirements are conflicting. For instance, to get a good delay spread tolerance, a large number of subcarriers with a small subcarrier spacing is desirable, but the opposite is true for a good tolerance against Doppler spread and phase noise. These design issues are discussed in Section 2.5. Section 2.6 gives an overview of OFDM signal processing functions, while Section 2. ends this chapter with a complexity comparison of OFDM versus single-carrier systems.

2.2 GENERATION OF SUBCARRIERS USING THE IFFT

An OFDM signal consists of a sum of subcarriers that are modulated by using *phase shift keying (PSK)* or *quadrature amplitude modulation (QAM)*. If d_i are the complex

QAM symbols, N_s is the number of subcarriers, T the symbol duration, and f_c the carrier frequency, then one OFDM symbol starting at $t = t_s$ can be written as

$$s(t) = \mathrm{Re}\left\{ \sum_{i=-\frac{N_s}{2}}^{\frac{N_s}{2}-1} d_{i+N_s/2} \exp(j2\pi(f_c - \frac{i+0.5}{T})(t-t_s)) \right\} \quad , t_s \le t \le t_s + T \tag{2.1}$$

$$s(t) = 0 \,, \quad t < t_s \ \wedge \ t > t_s + T$$

In the literature, often the equivalent complex baseband notation is used, which is given by (2.2). In this representation, the real and imaginary parts correspond to the in-phase and quadrature parts of the OFDM signal, which have to be multiplied by a cosine and sine of the desired carrier frequency to produce the final OFDM signal. Figure 2.1 shows the operation of the OFDM modulator in a block diagram.

$$s(t) = \sum_{i=-\frac{N_s}{2}}^{\frac{N_s}{2}-1} d_{i+N_s/2} \exp(j2\pi \frac{i}{T}(t-t_s)) \quad , t_s \le t \le t_s + T \tag{2.2}$$

$$s(t) = 0 \,, \quad t < t_s \ \wedge \ t > t_s + T$$

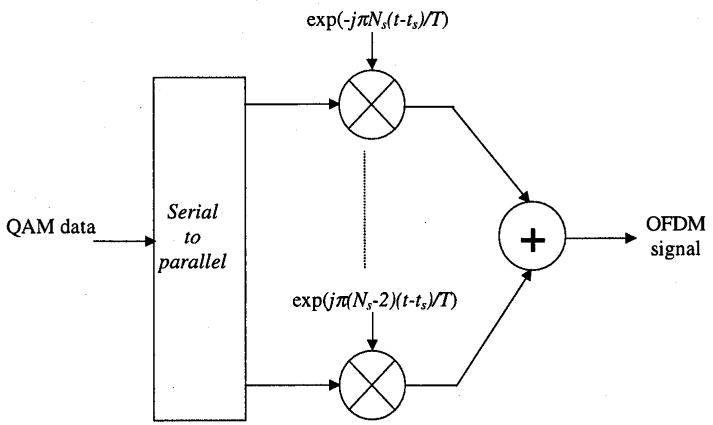

Figure 2.1 OFDM modulator.

As an example, Figure 2.2 shows four subcarriers from one OFDM signal. In this example, all subcarriers have the same phase and amplitude, but in practice the amplitudes and phases may be modulated differently for each subcarrier. Note that each subcarrier has exactly an integer number of cycles in the interval T, and the number of cycles between adjacent subcarriers differs by exactly one. This property accounts for

the orthogonality between the subcarriers. For instance, if the jth subcarrier from (2.2) is demodulated by downconverting the signal with a frequency of j/T and then integrating the signal over T seconds, the result is as written in (2.3). By looking at the intermediate result, it can be seen that a complex carrier is integrated over T seconds. For the demodulated subcarrier j, this integration gives the desired output $d_{j+N/2}$ (multiplied by a constant factor T), which is the QAM value for that particular subcarrier. For all other subcarriers, the integration is zero, because the frequency difference $(i\text{-}j)/T$ produces an integer number of cycles within the integration interval T, such that the integration result is always zero.

$$\int_{t_s}^{t_s+T} \exp(-j2\pi \frac{j}{T}(t-t_s)) \sum_{i=-\frac{N_s}{2}}^{\frac{N_s}{2}-1} d_{i+N_s/2} \exp(j2\pi \frac{i}{T}(t-t_s))\,\mathrm{dt}$$
$$= \sum_{i=-\frac{N_s}{2}}^{\frac{N_s}{2}-1} d_{i+N_s/2} \int_{t_s}^{t_s+T} \exp(j2\pi \frac{i-j}{T}(t-t_s))dt = d_{j+N_s/2}T \tag{2.3}$$

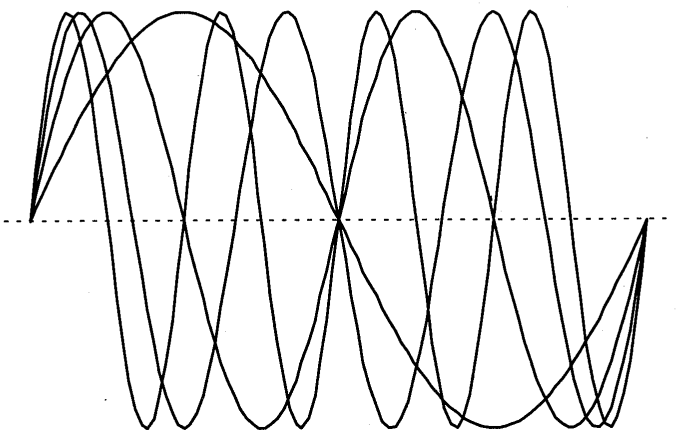

Figure 2.2 Example of four subcarriers within one OFDM symbol.

The orthogonality of the different OFDM subcarriers can also be demonstrated in another way. According to (2.1), each OFDM symbol contains subcarriers that are nonzero over a T-second interval. Hence, the spectrum of a single symbol is a convolution of a group of Dirac pulses located at the subcarrier frequencies with the spectrum of a square pulse that is one for a T-second period and zero otherwise. The amplitude spectrum of the square pulse is equal to $\mathrm{sinc}(\pi fT)$, which has zeros for all frequencies f that are an integer multiple of $1/T$. This effect is shown in Figure 2.2, which shows the overlapping sinc spectra of individual subcarriers. At the maximum of each subcarrier spectrum, all other subcarrier spectra are zero. Because an OFDM

receiver essentially calculates the spectrum values at those points that correspond to the maxima of individual subcarriers, it can demodulate each subcarrier free from any interference from the other subcarriers. Basically, Figure 2.3 shows that the OFDM spectrum fulfills Nyquist's criterium for an intersymbol interference free pulse shape. Notice that the pulse shape is present in the frequency domain and not in the time domain, for which the Nyquist criterium usually is applied. Therefore, instead of intersymbol interference (ISI), it is intercarrier interference (ICI) that is avoided by having the maximum of one subcarrier spectrum correspond to zero crossings of all the others.

The complex baseband OFDM signal as defined by (2.2) is in fact nothing more than the inverse Fourier transform of N_s QAM input symbols. The time discrete equivalent is the inverse discrete Fourier transform (IDFT), which is given by (2.4), where the time t is replaced by a sample number n. In practice, this transform can be implemented very efficiently by the inverse fast Fourier transform (IFFT). An N point IDFT requires a total of N^2 complex multiplications—which are actually only phase rotations. Of course, there are also additions necessary to do an IDFT, but since the hardware complexity of an adder is significantly lower than that of a multiplier or phase rotator, only the multiplications are used here for comparison. The IFFT drastically reduces the amount of calculations by exploiting the regularity of the operations in the IDFT. Using the radix-2 algorithm, an N-point IFFT requires only $(N/2)\cdot\log_2(N)$ complex multiplications [1]. For a 16-point transform, for instance, the difference is 256 multiplications for the IDFT versus 32 for the IFFT—a reduction by a factor of 8! This difference grows for larger numbers of subcarriers, as the IDFT complexity grows quadratically with N, while the IFFT complexity only grows slightly faster than linear.

$$s(n) = \sum_{i=0}^{N_s-1} d_i \exp(j2\pi \frac{in}{N}) \tag{2.4}$$

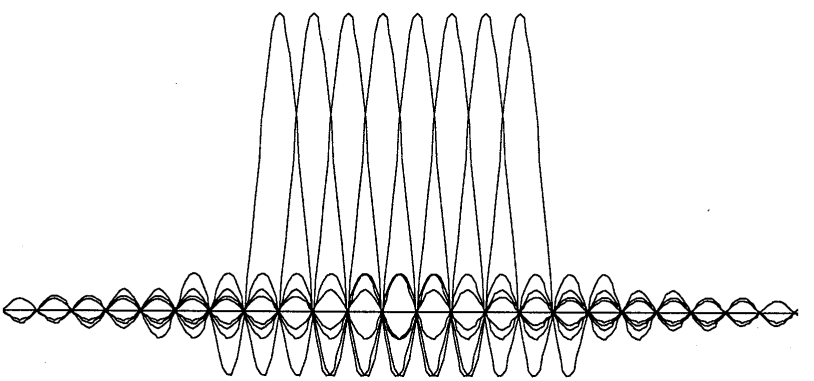

Figure 2.3 Spectra of individual subcarriers.

The number of multiplications in the IFFT can be reduced even further by using a radix-4 algorithm. This technique makes use of the fact that in a four-point IFFT, there are only multiplications by $\{1,-1,j,-j\}$, which actually do not need to be implemented by a full multiplier, but rather by a simple add or subtract and a switch of real and imaginary parts in the case of multiplications by j or $-j$. In the radix-4 algorithm, the transform is split into a number of these trivial four-point transforms, and non-trivial multiplications only have to be performed between stages of these four-point transforms. In this way, an N-point FFT using the radix-4 algorithm requires only $(3/8)N(\log_2 N-2)$ complex multiplications or phase rotations and $N\log_2 N$ complex additions [1]. For a 64-point FFT, for example, this means 96 rotations and 384 additions, or 1.5 and 6 rotations and additions per sample, respectively.

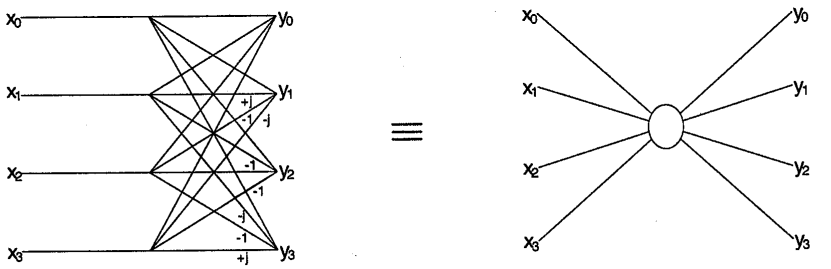

Figure 2.4 The radix-4 butterfly.

Figure 2.4 shows the four-point IFFT, which is known as the *radix-4 butterfly* that forms the basis for constructing larger IFFT sizes [1]. Four input values x_0 to x_3 are transformed into output values y_0 to y_3 by simple additions and trivial phase rotations. For instance, y_1 is given by $x_0 + jx_1 - x_2 - jx_3$, which can be calculated by doing four additions plus a few additional I/Q swappings and inversions to account for the multiplications by j and -1.

The radix-4 butterfly can be used to efficiently build an IFFT with a larger size. For instance, a 16-point IFFT is depicted in Figure 2.5. The 16-point IFFT contains two stages with four radix-4 butterflies, separated by an intermediate stage where the 16 intermediate results are phase rotated by the twiddle factor ω^i, which is defined as $exp(j2\pi i/N)$. Notice that for N=16, rotation by the twiddle factor ω^i reduces to a trivial operation for i=0, 4, 8 and 12, where ω^i is 1, j, -1 and $-j$, respectively. Taking this into account, the 16-point IFFT actually contains only eight non-trivial phase rotations, which is a factor of 32 smaller than the amount of phase rotations for the IDFT. These non-trivial phase rotations largely determine the implementation complexity, because the complexity of a phase rotation or complex multiplication is an order of magnitude larger than the complexity of an addition.

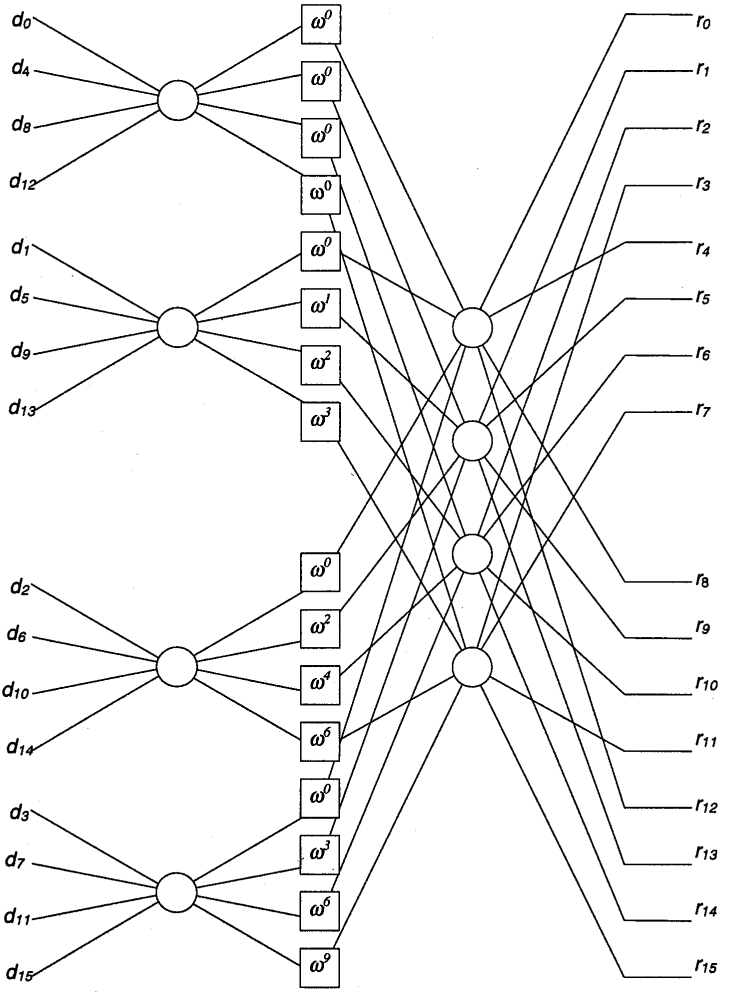

Figure 2.5 16-point IFFT using the radix-4 algorithm.

As an example of how to generate an OFDM symbol, let us assume that we want to transmit eight binary values {1 1 1 –1 1 1 –1 1} on eight subcarriers. The IDFT or IFFT then has to calculate:

$$\frac{1}{8}\begin{bmatrix} 1 & 1 & 1 & 1 & 1 & 1 & 1 & 1 \\ 1 & \frac{1}{2}\sqrt{2}(1+j) & j & \frac{1}{2}\sqrt{2}(-1+j) & -1 & \frac{1}{2}\sqrt{2}(-1-j) & -j & \frac{1}{2}\sqrt{2}(1-j) \\ 1 & j & -1 & -j & 1 & j & -1 & -j \\ 1 & \frac{1}{2}\sqrt{2}(-1+j) & -j & \frac{1}{2}\sqrt{2}(1+j) & -1 & \frac{1}{2}\sqrt{2}(1-j) & j & \frac{1}{2}\sqrt{2}(-1-j) \\ 1 & -1 & 1 & -1 & 1 & -1 & 1 & -1 \\ 1 & \frac{1}{2}\sqrt{2}(-1-j) & j & \frac{1}{2}\sqrt{2}(1-j) & -1 & \frac{1}{2}\sqrt{2}(1+j) & -j & \frac{1}{2}\sqrt{2}(-1+j) \\ 1 & -j & -1 & j & 1 & -j & -1 & j \\ 1 & \frac{1}{2}\sqrt{2}(1-j) & -j & \frac{1}{2}\sqrt{2}(-1-j) & -1 & \frac{1}{2}\sqrt{2}(-1+j) & j & \frac{1}{2}\sqrt{2}(1+j) \end{bmatrix} \begin{bmatrix} 1 \\ 1 \\ 1 \\ -1 \\ 1 \\ 1 \\ -1 \\ 1 \end{bmatrix} = \frac{1}{8}\begin{bmatrix} 4 \\ \sqrt{2}(1+j(\sqrt{2}-1)) \\ 2+2j \\ -\sqrt{2}(1+j(\sqrt{2}+1)) \\ 0 \\ -\sqrt{2}(1-j(\sqrt{2}+1)) \\ 2-2j \\ \sqrt{2}(1-j(\sqrt{2}-1)) \end{bmatrix} \tag{2.5}$$

The left-hand side of (2.5) contains the IDFT matrix, where every column corresponds to a complex subcarrier with a normalized frequency ranging from -4 to +3. The right-hand side of (2.5) gives the eight IFFT output samples that form one OFDM symbol. In practice, however, these samples are not enough to make a real OFDM signal. The reason is that there is no oversampling present, which would introduce intolerable aliasing if one would pass these samples though a digital-to-analog converter. To introduce oversampling, a number of zeros can be added to the input data. For instance, eight zeros could be added to the eight input samples of the previous example, after which a 16-point IFFT can be performed to get 16 output samples of a twice-oversampled OFDM signal. Notice that in the complex IFFT as in (2.5), the first half of the rows correspond to positive frequencies while the last half correspond to negative frequencies. Hence, if oversampling is used, the zeros should be added in the middle of the data vector rather than appending them at the end. This ensures the zero data values are mapped onto frequencies close to plus and minus half the sampling rate, while the nonzero data values are mapped onto the subcarriers around 0 Hz. For the data of the previous example, the oversampled input vector would become {1 1 1 –1 0 0 0 0 0 0 0 0 1 1 –1 1}.

2.3 GUARD TIME AND CYCLIC EXTENSION

One of the most important reasons to do OFDM is the efficient way it deals with multipath delay spread. By dividing the input datastream in N_s subcarriers, the symbol duration is made N_s times smaller, which also reduces the relative multipath delay spread, relative to the symbol time, by the same factor. To eliminate intersymbol interference almost completely, a guard time is introduced for each OFDM symbol. The guard time is chosen larger than the expected delay spread, such that multipath components from one symbol cannot interfere with the next symbol. The guard time could consist of no signal at all. In that case, however, the problem of intercarrier interference (ICI) would arise. ICI is crosstalk between different subcarriers, which means they are no longer orthogonal. This effect is illustrated in Figure 2.6. In this example, a subcarrier 1 and a delayed subcarrier 2 are shown. When an OFDM receiver

tries to demodulate the first subcarrier, it will encounter some interference from the second subcarrier, because within the FFT interval, there is no integer number of cycles difference between subcarrier 1 and 2. At the same time, there will be crosstalk from the first to the second subcarrier for the same reason.

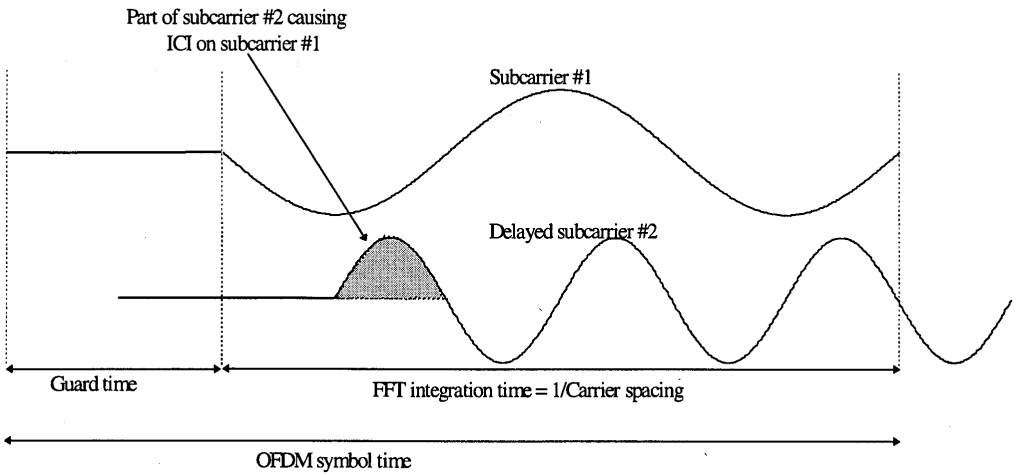

Figure 2.6 Effect of multipath with zero signal in the guard time; the delayed subcarrier 2 causes ICI on subcarrier 1 and vice versa.

To eliminate ICI, the OFDM symbol is cyclically extended in the guard time, as shown in Figure 2.7. This ensures that delayed replicas of the OFDM symbol always have an integer number of cycles within the FFT interval, as long as the delay is smaller than the guard time. As a result, multipath signals with delays smaller than the guard time cannot cause ICI.

As an example of how multipath affects OFDM, Figure 2.8 shows received signals for a two-ray channel, where the dotted curve is a delayed replica of the solid curve. Three separate subcarriers are shown during three symbol intervals. In reality, an OFDM receiver only sees the sum of all these signals, but showing the separate components makes it more clear what the effect of multipath is. From the figure, we can see that the OFDM subcarriers are BPSK modulated, which means that there can be 180-degree phase jumps at the symbol boundaries. For the dotted curve, these phase jumps occur at a certain delay after the first path. In this particular example, this multipath delay is smaller than the guard time, which means there are no phase transitions during the FFT interval. Hence, an OFDM receiver "sees" the sum of pure sine waves with some phase offsets. This summation does not destroy the orthogonality between the subcarriers, it only introduces a different phase shift for each subcarrier. The orthogonality does become lost if the multipath delay becomes larger than the

guard time. In that case, the phase transitions of the delayed path fall within the FFT interval of the receiver. The summation of the sine waves of the first path with the phase modulated waves of the delayed path no longer gives a set of orthogonal pure sine waves, resulting in a certain level of interference.

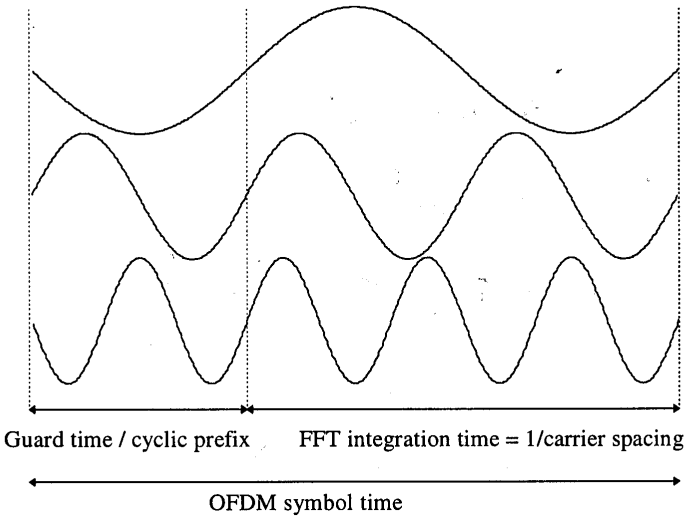

Figure 2.7 OFDM symbol with cyclic extension.

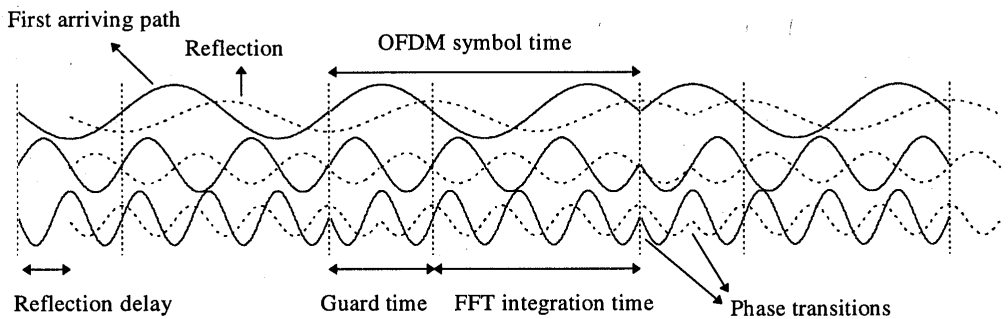

Figure 2.8 Example of an OFDM signal with three subcarriers in a two-ray multipath channel. The dashed line represents a delayed multipath component.

To get an idea what level of interference is introduced when the multipath delay exceeds the guard time, Figure 2.9 depicts three constellation diagrams that were derived from a simulation of an OFDM link with 48 subcarriers, each modulated by using 16-QAM. Figure 2.9(a) shows the undistorted 16-QAM constellation, which is observed whenever the multipath delay is below the guard time. In Figure 2.9(b), the multipath delay exceeds the guard time by a small 3% fraction of the FFT interval.

Hence, the subcarriers are not orthogonal anymore, but the interference is still small enough to get a reasonable received constellation. In Figure 2.9(c), the multipath delay exceeds the guard time by 10% of the FFT interval. The interference is now so large that the constellation is seriously blurred, causing an unacceptable error rate.

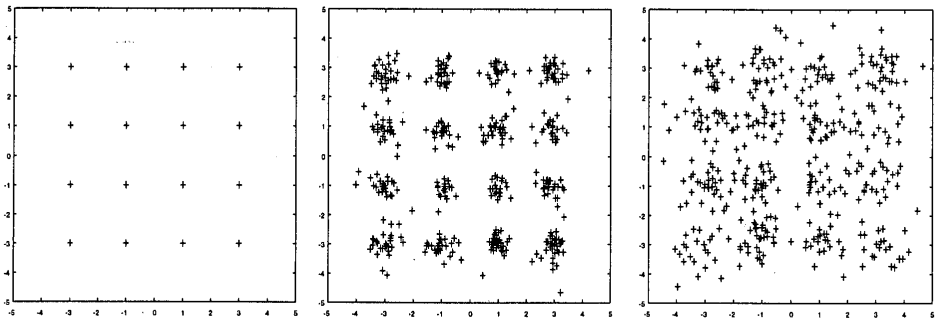

(a) (b) (c)

Figure 2.9 16-QAM constellation for a 48-subcarrier OFDM link with a two-ray multipath channel, the second ray being 6 dB lower than the first one. (a) delay < guard time; (b) delay exceeds guard time by 3% of the FFT interval; (c) delay exceeds guard time by 10% of the FFT interval.

2.4 WINDOWING

In the previous sections, it was explained how an OFDM symbol is formed by performing an IFFT and adding a cyclic extension. Looking at an example OFDM signal like in Figure 2.8, sharp phase transitions caused by the modulation can be seen at the symbol boundaries. Essentially, an OFDM signal like the one depicted in Figure 2.8 consists of a number of unfiltered QAM subcarriers. As a result, the out-of-band spectrum decreases rather slowly, according to a sinc function. As an example of this, the spectra for 16, 64, and 256 subcarriers are plotted in Figure 2.10. For larger number of subcarriers, the spectrum goes down more rapidly in the beginning, which is caused by the fact that the sidelobes are closer together. However, even the spectrum for 256 subcarriers has a relatively large –40-dB bandwidth that is almost four times the –3-dB bandwidth.

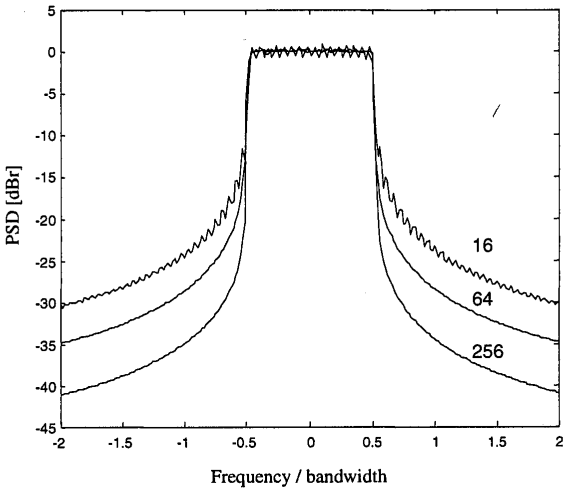

Figure 2.10 Power spectral density (PSD) without windowing for 16, 64, and 256 subcarriers.

To make the spectrum go down more rapidly, windowing can be applied to the individual OFDM symbols. Windowing an OFDM symbol makes the amplitude go smoothly to zero at the symbol boundaries. A commonly used window type is the raised cosine window, which is defined as

$$w(t)=\begin{cases} 0.5+0.5\cos(\pi+t\pi/(\beta T_s)) & 0 \le t \le \beta T_s \\ 1.0 & \beta T_s \le t \le T_s \\ 0.5+0.5\cos((t-T_s)\pi/(\beta T_s)) & T_s \le t \le (1+\beta)T_s \end{cases} \tag{2.6}$$

Here, T_s is the symbol interval, which is shorter than the total symbol duration because we allow adjacent symbols to partially overlap in the roll-off region. The time structure of the OFDM signal now looks like Figure 2.11.

In equation form, an OFDM symbol starting at time $t = t_s = kT_s$ is defined as

$$s_k(t)=\mathrm{Re}\left\{ w(t-t_s)\sum_{i=-\frac{N_s}{2}}^{\frac{N_s}{2}-1} d_{i+N_s(k+1/2)}\exp(j2\pi(f_c-\frac{i+0.5}{T})(t-t_s-T_{prefix}))\right\},\ t_s \le t \le t_s+T_s(1+\beta)$$

$$s_k(t)=0,\ t<t_s \wedge t>t_s+T_s(1+\beta) \tag{2.7}$$

In practice, the OFDM signal is generated as follows: first, N_c input QAM values are padded with zeros to get N input samples that are used to calculate an IFFT. Then, the last T_{prefix} samples of the IFFT output are inserted at the start of the OFDM symbol, and the first $T_{postfix}$ samples are appended at the end. The OFDM symbol is then multiplied by a raised cosine window $w(t)$ to more quickly reduce the power of out-of-band subcarriers. The OFDM symbol is then added to the output of the previous OFDM symbol with a delay of T_s, such that there is an overlap region of βT_s, where β is the rolloff factor of the raised cosine window.

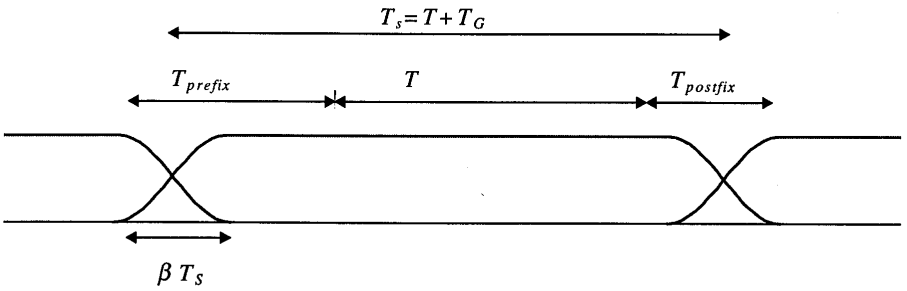

Figure 2.11 OFDM cyclic extension and windowing. T_s is the symbol time, T the FFT interval, T_G the guard time, T_{prefix} the preguard interval, $T_{postfix}$ the postguard interval, and β is the rolloff factor.

Figure 2.12 shows spectra for 64 subcarriers and different values of the rolloff factor β. It can be seen that a rolloff factor of 0.025—so the rolloff region is only 2.5% of the symbol interval—already makes a large improvement in the out-of-band spectrum. For instance, the –40-dB bandwidth is more than halved to about twice the –3-dB bandwidth. Larger rolloff factors improve the spectrum further, at the cost, however, of a decreased delay spread tolerance. The latter effect is demonstrated in Figure 2.13, which shows the signal structure of an OFDM signal for a two-ray multipath channel. The receiver demodulates the subcarriers by taking an FFT over the T-second interval between the dotted lines. Although the relative delay between the two multipath signals is smaller than the guard time, ICI and ISI are introduced because of the amplitude modulation in the gray part of the delayed OFDM symbol. The orthogonality between subcarriers as proved by (2.3) only holds when amplitude and phase of the subcarriers are constant during the entire T-second interval. Hence, a rolloff factor of β reduces the effective guard time by βT_s.

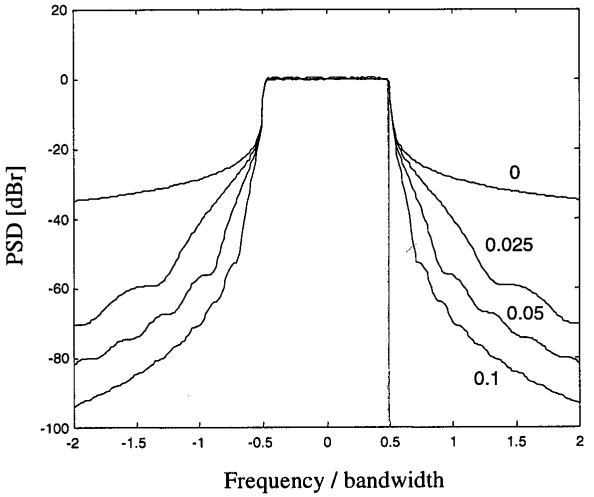

Figure 2.12 Spectra for raised cosine windowing with rolloff factors of 0 (rectangular window), 0.025, 0.05, and 0.1.

Instead of windowing, it is also possible to use conventional filtering techniques to reduce the out-of-band spectrum. Windowing and filtering are dual techniques; multiplying an OFDM symbol by a window means the spectrum is going to be a convolution of the spectrum of the window function with a set of impulses at the subcarrier frequencies. When filtering is applied, a convolution is done in the time domain and the OFDM spectrum is multiplied by the frequency response of the filter. When using filters, care has to be taken not to introduce rippling effects on the envelope of the OFDM symbols over a timespan that is larger than the rolloff region of the windowing approach. Too much rippling means the undistorted part of the OFDM envelope is smaller, and this directly translates into less delay spread tolerance. Notice that digital filtering techniques are more complex to implement than windowing. A digital filter requires at least a few multiplications per sample, while windowing only requires a few multiplications per symbol, for those samples which fall into the rolloff region. Hence, because only a few percent of the samples are in the rolloff region, windowing is an order of magnitude less complex than digital filtering.

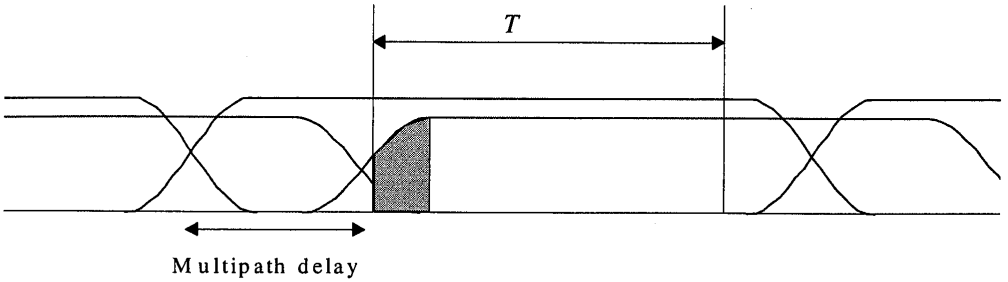

Figure 2.13 OFDM symbol windows for a two-ray multipath channel, showing ICI and ISI, because in the gray part, the amplitude of the delayed subcarriers is not constant.

2.5 CHOICE OF OFDM PARAMETERS

The choice of various OFDM parameters is a tradeoff between various, often conflicting requirements. Usually, there are three main requirements to start with: bandwidth, bit rate, and delay spread. The delay spread directly dictates the guard time. As a rule, the guard time should be about two to four times the root-mean-squared delay spread. This value depends on the type of coding and QAM modulation. Higher order QAM (like 64-QAM) is more sensitive to ICI and ISI than QPSK; while heavier coding obviously reduces the sensitivity to such interference.

Now that the guard time has been set, the symbol duration can be fixed. To minimize the signal-to-noise ratio (SNR) loss caused by the guard time, it is desirable to have the symbol duration much larger than the guard time. It cannot be arbitrarily large, however, because a larger symbol duration means more subcarriers with a smaller subcarrier spacing, a larger implementation complexity, and more sensitivity to phase noise and frequency offset [2], as well as an increased peak-to-average power ratio [3, 4]. Hence, a practical design choice is to make the symbol duration at least five times the guard time, which implies a 1-dB SNR loss because of the guard time.

After the symbol duration and guard time are fixed, the number of subcarriers follows directly as the required –3-dB bandwidth divided by the subcarrier spacing, which is the inverse of the symbol duration less the guard time. Alternatively, the number of subcarriers may be determined by the required bit rate divided by the bit rate per subcarrier. The bit rate per subcarrier is defined by the modulation type (e.g., 16-QAM), coding rate, and symbol rate.

As an example, suppose we want to design a system with the following requirements:

- Bit rate: 20 Mbps
- Tolerable delay spread: 200 ns
- Bandwidth: < 15 MHz

The delay-spread requirement of 200 ns suggests that 800 ns is a safe value for the guard time. By choosing the OFDM symbol duration 6 times the guard time (4.8 μs), the guard time loss is made smaller than 1 dB. The subcarrier spacing is now the inverse of 4.8 – 0.8 = 4 μs, which gives 250 kHz. To determine the number of subcarriers needed, we can look at the ratio of the required bit rate and the OFDM symbol rate. To achieve 20 Mbps, each OFDM symbol has to carry 96 bits of information (96/4.8 μs = 20 Mbps). To do this, there are several options. One is to use 16-QAM together with rate ½ coding to get 2 bits per symbol per subcarrier. In this case, 48 subcarriers are needed to get the required 96 bits per symbol. Another option is to use QPSK with rate ¾ coding, which gives 1.5 bits per symbol per subcarrier. In this case, 64 subcarriers are needed to reach the 96 bits per symbol. However, 64 subcarriers means a bandwidth of 64·250 kHz = 16 MHz, which is larger than the target bandwidth. To achieve a bandwidth smaller than 15 MHz, the number of subcarriers needs to be smaller than 60. Hence, the first option with 48 subcarriers and 16-QAM fulfills all the requirements. It has the additional advantage that an efficient 64-point radix-4 FFT/IFFT can be used, leaving 16 zero subcarriers to provide oversampling necessary to avoid aliasing.

An additional requirement that can affect the chosen parameters is the demand for an integer number of samples both within the FFT/IFFT interval and in the symbol interval. For instance, in the above example we want to have exactly 64 samples in the FFT/IFFT interval to preserve orthogonality among the subcarriers. This can be achieved by making the sampling rate 64/4 μs = 16 MHz. However, for that particular sampling rate, there is no integer number of samples with the symbol interval of 4.8 μs. The only solution to this problem is to change one of the parameters slightly to meet the integer constraint. For instance, the number of samples per symbol can be set to 78, which gives a sampling rate of 78/4.8 μs = 16.25 MHz. Now, the FFT interval becomes 64/16.25 MHz = 3.9385 μs, so both guard time and subcarrier spacing are slightly larger than in the case of the original FFT interval of 4 μs.

2.6 OFDM SIGNAL PROCESSING

The previous sections described how the basic OFDM signal is formed using the IFFT, adding a cyclic extension and performing windowing to get a steeper spectral rolloff. However, there is more to it to build a complete OFDM modem. Figure 2.14 shows the block diagram of an OFDM modem, where the upper path is the transmitter chain and the lower path corresponds to the receiver chain. In the center we see the IFFT, which modulates a block of input QAM values onto a number of subcarriers. In the receiver, the subcarriers are demodulated by an FFT, which performs the reverse operation of an IFFT. An interesting feature of the FFT/IFFT is that the FFT is almost identical to an IFFT. In fact, an IFFT can be made using an FFT by conjugating input and output of the FFT and dividing the output by the FFT size. This makes it possible to use the same hardware for both transmitter and receiver. Of course, this saving in complexity is only possible when the modem does not have to transmit and receive simultaneously.

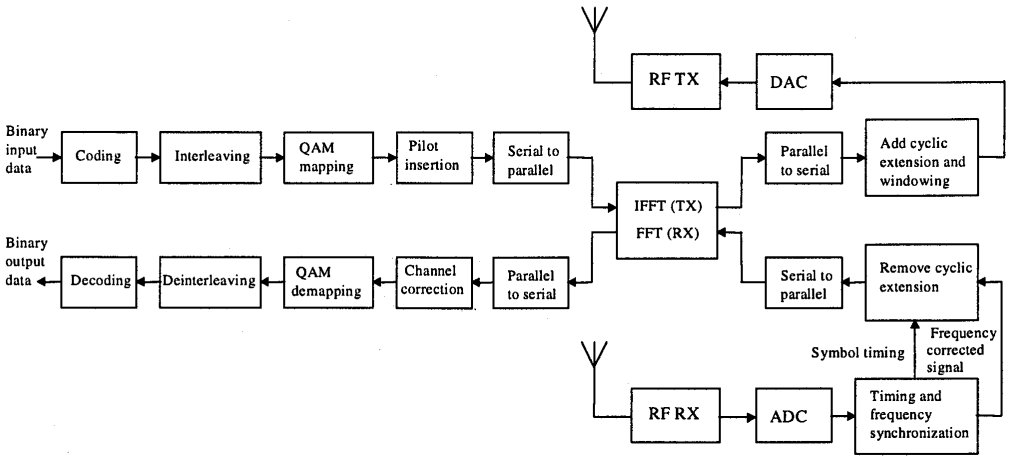

Figure 2.14 Block diagram of an OFDM transceiver.

The functions before the IFFT have not been discussed till now. Binary input data is first encoded by a forward error correction code. The encoded data is then interleaved and mapped onto QAM values. These functions are discussed in more detail in the next chapter.

In the receiver path, after passing the RF part and the analog-to-digital conversion, the digital signal processing starts with a training phase to determine symbol timing and frequency offset. An FFT is used to demodulate all subcarriers. The output of the FFT contains N_s QAM values, which are mapped onto binary values and decoded to produce binary output data. To successfully map the QAM values onto binary values, first the reference phases and amplitudes of all subcarriers have to be acquired. Alternatively, differential techniques can be applied. All of these receiver functions are highlighted in the following chapters.

2.7 IMPLEMENTATION COMPLEXITY OF OFDM VERSUS SINGLE-CARRIER MODULATION

One of the main reasons to use OFDM is its ability to deal with large delay spreads with a reasonable implementation complexity. In a single-carrier system, the implementation complexity is dominated by equalization, which is necessary when the delay spread is larger than about 10% of the symbol duration. OFDM does not require an equalizer. Instead, the complexity of an OFDM system is largely determined by the FFT, which is used to demodulate the various subcarriers. In the following example, it is demonstrated that the processing complexity of an OFDM modem can be significantly less than that of a single carrier modem, given the fact that both can deal with the same amount of delay spread. Notice that some papers mention the use of a

single-tap equalizer for OFDM, when they are referring to the phase correction in case of a coherent OFDM receiver. We will not use this somewhat confusing terminology, because the term equalization suggests that an attempt is made to invert the channel, while an OFDM receiver is doing the opposite; weak subcarriers are not being extra amplified to equalize the channel, but rather, they get a low weight in the decoding. In this way, OFDM avoids the problem of noise enhancement that is present in linear equalization techniques.

Figure 2.15 shows the block diagram of a decision feedback equalizer with symbol-spaced taps. Such an equalizer can be used to combat delay spread in single-carrier systems using quadrature amplitude modulation (QAM) or some form of constant amplitude modulation such as Gaussian Minimum Shift Keying (GMSK) or offset-QPSK. From references [5, 6], it can be learned that at least 8 feedforward and 8 feedback taps are required to handle a delay spread of 100 ns for a GMSK modem at a data rate of 24 Mbps. We can use this information to compare a single carrier system with the 24 Mbps mode of the new IEEE 802.11 OFDM standard, which can handle delay spreads up to 250 ns using a 64-point FFT. In order to increase the delay spread tolerance of a GMSK modem to the same level, the equalizer length has to be increased by a factor of 250/100, so it has 20 feedforward and feedback taps. Fortunately, for GMSK only the real outputs of the complex multiplications are used, so each multiplier has to perform two real multiplications per sample. Hence, the number of real multiplications per second becomes $2 \cdot 20 \cdot 24 \cdot 10^6 = 960 \cdot 10^6$. Notice we only count the feedforward taps here, since the feedback taps consist of trivial rotations, while the feedforward taps consist of full multiplications. For the OFDM system, a 64-point FFT has to be processed by every OFDM symbol duration which is 4 μs, see chapter 10. With a radix-4 algorithm, this requires 96 complex multiplications [1], which gives a processing load of $96 \cdot 10^6$ real multiplications per second. So, in terms of multiplications per second, the equalizer of the single carrier system is 10 times more complex than the FFT of the OFDM system! This complexity difference grows with the bit rate, or rather with the bandwidth – delay spread product, which is a measure of the relative amount of inter-symbol interference. For instance, if we want to double the bit rate in the previous example by doubling the bandwidth, but the delay spread tolerance has to stay the same, then the number of subcarriers and the guard time has to be doubled for OFDM, while for the single-carrier system, both the number of equalizer taps and the sampling rate are doubled. The latter means that the number of multiplications per second is quadrupled, so the equalizer complexity grows quadratically with the bandwidth – delay spread product. For OFDM, a double-sized FFT has to be calculated in the same amount of time in order to double the rate. For the radix-2 algorithm, this means an increase in the number of multiplications of $N\log_2(2N)/(N/2)\log_2 N = 2(1+1/\log_2 N)$, where N is the FFT size for the half-rate system. The complexity of the FFT grows only slightly faster than linear with the bandwidth – delay spread product, which explains why OFDM is more attractive than a single carrier system with equalization for relatively large bandwidth – delay spread products (values around 1 or larger). It should be noted that the complexity difference between the FFT and the equalizer is less if the equalization is done in the frequency domain, as

described in [7]. In this case, equalization is twice as complex, because both an FFT and an IFFT have to be performed to do frequency domain equalization on a signal block.

Another complexity advantage of OFDM is the fact that the FFT does not really require full multiplications, but rather phase rotations, which can be efficiently implemented by the CORDIC algorithm [8]. Because phase rotations do not change the amplitude, they do not increase the dynamic range of the signals, which simplifies the fixed point design.

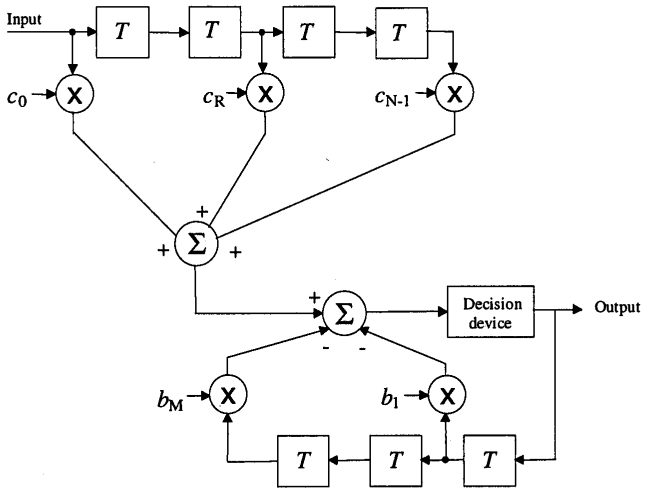

Figure 2.15 Decision-feedback equalizer.

Except for the difference in complexity, OFDM has another advantage over single carrier systems with equalizers. For the latter systems, the performance degrades abruptly if the delay spread exceeds the value for which the equalizer is designed. Because of error propagation, the raw bit error probability increases so quickly that inroducing lower rate coding or a lower constellation size does not significantly improve the delay spread robustness. For OFDM, however, there are no such nonlinear effects as error propagation, and coding and lower constellation sizes can be employed to provide fallback rates that are significantly more robust against delay spread. This is an important consideration, as it enhances the coverage area and avoids the situation that users in bad spots cannot get any connection at all.

REFERENCES

[1] Blahut, R. E., *Fast Algorithms for Digital Signal Processing*. Reading, MA: Addison-Wesley, 1985.

[2] Pollet, T., M. van Bladel and M. Moeneclaey, "BER Sensitivity of OFDM Systems to Carrier Frequency Offset and Wiener Phase Noise," *IEEE Trans. on Comm.*, Vol. 43, No. 2/3/4, pp. 191–193, Feb.–Apr. 1995.

[3] Pauli, M., and H. P. Kuchenbecker, "Minimization of the Intermodulation Distortion of a Nonlinearly Amplified OFDM Signal," *Wireless Personal Communications*, Vol. 4, No. 1, pp. 93–101, Jan. 1997.

[4] Rapp, C., "Effects of HPA-Nonlinearity on a 4-DPSK/OFDM Signal for a Digital Sound Broadcasting System," *Proc. of the Second European Conference on Satellite Communications*, Liège, Belgium, pp.179–184, Oct. 22–24, 1991.

[5] Tellado-Mourelo, J., E. K.Wesel, J. M.Cioffi, "Adaptive DFE for GMSK in Indoor Radio Channels," *IEEE Trans. on Sel. Areas in Comm.*, Vol. 14, No. 3, pp. 492–501, Apr. 1996.

[6] Wales, S. W., "Modulation and Equalization Techniques for HIPERLAN," *Proc. of PIMRC/WCN*, The Hague, The Netherlands, Sept. 21–23, pp. 959–963, 1994.

[7] Sari, H., G. Karam, I. Jeanclaude, "Transmission Techniques for Digital Terrestrial TV Broadcasting," *IEEE Communications Magazine*, Feb. 1995, pp. 100–109.

[8] Parhi, K. K., and T. Nishitani, *Digital Signal Processing for Multimedia Systems*. New York: Marcel Dekker, Inc., 1999.

Chapter 3

Coding and Modulation

3.1 INTRODUCTION

We explained in the previous chapter how OFDM avoids the problem of intersymbol interference by transmitting a number of narrowband subcarriers together with using a guard time. This does give rise to another problem, however, which is the fact that in a multipath fading channel, all subcarriers will arrive at the receiver with different amplitudes. In fact, some subcarriers may be completely lost because of deep fades. Hence, even though most subcarriers may be detected without errors, the overall bit-error ratio (BER) will be largely dominated by a few subcarriers with the smallest amplitudes, for which the bit-error probability is close to 0.5. To avoid this domination by the weakest subcarriers, forward-error correction coding is essential. By using coding across the subcarriers, errors of weak subcarriers can be corrected up to a certain limit that depends on the code and the channel. A powerful coding means that the performance of an OFDM link is determined by the average received power, rather than by the power of the weakest subcarrier.

This chapter starts with a review of block codes and convolutional codes. Then, it introduces interleaving as a way to randomize error bursts that occur when adjacent subcarriers are lost in a deep fade. Section 3.4 describes QAM as the most commonly used modulation technique in OFDM, after which Section 3.5 shows the important relation between coding and modulation. Thus, this chapter presents a brief overview of coding and modulation [1–9].

3.2 FORWARD-ERROR CORRECTION CODING

3.2.1 Block Codes

A *block code* encodes a block of k input symbols into n coded symbols, with n being larger than k. The purpose of adding the redundant n-k symbols is to increase the *minimum Hamming distance*, which is the minimum number of different symbols between any pair of code words. For a minimum Hamming distance of d_{min}, the code can correct t errors where t is given by

$$t \leq floor(\frac{d_{\min} - 1}{2}) \tag{3.1}$$

Here, *floor(x)* denotes the floor function that rounds x downward to the closest integer value. The minimum Hamming distance is upperbound by the number of redundant symbols n-k as

$$d_{\min} \leq n - k + 1 \tag{3.2}$$

For binary codes, only repetition codes and single-parity check codes reach this upperbound. A class of nonbinary codes that does reach the above bound are the *Reed-Solomon codes*. Because of their good distance properties and the availabity of efficient coding and decoding algorithms [6, 7], Reed-Solomon codes are the most popularly used block codes. Reed-Solomon codes are defined for blocks of symbols with m bits per symbol, where the code length n is related to m by

$$n = 2^m - 1 \tag{3.3}$$

The number of input symbols k is related to m and the required minimum Hamming distance d_{min} as

$$k = 2^m - d_{\min} \tag{3.4}$$

There appears to be little flexibility in the available code lengths as indicated by (3.3). However, a Reed-Solomon code can easily be shortened to any arbitrary length

by leaving a number of input bits zero and deleting the same amount of output bits. It is also possible to extend the code length to a power of 2 by adding an extra parity symbol.

According to (3.1) and (3.2), a Reed-Solomon code can correct up to floor((n-k)/2) erroneous symbols. Each symbol contains m bits, so a maximum amount of m·floor((n-k)/2) erroneous bits may be corrected. The latter is only true, however, if all bit errors occur within the maximum amount of correctable symbol errors. So if a Reed-Solomon is designed to correct up to two symbol errors containing 8 bits per symbol, it cannot correct an arbitrary combination of three bit errors, as these errors may occur in three different symbols. This characteristic makes Reed-Solomon codes particularly useful for correcting bursty channels. One example of such a channel is an OFDM link in the presence of multipath fading, which causes the errors to be concentrated in a few subcarriers that are hit by deep fades.

3.2.2 Convolutional Codes

A convolutional code maps each k bits of a continuous input stream on n output bits, where the mapping is performed by convolving the input bits with a binary impulse response. The convolutional encoding can be implemented by simple shift registers and modulo-2 adders. As an example, Figure 3.1 shows the encoder for a rate 1/2 code which is actually one of the most frequently applied convolutional codes. This encoder has a single data input and two outputs A_i and B_i, which are interleaved to form the coded output sequence $\{A_1B_1A_2B_2 \ldots\}$. Each pair of output bits $\{A_i,B_i\}$ depends on seven input bits, being the current input bit plus six previous input bits that are stored in the length 6 shift register. This value of 7—or in general the shift register length plus 1—is called the *constraint length.* The shift register taps are often specified by the corresponding generator polynomials or generator vectors. For the example of Figure 3.1, the generator vectors are {1011011,1111001} or {133,171} octal. The ones in the generator vectors correspond with taps on the shift register.

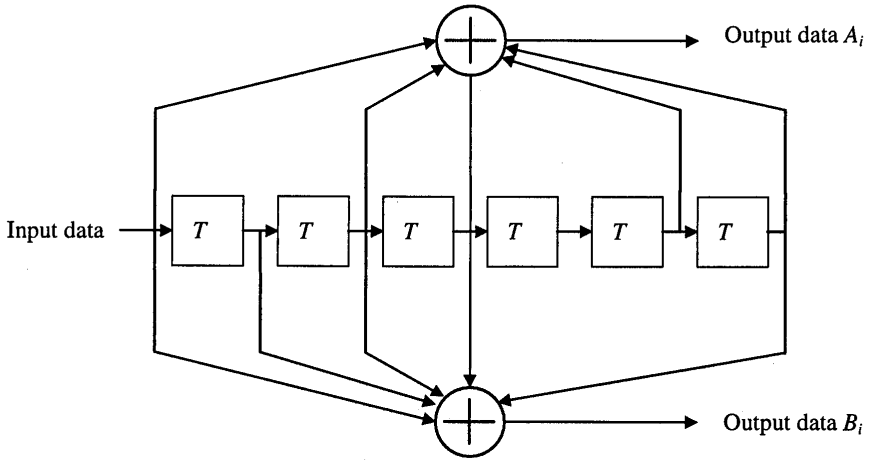

Figure 3.1 Block diagram of a constraint length 7 convolutional encoder.

Decoding of convolutional codes is most often performed by *soft decision Viterbi decoding*, which is an efficient way to obtain the optimal maximum likelihood estimate of the encoded sequence. A description of this decoding technique can be found in [8]. The complexity of Viterbi decoding grows exponentially with the constraint length. Hence, practical implementations do not go further than a constraint length of about 10. Decoding of convolutional codes with larger constraint length is possible by using suboptimal decoding techniques like sequential decoding [8].

Because convolutional codes do not have a fixed length, it is more difficult to specify their performance in terms of Hamming distance and a number of correctable errors. One measure that is used is the *free distance*, which is the minimum Hamming distance between arbitrarily long different code sequences that begin and end with the same state of the encoder, where the state is defined by the contents of the shift registers of the encoder. For example, the code of Figure 3.1 has a free distance of 10. When hard decision decoding is used, this code can correct up to floor((10-1)/2) = 4 bit errors within each group of encoded bits with a length of about 3 to 5 times the constraint length. When soft decision decoding is used, however, the number of correctable errors does not really give a useful measure anymore. A better performance measure is the *coding gain*, which is defined as the gain in the bit energy-to-noise density ratio E_b/N_o relative to an uncoded system to achieve a certain bit error ratio. The E_b/N_o gain is equivalent to the gain in input signal-to-noise ratio (SNR) minus the rate loss in dB because of the redundant bits. As an example, Figure 3.2 shows the bit error ratio versus E_b/N_o for uncoded QPSK and for coded QPSK using the previously mentioned constraint length 7 code. It can be seen from the figure that for a bit-error ratio of 10^{-4}, the coded link needs about 5 dB less E_b/N_o compared with that of the uncoded link. For lower bit error ratios, this coding gain converges to a maximum value of about 5.5 dB.

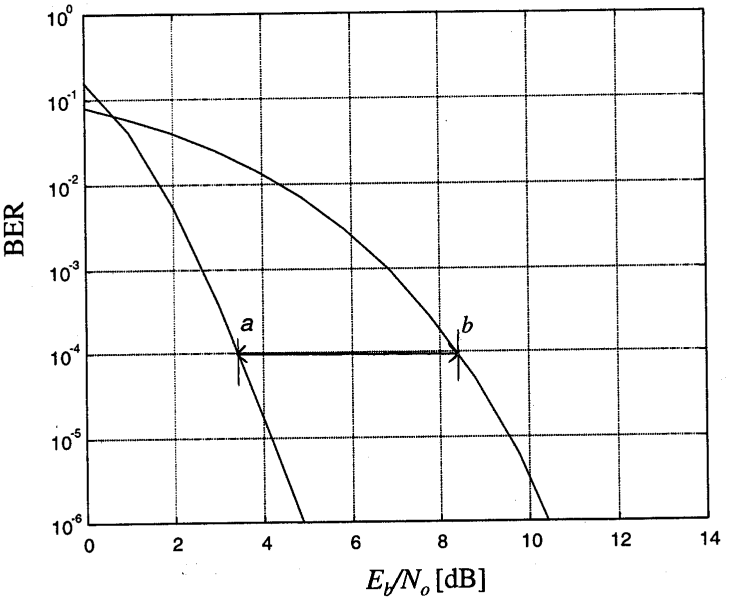

Figure 3.2 BER versus E_b/N_o for coded and uncoded QPSK in AWGN.

In the above curves, we have used the bit energy-to-noise density ratio E_b/N_o, which is equivalent to the ratio of the signal power P and the noise power in a bandwidth equal to the bit rate N_o/T_b, where T_b is the bit time. Some other useful SNR definitions are the input SNR and the symbol energy-to-noise density ratio E_s/N_o, which is equivalent to the ratio of the signal power and the noise power within a bandwidth equal to the symbol rate N_o/T_s, where T_s is the symbol duration. E_s/N_o is equivalent to the SNR for individual subcarriers, plus the guard time loss in dB. It is related to E_b/N_o as

$$\frac{E_s}{N_o} = \frac{E_b}{N_o}\frac{T_s}{T_b} \tag{3.5}$$

The input signal-to-noise ratio SNR_i is related to E_b/N_o as

$$SNR_i = \frac{E_b}{N_o}\frac{1}{BT_b} = \frac{E_b}{N_o}\frac{bN_s r}{BT_s} \tag{3.6}$$

Here, B is the input noise bandwidth, b is the number of coded bits per subcarrier, N_s the number of subcarriers, and r the coding rate. Basically, the SNR_i is equal to E_b/N_o multiplied by the ratio of bit rate and bandwidth. The latter ratio is equivalent to the spectral efficiency in bps/Hz. The spectral efficiency depends on the number of bits per subcarrier b, which is determined by the constellation size, the coding rate r, and the guard time, which appears indirectly in (3.6) as a part of the

symbol duration T_s. The number of subcarriers has no influence on the spectral efficiency, because the noise bandwidth increases linearly with the number of subcarriers.

A convolutional code can be punctured to increase the coding rate. For instance, increasing the rate of the above rate 1/2 code to 3/4 is done by deleting 2 of every 6 bits at the output of the encoder. The punctured output sequence for a rate 3/4 code is $\{A_1B_1A_2B_3A_4B_4A_5B_6A_7B_7 \ldots\}$. For a rate 2/3 code, the punctured output sequence is $\{A_1B_1A_2A_3B_3A_4A_5B_5 \ldots\}$. To decode the punctured sequence, the original rate 1/2 decoder can be used. Before decoding, erasures have to be inserted in the data at the locations of the punctured bits.

3.2.3 Concatenated Codes

Instead of using a single block code or convolutional code, it is also possible to combine or concatenate two codes. The main advantage of a concatenated code is that it can provide a large coding gain with less implementation complexity as a comparable single code. Figure 3.3 shows the block diagram of a concatenated coding scheme. The input bits are first coded and interleaved by an outer coder and interleaver. The coded bits are then again coded and interleaved by an inner coder and interleaver. Usually, the inner code is a convolutional code and the outer code a block code; for instance, a Reed-Solomon code. The motivation behind this is that the convolutional code with soft decision decoding performs better for relatively low-input SNRs. The hard decision block decoder then cleans up the relatively few remaining errors in the decoded output bits of the convolutional decoder. The task of the interleavers is to break up bursts of errors as much as possible. In case of an outer block code, the outer interleaver preferably separates symbols by more than the block length of the outer encoder. Compared with a single-code system, concatenated coding has more delay because of the extra interleaving, which can be a disadvantage for packet communications where the interleaving delay affects turnaround time and throughput. A good overview of achievable performance of concatenated coding is given in [3].

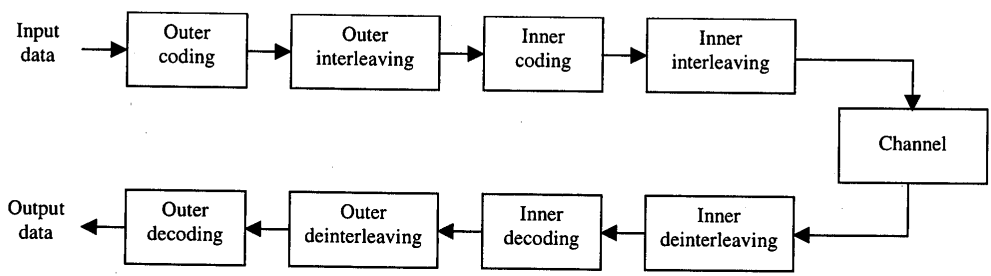

Figure 3.3 Concatenated coding/decoding.

3.3 INTERLEAVING

Because of the frequency selective fading of typical radio channels, the OFDM subcarriers generally have different amplitudes. Deep fades in the frequency spectrum may cause groups of subcarriers to be less reliable than others, thereby causing bit errors to occur in bursts rather than being randomly scattered. Most forward error-correction codes are not designed to deal with error bursts. Therefore, interleaving is applied to randomize the occurrence of bit errors prior to decoding. At the transmitter, the coded bits are permuted in a certain way, which makes sure that adjacent bits are separated by several bits after interleaving. At the receiver, the reverse permutation is performed before decoding. A commonly used interleaving scheme is the block interleaver, where input bits are written in a matrix column by column and read out row by row. As an example of such an interleaver, Figure 3.4 shows the bit numbers of a block interleaver operating on a block size of 48 bits. After writing the 48 bits in the matrix according to the order as depicted in the figure, the interleaved bits are read out row by row, so the output bit numbers are 0, 8, 16, 24, 32, 40, 1, 9, . . . , 47. Instead of bits, the operation can also be applied on symbols; for instance, the matrix can be filled with 48 16-QAM symbols containing 4 bits per symbol, so the interleaving changes the symbol order but not the bit order within each symbol. Interleaving on a symbol-basis is especially useful for Reed-Solomon codes, as these codes operate on symbols rather than bits. A Reed-Solomon code can correct up to a certain number of symbol errors per block length, so interleaving should be done over several block lengths, in order to spread bursts of symbol errors over a number of different Reed-Solomon blocks.

0	8	16	24	32	40
1	9	17	25	33	41
2	10	18	26	34	42
3	11	19	27	35	43
4	12	20	28	36	44
5	13	21	29	37	45
6	14	22	30	38	46
7	15	23	31	39	47

Figure 3.4 Interleaving scheme.

For a general block interleaver with a block size of N_B bits and d columns, the ith interleaved bit is equal to the kth encoded input bit, where k is given by

$$k = id - (N_B - 1)\,floor(\frac{id}{N_B}) \tag{3.7}$$

Instead of a block interleaver, it is also possible to use a convolutional interleaver. An example of this type of interleaver is shown in Figure 3.5. The interleaver cyclically writes each input symbol or bit into one of K shift registers that introduce a delay of 0 to k-1 symbol durations. The shift registers are read out cyclically to produce the interleaved symbols.

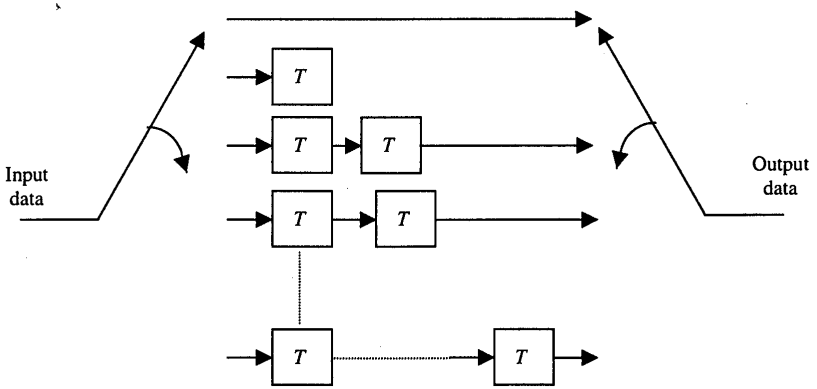

Figure 3.5 Convolutional interleaver.

3.4 QUADRATURE AMPLITUDE MODULATION

Quadrature amplitude modulation (QAM) is the most popular type of modulation in combination with OFDM. Especially rectangular constellations are easy to implement as they can be split into independent *Pulse amplitude modulated* (PAM) components for both the in-phase and the quadrature part. Figure 3.6 shows the rectangular constellations of Quadrature Phase Shift Keying (QPSK), 16-QAM, and 64-QAM. The constellations are not normalized; to normalize them to an average power of one—assuming that all constellation points are equally likely to occur—each constellation has to be multiplied by the normalization factor listed in Table 3.1. The table also mentions Binary Phase Shift Keying (BPSK), which uses two of the four QPSK constellation points (1+j, –1–j).

Table 3.1 also gives the loss in the minimum squared Euclidean distance between two constellation points, divided by the gain in data rate of that particular QAM type relative to BPSK. This value defines the maximum loss in E_b/N_o relative to BPSK that is needed to achieve a certain bit-error ratio in an uncoded QAM link. The BER curves in Figure 3.7 illustrate that the E_b/N_o loss values of Table 3.1 are quite accurate for BER values below 10^{-2}. The difference between QPSK and 16-QAM is about 4 dB. From 16-QAM to 64-QAM, almost 4.5 dB extra E_b/N_o is required. For larger constellation sizes, the E_b/N_o penalty of increasing the number of bits per symbol by 1 converges to 3 dB.

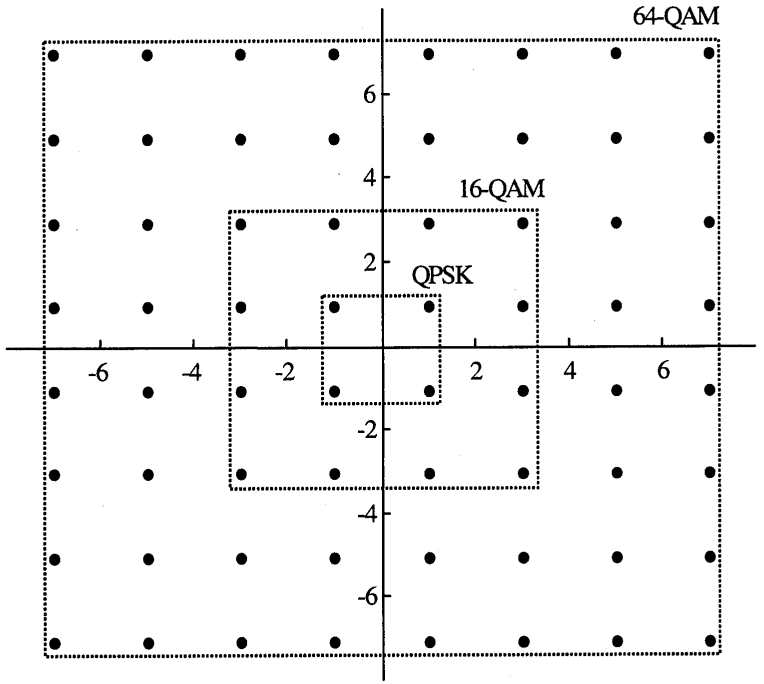

Figure 3.6 QPSK, 16-QAM, and 64-QAM constellations.

Table 3.1
QAM normalization factors and normalized Euclidean distance differences.

Modulation	**Normalization factor**	**Maximum E_b/N_o loss relative to BPSK in dB**
BPSK	$1/\sqrt{2}$	0
QPSK	$1/\sqrt{2}$	0
16-QAM	$1/\sqrt{10}$	3.98
64-QAM	$1/\sqrt{42}$	8.45

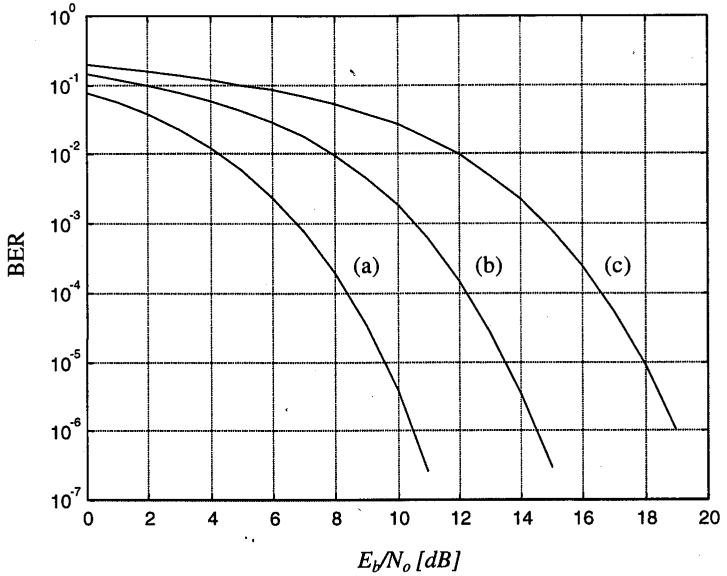

Figure 3.7 BER versus E_b/N_o for (a) BPSK/QPSK, (b) 16-QAM, (c) 64-QAM.

3.5 CODED MODULATION

When coding is applied to a QAM signal, it is important to consider the relation between coding and modulation to obtain the best result. In [9], Trellis coding was introduced as a way to attain coding gain without bandwidth expansion, meaning that all redundancy is obtained by increasing the constellation size. It was demonstrated in [9] that coding gains up to 6 dB can be obtained by going from uncoded QPSK to Trellis-coded 8-PSK using rate 2/3 coding. This technique is based on partitioning the PSK or QAM constellations into subsets with a high Euclidean distance within each subset. For instance, each 2 8-PSK constellation points with a relative phase difference of 180° define a subset with the same Euclidean distance as BPSK. The minimum Euclidean distance between different subsets is much smaller. Hence, coding is applied on the bits defining the subset number, such that the minimum Euclidean distance of the coded signal becomes equal to the distance within each subset.

A disadvantage of the above Trellis coding approach is that although the codes can have a large minimum Euclidean distance, the minimum Hamming distance is only 1, because bits within a subset are left uncoded. Hence, if one Trellis-coded symbol is lost, this immediately results in one or more bit errors. For OFDM this is a very undesirable property, as the data of several subcarriers may be lost by deep fades. This illustrates that the minimum Euclidean distance is not the only relevant parameter when selecting a good code for OFDM. For frequency selective channels, an additional criterion is that the Euclidean distance should be spread over as many symbols as possible, such that a few lost symbols have the smallest possible impact on the

probability of a decoding error [1]. As a consequence, in fading channels it is preferable to use high-order QAM constellations in combination with low-rate coding schemes. It is demonstrated in [1] that a specially designed rate 1/4 code with constraint length 7 together with a 16-QAM constellation can give good performance even on channels where more than half of the subcarriers are lost, with a degradation of less than 2 dB in the required signal-to-noise ratio relative to an ideal AWGN channel.

One of the disadvantages of special Trellis codes is that they are designed for specific constellations, such that you need a different encoder and decoder for different constellations. A practical approach to avoid this problem is to use standard binary codes together with Gray-encoded QAM. In [4], for instance, an efficient way is described to use a standard binary convolutional code together with 16-QAM. This scheme can easily be extended to an arbitrary rectangular QAM constellation. To do this, binary input data are converted into QAM symbols according to a Gray code mapping. For 16-QAM, for instance, the in-phase and quadrature parts are separately formed as 4 level PAM values, determined by two bits $b0$ and $b1$, as shown in Figure 3.8. The vertical lines indicate the regions for which the bit values are 1.

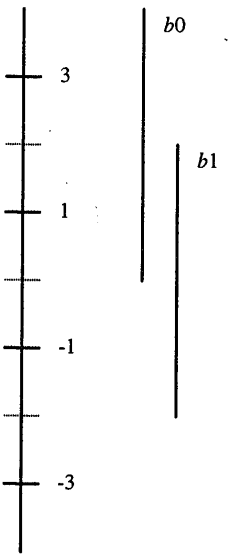

Figure 3.8 Gray mapping of two bits into 4 level PAM.

In the receiver, the incoming QAM symbols have to be demapped into one-dimensional values with corresponding metrics for the Viterbi decoder. For QPSK, the demapping is simply taking the in-phase and quadrature values as the two desired metrics. For the case of 16-QAM, the in-phase and quadrature values are treated as independent 4 level PAM signals, which are demapped into 2 metrics as shown in Figure 3.9. Here, the input values are normalized such that 2 corresponds to a decision

level, above which $b1$ is zero. The scale of the output values depends on the required quantization level of the Viterbi decoder, which typically ranges from 3 to 8 bits. Notice that the metric for b0 can be twice as large as for b1 in case the in-phase or quadrature value is –3 or +3. This indicates the fact that the b0 values are indeed more reliable in this case, as the minimum Euclidean distance from a +3 value to an erroneous $b0$ value of –1 is 4, while the minimum distance between two different $b1$ values is always 2. This difference in reliability of bits becomes even larger for higher order QAM. For instance, Figure 3.10 shows the demapping of 3-bit metrics for the case of 8 level PAM, which is used to make a 64-QAM constellation.

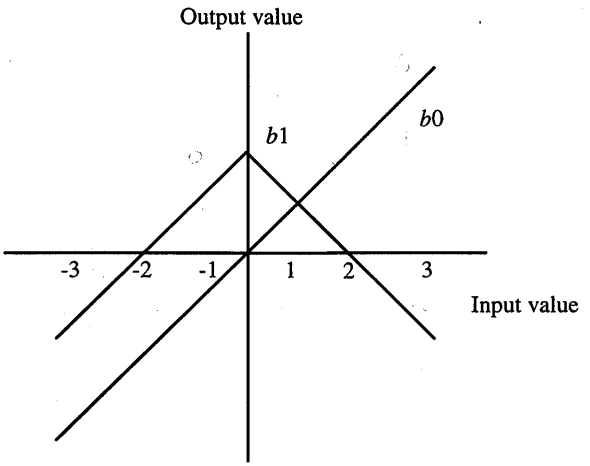

Figure 3.9 Demapping of 4 level PAM into 2 metrics.

Figure 3.11 shows the BERs versus E_b/N_o for several combinations of coding rates and QAM types in an AWGN channel. An interesting effect is that the coding gain relative to the uncoded QAM curves of Figure 3.7 becomes larger for larger QAM constellations. At a BER of 10^{-5}, for instance, the coding gains for a rate 1/2 code are approximately 5.5, 7, and 8.5 dB for QPSK, 16-QAM, and 64-QAM, respectively. This is explained by the fact that the uncoded error probability is determined mainly by the least significant bits in the Gray mapping; for instance, the b3 values in Figure 3.10. When coding is used, then the error probability depends on an average over several coded bits; for instance, several b1, b2, and b3 values in the case of 64-QAM. As a result of this averaging, the minimum squared Euclidean distance between different coded QAM sequences is larger than in the situation where only the least significant bits like b3 in Figure 3.10 are transmitted. Therefore, the coding gain is larger than in the case of QPSK or BPSK, where all bits have the same weight.

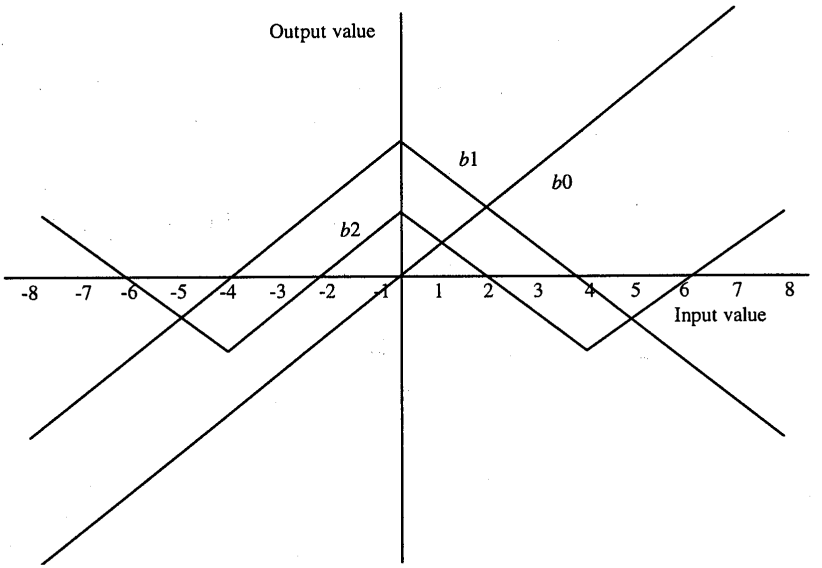

Figure 3.10 Demapping of 8 level PAM into 3 metrics.

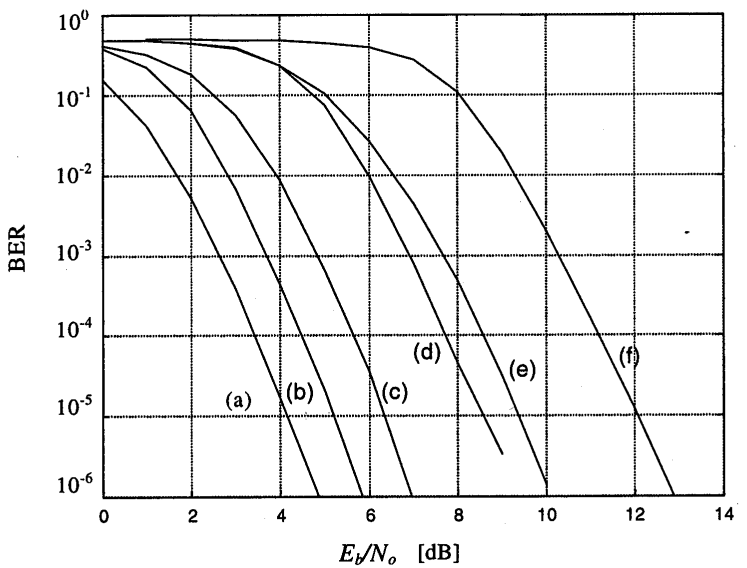

Figure 3.11 BERs versus E_b/N_o in AWGN for a constraint length 7 convolutional code with (a) QPSK, rate ½, (b) QPSK, rate ¾; (c) 16-QAM, rate ½; (d) 16-QAM, rate ¾; (e) 64-QAM, rate ½; (f) 64-QAM, rate ¾.

Other interesting information that can be derived from Figure 3.11 is the coding gain of a particular coded modulation type when compared with the uncoded QAM constellation that gives the same net data rate or the same efficiency in bps/Hz. For instance, the curve for 16-QAM with rate 1/2 coding can be compared with the curve for uncoded QPSK in Figure 3.7, as both have the same efficiency of 2 bps/Hz. It can be seen from the figures that for a BER of 10^{-5}, coded 16-QAM gives a coding gain of about 3 dB, compared with that of uncoded QPSK.

Figure 3.12 shows simulated BERs versus mean E_b/N_o for a Rayleigh fading channel with an exponentially decaying power delay profile. This channel was introduced in Chapter 1. Curves are drawn for various normalized delay spreads $\tau_{rms}N_s/T$, which is the rms delay spread as defined in Chapter 1 multiplied by the bandwidth of the OFDM signal. The normalized delay spread makes it possible to generalize delay spread results, independent of the number of subcarriers or the absolute bandwidth value of an OFDM system. It is required though that the number of subcarriers be significantly larger (a factor of 4 is sufficient) than the constraint length of the convolutional code, such that the code is able to fully benefit from the frequency diversity of the channel. The fact that the performance of an OFDM link depends only on the normalized delay spread $\tau_{rms}N_s/T$ can be understood better by realizing that the rms delay spread is approximately equal to the inverse of the coherence bandwidth of the channel, which determines the characteristics of bandwidth and spacing of fades in the channel frequency response. A small normalized delay spread is equivalent to a small ratio of OFDM signal bandwidth and coherence bandwidth. In such a situation, the channel frequency response is relatively flat within the OFDM signal bandwidth, so if there is a deep fade, all the subcarriers are significantly attenuated. In the case of a large normalized delay spread, a fade only affects a few adjacent subcarriers. There can be several fades within the OFDM signal bandwidth, with relatively strong subcarriers between the fades. As a result, the average signal power is much more constant over several channels than in the case of small delay spreads. The coding benefits from this by using the stronger subcarriers to compensate for the attenuated subcarriers.

Except for the delay spread, the guard time T_G is also normalized in Figure 3.12 and all other figures in this chapter. The normalized guard time is defined here as T_GN_s/T; the same normalization as for the guard time is applied to maintain a fixed ratio between delay spread and guard time, independent of the number of subcarriers N_s and the FFT interval T. Because the E_b/N_o loss caused by the guard time depends on the ratio T_G/T_s rather than the normalization chosen here, the guard time loss is not included in the following figures. This makes it possible to see from Figure 3.12 for what ratio of guard time and delay spread the system breaks down because of ISI and ICI. In Figure 3.12, for instance, an error floor is starting to appear for a normalized delay spread of 4; the ratio of guard time and delay spread is 3 for this case. Hence, for QPSK with rate 3/4 coding, the guard time should be at least three times the delay spread to achieve an average BER less than 10^{-4}.

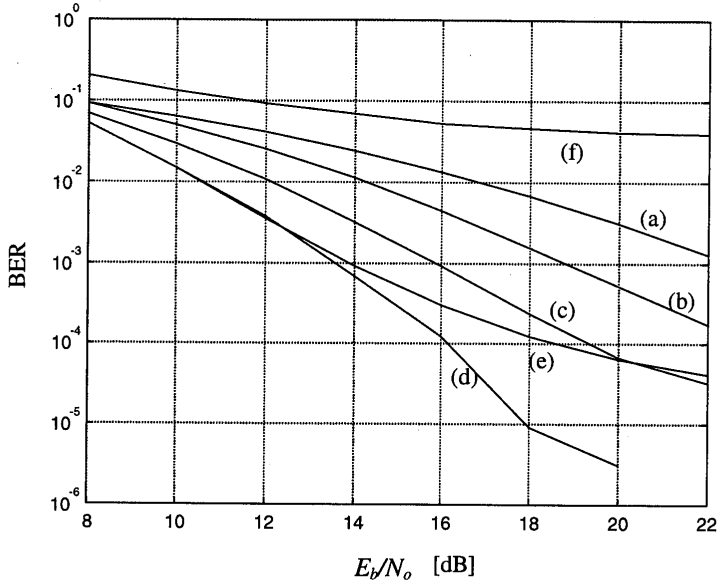

Figure 3.12 BERs versus mean E_b/N_o in a Rayleigh fading channel for QPSK, rate 3/4 convolutional coding, normalized guard time $T_G N_s/T = 12$, normalized delay spread $\tau_{rms} N_s/T$ = (a) 0.25, (b) 0.5, (c) 1, (d) 2, (e) 4, (f) 8.

Notice that Figure 3.12 uses the mean E_b/N_o, which is the average value over a large number of independent channels. The instantaneous E_b/N_o of an individual channel can be significantly smaller or larger than this mean value, especially for low delay spreads where the instantaneous signal power is determined by a single Rayleigh fading path. For larger delay spreads, the variation in the instantaneous signal power becomes much smaller because of the increased frequency diversity of the channel. Low instantaneous E_b/N_o values, which dominate the error ratio, occur much less frequently than at low delay spreads, hence the improved performance. The larger the delay spread, the smaller the E_b/N_o can be, until the delay spread becomes so large that ISI and ICI become limiting factors.

Figure 3.13 shows packet-error ratios (PERs) for 256-byte packets, simulated for the same conditions as Figure 3.12. For relatively slowly time-varying channels, as encountered for instance in indoor wireless LAN applications, the packet-error ratio averaged over a large number of fading channels is equivalent to the coverage outage probability, which is the probability of an unacceptably large packet-error ratio at a certain location within the coverage range. For instance, at an E_b/N_o value of 18 dB and a normalized delay spread between 0.5 and 4, a packet error ratio of 1% means that 1% of the channels generate most of the packet errors—caused by deep fades or ISI/ICI—while the remaining 99% of the channels have a much lower error ratio.

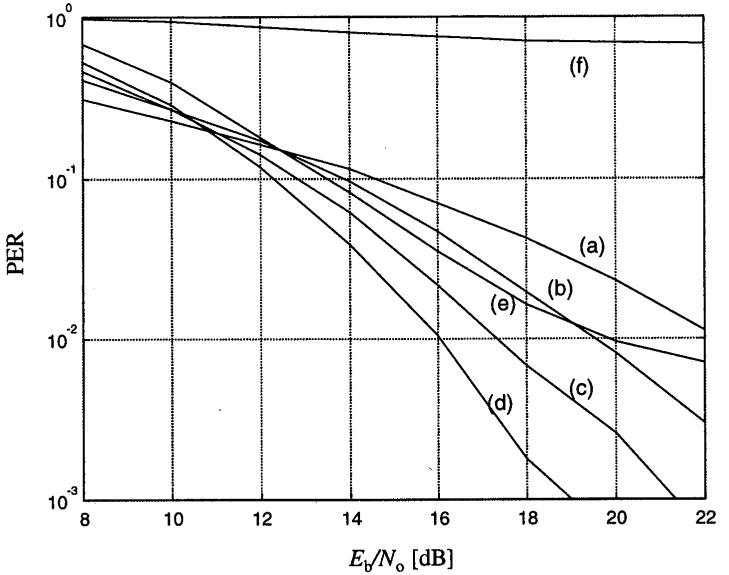

Figure 3.13 PERs versus mean E_b/N_o in a Rayleigh fading channel for QPSK, rate 3/4 convolutional coding, packet length = 256 bytes, normalized guard time $T_G N/T$ = 12, normalized delay spread $\tau_{rms} N_s/T$ = (a) 0.25, (b) 0.5, (c) 1, (d) 2, (e) 4, (f) 8.

Figure 3.14 shows simulated BERs and PERs for 256-byte packets in a Rayleigh fading channel with an exponentially decaying power delay profile. Two different combinations of coding rate and QAM type are used. Curves (a) and (c) are based on 16-QAM with rate 1/2 coding, giving a spectral efficiency of 2 bps/Hz, while curves (b) and (d) use QPSK with rate 3/4 coding, giving an efficiency of 1.5 bps/Hz. This example leads to the surprising result that in a fading channel, a higher order QAM system with a better spectral efficiency can be actually better in terms of E_b/N_o performance than a system with a lower spectral efficiency based on a lower order QAM, while the opposite is true in AWGN as demonstrated by Figure 3.11. The explanation for this effect is that in a frequency selective channel where a certain percentage of the subcarriers can be completely lost in deep fades, the ability to correct for those lost subcarriers by having a large Hamming distance is more important than a large minimum Euclidean distance for each individual subcarrier. In the example of Figure 3.11, the rate 1/2 code combined with 16-QAM can tolerate more weak subcarriers than the rate 3/4 code with QPSK, resulting in an E_b/N_o gain that is larger than the loss in Euclidean distance of 16-QAM versus QPSK.

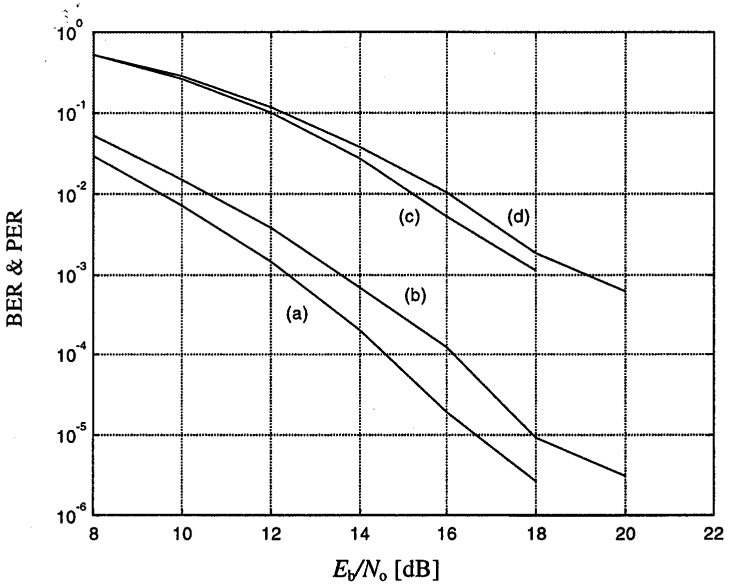

Figure 3.14 PER and BER versus mean E_b/N_0 in a Rayleigh fading channel for a packet length of 256 bytes and a normalized delay spread $\tau_{rms}N_s/T = 2$. (a) BER of 16-QAM, rate 1/2 coding; (b) BER of QPSK, rate 3/4 coding; (c) PER of 16-QAM, rate 1/2 coding; (d) PER of QPSK, rate 3/4 coding.

As mentioned before, when the delay spread increases, the performance of an OFDM link increases until a limit is reached where ISI and ICI cause an unacceptably high error floor. This error floor depends on the type of modulation and coding rate. Figure 3.15 illustrates this with simulation curves of the packet error floor versus the normalized delay spread τ_{rms}/T_G. No noise was present in the simulations, so all errors are purely caused by ISI and ICI. As expected, more delay spread can be tolerated for smaller QAM constellations. There is little difference, however, in the robustness of, for instance QPSK with rate 3/4 coding and 16-QAM with rate 1/2 coding, thanks to the fact that the latter is able to tolerate more erroneous subcarriers, which partly compensates the smaller distance between constellation points.

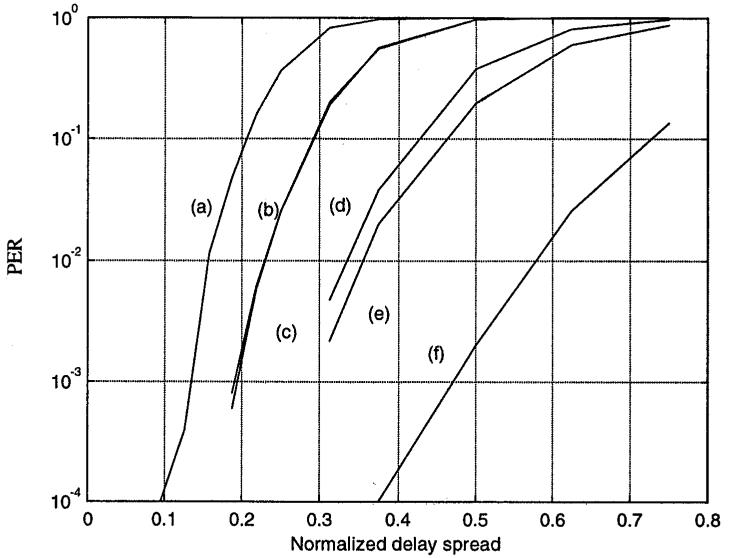

Figure 3.15 Irreducible packet error ratios versus normalized delay spread τ_{rms}/T_G for 256 byte packets and (a) 64-QAM, rate ¾; (b) 64-QAM, rate ½; (c) 16-QAM, rate ¾; (d) 16-QAM, rate ½; (e) QPSK, rate ¾; (f) QPSK, rate ½.

When an OFDM system has to be designed, Figure 3.15 can be used to derive a minimum requirement on the guard time, based on the maximum delay spread for which the system should work. For instance, for a tolerable packet-error floor of 1%, the guard time has to be about twice the delay spread for QPSK with rate 1/2 coding, but it has to be six times the delay spread for 64-QAM with rate 3/4 coding.

REFERENCES

[1] Wesel, R. D., "Joint Interleaver and Trellis Code Design," *Proceedings of IEEE Globecom*, 1997.

[2] Le Floch, B., M. Alard, and C. Berrou, "Coded Orthogonal Frequency Division Multiplex," *Proceedings of the IEEE*, Vol. 83, no. 6, June 1995.

[3] Alard, M., and R. Lasalle, "Principles of Modulation and Channel Coding for Digital Broadcasting for Mobile Receivers," *EBU Technical Review*, No. 224, pp. 168 - 190.

[4] Wang, Q., and L. Y. Onotera, "Coded QAM Using a Binary Convolutional Code," *IEEE Transactions on Communications*, Vol. 43, No. 6, June 1995.

[5] Wesel, R. D., and J. M. Cioffi, "Fundamentals of Coding for Broadcast OFDM," *Proceedings of IEEE ASILOMAR-29*, 1996.

[6] Massey, J. L., "Shift-Register Synthesis and BCH Decoding," *IEEE Transactions on Information Theory*, IT-15, pp. 122 - 127, Jan. 1979.

[7] Berlekamp, E. R., "The Technology of Error Correcting Codes," *Proceedings of the IEEE*, Vol.68, No.5, pp.564 – 593, May 1980.

[8] Charles Lee, L. H., "*Convolutional Coding: Fundamentals and Applications*," London: Artech House, 1997.

[9] Ungerboeck, G., "Channel Coding with Multilevel/Phase Signals," *IEEE Transactions on Information Theory*, Vol. IT-28, No.1, pp.55-67, Jan. 1982.

CHAPTER 4

Synchronization

Before an OFDM receiver can demodulate the subcarriers, it has to perform at least two synchronization tasks. First, it has to find out where the symbol boundaries are and what the optimal timing instants are to minimize the effects of intercarrier interference (ICI) and intersymbol interference (ISI). Second, it has to estimate and correct for the carrier frequency offset of the received signal, because any offset introduces ICI. In this chapter, we discuss the effects of timing and frequency offsets and describe several synchronization techniques that can be used to obtain symbol timing and frequency synchronization. Notice that these two synchronization tasks are not the only training required in an OFDM receiver. For coherent receivers, except for the frequency, the carrier phase also needs to be synchronized. Further, a coherent QAM receiver needs to learn the amplitudes and phases of all subcarriers to find out the decision boundaries for the QAM constellation of each subcarrier. The latter training tasks are described in the next chapter.

4.1 INTRODUCTION

In an OFDM link, the subcarriers are perfectly orthogonal only if transmitter and receiver use exactly the same frequencies. Any frequency offset immediately results in ICI. A related problem is phase noise; a practical oscillator does not produce a carrier at exactly one frequency, but rather a carrier that is phase modulated by random phase jitter. As a result, the frequency, which is the time derivative of the phase, is never perfectly constant, thereby causing ICI in an OFDM receiver. For single-carrier systems, phase noise and frequency offsets only give a degradation in the received signal-to-noise ratio (SNR), rather than introducing interference. This is the reason that the sensitivity to phase noise and frequency offset are often mentioned as disadvantages of OFDM relative to single-carrier systems. Although it is true that OFDM is more susceptible to phase noise and frequency offset than single-carrier systems, the following sections show that degradation can be kept to a minimum. They describe

techniques to achieve symbol timing and frequency synchronization by using the cyclic prefix or special OFDM training symbols. They also demonstrate that OFDM is rather insensitive to timing offsets, although such offsets do reduce the delay spread robustness. An optimal symbol timing technique is derived that maximizes the delay spread robustness.

4.2 SENSITIVITY TO PHASE NOISE

The issue of phase noise in OFDM systems has been the subject of many studies [1–5]. In [1], the power density spectrum of an oscillator signal with phase noise is modeled by a Lorentzian spectrum, which is equal to the squared magnitude of a first order lowpass filter transfer function. The single-sided spectrum $S_s(f)$ is given by

$$S_s(f) = \frac{2/\pi f_l}{1 + f^2 / f_l^2} \tag{4.1}$$

Here, f_l is the –3 dB linewidth of the oscillator signal. In practice, only double-sided spectra are measured, which are equal to mirrored versions of the one-sided spectrum around the carrier frequency f_c. Further, because the bandwidth is doubled, the spectrum is divided by 2 in order to keep the total power normalized to 1. Hence, the double-sided phase noise spectrum is given by

$$S_d(f) = \frac{1/\pi f_l}{1 + |f - f_c|^2 / f_l^2} \tag{4.2}$$

Figure 4.1 shows an example of a Lorentzian phase noise spectrum with a single-sided –3-dB linewidth of 1 Hz. The slope of –20 dB per decade of this model agrees with measurements in [3], which shows measured phase noise spectra for two oscillators at 5 and 54 GHz.

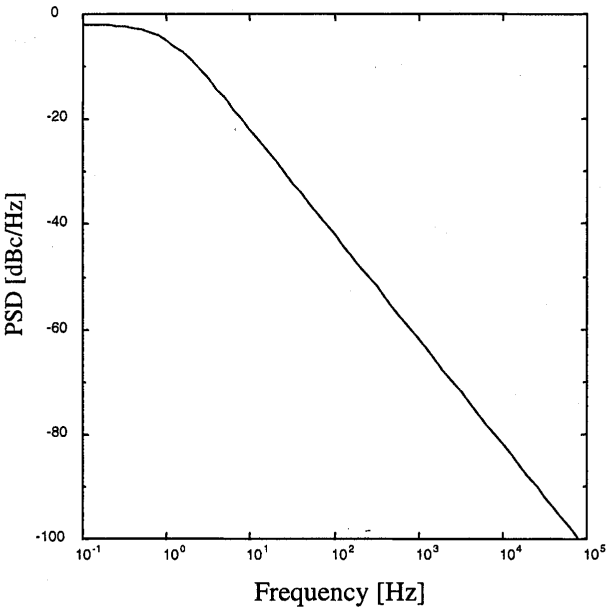

Figure 4.1 Phase noise power spectral density (PSD) with a single-sided –3-dB linewidth of 1 Hz and a –100 dBc/Hz density at 100 kHz offset.

Phase noise basically has two effects. First, it introduces a random phase variation that is common to all subcarriers. If the oscillator linewidth is much smaller than the OFDM symbol rate, which is usually the case, then the common phase error is strongly correlated from symbol to symbol, so tracking techniques or differential detection can be used to minimize the effects of this common phase error. The second and more disturbing effect of phase noise is that it introduces ICI, because the subcarriers are no longer spaced at exactly $1/T$ in the frequency domain. In [1], the amount of ICI is calculated and translated into a degradation in SNR that is given as

$$D_{phase} \cong \frac{11}{6\ln 10} 4\pi\beta T \frac{E_s}{N_o} \tag{4.3}$$

Here, β is the –3-dB one-sided bandwidth of the power density spectrum of the carrier. The phase noise degradation is proportional to βT, which is the ratio of the linewidth and subcarrier spacing $1/T$. Figure 4.2 shows the SNR degradation in dB as a function of the normalized linewidth βT. Curves are shown for three different E_s/N_o values, corresponding to the required values to obtain a bit-error ratio (BER) of 10^{-6} for uncoded QPSK, 16-QAM, and 64-QAM, respectively. The main conclusion that we can draw from this figure is that for a negligible SNR degradation of less than 0.1 dB, the –3-dB phase noise bandwidth has to be about 0.1 to 0.01 percent of the subcarrier spacing, depending on the modulation. For instance, to support 64-QAM in an OFDM link with a subcarrier spacing of 300 kHz, the –3-dB linewidth should be 30 Hz at

most. According to (4.2), this means that at a distance of 1 MHz from the carrier frequency, the phase noise spectral density has to have a value of approximately –110 dBc/Hz.

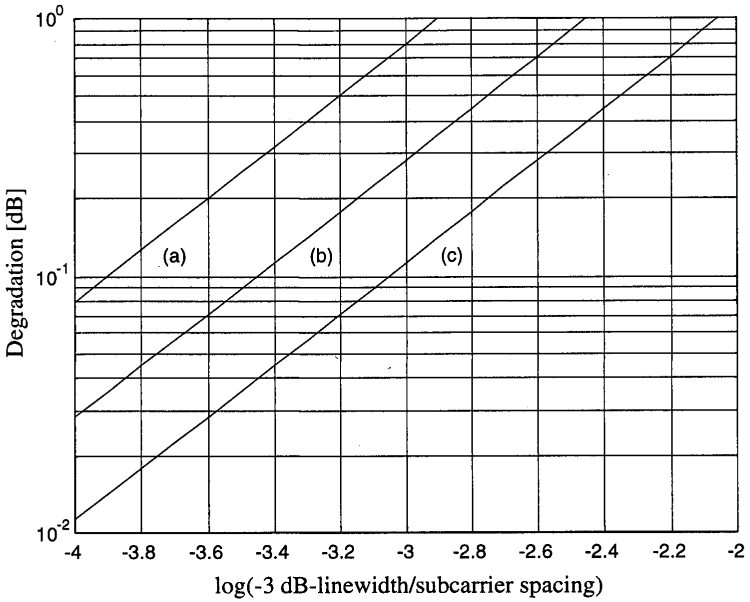

Figure 4.2 SNR degradation in dB versus the –3-dB bandwidth of the phase noise spectrum for (a) 64-QAM (E_s/N_o=19 dB), (b) 16-QAM (E_s/N_o=14.5 dB), (c) QPSK (E_s/N_o=10.5 dB).

The phase noise analysis in [1] assumed a free-running voltage-controlled oscillator (VCO). In practice, however, normally a phase-locked loop (PLL) is used to generate a carrier with a stable frequency. In a PLL, the frequency of a VCO is locked to a stable reference frequency, which is usually produced by a crystal oscillator. The PLL is able to track the phase jitter of the free-running VCO for jitter frequency components that fall within the *tracking loop bandwidth* of the loop. As a result, for frequencies below the tracking loop bandwidth the phase noise of the PLL output is determined mainly by the phase noise of the reference oscillator, which is usually smaller than the VCO phase noise, while for frequencies larger than the tracking loop bandwidth, the phase noise is dominated by the VCO phase noise. In this case, a typical phase noise spectrum will have a shape as depicted in Figure 4.3. The loop bandwidth of this example is around 100 Hz. For such phase noise spectra, the above analysis does not directly apply. We can, however, use the above results to get some requirements for a practical phase noise spectrum. For example, a heuristic approach is to require that the total power in the range of a minimum frequency offset of 10% of the subcarrier spacing to a maximum offset equal to the total bandwidth of the OFDM signal is equal to that of the Lorentzian model. For instance, suppose we have an OFDM system with a subcarrier spacing of 300 kHz and a bandwidth of 20 MHz. For the above-mentioned

example of a 30-Hz linewidth, the total power in the range of 30 kHz to 20 MHz is $(\pi/2)(\text{atan}(2\cdot10^6/30)-\text{atan}(3\cdot10^4/30)) \cong -32$ dBc. In fact, for this case, the exact value of the total bandwidth does not matter much, as the amount of phase noise power for frequency offsets larger than 20 MHz is negligible. The value of –32 dBc means that the total amount of phase noise for frequency offsets larger than 10% of the subcarrier spacing is less than 0.1% of the total carrier power. For a practical PLL, the phase noise spectrum can be measured and integrated over the same frequency interval to check whether the total phase noise power meets the requirement.

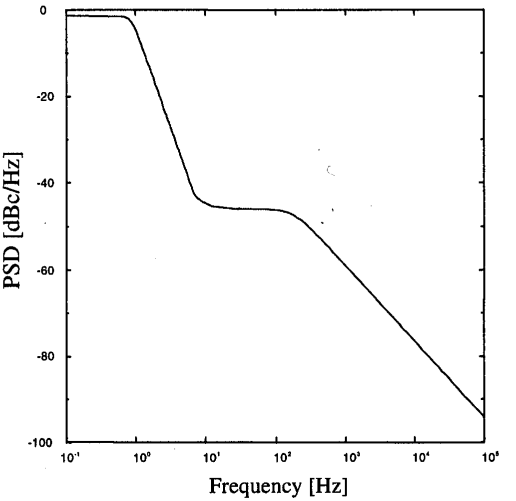

Figure 4.3 Example of a PLL phase noise spectrum.

4.3 SENSITIVITY TO FREQUENCY OFFSET

Chapter 2 explained that all OFDM subcarriers are orthogonal if they all have a different integer number of cycles within the FFT interval. If there is a frequency offset, then the number of cycles in the FFT interval is not an integer anymore, with the result that ICI occurs after the FFT. The FFT output for each subcarrier will contain interfering terms from all other subcarriers, with an interference power that is inversely proportional to the frequency spacing. The amount of ICI for subcarriers in the middle of the OFDM spectrum is approximately twice as large as that for subcarriers at the band edges, because the subcarriers in the middle have interfering subcarriers on both sides, so there are more interferers within a certain frequency distance. In [1], the degradation in SNR caused by a frequency offset that is small relative to the subcarrier spacing is approximated as

$$D_{freq} \cong \frac{10}{3\ln 10}(\pi \Delta f T)^2 \frac{E_s}{N_o} \tag{4.4}$$

This degradation is depicted in Figure 4.4 as a function of the frequency offset, normalized to the subcarrier spacing, and for three different E_s/N_o values. Note that for a negligible degradation of about 0.1 dB, the maximum tolerable frequency offset is less than 1% of the subcarrier spacing. For instance, for an OFDM system at a carrier frequency of 5 GHz and a subcarrier spacing of 300 kHz, the oscillator accuracy needs to be 3 kHz or 0.6 ppm. The initial frequency error of a low-cost oscillator will normally not meet this requirement, which means that a frequency synchronization technique has to be applied before the FFT. Examples of such synchronization techniques are described further in this chapter.

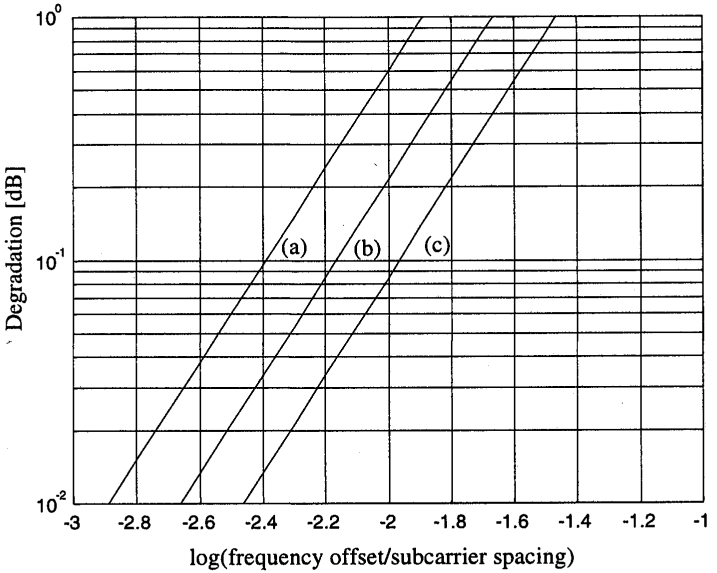

Figure 4.4 SNR degradation in dB versus the normalized frequency offset for (a) 64-QAM (E_s/N_o=19 dB), (b) 16-QAM (E_s/N_o=14.5 dB), (c) QPSK (E_s/N_o=10.5 dB).

4.4 SENSITIVITY TO TIMING ERRORS

The previous section explained that frequency offset and phase jitter introduce a certain amount of ICI. With respect to timing offsets, OFDM is relatively more robust; in fact, the symbol timing offset may vary over an interval equal to the guard time without causing ICI or ISI, as depicted in Figure 4.5. ICI and ISI occur only when the FFT interval extends over a symbol boundary or extends over the rolloff region of a symbol. Hence, OFDM demodulation is quite insensitive to timing offsets. To achieve the best possible multipath robustness, however, there exists an optimal timing instant as explained in Section 4.7. Any deviation from this timing instant means that the sensitivity to delay spread increases, so the system can handle less delay spread than

the value it was designed for. To minimize this loss of robustness, the system should be designed such that the timing error is small compared with the guard interval.

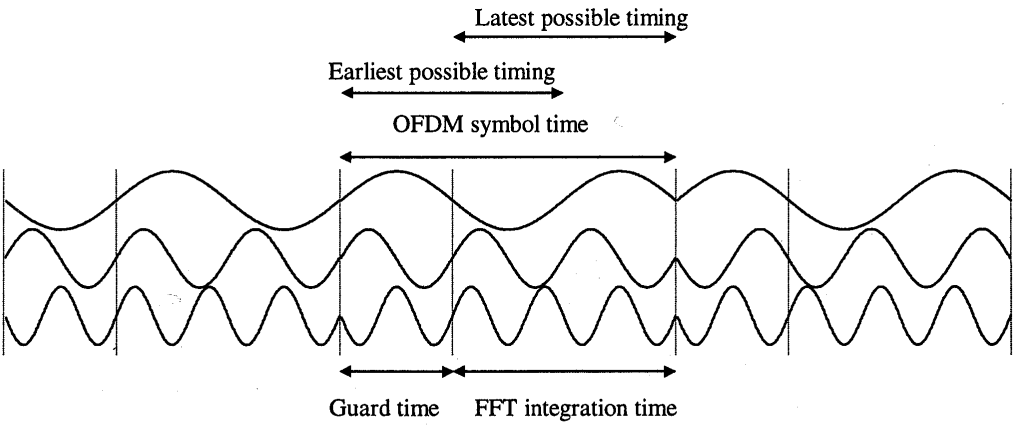

Figure 4.5 Example of an OFDM signal with three subcarriers, showing the earliest and latest possible symbol timing instants that do not cause ISI or ICI.

An interesting relationship exists between symbol timing and the demodulated subcarrier phases [6]. Looking at Figure 4.5, we can see that as the timing changes, the phases of the subcarriers change. The relation between the phase φ_i of subcarrier i and the timing offset τ is given by

$$\varphi_i = 2\pi f_i \tau \tag{4.5}$$

Here, f_i is the frequency of the ith subcarrier before sampling. For an OFDM system with N subcarriers and a subcarrier spacing of $1/T$, a timing delay of one sampling interval of T/N causes a significant phase shift of $2\pi(1\text{-}1/N)$ between the first and last subcarrier. These phase shifts add to any phase shifts that are already present because of multipath propagation. In a coherent OFDM receiver, channel estimation is performed to estimate these phase shifts for all subcarriers, which is described in the next chapter. Figure 4.6(a) shows an example of the QPSK constellation of a received OFDM signal with 48 subcarriers, an SNR of 30 dB, and a timing offset equal to 1/16 of the FFT interval. The timing offset translates into a phase offset of a multiple of $2\pi/16$ between the subcarriers. Because of this phase offset, the QPSK constellation points are rotated to 16 possible points on a circle. After estimation and correction of the phase rotations, the constellation diagram of Figure 4.6(b) is obtained. Chapter 5 describes methods to estimate the unknown phase rotations.

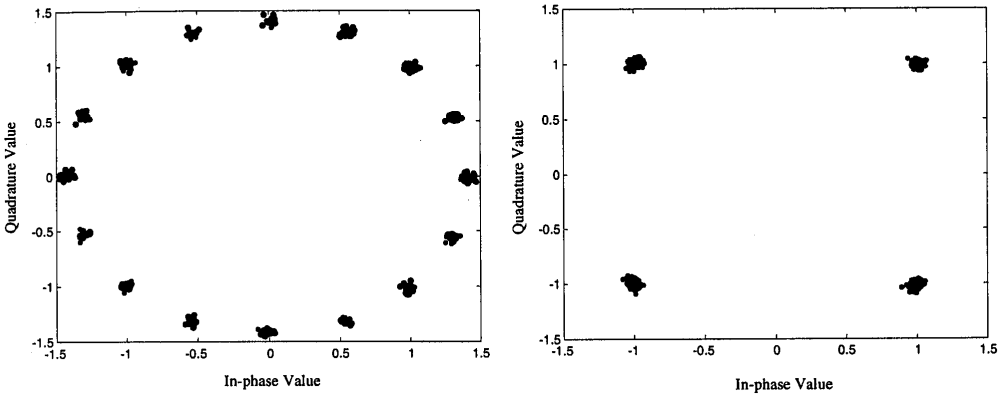

(a) (b)

Figure 4.6 Constellation diagram with a timing error of T/16 before (a) and after (b) phase correction.

In the above analysis, we implicitly assumed that there is an error only in the timing offset and not in the sampling frequency. An error in the sampling frequency has two effects [7]. First, it gives a time-varying timing offset, resulting in time-varying phase changes that have to be tracked by the receiver. Second, it causes ICI because an error in the sampling frequency means an error in the FFT interval duration, such that the sampled subcarriers are not orthogonal anymore. Fortunately, for practically achievable sampling offsets of 10 ppm, the amount of ICI is rather small, about 0.01 dB at an E_s/N_o of 20 dB, as shown in [7].

4.5 SYNCHRONIZATION USING THE CYCLIC EXTENSION

Because of the cyclic prefix, the first T_G seconds part of each OFDM symbol is identical to the last part. This property can be exploited for both timing and frequency synchronization by using a synchronization system like depicted in Figure 4.7. Basically, this device correlates a T_G long part of the signal with a part that is T seconds delayed [8, 9]. The correlator output can be written as

$$x(t) = \int_0^{T_G} r(t-\tau)r(t-\tau-T)d\tau \tag{4.6}$$

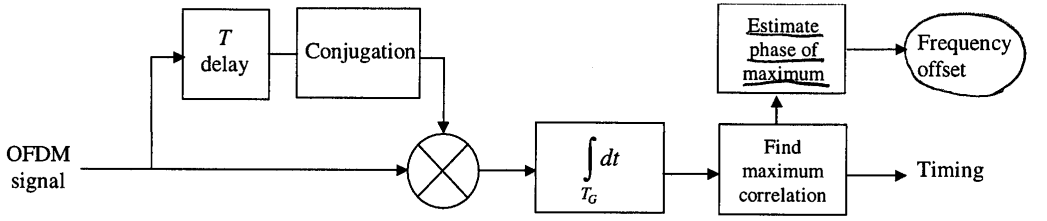

Figure 4.7 Synchronization using the cyclic prefix.

Two examples of the correlation output are shown in Figures 4.8 and 4.9 for eight OFDM symbols with 192 and 48 subcarriers, respectively. These figures illustrate a few interesting characteristics of the cyclic extension correlation method. First, both figures clearly show eight peaks for the eight different symbols, but the peak amplitudes show a significant variation. The reason for this is that although the average power for a T-seconds interval of each OFDM symbol is constant, the power in the guard time can substantially vary from this average power level. Another effect is the level of the undesired correlation sidelobes between the main correlation peaks. These sidelobes reflect the correlation between two pieces of the OFDM signal that belong partly or totally to two different OFDM symbols. Because different OFDM symbols contain independent data values, the correlation output is a random variable, which may reach a value that is larger than the desired correlation peak. The standard deviation of the random correlation magnitude is related to the number of independent samples over which the correlation is performed. The larger the number of independent samples, the smaller the standard deviation is. In the extreme case where the correlation is performed over only one sample, the output magnitude is proportional to the signal power, and there is no distinct correlation peak in this case. In the other extreme case where the correlation is performed over a very large number of samples, the ratio of sidelobes-to-peak amplitude will go to zero. Because the number of independent samples is proportional to the number of subcarriers, the cyclic extension correlation technique is only effective when a large number of subcarriers are used, preferably more than 100. An exception to this is the case where instead of random data symbols, specially designed training symbols are used [10]. In this case, the integration can be done over the entire symbol duration instead of the guard time only. The level of undesired correlation sidelobes can be minimized by a proper selection of the training symbols.

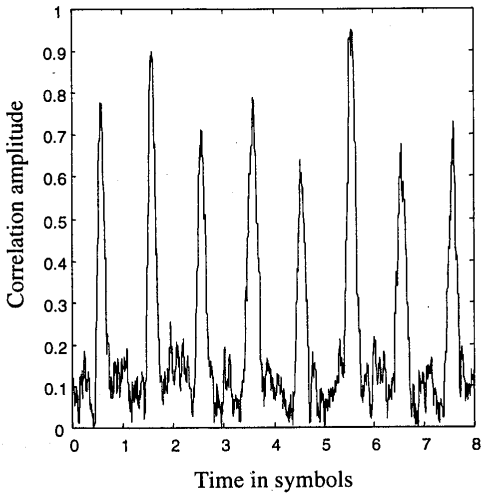

Figure 4.8 Example of correlation output amplitude for eight OFDM symbols with 192 subcarriers and a 20% guard time.

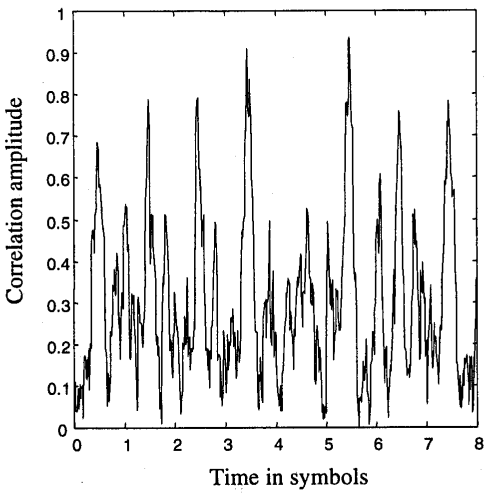

Figure 4.9 Example of correlation output amplitude for eight OFDM symbols with 48 subcarriers and a 20% guard time.

Notice that the undesired correlation sidelobes only create a problem for symbol timing. For frequency offset estimation, they do not play a role. Once symbol timing is known, the cyclic extension correlation output can be used to estimate the frequency offset. The phase of the correlation output is equal to the phase drift between samples that are T seconds apart. Hence, the frequency offset can simply be found as the correlation phase divided by $2\pi T$. This method works up to a maximum absolute

frequency offset of half the subcarrier spacing. To increase this maximum range, shorter symbols can be used, or special training symbols with different PN sequences on odd and even subcarrier frequencies to identify a frequency offset of an integer number of subcarrier spacings [13].

The noise performance of the frequency offset estimator is now determined for an input signal *r(t)* that consists of an OFDM signal *s(t)* with power *P* and additive Gaussian noise *n(t)* with a one-sided noise power spectral density of N_0 within the bandwidth of the OFDM signal:

$$r(t) = s(t) + n(t) \tag{4.7}$$

The frequency offset estimator multiplies the signal by a delayed and conjugated version of the input to produce an intermediate signal *y(t)* given by

$$y(t) = r(t)r^*(t-T) = \|s(t)\|^2 \exp(j\varphi) + n(t)s^*(t-T) + n^*(t-T)s(t) + n(t)n^*(t-T) \tag{4.8}$$

The first term in the right-hand side of (4.8) is the desired output component with a phase equal to the phase drift over a *T*-second interval and a power equal to the squared signal power. The next two terms are products of the signal and the Gaussian noise. Because the signal and noise are uncorrelated, and because noise samples separated by *T* seconds are uncorrelated, the power of the two terms is equal to twice the product of signal power and noise power. Finally, the power of the last term of (4.8) is equal to the squared noise power. If the input SNR is much larger than one, the power of the squared noise component becomes negligible compared with the power of the other two noise terms. For practical OFDM systems, the minimum input SNR is about 6 dB, so the signal power is four times the noise power. In this case, the power of the squared noise component is eight times smaller than the power of the two signal-noise product terms.

The frequency offset is estimated by averaging *y(t)* over an interval equal to the guard time T_G and then estimating the phase of *y(t)*. Because the desired output component of (4.8) is a constant vector, averaging reduces the noise that is added to this vector. Assuming that the squared noise component may be neglected, the output SNR is approximated as

$$SNR_o \cong \frac{P^2}{2PN_o / T_G} = \frac{PT_G}{2N_o} \tag{4.9}$$

Figure 4.10 shows a vector representation of the phase estimation, where the noise is divided into in-phase and quadrature components, both having a noise power of N_o/T_G.

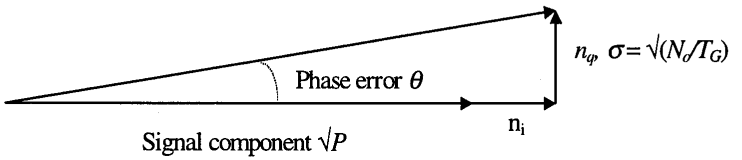

Figure 4.10 Vector representation of phase drift estimation.

The phase error θ is given by (4.10), where the approximation has been made that n_i and n_q are small compared with the signal amplitude $\sqrt{P}$.

$$\theta = \tan^{-1}\left(\frac{n_q}{\sqrt{P} + n_i}\right) \cong \frac{n_q}{\sqrt{P}} \tag{4.10}$$

Because the frequency offset estimation error is equal to the phase error θ divided by $2\pi T$, the standard deviation of the frequency error is given by

$$\sigma_f \cong \frac{1}{2\pi T}\sqrt{\frac{N_o}{PT_G}} = \frac{1}{2\pi T}\sqrt{\frac{1}{E_s / N_o}\frac{T_G}{T_s}} \tag{4.11}$$

Here, T_s is the symbol interval and E_s/N_o is the symbol-to-noise energy ratio, defined as

$$\frac{E_s}{N_o} = \frac{PT_s}{N_o} \tag{4.12}$$

E_s/N_o is equal to the bit energy-to-noise density E_b/N_o multiplied by the number of bits per symbol. Because OFDM typically has a large number of bits per symbol and E_b/N_o is larger than 1 for successful communications, typical E_s/N_o values are much larger than 1. For instance, with 48 subcarriers using 16-QAM and rate ½ coding, there are 96 bits per OFDM symbol. In this case, E_s/N_o is about 20 dB larger than E_b/N_o. So for typical E_b/N_o values around 10 dB, typical E_s/N_o values are around 30 dB.

Figure 4.11 shows the frequency estimation error versus E_s/N_o for three different T_G/T_s ratios. The frequency error is normalized to the subcarrier spacing $1/T$, so a value of 0.01 means 1% of the subcarrier spacing. The solid lines represent calculated values according to equation (4.11), while the dotted lines are derived from simulations. The difference between the two set of curves show the effect of the simplifications made in the derivation of (4.11). For E_s/N_o values of 30 dB or more, the difference is negligible, but around 20 dB, the simulated errors are about 50% larger than the calculated values.

Section 4.3 explained that the frequency error preferably had to be less than 1% of the subcarrier spacing to have a negligible performance degradation. From Figure 4.11, we can learn that such an error level can be achieved at an E_s/N_o value of 26, 31, and 34 dB for a T_G/T_s ratio of 1, 0.2, and 0.1, respectively. A lower T_G/T_s ratio means that a smaller fraction of an OFDM symbol is used for synchronization, hence more SNR is required to attain the same performance as for a larger T_G/T_s value.

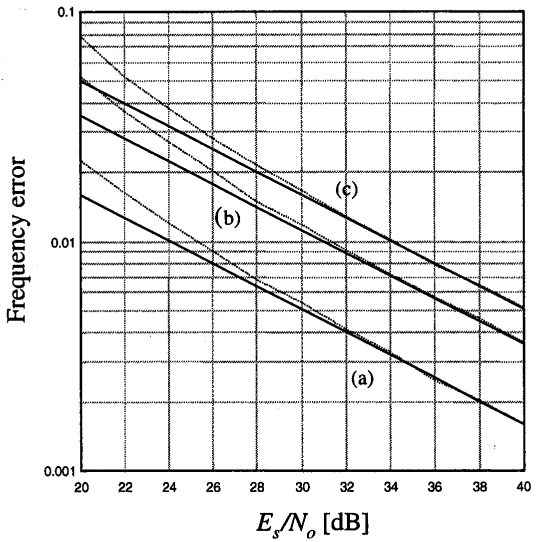

Figure 4.11 Frequency estimation error normalized to the subcarrier spacing. Solid lines are calculated; dotted lines are simulated. (a) T_G/T_s=1, (b) T_G/T_s=0.2, (c) T_G/T_s=0.1.

If the required E_s/N_o value for an acceptable frequency error level is too large, then averaging the vector $y(t)$ in (4.8) over multiple OFDM symbols can be used to increase the effective signal-to-noise ratio. For averaging over K symbols, the frequency error standard deviation becomes

$$\sigma_f \cong \frac{1}{2\pi T}\sqrt{\frac{1}{KE_s/N_o}\frac{T_G}{T_s}} \tag{4.13}$$

Averaging over K symbols has the effect that the curves of Figure 4.11 shift to the left by 10log$K$ dB. For instance, when averaging over four OFDM symbols, a 1% frequency error is achieved at an E_s/N_o value of 28 dB for a T_G/T_s ratio of 0.1 instead of 34 dB without averaging.

Notice that a T_G/T_s ratio of one – curve (*a*) in Figure 4.11 – is a special case where the guard time is equal to the symbol period. For normal OFDM data symbols, this is not possible, as it would mean that the FFT interval is zero. It does, however,

correspond to the interesting case where two identical OFDM symbols are used to estimate the frequency offset. In this case, all samples of a symbol can be used to estimate the phase difference with the corresponding samples of the other symbol. Hence, (4.11) applies with T_G/T_s set to 1, although T_G is not really a guard time in this case.

4.6 SYNCHRONIZATION USING SPECIAL TRAINING SYMBOLS

The synchronization technique based on the cyclic extension is particularly suited to tracking or to blind synchronization in a circuit-switched connection, where no special training signals are available. For packet transmission, however, there is a drawback because an accurate synchronization needs an averaging over a large (>10) number of OFDM symbols to attain a distinct correlation peak and a reasonable SNR. For high-rate packet transmission, the synchronization time needs to be as short as possible, preferably a few OFDM symbols only. To achieve this, special OFDM training symbols can be used for which the data content is known to the receiver [11-13]. In this way, the entire received training signal can be used to achieve synchronization, whereas the cyclic extension method only uses a fraction of each symbol.

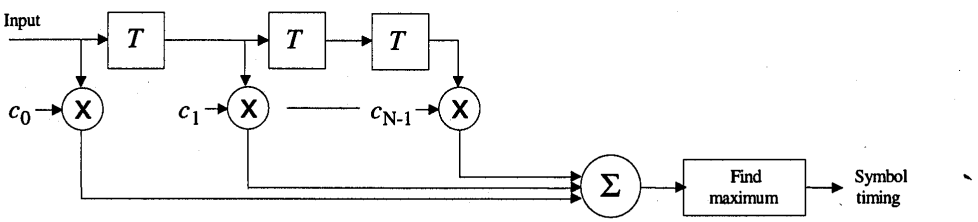

Figure 4.12 Matched filter that is matched to a special OFDM training symbol.

Figure 4.12 shows a block diagram of a matched filter that can be used to correlate the input signal with the known OFDM training signal. Here, T is the sampling interval and c_i are the matched filter coefficients, which are the complex conjugates of the known training signal. From the correlation peaks in the matched filter output signal, both symbol timing and frequency offset can be estimated, as will be explained in this section. Notice that the matched filter correlates with the OFDM time signal, *before* performing an FFT in the receiver. Hence, this technique is very similar to synchronization in a direct-sequence spread-spectrum receiver, where the input signal is correlated with a known spreading signal. In fact, the latter approach of using a single-carrier training signal can also be combined with OFDM, as proposed in [14], but here we will assume that the training signal consists of normal OFDM data symbols.

Figure 4.13 shows an example of the matched filter output for an OFDM training symbol with 48 subcarriers. The training signal for this case consisted of five

identical OFDM symbols without a guard time. Alternatively, it could be stated that there is only one OFDM symbol with a guard time equal to four IFFT intervals, because the IFFT output is repeated four times. The reason for having the training symbol interval equal to the IFFT interval is that this gives the best possible cyclic autocorrelation properties in terms of low undesired sidelobes. This can be seen in Figure 4.13(a), which shows the undesired sidelobes to be at least 20 dB lower than the main correlation peaks. An exception to this occurs at the beginning of the correlation. The reason for this is that at this point, an aperiodic correlation is performed instead of a cyclic correlation, because the matched filter is partly filled with zero values until a full OFDM symbol has been received. A similar effect happens at the end of the training—not shown in the picture—when the matched filter will partly correlate with samples from the following OFDM data symbol that is different from the training symbol. Hence, to avoid undesired partial correlations, the matched filter outputs during the first and last symbol intervals should be skipped. The values in between can be used to detect the main correlation peak, which gives the desired symbol timing information.

The correlation function of Figure 4.13(a) was made for the case of a zero fractional timing offset between the input signal and the known training signal. This means that the matched filter tap values, which are equal to the conjugated training signal samples, are exactly equal to the conjugated sample values of the incoming OFDM signal. This ideal situation does not occur when there is a timing offset of some fraction of a sample interval between the input signal and the known training signal. To see the effect of a fractional timing offset, Figure 4.13(b) shows the correlation output for the worst case timing offset of half a sampling interval. In this case, instead of one main peak per symbol interval, there are two equally strong peaks with a slightly smaller amplitude than the single peak in the case of no timing offset. However, the relative level of undesired correlation sidelobes is still 20 dB below the main peaks.

The plots of Figure 4.13 assumed unquantized input signals and tap values. In practice, it is desirable to have a low number of quantization bits to keep the implementation simple. Figure 4.14 shows the correlation output where the matched filter tap values are quantized to {-1, 0, 1} values for both the real and imaginary parts. This reduces the complexity of the multiplications in the matched filter to additions, having a relatively low hardware complexity. As we can see from Figure 4.14, the correlation output looks different from the unquantized case in Figure 4.13, but the undesired sidelobe level is still about 20 dB below the main peak. Such good correlation properties cannot be achieved with any arbitrary quantized OFDM signal. To minimize the effects of the quantization, the best results are obtained with OFDM signals that have minimum amplitude fluctuations. In the case of Figure 4.14, the OFDM symbol consists of the IFFT of a length 48 complementary code, which results in a signal with peak amplitude fluctuations that are no more than 3 dB larger than the root mean square value. More details about these complementary codes can be found in Chapter 6, which deals with the OFDM peak-to-average power issue.

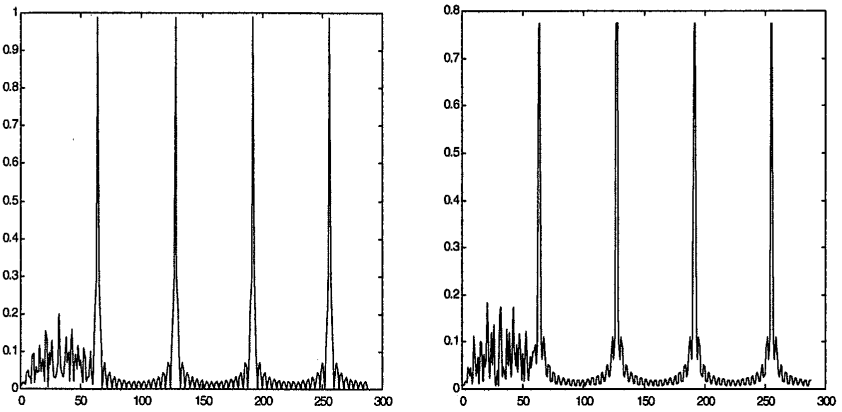

Figure 4.13 Matched filter output versus sample number for 4 training symbols, using 48 subcarriers and 64 samples per symbol. (a) Zero fractional timing offset between input signals and matched filter coefficients, (b) worst case fractional offset of half a sample between input signal and reference pulse.

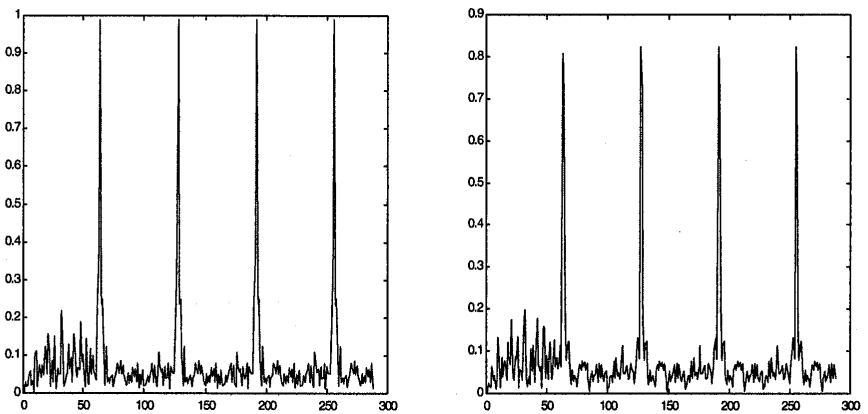

Figure 4.14 Matched filter output versus sample number with {1,–1,0} values for in-phase and quadrature coefficients. (a) Zero fractional timing offset between input signals and matched filter coefficients, (b) worst case fractional offset of half a sample between input signal and reference pulse.

4.7 OPTIMAL TIMING IN THE PRESENCE OF MULTIPATH

The task of OFDM symbol timing is to minimize the amount of ISI and ICI. This type of interference is absent when the FFT is taken over the flat part of the signaling

window, which is shown in Figure 4.15. This window is the envelope of the transmitted OFDM symbols. Within the flat part of the window, all subchannels maintain perfect orthogonality. In the presence of multipath, however, orthogonality is lost if the multipath delays exceed the effective guard time, which is equal to the duration of the flat window part minus the FFT period.

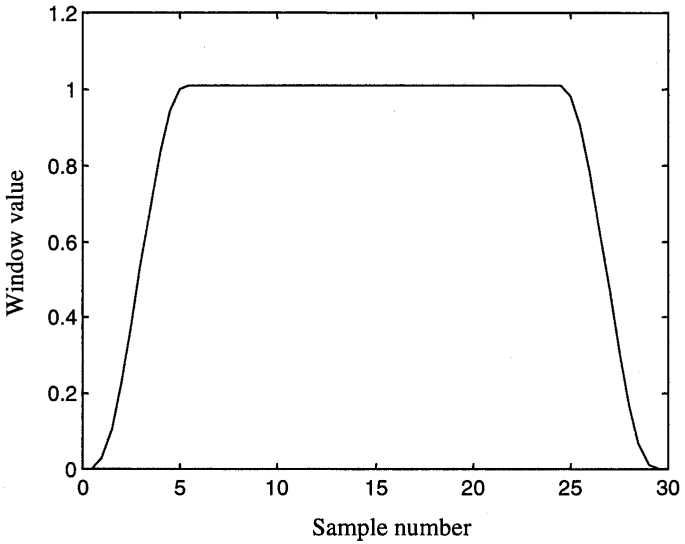

Figure 4.15 Raised cosine window.

The effect of multipath propagation on ISI and ICI is illustrated in Figure 4.16. It shows the windowing envelopes of three OFDM symbols. The radio channel consists of two paths with a relative delay of almost half a symbol and a relative amplitude of 0.5. The receiver selects the FFT timing such that the FFT is taken over the flat envelope part of the strongest path. Because the multipath delay is larger than the guard time, however, the FFT period cannot at the same time cover a totally flat envelope part of the weaker signal. As a result, the nonflat part of the symbol envelope causes ICI. At the same time, the partial overlap of the previous OFDM symbol in the FFT period causes ISI.

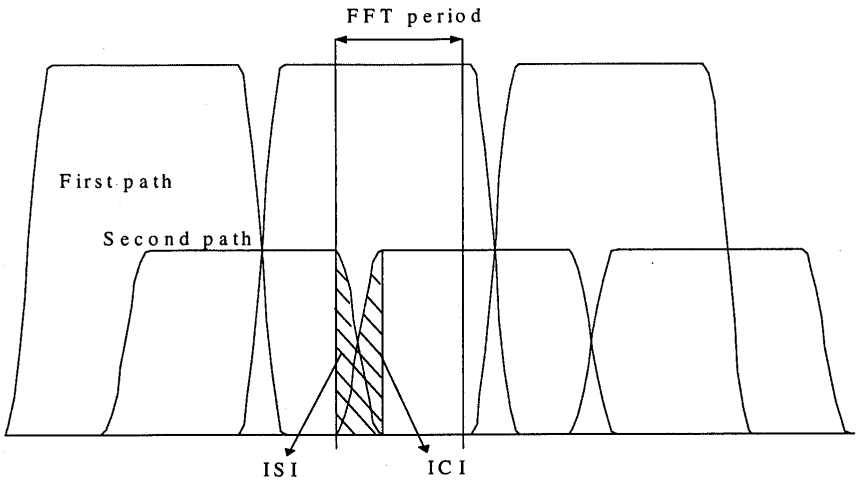

Figure 4.16 ISI/ICI caused by multipath signals.

The solution to the timing problem is to find the delay window—with a width equal to the guard time—that contains maximum signal power. The optimal FFT starting time, then, is equal to the starting delay of the found delay window, plus the delay that occurs between a matched filter peak output from a single OFDM pulse and the delay of the last sample on the flat part of the OFDM signal envelope, minus the length of the FFT interval.

As an example of the timing procedure, Figure 4.17 depicts a simulated matched filter output. By performing a moving average over four samples (which is assumed here to be the length of the guard interval) of the matched filter output power, it is detected that samples 21 to 24 contain the most power. Hence, the starting sample for the FFT is 21 minus some constant number which is mentioned above.

Figure 4.17 clearly shows the advantage of looking for maximum power in the whole guard interval, rather than looking for the maximum correlation output only. If the latter is applied to the example of Figure 4.17, then sample 23 would be chosen instead of sample 21. As a result, the multipath power at samples 21 and 22 would cause extra ISI and ICI, while the useful signal power of samples 24 to 27 would be less than the power of the samples 21 to 24. Hence, the signal-to-interference ratio can easily be degraded by several dB if the suboptimal maximum peak detection is used.

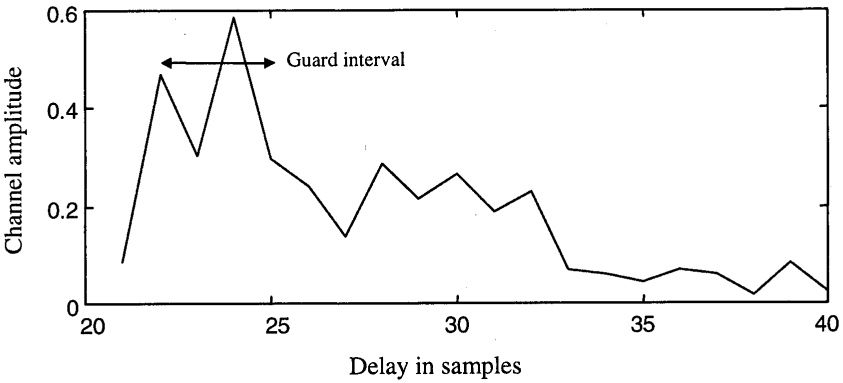

Figure 4.17 Example of channel impulse response.

We now prove that maximizing power in a certain delay window actually maximizes the signal-to-interference ratio. Figure 4.18 shows the OFDM symbol structure, where T is the time needed by the FFT. If a multipath signal is introduced with a relative[1] delay exceeding T_{g1}, it will cause ISI and ICI. Similarly, multipath signals with relative delays less than $-T_{g2}$ cause ISI and ICI. The timing problem is now to choose T_{g1} and T_{g2} such that the amount of ICI and ISI after the FFT is minimized.

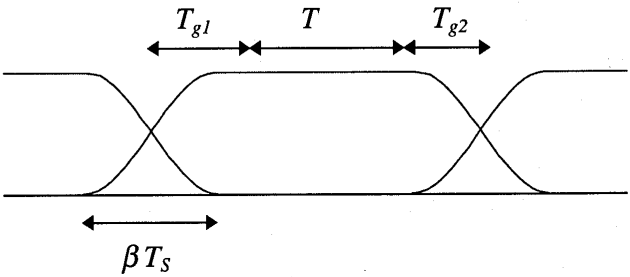

Figure 4.18 OFDM symbol structure.

From the above, it is clear that ISI and ICI are caused by all multipath signals, which delays fall outside a window of $T_g = T_{g1} + T_{g2}$. All multipath signals within this delay window contribute to the effectively used signal power. Hence, the optimal timing circuit maximizes the signal-to-(ISI+ICI) ratio (SIR), given by

[1] Relative to the delay of the shown reference OFDM signal.

$$SIR = \frac{S_u}{S_t - S_u},\ S_u = \int_{T_o}^{T_o+T_g} \|h(\tau)\|^2 d\tau,\ S_t = \int_{-\infty}^{\infty} \|h(\tau)\|^2 d\tau \qquad (4.14)$$

Here, $T_o=-T_{g2}$ is the timing offset of the guard time window T_g. S_t denotes the total received signal power and S_u is the useful signal power. Because only S_u depends on the timing offset T_o, the SIR is maximized by maximizing S_u; that is, choosing the T_o value that contains the largest power of $h(\tau)$ in the interval $\{T_o, T_o+T_G\}$.

REFERENCES

[1] Pollet, T., M. van Bladel and M. Moeneclaey, "BER Sensitivity of OFDM Systems to Carrier Frequency Offset and Wiener Phase Noise," *IEEE Trans. on Comm.*, Vol. 43, No. 2/3/4, pp. 191–193, Feb.-Apr. 1995.

[2] Pollet, T., and M. Moeneclaey, "Synchronizability of OFDM Signals," *Proceedings of Globecom '95*, Vol. 3, Singapore, pp. 2054–2058, Nov. 1995.

[3] Kivinen, J., and P. Vainikainen, "Phase Noise in a Direct Sequence Based Channel Sounder," *Proceedings of IEEE PIMRC '97*, Helsinki, pp. 1115–1119, Sep. 1–4, 1997.

[4] Robertson, P., and S. Kaiser, "Analysis of the Effects of Phase-Noise in Orthogonal Frequency Division Multiplex Systems," *Proceedings of IEEE VTC '95*, pp. 1652–1657.

[5] Tomba, L., "On the Effects of Wiener Phase Noise in OFDM systems," *IEEE Trans. on Comm.*, Vol. 46, No. 5, pp. 580–583, May 1998.

[6] Zogakis, T. N., and J. M. Cioffi, "The Effect of Timing Jitter on the Performance of a Discrete Multitone System," *IEEE Trans. on Comm.*, Vol. 44, No. 7, pp. 799–808, July 1996.

[7] Pollet, T., P. Spruyt and M. Moeneclaey, "The BER Performance of OFDM Systems Using Non-Synchronized Sampling," *Proceedings of Globecom '94*, pp. 253–257, Nov. 1994.

[8] Van de Beek, J. J., M. Sandell, M. Isaksson, and P. O. Börjesson, "Low-Complex Frame Synchronization in OFDM Systems," *Proceedings of International Conference on Universal Personal Communications ICUPC '95*, Nov. 1995.

[9] Sandell, M., J. J. van de Beek, and P. O. Börjesson, "Timing and Frequency Synchronization in OFDM Systems Using the Cyclic Prefix," *Proceedings of Int. Symp. On Synchronization*, Saalbau, Essen, Germany, 1995, pp. 16–19, Dec. 14–15, 1995

[10] Böhnke, R., and T. Dölle, "Preamble Structures for HiperLAN Type 2 System," ETSI BRAN Document No. HL13SON1A, Apr. 7, 1999.

[11] Moose, P. H., "A Technique for Orthogonal Frequency Division Multiplexing Frequency Offset Correction," *IEEE Trans. on Comm.*, Vol. 42, No. 10, pp. 2908–2914, Oct. 1994.

[12] Warner, W. D., and C. Leung, "OFDM/FM Frame Synchronization for Mobile Radio Data Communization," *IEEE Trans. on Vehicular Tech.*, Vol. 42, No. 3, pp. 302–313, Aug. 1993.

[13] Schmidl, T. M., and D. C. Cox, "Robust Frequency and Timing Synchronization for OFDM," *IEEE Trans. on Comm.*, Vol. 45, No. 12, pp. 1613–1621, Dec. 1997.

[14] Lambrette, U., M. Speth, and H. Meyr, "OFDM Burst Frequency Synchronization by Single Carrier Training Data," *IEEE Communications Letters*, Vol. 1, No. 2, pp. 46–48, Mar. 1997.

CHAPTER 5

Coherent and Differential Detection

5.1 INTRODUCTION

In an OFDM link, the data bits are modulated on the subcarriers by some form of phase shift keying (PSK) or quadrature amplitude modulation (QAM). To estimate the bits at the receiver, knowledge is required about the reference phase and amplitude of the constellation on each subcarrier. In general, the constellation of each subcarrier shows a random phase shift and amplitude change, caused by carrier frequency offset, timing offset, and frequency selective fading. To cope with these unknown phase and amplitude variations, two different approaches exist. The first one is coherent detection, which uses estimates of the reference amplitudes and phases to determine the best possible decision boundaries for the constellation of each subcarrier. The main issue with coherent detection is how to find the reference values without introducing too much training overhead. To achieve this, several channel estimation techniques exist that will be described in the next section. The second approach is differential detection, which does not use absolute reference values, but only looks at the phase and/or amplitude differences between two QAM values. Differential detection can be done both in the time domain or in the frequency domain; in the first case, each subcarrier is compared with the subcarrier of the previous OFDM symbol. In the case of differential detection in the frequency domain, each subcarrier is compared with the adjacent subcarrier within the same OFDM symbol.

5.2 COHERENT DETECTION

Figure 5.1 shows a block diagram of a coherent OFDM receiver. After downconversion and analog-to-digital conversion, the fast Fourier transform (FFT) is used to demodulate the N subcarriers of the OFDM signal. For each symbol, the FFT output contains N QAM values. However, these values contain random phase shifts and amplitude variations caused by the channel response, local oscillator drift, and timing

offset. It is the task of the channel estimation block to learn the reference phases and amplitudes for all subcarriers, such that the QAM symbols can be converted to binary soft decisions as explained in Chapter 3. The next subsections present several techniques to obtain the channel estimates that are required for coherent detection.

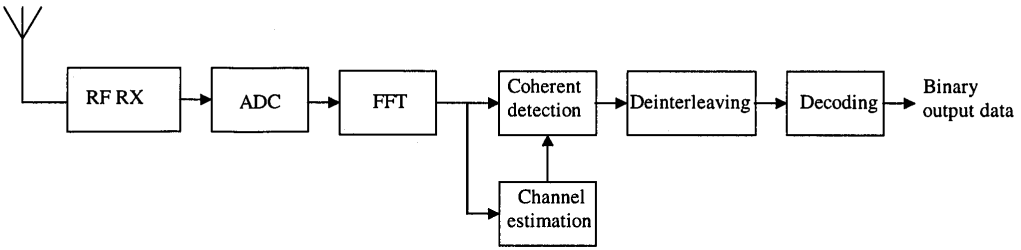

Figure 5.1 Block diagram of an OFDM receiver with coherent detection.

5.2.1 Two-Dimensional Channel Estimators

In general, radio channels are fading both in time and in frequency. Hence, a channel estimator has to estimate time-varying amplitudes and phases of all subcarriers. One way to do this is to use a two-dimensional channel estimator that estimates the reference values based on a few known pilot values. This concept is demonstrated in Figure 5.2, which shows a block of 9 OFDM symbols with 16 subcarriers. The gray subcarrier values are known pilots. Based on these pilots, all other reference values can be estimated by performing a two-dimensional interpolation [1–4].

To be able to interpolate the channel estimates both in time and frequency from the available pilots, the pilot spacing has to fulfill the Nyquist sampling theorem, which states that the sampling interval must be smaller than the inverse of the double-sided bandwidth of the sampled signal. For the case of OFDM, this means that there exist both a minimum subcarrier spacing and a minimum symbol spacing between pilots. By choosing the pilot spacing much smaller than these minimum requirements, a good channel estimation can be made with a relatively easy algorithm. The more pilots are used, however, the smaller the effective Signal-to-Noise ratio, SNR, becomes that is available for data symbols. Hence, the pilot density is a tradeoff between channel estimation performance and SNR loss.

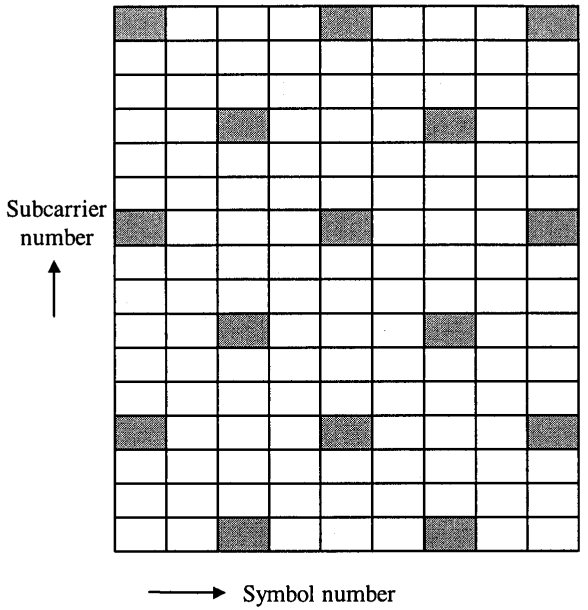

Figure 5.2 Example of pilots (marked gray) in a block of 9 OFDM symbols with 16 subcarriers.

To determine the minimum pilot spacing in time and frequency, we need to find the bandwidth of the channel variation in time and frequency. These bandwidths are equal to the Doppler spread B_d in the time domain and the maximum delay spread τ_{max} in the frequency domain [5]. Hence, the requirements for the pilot spacings in time and frequency s_t and s_f are

$$s_t < \frac{1}{B_d} \tag{5.1}$$

$$s_f < \frac{1}{\tau_{\max}} \tag{5.2}$$

Assume now the available pilot values are arranged in a vector $\hat{\mathbf{p}}$ and the channel values that have to be estimated from $\hat{\mathbf{p}}$ are in a vector $\mathbf{h}$. Notice that we use bold letters to distinguish vectors from scalar variables. It is assumed that any known modulation of the pilots is removed before the estimation; for instance, if the transmitter applies some phase shifts to the pilots, then the receiver has to back-rotate those known phases. The channel estimation problem is now to find the channel estimates $\hat{\mathbf{h}}$ as a linear combination of the pilot estimates $\hat{\mathbf{p}}$. According to [6], the minimum mean square error estimate for this problem is given by

$$\hat{\mathbf{h}} = \mathbf{R}_{\mathbf{h}\hat{\mathbf{p}}}\mathbf{R}_{\hat{\mathbf{p}}\hat{\mathbf{p}}}^{-1}\hat{\mathbf{p}} \tag{5.3}$$

$\mathbf{R}_{\mathbf{h}\hat{\mathbf{p}}}$ is the cross-covariance matrix between $\mathbf{h}$ and the noisy pilot estimates $\hat{\mathbf{p}}$, given by

$$\mathbf{R}_{\mathbf{h}\hat{\mathbf{p}}} = \mathrm{E}\left\{ \mathbf{h}\hat{\mathbf{p}}^{\mathbf{H}} \right\} \tag{5.4}$$

$\mathbf{R}_{\hat{\mathbf{p}}\hat{\mathbf{p}}}$ is the auto-covariance matrix of the pilot estimates:

$$\mathbf{R}_{\hat{\mathbf{p}}\hat{\mathbf{p}}} = \mathrm{E}\left\{ \hat{\mathbf{p}}\hat{\mathbf{p}}^{\mathbf{H}} \right\} = \mathbf{R}_{\mathbf{pp}} + \sigma_n^2(\mathbf{pp}^{\mathbf{H}})^{-1} \tag{5.5}$$

Assuming the pilots all have the same power, which is the case if all pilots are for instance known QPSK symbols, then the pilots' auto-covariance matrix can be rewritten as

$$\mathbf{R}_{\hat{\mathbf{p}}\hat{\mathbf{p}}} = \mathbf{R}_{\mathbf{pp}} + \frac{1}{\mathrm{SNR}}\mathbf{I} \tag{5.6}$$

where SNR is the signal-to-noise ratio per pilot and $\mathbf{R}_{\mathbf{pp}}$ is the autocovariance matrix of the noiseless pilots. With this, the channel estimates can be written as

$$\hat{\mathbf{h}} = \mathbf{R}_{\mathbf{h}\hat{\mathbf{p}}}(\mathbf{R}_{\mathbf{pp}} + \frac{1}{\mathrm{SNR}}\mathbf{I})^{-1}\hat{\mathbf{p}} \tag{5.7}$$

(5.7) basically gives the desired channel estimates as the multiplication of an interpolation matrix with the pilot estimates. Notice that the interpolation matrix does not depend on the received symbols; it only depends on the position of the pilots and the number of pilots and channel estimates. Hence, the interpolation matrix can be designed as a constant matrix, avoiding the need to do matrix inversions in the OFDM receiver.

The elements covariance matrices $\mathbf{R}_{\mathbf{h}\hat{\mathbf{p}}}$ and $\mathbf{R}_{\hat{\mathbf{p}}\hat{\mathbf{p}}}$ can be calculated as follows. Both matrices contain correlation values between subcarrier values for different time and frequency spacings. If k and l are the subcarrier number and OFDM symbol number, respectively, the correlation values are given by

$$E\{h_{k,l}\hat{p}^*_{k',l'}\} = E\{p_{k,l}\hat{p}^*_{k',l'}\} = r_f(k-k')r_t(l-l') \tag{5.8}$$

Here, $r_t(l)$ and $r_f(k)$ are the correlation functions in time and frequency, respectively. For an exponentially decaying multipath power delay profile, $r_f(k)$ is given by

$$r_f(k) = \frac{1}{1 + j2\pi\tau_{rms}k/T} \tag{5.9}$$

Here, $1/T$ is the subcarrier spacing, which is the inverse of the FFT interval T. For a time-fading signal with a maximum Doppler frequency f_{max} and a Jakes spectrum, the time correlation function $r_t(l)$ is given as

$$r_t(l) = J_o(2\pi f_{\max} l T_s) \tag{5.10}$$

where $J_o(x)$ is the zero*th* order Bessel function of the first kind and T_s is the OFDM symbol duration, which is the FFT interval T plus the guard time. To illustrate the channel estimation technique described above, an example will be given for the case of five pilots in a block of five OFDM symbols with five subcarriers. Four pilots are located at the corners of the block and one in the middle, being the third subcarrier of the third OFDM symbol. Using the Jakes fading channel model, an OFDM signal was generated that experienced fading both in time and frequency. Table 5.1 lists the 25 reference channel values for the five subcarriers in each of the five symbols for this example. Of course, an OFDM receiver does not know these reference values; it only has knowledge about the five pilot values, which are located at row and column numbers {1,1}, {1,5}, {3,3}, {5,1}, and {5,5}. In this particular example, no noise is added to the pilot values. Each column represents one symbol with five subcarrier values. We can see from the table that there is fading both in frequency—across the rows—and in time.

Table 5.1
Example channel values for a block of five OFDM symbols and five subcarriers.

1.0386–0.2468i	1.1333–0.2441i	1.1777–0.2491i	1.1693–0.2617i	1.1048–0.2761i
0.8938–0.4782i	0.9798–0.4821i	1.0172–0.4842i	1.0040–0.4847i	0.9386–0.4778i
0.6726–0.6302i	0.7479–0.6398i	0.7802–0.6402i	0.7675–0.6316Ii	0.7099–0.6082i
0.4173–0.6794i	0.4809–0.6913i	0.5093–0.6897i	0.5007–0.6750i	0.4567–0.6421i
0.1794–0.6258i	0.2321–0.6349i	0.2578–0.6303i	0.2548–0.6125i	0.2258–0.5774i

Table 5.2 gives the elements of the pilot auto-covariance matrix. This matrix is independent of the received signal, so it can be precalculated using (5.8), (5.9), and (5.10). The first row of $\mathbf{R}_{pp}$ consists of the correlations between the first pilot and all five pilots. The first value is 1, as this is the correlation of the first pilot with itself. The second value of the first row is the correlation between the first pilot at the first subcarrier with the pilot of the first subcarrier of the fifth symbol. Because these pilots are both on the same subcarrier, the frequency correlation component $r_f(k)$ is equal to 1, and the correlation value is purely determined by the time fading component $r_t(k)$. This explains why the imaginary component of the second correlation value is zero, because $r_t(k)$ (5.10) is a strictly real function. Notice that from the matrix $\mathbf{R}_{pp}$ the matrix $\mathbf{R}_{\hat{p}\hat{p}}$ is formed by adding an identity matrix multiplied by the inverse of the SNR (5.6). In practice, the SNR is not known *a priori*, so an expected value is used. In our example, we will use an SNR of 10 dB. Using a large SNR value gives a relatively large weight on $\mathbf{R}_{pp}$ in (5.7).

Table 5.2
Example of covariance matrix $\mathbf{R}_{pp}$.

1.0000	0.4720	0.7967–0.2589i	0.7568–0.5499i	0.3572–0.2595i
0.4720	1.0000	0.7967–0.2589i	0.3572–0.2595i	0.7568–0.5499i
0.7967–0.2589i	0.7967–0.2589i	1.0000	0.7967–0.2589i	0.7967–0.2589i
0.7568–0.5499i	0.3572–0.2595i	0.7967–0.2589i	1.0000	0.4720
0.3572–0.2595i	0.7568–0.5499i	0.7967–0.2589i	0.4720	1.0000

Table 5.3 gives the example matrix $\mathbf{R}_{h\hat{p}}$. This matrix contains the correlation values between all 25 channel values—in the block of five symbols by five subcarriers—with each of the five pilots. Hence, the matrix has 25 rows and 5 columns. Because the pilots are also part of the 25 channel values, the rows of $\mathbf{R}_{pp}$ are all part of $\mathbf{R}_{h\hat{p}}$; for instance, the first row of $\mathbf{R}_{h\hat{p}}$ is the same as the first row of $\mathbf{R}_{pp}$.

Table 5.3

Example of covariance matrix $\mathbf{R}_{h\hat{p}}$.

1.0000	0.4720	0.7967–0.2589i	0.7568–0.5499i	0.3572–0.2595i
0.9836–0.1558i	0.4643–0.0735i	0.8377–0.1327i	0.8584–0.4374i	0.4052–0.2064i
0.9355–0.3040i	0.4416–0.1435i	0.8516	0.9355–0.3040i	0.4416–0.1435i
0.8584–0.4374i	0.4052–0.2064i	0.8377–0.1327i	0.9836–0.1558i	0.4643–0.0735i
0.7568–0.5499i	0.3572–0.2595i	0.7967–0.2589i	1.0000	0.4720
0.9618	0.6820	0.8998–0.2924i	0.7279–0.5289i	0.5161–0.3750i
0.9461–0.1498i	0.6708–0.1062i	0.9461–0.1498i	0.8256–0.4207i	0.5854–0.2983i
0.8998–0.2924i	0.6380–0.2073i	0.9618	0.8998–0.2924i	0.6380–0.2073i
0.8256–0.4207i	0.5854–0.2983i	0.9461–0.1498i	0.9461–0.1498i	0.6708–0.1062i
0.7279–0.5289i	0.5161–0.3750i	0.8998–0.2924i	0.9618	0.6820
0.8516	0.8516	0.9355–0.3040i	0.6445–0.4683i	0.6445–0.4683i
0.8377–0.1327i	0.8377–0.1327i	0.9836–0.1558i	0.7310–0.3725i	0.7310–0.3725i
0.7967–0.2589i	0.7967–0.2589i	1.0000	0.7967–0.2589i	0.7967–0.2589i
0.7310–0.3725i	0.7310–0.3725i	0.9836–0.1558i	0.8377–0.1327i	0.8377–0.1327i
0.6445–0.4683i	0.6445–0.4683i	0.9355–0.3040i	0.8516	0.8516
0.6820	0.9618	0.8998–0.2924i	0.5161–0.3750i	0.7279–0.5289i
0.6708–0.1062i	0.9461–0.1498i	0.9461–0.1498i	0.5854–0.2983i	0.8256–0.4207i
0.6380–0.2073i	0.8998–0.2924i	0.9618	0.6380–0.2073i	0.8998–0.2924i
0.5854–0.2983i	0.8256–0.4207i	0.9461–0.1498i	0.6708–0.1062i	0.9461–0.1498i
0.5161–0.3750i	0.7279–0.5289i	0.8998–0.2924i	0.6820	0.9618
0.4720	1.0000	0.7967–0.2589i	0.3572–0.2595i	0.7568–0.5499i
0.4643–0.0735i	0.9836–0.1558i	0.8377–0.1327i	0.4052–0.2064i	0.8584–0.4374i
0.4416–0.1435i	0.9355–0.3040i	0.8516	0.4416–0.1435i	0.9355–0.3040i
0.4052–0.2064i	0.8584–0.4374i	0.8377–0.1327i	0.4643–0.0735i	0.9836–0.1558i
0.3572–0.2595i	0.7568–0.5499i	0.7967–0.2589i	0.4720	1.0000

The above matrices can be combined to the final interpolation matrix listed in Table 5.4. The matrix has 25 rows and 5 columns; when multiplied by the row vector containing five measured pilots, 25 channel estimates are obtained. Figure 5.3 shows the estimation errors for the channel example of Table 5.1. We can see that the relative estimation error is between 3% and 14%. The largest errors are located at the edges of the block, which is a typical phenomenon of this kind of interpolation. It suggests that to minimize the interpolation error, pilots should be used that surround the channel positions that have to be estimated.

Table 5.4

Example of interpolation matrix $\mathbf{R}_{h\hat{p}}(\mathbf{R}_{pp}+\frac{1}{SNR}\mathbf{I})^{-1}$

0.9044+0.0902i	0.0331–0.0034i	0.0333–0.0749i	0.0145–0.0630i	–0.0241 + 0.0562i
0.6009+0.0022i	–0.0908–0.0346i	0.4006+0.0861i	0.1446–0.0753i	–0.1200–0.0040i
0.2760–0.0836i	–0.2100–0.0647i	0.7484+0.2459i	0.2760–0.0836i	–0.2100–0.0647i
0.1446–0.0753i	–0.1200–0.0040i	0.4006+0.0861i	0.6009+0.0022i	–0.0908–0.0346i
0.0145–0.0630i	–0.0241+0.0562i	0.0333–0.0749i	0.9044+0.0902i	0.0331–0.0034i
0.7534+0.0819i	0.2917+0.0323i	0.0409–0.1125i	0.0040–0.0267i	–0.0165+0.0364i
0.4658+0.0002i	0.0993–0.0193i	0.4555+0.0678i	0.0816–0.0547i	–0.0587–0.0169i
0.1620–0.0797i	–0.0955–0.0697i	0.8483+0.2478i	0.1620–0.0797i	–0.0955–0.0697i
0.0816–0.0547i	–0.0587–0.0169i	0.4555+0.0678i	0.4658+0.0002i	0.0993–0.0193i
0.0040–0.0267i	–0.0165+0.0364i	0.0409–0.1125i	0.7534+0.0819i	0.2917+0.0323i
0.5412+0.0619i	0.5412+0.0619i	0.0435–0.1257i	–0.0067+0.0077i	–0.0067+0.0077i
0.2920–0.0072i	0.2920–0.0072i	0.4746+0.0614i	0.0111–0.0344i	0.0111–0.0344i
0.0333–0.0749i	0.0333–0.0749i	0.8830+0.2483i	0.0333–0.0749i	0.0333–0.0749i
0.0111–0.0344i	0.0111–0.0344i	0.4746+0.0614i	0.2920–0.0072i	0.2920–0.0072i
–0.0067+0.0077i	–0.0067+0.0077i	0.0435–0.1257i	0.5412+0.0619i	0.5412+0.0619i
0.2917+0.0323i	0.7534+0.0819i	0.0409–0.1125i	–0.0165+0.0364i	0.0040–0.0267i
0.0993–0.0193i	0.4658+0.0002i	0.4555+0.0678i	–0.0587–0.0169i	0.0816–0.0547i
–0.0955–0.0697i	0.1620–0.0797i	0.8483+0.2478i	–0.0955–0.0697i	0.1620–0.0797i
–0.0587–0.0169i	0.0816–0.0547i	0.4555+0.0678i	0.0993–0.0193i	0.4658+0.0002i
–0.0165+0.0364i	0.0040–0.0267i	0.0409–0.1125i	0.2917+0.0323i	0.7534+0.0819i
0.0331–0.0034i	0.9044+0.0902i	0.0333–0.0749i	–0.0241+0.0562i	0.0145–0.0630i
–0.0908–0.0346i	0.6009+0.0022i	0.4006+0.0861i	–0.1200–0.0040i	0.1446–0.0753i
–0.2100–0.0647i	0.2760–0.0836i	0.7484+0.2459i	–0.2100–0.0647i	0.2760–0.0836i
–0.1200–0.0040i	0.1446–0.0753i	0.4006+0.0861i	–0.0908–0.0346i	0.6009+0.0022i
–0.0241+0.0562i	0.0145–0.0630i	0.0333–0.0749i	0.0331–0.0034i	0.9044+0.0902i

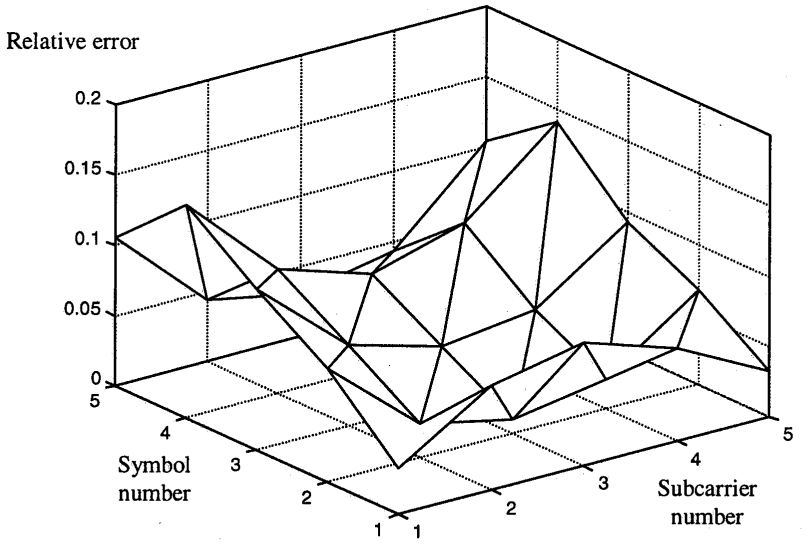

Figure 5.3 Example of relative channel estimation errors versus subcarrier number and symbol number.

5.2.2 One-Dimensional Channel Estimators

The channel estimation technique described in the previous section basically performed a two-dimensional interpolation to estimate points on a time-freqency grid based on several pilots. Instead of directly calculating the two-dimensional solution, it is also possible to separate the interpolation into two one-dimensional interpolations, as illustrated by Figure 5.4 [7]. With this technique, first an interpolation in the frequency domain is performed for all symbols containing pilots. Then, for each subcarrier an interpolation in the time domain is performed to estimate the remaining channel values.

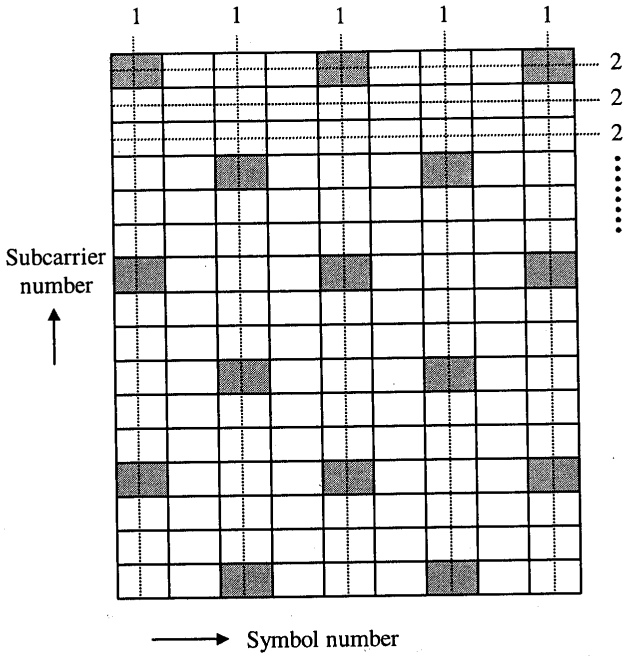

Figure 5.4 Channel estimation with separable filters in frequency (1) and time (2) direction.

5.2.3 Special Training Symbols

The channel estimation techniques from the previous sections were designed to estimate a channel that varied both in time and frequency. These techniques are especially suitable for continuous transmission systems such as Digital Audio Broadcasting or Digital Video Broadcasting, which are both described in Chapter 10. They are not very suited, however, for packet-type communications for two reasons. First, in many packet transmission systems, such as wireless LAN, the packet length is short enough to assume a constant channel during the length of the packet. This means there is no need to estimate time fading, which greatly simplifies the channel estimation problem. Second, using pilots scattered over several OFDM data symbols introduces a delay of several symbols before the first channel estimates can be calculated. Such a delay is undesirable in packet transmission like in an IEEE 802.11 wireless LAN, which requires an acknowledgment to be sent after each packet transmission. Any delay in the reception of a packet will also delay the acknowledgment and hence decrease the effective throughput of the system. An additional disadvantage is the fact that the receiver needs to buffer several OFDM symbols, thereby requiring extra hardware.

For the specific problem of channel estimation in packet transmission systems, the most appropriate approach seems to be the use of a preamble consisting of one or more known OFDM symbols. This approach is sketched in Figure 5.5. The figure shows the time-frequency grid with subcarriers on the vertical axis and symbols on the horizontal axis. All gray subcarriers are pilots. The packet starts with two OFDM symbols for which all data values are known. These training symbols can be used to obtain channel estimates, as well as a frequency offset estimate, as was explained in Chapter 4. After the first two training symbols, Figure 5.5 shows two pilot subcarriers within the data symbols. These pilots are not meant for channel estimation, but for tracking the remaining frequency offset after the initial training. Because this frequency offset affects all subcarriers in a similar way, there is no need to have many pilots with a small frequency spacing as in the case of channel estimation. This type of pilot structure was first mentioned in a proposal for the IEEE 802.11 OFDM standard [8], which is described in detail in Chapter 9.

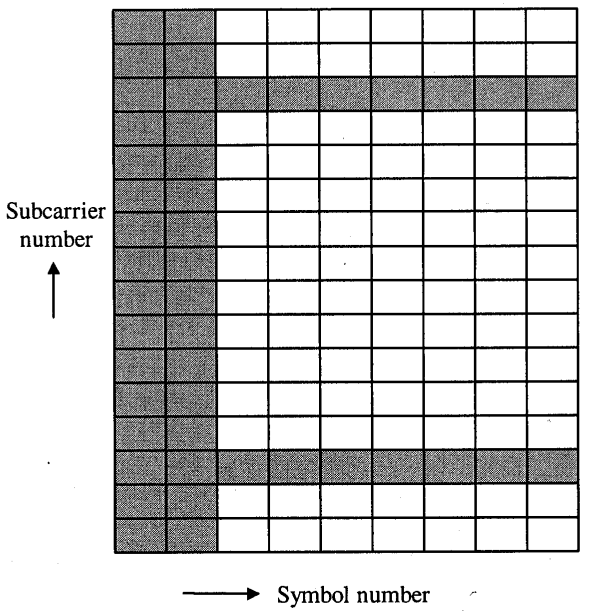

Figure 5.5 Example of a packet with two training symbols for channel estimation and two pilot subcarriers used for frequency synchronization.

The choice of the number of training symbols is a tradeoff between a short training time and a good channel estimation performance. Using two training symbols is a reasonable choice, because it gives a 3-dB-lower noise level in the channel estimates by a simple averaging of the two training symbols, and a minimum of two training symbols is convenient anyway to estimate the frequency offset by comparing the phase shift of the two identical symbols.

If multiple training symbols are used, there is actually no need to repeat an entire OFDM symbol including guard time. A more efficient way is to repeat the IFFT interval and to keep a single guard time, as depicted in Figure 5.6. This can also be viewed as extending the guard time to twice the original guard time plus an extra time equal to the IFFT interval. The advantage of this approach is that it makes the training extra robust to multipath; a receiver can perform a channel estimation by taking the FFT of the averaged IFFT intervals of the long training symbol. This channel estimate will be free from ISI and ICI as long as the relative multipath delays are smaller than the guard time of the training symbol, which is now doubled relative to the guard time of the OFDM data symbols.

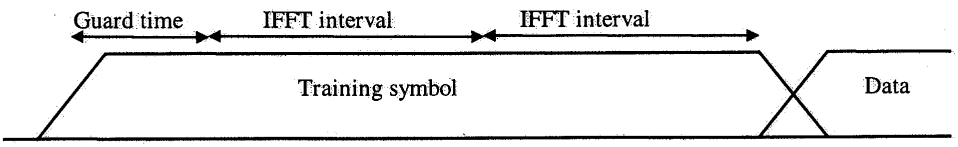

Figure 5.6 Extended training symbol for channel estimation with a single guard time and multiple IFFT intervals.

One of the main assumptions when using pilot symbols only at the start of a packet is that channel variations during the rest of the packet are negligible. Whether this is a valid assumption depends on the packet duration and the Doppler bandwidth. This issue is discussed further in Section 5.3.1. This section describes a related differential detection technique that relies on the same assumption of a channel that is nearly constant in time.

5.2.4 Decision-Directed Channel Estimation

The previously described coherent detection techniques are all based on pilots to estimate the channel. A disadvantage of those pilots is that they cost a certain percentage of the transmitted power. To avoid this loss, decision-directed channel estimation can be used. Here, instead of pilots, data estimates are used to remove the data modulation from the received subcarriers, after which all subcarriers can be used to estimate the channel. Of course, it is not possible to make reliable data decisions before a good channel estimate is available. Therefore, only decisions from previous symbols are used to predict the channel in the current symbol [9]. This is in contrast to the pilot methods, where the channel for a certain symbol is estimated from pilots within, before, and after that particular symbol. If the channel is relatively slowly varying in time, however, such that there is a large correlation between adjacent symbols, then there is a negligible impact on performance if only earlier symbols are used to estimate the channel for a particular OFDM symbol.

To start the decision-directed channel estimation, at least one known OFDM symbol must be transmitted. This enables the receiver to attain channel estimates for all subcarriers, which are then used to detect the data in the following OFDM symbol. Once data estimates are available for a symbol, these estimates are used to remove the data modulation from the subcarriers, after which those subcarrier values can be used as pilots in exactly the same way as described in Sections 5.2.1 and 5.2.2.

5.3 DIFFERENTIAL DETECTION

The key idea behind all coherent detection techniques discussed in the previous subsections is that they somehow estimate the channel to obtain an absolute reference phase and amplitude for each subcarrier in each OFDM symbol. In contrast to this, differential detection does not perform any channel estimation, thereby saving both complexity and pilots at the cost of a somewhat reduced SNR performance. A general block diagram of an OFDM receiver using differential detection is shown in Figure 5.7. Instead of using an absolute reference, differential detection compares each subsymbol with another subsymbol, which can be a previous subcarrier in the same OFDM symbol, or the same subcarrier of a previous OFDM symbol. The next sections explain both variations of differential detection and show how differential detection can even be applied to multi-amplitude modulation.

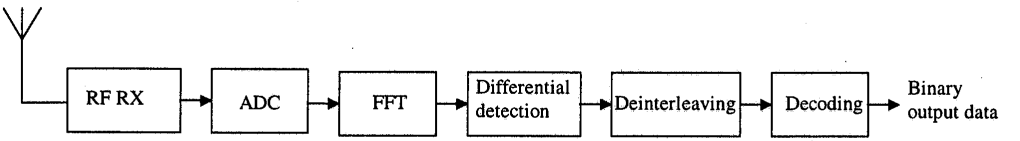

Figure 5.7 Block diagram of an OFDM receiver with differential detection.

5.3.1 Differential Detection in the Time Domain

If differential detection is applied in the time domain, then each subsymbol is compared to the subsymbol on the same subcarrier of the previous OFDM symbol, as depicted in Figure 5.8.

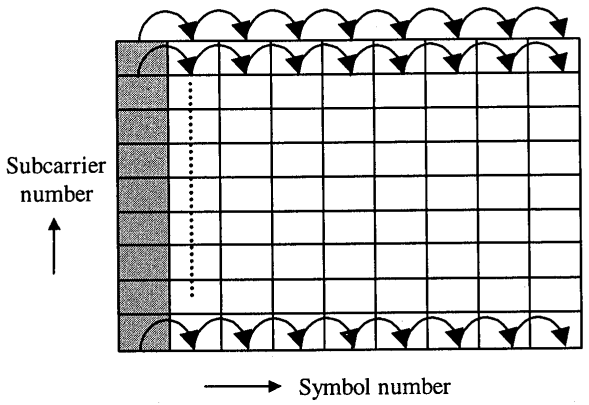

Figure 5.8 Differential detection in the time domain. Gray subcarriers are pilots that are needed as initial phase references.

To make differential detection possible, the transmitter has to apply differential encoding. For a PSK signal with input phases φ_{kj}, the differentially encoded phases θ_{ij} are

$$\theta_{ij} = \sum_{k=0}^{i} \varphi_{kj} \mod(2\pi) \tag{5.11}$$

where i and k are the symbol number and j is the subcarrier number. Differential detection is essentially applied to each subcarrier separately. Because at the start of a transmission no previous symbol values are yet available, the subcarrier values of the first symbol are chosen to be some arbitrary values.

At the receiver, the FFT output of symbol i and subcarrier j can be written as

$$x_{ij} = a_{ij} e^{\theta_{ij}+\beta_{ij}} + n_{ij} \tag{5.12}$$

where a_{ij}, β_{ij}, and n_{ij} are the channel amplitude, channel phase, and additive noise component of symbol i and subcarrier j. A differential phase detection in the time domain is performed by multiplying each FFT output with the conjugated FFT output of the same subcarrier from the previous OFDM symbol.

$$y_{ij} = x_{ij} x_{i-1,j}^{*} = a_{ij} a_{i-1,j} e^{\varphi_{ij}+\beta_{ij}-\beta_{i-1,j}} + n_{ij} a_{i-1,j} e^{\theta_{i-1,j}+\beta_{i-1,j}} + n_{i-1,j} a_{ij} e^{\theta_{ij}+\beta_{ij}} + n_{ij} n_{i-1,j}^{*} \tag{5.13}$$

The first term of (5.13) has the desired phase φ_{kj}, but it also has an undesired phase disturbance $\beta_{ij} - \beta_{i-1,j}$, which is the channel phase shift on subcarrier j from symbol $i - 1$ to i. The latter disturbance depends only on the time fading, so to have a negligible impact on the phase detection, the OFDM symbol duration has to be small relative to the channel coherence time.

Figure 5.9 shows the correlation between signal samples as a function of the normalized time difference $f_{max}T_s$, where f_{max} is the maximum Doppler spread and T_s is the OFDM symbol duration. The correlation is calculated according to (5.10), with the number of OFDM symbols l set to one. Figure 5.9 can be used to determine the maximum tolerable Doppler spread, depending on the allowable phase error and the OFDM symbol duration. The maximum tolerable level of channel estimation errors can be related to the correlation between two OFDM symbols by writing the channel value y_{ij} as a function of the channel value $y_{i-1,j}$ of the previous symbol

$$y_{ij} = r_t y_{i-1,j} + \sqrt{(1-r_t^2)}\, q_{ij} \tag{5.14}$$

Here, r_t is the correlation between channel values of two OFDM symbols on the same subcarrier, as given by (5.10). q_{ij} is a randomly distributed component with unity power. The difference between the channel values $y_{i-1,j}$ and y_{ij} is given by

$$y_{i-1,j} - y_{ij} = y_{i-1,j}(1-r_t) + \sqrt{(1-r_t^2)}\, q_{ij} \tag{5.15}$$

This difference in channel values between two OFDM symbols determines the loss in SNR performance. For a negligible loss of performance, the signal-to-distortion ratio (SDR) should be much larger than the SNR that is needed to achieve a certain maximum BER or PER.

Assuming $y_{i-1,j}$ and q_{ij} are uncorrelated, the distortion power is the sum of the powers of both components in (5.15). Because both $y_{i-1,j}$ and q_{ij} have unity power, the SDR can be written as

$$SDR = \frac{1}{2(1-r_t)} \tag{5.16}$$

The required SNR values depend on coding rate and type of modulation. Some practical values can be deduced from Chapter 3. For instance, an SNR of 4 dB is required to get a BER of 10^{-5} using QPSK and rate 1/2 convolutional coding. For a loss in SNR performance of less than 1 dB, the distortion power should be at least 6 dB lower than the noise power, so the SDR needs to be 10 dB or more. Using (5.16), an

SDR of 10 dB requires a correlation value r_t of 0.95. From Figure 5.10—which is a zoom-in on the first part of Figure 5.9—we can see that a correlation value of 0.95 corresponds to a normalized time distance $f_{max}T_s$ of approximately 0.07. Hence, the maximum allowable Doppler frequency in this case is $0.07/T_s$. The Doppler frequency can be related to the maximum allowable velocity v as

$$f_{\max} = f_c \frac{v}{c} \tag{5.17}$$

where f_c is the carrier frequency and c the speed of light. For example, for a carrier frequency of 5 GHz and a symbol duration of 4 μs, a maximum Doppler frequency of $0.07/T_s = 17.5$ kHz leads to a maximum allowable user velocity of 1,050 m/s. Because this speed is orders of magnitudes above practical values, we can conclude that for normal speeds, the channel change between two OFDM symbols is negligible for the parameters of the above example.

An interesting analogy exists between differential detection in the time domain and the coherent detection method using pilot symbols at the beginning of a packet, which was described in Section 5.2.3. Both methods rely on the fact that the channel is relatively constant in time. When the first symbols of a packet are used as a coherent reference for the rest of the packet, a nonzero Doppler bandwidth will cause the channel estimation errors to grow with the packet length. Hence, the maximum possible packet length is determined by the allowable level of channel estimation errors. To calculate the errors in the channel estimation, the same equations can be used as for differential detection in the time domain, with the only difference that T_s is replaced by the packet duration T_p. For instance, for the parameters of the previous example, it is required that $f_{max}T_p$ is approximately 0.07. Because f_{max} is equal to $f_c v/c$, the maximum possible packet duration T_p becomes $0.07c/f_c v \cong 2.8$ ms at a walking speed of v=1.5 m/s. At a vehicle speed of 30 m/s, however, the maximum packet duration is limited to about 0.1 ms.

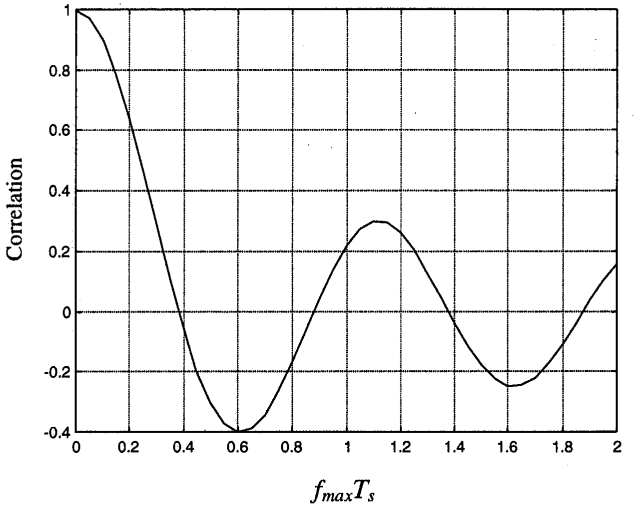

Figure 5.9 Correlation between symbols versus the normalized time distance $f_{max}T_s$.

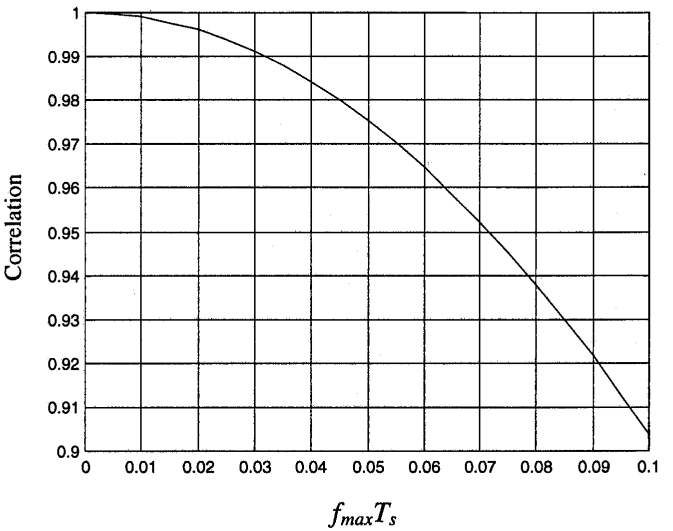

Figure 5.10 Correlation between symbols versus the normalized time distance $f_{max}T_s$, zoom-in of Figure 5.9.

The remaining three terms of (5.13) are noise components. If the difference between the amplitudes $a_{i-1,j}$ and a_j is neglected, the power of the second and third term is equal to $2P_sP_n$, where P_s and P_n are signal and noise power, respectively. The power of the last term in (5.13) is equal to the squared noise power P_n^2. For an SNR that is much larger than one, the cross products dominate the squared noise component, and the output SNR can be written as

$$SNR_y = \frac{P_s^2}{P_n^2 + 2P_sP_n} \cong \frac{P_s}{2P_n} = \frac{SNR_x}{2} \tag{5.18}$$

Hence, the SNR after differential detection is approximately 3 dB worse than the input SNR. This 3 dB is the worst case SNR loss of differential detection relative to coherent detection. In practice, coherent detection also has an SNR loss because of imperfect channel estimates and because a part of the signal power is spent on pilots. This typically reduces the difference between differential and coherent detection from 3 to about 1 to 2 dB.

5.3.2 Differential Detection in the Frequency Domain

Differential detection can also be applied across subcarriers instead of symbols. In this case, for a PSK signal with input phases φ_{kj}, the differentially encoded phases θ_{ij} are

$$\theta_{ij} = \sum_{k=0}^{j} \varphi_{ik} \mod(2\pi) \tag{5.19}$$

where i is the symbol number and j and k are subcarrier numbers. Differential detection is now applied to each symbol separately, as depicted in Figure 5.11. The first subcarrier of each symbol is a known pilot value that is needed to provide an initial value to start the differential detection process.

A differential phase detection in the frequency domain is performed by multiplying each FFT output with the conjugated FFT output of the same symbol from the previous subcarrier:

$$y_{ij} = x_{ij}x_{i,j-1}^* = a_{ij}a_{i,j-1}e^{\varphi_{ij}+\beta_{ij}-\beta_{i,j-1}} + n_{ij}a_{i,j-1}e^{\theta_{i,j-1}+\beta_{i,j-1}} + n_{i,j-1}a_{ij}e^{\theta_{ij}+\beta_{ij}} + n_{ij}n_{i,j-1}^* \tag{5.20}$$

Here, x_{ij} is the FFT output at the receiver as defined by (5.12). Equation (5.20) has exactly the same structure as (5.13), which described differential detection in the time domain. Because of this, a similar signal-to-noise analysis can be made, showing that differential detection in the frequency domain also has an SNR loss of 3 dB compared with ideal coherent detection. The main difference between differential detection in frequency and time is the phase disturbance component in the first term of (5.20). This first term contains the desired phase φ_{kj}, but also an undesired phase $\beta_{ij}-\beta_{i,j-1}$, which is the channel phase shift on symbol i from subcarrier $j-1$ to j.

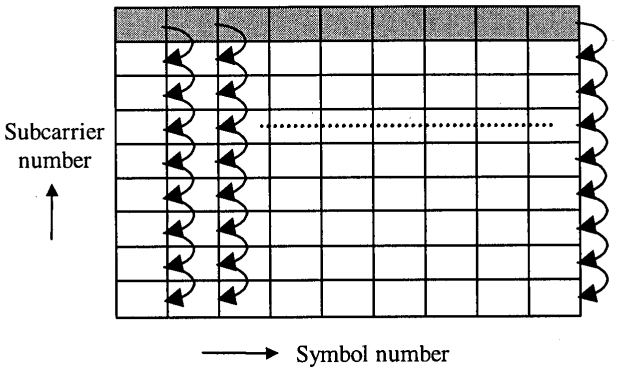

Figure 5.11 Differential detection in the frequency domain. Gray subcarriers are pilots.

The influence of the phase disturbance can be analyzed by looking at the correlation between adjacent subcarriers as a function of the normalized frequency difference τ_{max}/T. This correlation can be calculated from (5.9) by setting the number of subcarriers k to one. A plot of the correlation versus the normalized frequency difference is drawn in Figure 5.12.

Similar to the case of correlation in the time domain as described in the previous section, we can deduce that the SDR for a correlation value r_f is given by

$$SDR = \frac{1}{2(1-r_f)} \tag{5.21}$$

If we use the same example as in the previous section, which required an SDR of 10 dB, then the correlation r_f has to be 0.95. From Figure 5.12 we can deduce that the normalized subcarrier spacing τ_{rms}/T has to be approximately 0.03. This means that the subcarrier spacing has to be $0.03/\tau_{rms}$ at most. Equivalently, it can be stated that the maximum tolerable delay spread is 3% of the FFT period T. The latter means that the delay spread robustness of differential detection in the frequency domain is generally significantly worse than other detection techniques, where the delay spread robustness is related only to the guard time and not to the FFT period.

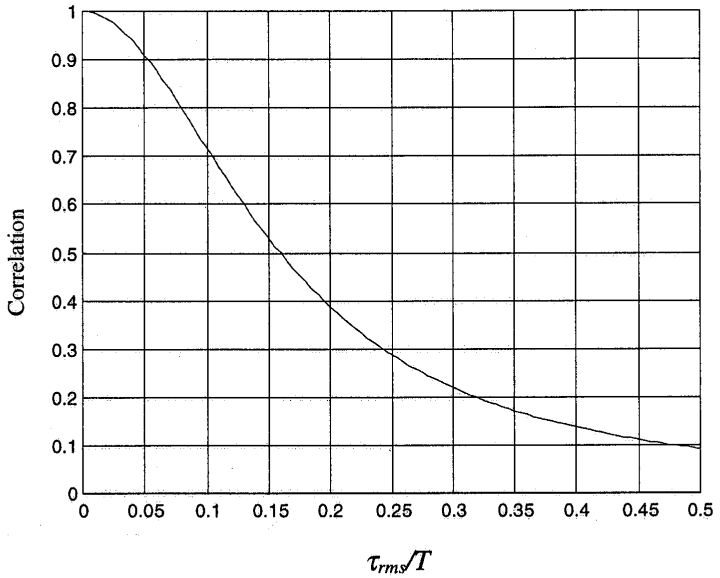

Figure 5.12 Correlation between subcarriers versus the normalized subcarrier spacing τ_{rms}/T.

Figure 5.13 presents some simulation results which compare coherent demodulation and differential detection for an OFDM system for wireless LAN applications. Table 5.5 lists the main system parameters. The data rates for this system are variable, dependent on the coding rate and the modulation type. Some possible data rates for this system are 32 Mbps with 16-QAM and rate ½ coding, or 8-PSK with rate 2/3 coding, 24 Mbps with QPSK and rate 3/4 coding, or 8-PSK with rate ½ coding, and 16 Mbps with QPSK and rate 1/2 coding.

Table 5.5
Main parameters of the simulated OFDM system.

Number of subcarriers	48
OFDM symbol duration	3 μs
Guard interval	600 ns
T_{prefix}: Pre-guard interval	600 ns
$T_{postfix}$: Post-guard interval	75 ns
Subcarrier spacing	416.666 kHz
Roll-off factor β	0.025
Channel spacing	25 MHz
Occupied -3 dB bandwidth	20 MHz

Figure 5.13 shows the irreducible packet-error probabilities versus rms delay spread for an exponentially decaying multipath delay profile. No noise was present in the simulation, so all errors are caused by ISI and ICI because of multipath components with relative delays extending the guard time of the OFDM symbols. To obtain channel estimates for coherent detection, a training symbol was present at the start of each packet. All subcarrier values of this training symbol are known to the receiver, so this is the channel estimation method discussed in Section 5.2.3.

Clearly, coherent demodulation [curves (a) and (b)] performs much better than differential detection in the frequency domain. For the same data rate and packet-error probability, coherent demodulation can tolerate about three times as much delay spread as differential detection. The reason for the relatively poor performance of differential in frequency detection is the significant phase fluctuation between subcarriers. Differential detection in the frequency domain assumes that there is a negligible phase difference between two adjacent subcarriers. For delay spreads around 50 ns, however, a significant percentage of channels show several phase changes exceeding $\pi/8$ within the 48 OFDM subcarriers per symbol. Differential 8-PSK will generate two erroneous subcarriers if the phase changes more than $\pi/8$, and that explains why the error curves for 8-PSK quickly converge to 1 for delay spreads exceeding 50 ns. Differential QPSK is more robust, but still worse than coherent 16-QAM, which operates at twice the data rate. Coherent demodulation is not affected by phase changes across the subcarriers, because it uses training symbols to estimate reference phases and amplitudes of all subcarriers. The same holds for differential detection in the time domain, which will have approximately the same delay spread robustness as coherent detection.

5.3.3 Differential Amplitude and Phase Shift Keying

Traditionally, differential detection is applied to phase-modulated systems only, as it is not obvious how differential detection can be applied to amplitude-modulated systems. It is possible to use differential amplitude and phase shift keying (DAPSK), however, by using a star constellation like depicted in Figure 5.14 [10–12].

The main advantage of DAPSK is that it does not require pilot symbols to estimate a time-varying channel or a remaining local oscillator offset. It only requires a single pilot symbol to initialize the differential detection, as depicted in the Figures 5.8 and 5.11. The disadvantage, however, is a loss in SNR performance, because the minimum distance for the DAPSK constellation is clearly worse than for the corresponding square QAM constellation. Added to this is the loss of doing differential versus coherent detection, although this loss is partly compensated by the fact that DAPSK uses fewer pilot subcarriers.

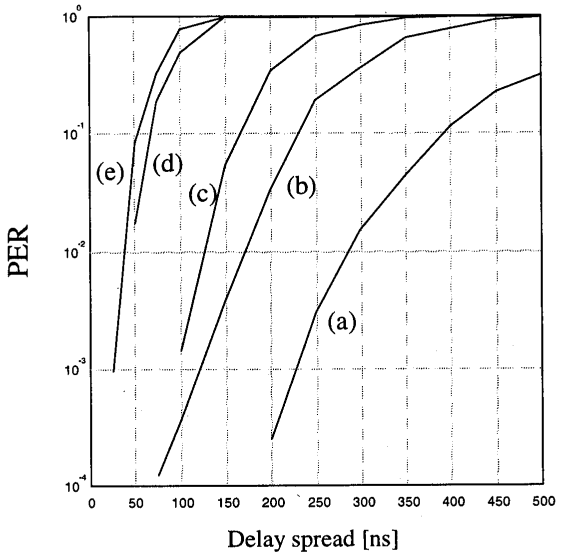

Figure 5.13 Irreducible packet error ratio versus rms delay spread, simulated for an exponentially decaying power delay profile with Rayleigh fading paths. (a) 16 Mbps with coherent QPSK and rate ½ coding, (b) 32 Mbps with coherent 16-QAM and rate ½ coding, (c) 16 Mbps with differential QPSK (in frequency domain) and rate ½ coding, (d) 24 Mbps with differential 8-PSK (in frequency domain) and rate ½ coding, (e) 32 Mbps with differential 8-PSK (in frequency domain) and rate 2/3 coding.

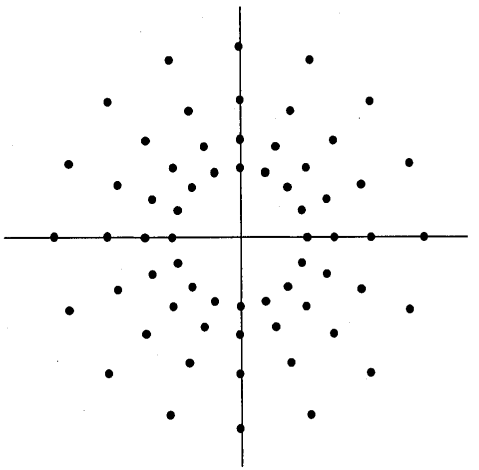

Figure 5.14 64-DAPSK constellation.

REFERENCES

[1] Sandell, M., and O. Edfors, "A Comparative Study of Pilot-Based Channel Estimators for Wireless OFDM," Research Report TULEA 1996:19, Division of Signal Processing, Luleå University of Technology, Sep. 1996.

[2] Edfors, O., M. Sandell, J. J. van de Beek, S. K. Wilson, and P. O. Börjesson, "OFDM Channel Estimation by Singular Value Decomposition," *Proceedings of the 46th IEEE Vehicular Technology Conference*, pp. 923–927, Apr. 28–May 1, 1996.

[3] Sandell, M., S. K. Wilson, and P. O. Börjesson, "Performance Analysis of Coded OFDM on Fading Channels with Non-Ideal Interleaving and Channel Knowledge," Research Report TULEA 1996:20, Division of Signal Processing, Luleå University of Technology, Sep. 1996.

[4] van de Beek, J. J., O. Edfors, M. Sandell, S. K. Wilson, and P. O. Börjesson, "On Channel Estimation in OFDM Systems," *Proceedings of the 45th IEEE Vehicular Technology Conference*, Rosemont, IL, pp. 715–719, July 1995.

[5] Proakis, J. G., *Digital Communications*, Prentice-Hall, 3rd ed., 1995.

[6] Scharf, L. L., *Statistical Signal Processing: Detection, Estimation and Time Series Analysis*, Addison-Wesley, 1991.

[7] Höher, P., "TCM on Frequency-Selective Land-Mobile Fading Channels," *Proceedings of the Tirrenia International Workshop on Digital Communications*, Tirrenia, Italy, Sep. 1991.

[8] Takanashi, H., and R. van Nee, "Merged Physical Layer Specification for the 5 GHz Band," *IEEE P802.11-98/72-r1*, March 1998.

[9] Frenger, P., and A. Svensson, "Decision directed Coherent Detection in Multicarrier Systems on Rayleigh Fading Channels," *IEEE Trans. on Veh. Technology*, Vol. 48, No. 2, pp. 490–498, 1999.

[10] Engels, V., and H. Rohling, "Multilevel Differential Modulation Techniques (64-DAPSK) for Multicarrier Transmission Techniques," *European Transactions on Telecommunication Related Technologies*, Vol. 6, No. 6, pp. 633–640, Nov.–Dec. 1995.

[11] Engels, V., and H. Rohling, "Differential Modulation Techniques for a 34 Mbit/s Radio Channel Using OFDM," *Wireless Personal Communications*, Vol. 2, pp. 29–44, 1995.

[12] May, T., H. Rohling, and V. Engels, "Performance Analysis of Viterbi Decoding for 64-DAPSK and 64-QAM Modulated Signals," *IEEE Trans. on Comm.*, Vol. 46, No. 2, pp. 182-190, February 1998.

CHAPTER 6

The Peak Power Problem

6.1 INTRODUCTION

An OFDM signal consists of a number of independently modulated subcarriers, which can give a large peak-to-average power (PAP) ratio when added up coherently. When N signals are added with the same phase, they produce a peak power that is N times the average power. This effect is illustrated in Figure 6.1. For this example, the peak power is 16 times the average value. The peak power is defined as the power of a sine wave with an amplitude equal to the maximum envelope value. Hence, an unmodulated carrier has a PAP ratio of 0 dB. An alternative measure of the envelope variation of a signal is the *Crest factor*, which is defined as the maximum signal value divided by the rms signal value. For an unmodulated carrier, the Crest factor is 3 dB. This 3 dB difference between PAP ratio and Crest factor also holds for other signals, provided that the center frequency is large in comparison with the signal bandwidth.

A large PAP ratio brings disadvantages like an increased complexity of the analog-to-digital and digital-to-analog converters and a reduced efficiency of the RF power amplifier. To reduce the PAP ratio, several techniques have been proposed, which basically can be divided in three categories. First, there are signal distortion techniques, which reduce the peak amplitudes simply by nonlinearly distorting the OFDM signal at or around the peaks. Examples of distortion techniques are clipping, peak windowing and peak cancellation. The second category is coding techniques that use a special forward-error correcting code set that excludes OFDM symbols with a large PAP ratio. The third technique is based on scrambling each OFDM symbol with different scrambling sequences and selecting that sequence that gives the smallest PAP ratio. This chapter discusses all of these techniques, but first makes an analysis of the PAP ratio distribution function. This will give a better insight in the PAP problem and will explain why PAP reduction techniques can be quite effective.

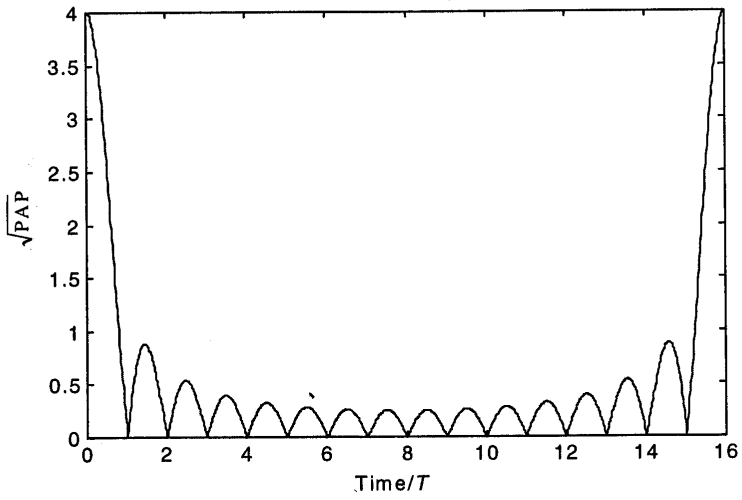

Figure 6.1 Square root of peak-to-average power ratio for a 16-channel OFDM signal, modulated with the same initial phase for all subchannels.

6.2 DISTRIBUTION OF THE PEAK-TO-AVERAGE POWER RATIO

For one OFDM symbol with N subcarriers, the complex baseband signal can be written as

$$x(t) = \frac{1}{\sqrt{N}} \sum_{n=1}^{N} a_n \exp(j\omega_n t) \tag{6.1}$$

Here, a_n are the modulating symbols. For QPSK, for instance, $a_n \in \{-1,1,j,-j\}$. From the central limit theorem it follows that for large values of N, the real and imaginary values of $x(t)$ become Gaussian distributed, each with a mean of zero and a variance of 1/2. The amplitude of the OFDM signal therefore has a Rayleigh distribution, while the power distribution becomes a central chi-square distribution with two degrees of freedom and zero mean, with a cumulative distribution given by

$$F(z) = 1 - e^{-z} \tag{6.2}$$

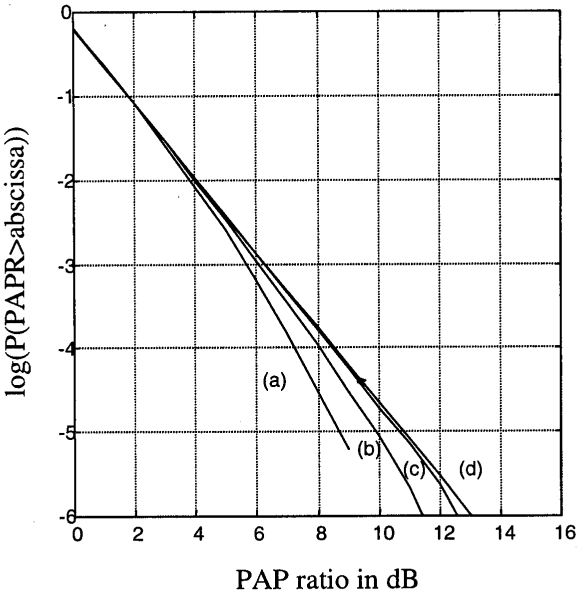

Figure 6.2 PAP distribution of an OFDM signal with (a) 12, (b) 24, (c) 48 and (d) an infinite number of subcarriers (pure Gaussian noise). Four times oversampling used in simulation, total number of simulated samples = 12 million.

Figure 6.2 shows the probability that the PAP ratio exceeds a certain value. We can see that the curves for various numbers of subcarriers are close to a Gaussian distribution (d) until the PAP value comes within a few dB from the maximum PAP level of 10log$N$, where N is the number of subcarriers.

What we want to derive now is the cumulative distribution function for the peak power per OFDM symbol. Assuming the samples are mutually uncorrelated—which is true for non-oversampling—the probability that the PAP ratio is below some threshold level can be written as

$$P(PAPR \le z) = F(z)^N = \left(1 - \exp(-z)\right)^N \tag{6.3}$$

This theoretical derivation is plotted against simulated values in Figure 6.3 for different values of N.

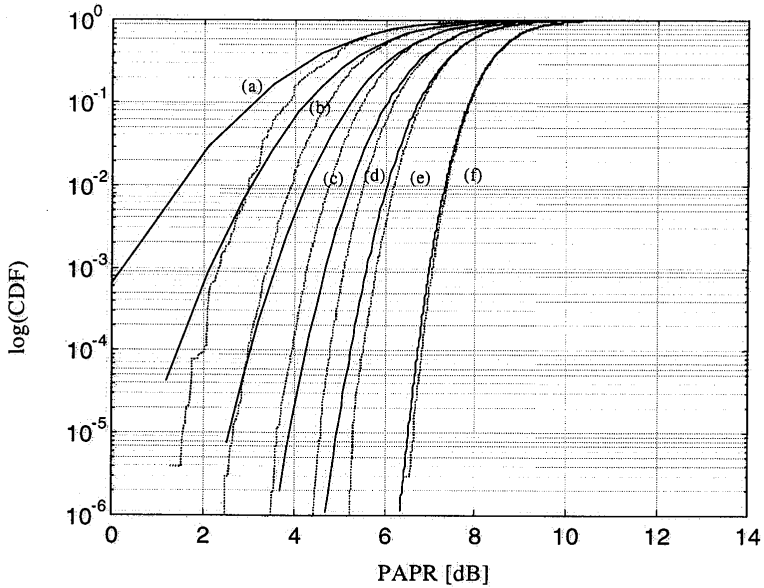

Figure 6.3 PAP distribution without oversampling for a number of subcarriers of (a) 16, (b) 32, (c) 64, (d) 128, (e) 256, and (f) 1024 (dotted lines are simulated).

The assumption made in deriving (6.3) that the samples should be mutually uncorrelated is not true anymore when oversampling is applied. Because it seems quite difficult to come up with an exact solution for the peak power distribution, we propose an approximation by assuming that the distribution for N subcarriers and oversampling can be approximated by the distribution for αN subcarriers without oversampling, with α larger than one. Hence, the effect of oversampling is approximated by adding a certain number of extra independent samples. The distribution of the PAP ratio is then given by

$$P(PAPR \le z) = \left(1 - \exp(-z)\right)^{\alpha \cdot N} \tag{6.4}$$

In Figure 6.4, the PAP distribution for different amounts of carriers is given for $\alpha = 2.8$. The dotted lines are simulated curves. We see in Figure 6.4 that Equation (6.4) is quite accurate for N>64. For large values of the cumulative distribution function close to one (>0.5), however, (6.3) is actually more accurate.

From Figure 6.4, we can deduce that coding techniques to reduce the PAP ratio may be a viable option, as reasonable coding rates are possible for a PAP ratio around 4 dB. For 64 subcarriers, for instance, about 10^{-6} of all possible QPSK symbols have a PAP ratio of less than 4.2 dB. This means that only 20 out of a total of 128 bits would be lost if only the symbols with a low PAP ratio would be transmitted. However, the main problem with this approach is to find a coding scheme with a reasonable coding rate ($\geq$ 1/2) that produces only these low PAP ratio symbols and that also has

reasonable error correcting properties. Section 6.5 describes a solution to this problem.

A different approach to the PAP problem is to use the fact that because large PAP ratios occur only infrequently, it is possible to remove these peaks at the cost of a slight amount of self-interference. Now, the challenge is to keep the spectral pollution of this self-interference as small as possible. Clipping is one example of a PAP reduction technique creating self interference. In the next sections, two other techniques are described which have better spectral properties than clipping.

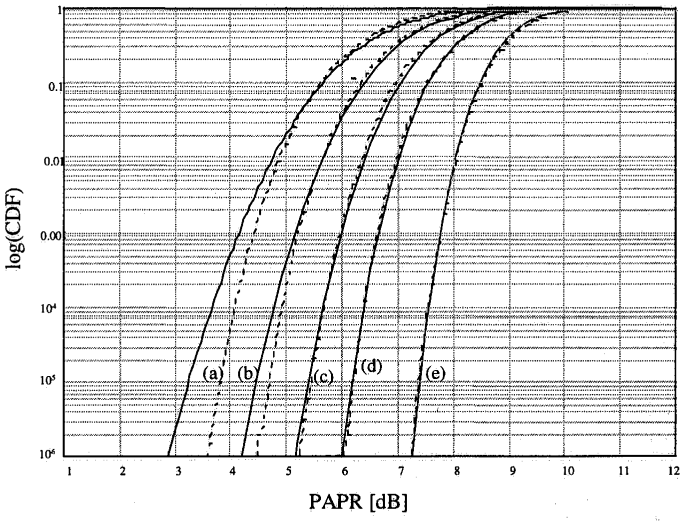

Figure 6.4 Cumulative distribution function of the PAPR for a number of subcarriers of (a) 32, (b) 64, (c) 128, (d) 256, and (e) 1,024. Solid lines are calculated; dotted lines are simulated.

6.3 CLIPPING AND PEAK WINDOWING

The simplest way to reduce the PAP ratio is to clip the signal, such that the peak amplitude becomes limited to some desired maximum level. Although clipping is definitely the simplest solution, there are a few problems associated with it. First, by distorting the OFDM signal amplitude, a kind of self-interference is introduced that degrades the BER. Second, the nonlinear distortion of the OFDM signal significantly increases the level of the out-of-band radiation. The latter effect can be understood easily by viewing the clipping operation as a multiplication of the OFDM signal by a rectangular window function that is 1 if the OFDM amplitude is below a threshold and smaller than 1 if the amplitude needs to be clipped. The spectrum of the clipped OFDM signal is found as the input OFDM spectrum convolved with the spectrum of the window function. The out-of-band spectral properties are mainly determined by the

wider spectrum of the two, which is the spectrum of the rectangular window function. This spectrum has a very slow rolloff that is inversely proportional to the frequency.

To remedy the out-of-band problem of clipping, a different approach is to multiply large signal peaks with a certain nonrectangular window. In [1], a Gaussian shaped window is proposed for this, but in fact any window can be used, provided it has good spectral properties. To minimize the out-of-band interference, ideally the window should be as narrowband as possible. On the other hand, the window should not be too long in the time domain, because that implies that many signal samples are affected, which increases the BER. Examples of suitable window functions are the cosine, Kaiser, and Hamming windows. Figure 6.5 gives an example of reducing the large peaks in OFDM with the use of windowing.

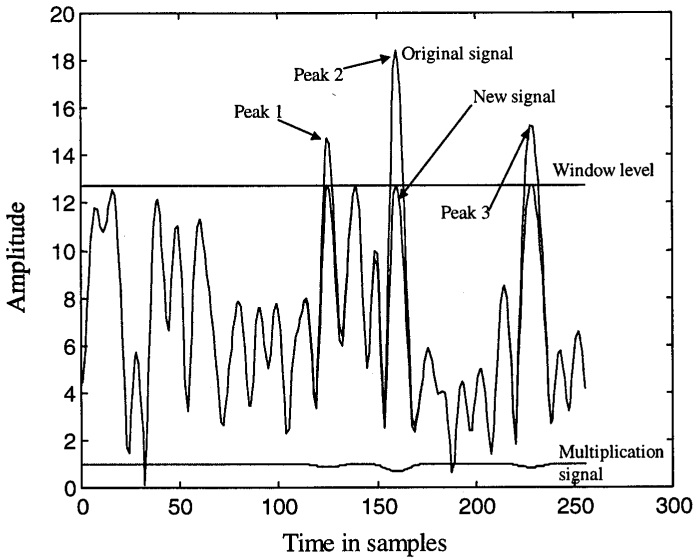

Figure 6.5 Windowing an OFDM time signal.

In Figure 6.6, the difference between clipping the signal and windowing the signal can be seen. Figure 6.7 shows how the spectral distortion can be decreased by increasing the window width.

Figure 6.8 shows PER curves with and without clipping, using a rate 1/2 convolutional code with constraint length 7. The simulated OFDM signal used 48 subcarriers with 16-QAM. The plots demonstrate that nonlinear distortion only has a minor effect on the PER; the loss in SNR is about 0.25 dB when the PAP ratio is decreased to 6 dB. When peak windowing is applied, the results are slightly worse; see Figure 6.9. This is caused by the fact that peak windowing distorts a larger part of the signal than clipping for the same PAP ratio.

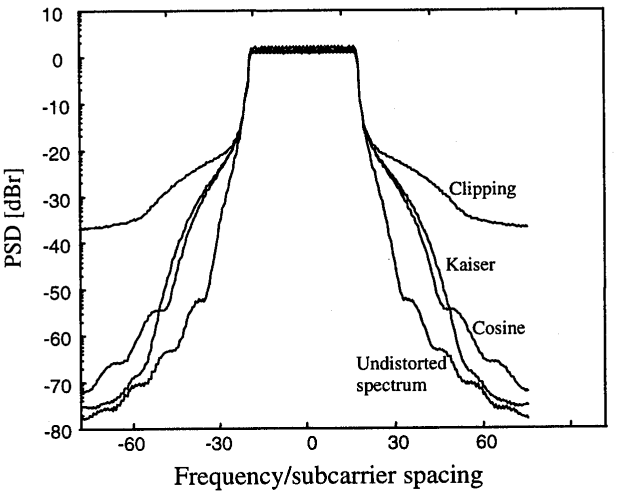

Figure 6.6 Frequency spectrum of an OFDM signal with 32 subcarriers with clipping and peak windowing at a threshold level of 3 dB above the rms amplitude.

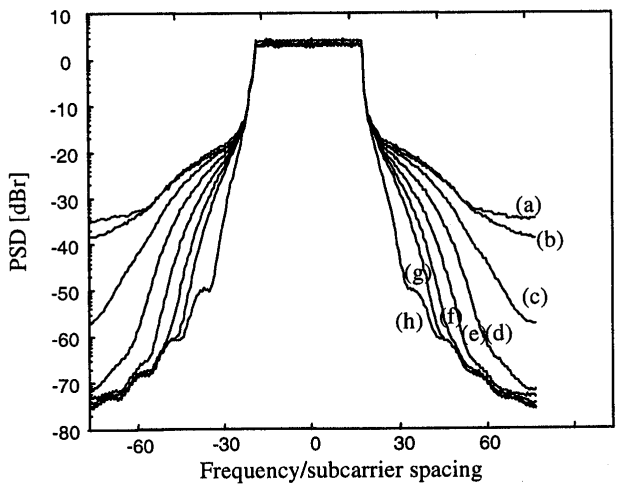

Figure 6.7 Frequency spectrum of an OFDM signal with 32 subcarriers with peak windowing at a threshold level of 3 dB above the rms amplitude. Symbol length is 128 samples (4 times oversampled) and window length is (a) 3, (b) 5, (c) 7, (d) 9, (e) 11, (f) 13, and (g) 15 samples. Curve (h) is the ideal OFDM spectrum.

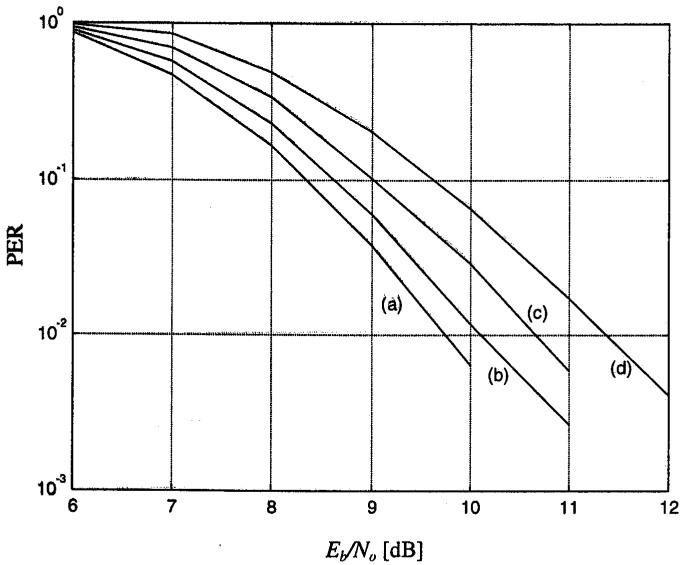

Figure 6.8 Packet error ratio versus E_b/N_o for 64 byte packets in AWGN. OFDM signal is clipped to a PAP ratio of (a) 16 (= no distortion), (b) 6, (c) 5, and (d) 4 dB.

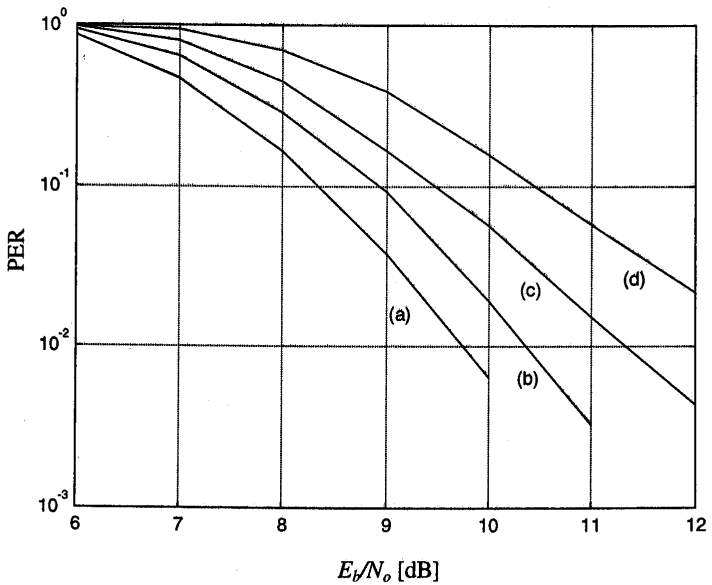

Figure 6.9 PER versus E_b/N_o for 64-byte packets in AWGN. Peak windowing is applied with a window width of 1/16 of the FFT duration. The PAP ratio is reduced to (a) 16 (= no distortion), (b) 6, (c) 5, and (d) 4 dB.

6.3.1 Required Backoff with a Non-Ideal Power Amplifier

The previous section demonstrated that peak windowing is very effective in reducing the PAP ratio. This does not immediately tell us, however, what backoff is required for a practical power amplifier to attain an acceptable level of out-of-band radiation. The backoff is defined here as the ratio of the output power and the maximum output power (saturation power) with a sinusoidal input signal. Another definition that is frequently used in the literature uses the power at the 1-dB compression point instead of the saturation power. Because the 1-dB compression point is typically 1 to 3 dB lower than the maximum power level, depending on the amplifier transfer function, the backoff values according to the latter definition are 1 to 3 dB smaller than the values mentioned in this section.

To simulate a power amplifier, the following model is used for the AM/AM conversion [2]:

$$g(A) = \frac{A}{\left(1 + A^{2p}\right)^{\frac{1}{2p}}} \tag{6.5}$$

The AM/PM conversion of a solid-state power amplifier is small enough to be neglected. Figure 6.10 gives some examples of the transfer function for various values of p. A good approximation of existing amplifiers is obtained by choosing p in the range of 2 to 3 [2]. For large values of p, the model converges to a clipping amplifier that is perfectly linear until it reaches its maximum output level.

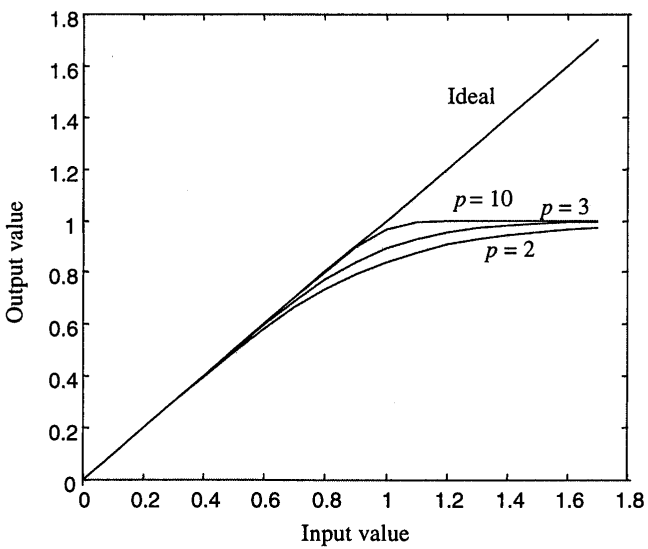

Figure 6.10 Rapp's model of AM/AM conversion.

Figure 6.11 shows the output spectra of an undistorted OFDM signal and the spectra of two distorted signals, assuming a highly linear amplifier model (p = 10 in (6.5). The backoff relative to the maximum output power was determined such that any significant distortion of the spectrum is at least 50 dB below the in-band spectral density. In this case, peak windowing gives a gain of almost 3 dB in the required backoff relative to clipping. This difference in backoff is much less than the difference in PAP ratio at the input of the power amplifier; without peak windowing, the PAP ratio is about 18 dB for the OFDM signal with 64 subcarriers. With peak windowing, this PAP ratio is reduced to approximately 5 dB. Hence, for the latter case, it is clear that the backoff of a highly linear amplifier must be slightly above this 5 dB to achieve a minimal spectral distortion. It is not true, however, that without peak windowing, the backoff must be in the order of 18 dB for the same amount of distortion as with peak windowing. The reason is that there is little energy in the signal parts that have a relatively large PAP ratio, so it does not affect the spectrum that much if those parts are distorted. After peak windowing or any other PAP reduction technique, however, a significant part of the signal samples are close to the maximum PAP ratio (e.g., 5 dB); in this case, any distortion of samples that is a dB or so below this maximum produces more spectral distortion than clipping the original OFDM signal at 10 dB below its maximum PAP level, simply because for the latter, a much smaller fraction of the signal is affected. Thus, the lower the PAP ratio is made by PAP-reduction techniques, the less tolerant the signal becomes against nonlinearities in the area of its maximum PAP ratio.

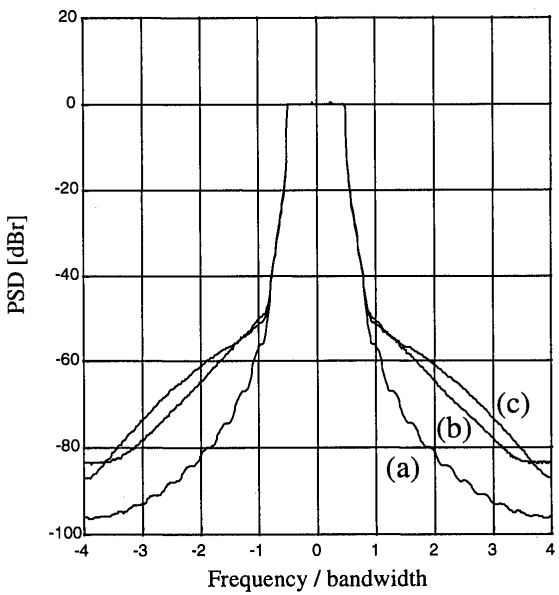

Figure 6.11 (a) Ideal OFDM spectrum for 64 subcarriers, (b) spectrum after highly linear amplifier (Rapp's parameter p = 10) with 8.7-dB backoff, (c) spectrum using peak windowing with 5.9-dB backoff.

Figure 6.12 shows OFDM spectra for a more realistic amplifier model with $p = 3$. The target for undesired spectrum distortion has now been set to a less stringent level of 30 dB below the in-band density. The difference in backoff with and without peak windowing is now reduced to 1 dB. This demonstrates that the more spectral pollution can be tolerated, the less gain can be achieved with PAP reduction techniques.

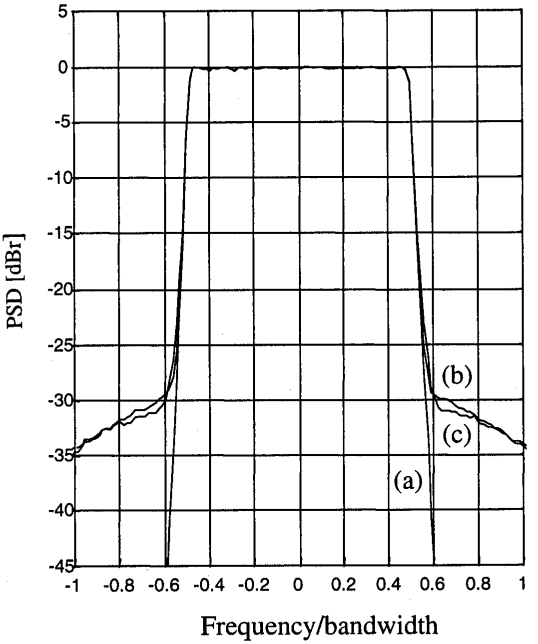

Figure 6.12 (a) Ideal OFDM spectrum for 64 subcarriers, (b) plain OFDM with 6.3-dB backoff and Rapp's parameter $p = 3$, (c) peak windowing with 5.3-dB backoff.

Figure 6.13 shows similar plots as Figure 6.12, but now for 256 subcarriers. This demonstrates that the required backoff with or without peak windowing is almost independent from the number of subcarriers, as long as this number is large compared with 1. In fact, the difference in backoff with and without peak windowing reduced slightly to 0.8 dB by going from 64 to 256 subcarriers.

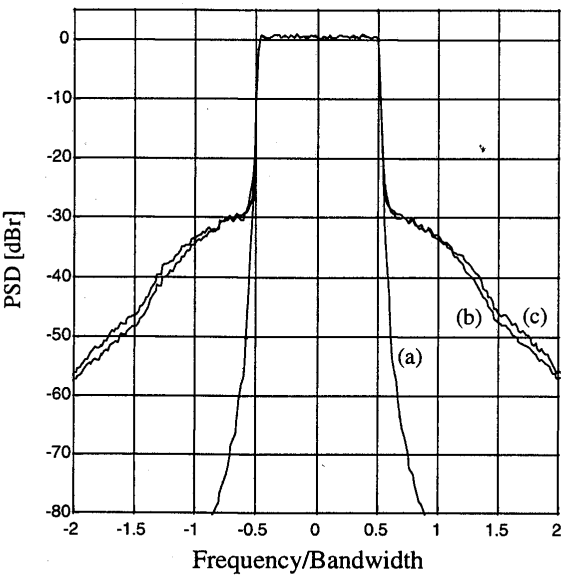

Figure 6.13 (a) Ideal OFDM spectrum for 256 subcarriers, (b) plain OFDM with 6.3-dB backoff and Rapp's parameter $p = 3$, and (c) peak windowing with 5.5-dB backoff.

6.3.2 Coding and Scrambling

A disadvantage of distortion techniques is that symbols with a large PAP ratio suffer more degradation, so they are more vulnerable to errors. To reduce this effect, forward-error correction coding can be applied across several OFDM symbols. By doing so, errors caused by symbols with a large degradation can be corrected by the surrounding symbols. In a coded OFDM system, the error probability is no longer dependent on the power of individual symbols, but rather on the power of a number of consecutive symbols. As an example, assume that the forward-error correction code produces an error if more than 4 out of every 10 symbols have a PAP ratio exceeding 10 dB[1]. Further, assume that the probability of a PAP ratio larger than 10 dB is 10^{-3}. Then, the error probability of the peak cancellation technique is $1-\sum_{i=0}^{3}\binom{10}{i}(10^{-3})^{i}(1-10^{-3})^{10-i} \cong 2\cdot 10^{-10}$, which is much less than the 10^{-3} in case no forward-error correction coding is used.

Although such a low symbol error probability may be good enough for real-time circuit-switched traffic, such as voice, it may still cause problems for packet data. A packet with too many large PAP ratio symbols will have a large probability of error. Such packets occur only very infrequently, as shown above, but when they occur, they

[1] The simplifying assumption is made here that 4 symbols with reduced power always result in an error, while in reality there is always a certain error probability < 1, depending on the SNR.

may never come through, because every retransmission of the packet has the same large error probability. To solve this problem, standard scrambling techniques can be used to ensure that the transmitted data between initial transmission and retransmissions are uncorrelated. To achieve this, the scrambler has to use a different seed for every transmission, which can be realized for instance by simply adding one to the seed after every transmission. Further, the length of the scrambling sequence has to be in the order of the number of bits per OFDM symbol to guarantee uncorrelated PAP ratios for different seeds. Different scrambling in every transmission will then guarantee independent PAP ratios for the OFDM symbols in retransmissions and hence, independent error probabilities. For example, if the probability of a worst case packet is 10^{-6}, the probability that it does not come through within two transmissions is 10^{-12}.

6.4 PEAK CANCELLATION

The key element of all distortion techniques is to reduce the amplitude of samples whose power exceeds a certain threshold. In the case of clipping and peak windowing, this was done by a nonlinear distortion of the OFDM signal, which resulted in a certain amount of out-of-band radiation. This undesirable effect can be avoided by doing a linear peak cancellation technique, whereby a time-shifted and scaled reference function is subtracted from the signal, such that each subtracted reference function reduces the peak power of at least one signal sample. By selecting an appropriate reference function with approximately the same bandwidth as the transmitted signal, it can be assured that the peak power reduction does not cause any out-of-band interference. One example of a suitable reference signal is a *sinc function*. A disadvantage of a sinc function is that it has an infinite support. Hence, for practical use, it has to be time-limited in some way. One way to do this without creating unnecessary out-of-band interference is multiplication by a windowing function; for instance, a raised cosine window. Figure 6.14 shows an example of a reference function, obtained by multiplication of a sinc function and a raised cosine window. If the windowing function is the same as used for windowing of the OFDM symbols, then it is assured that the reference function has the same bandwidth as the regular OFDM signals. Hence, peak cancellation will not degrade the out-of-band spectrum properties. By making the reference signal window narrower, a tradeoff can be made between less complexity of the peak cancellation calculations and some increase of the out-of-band power. The peak cancellation method was first published in [3], while later it was independently described in [4].

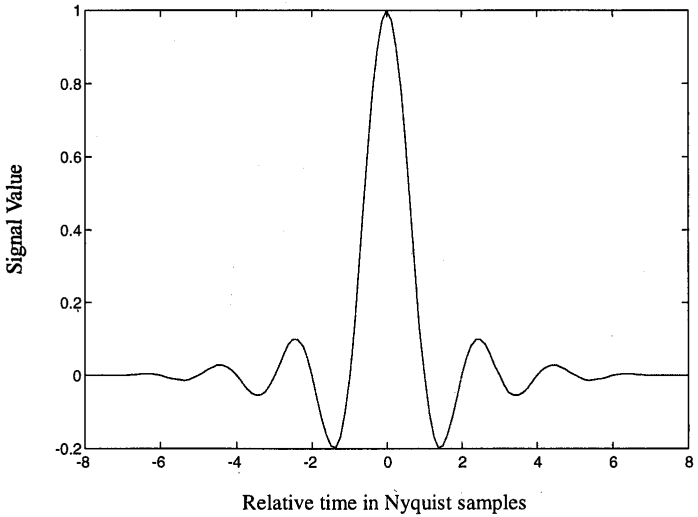

Figure 6.14 Sinc reference function, windowed with a raised cosine window.

Peak cancellation can be done digitally after generation of the digital OFDM symbols. It involves a peak power (or peak amplitude) detector, a comparator to see if the peak power exceeds some threshold, and a scaling of the peak and surrounding samples. Figure 6.15 shows the block diagram of an OFDM transmitter with peak cancellation. Incoming data are first coded and converted from a serial bit stream to blocks of N complex signal samples. On each of these blocks, an IFFT is performed. Then, a cyclic prefix is added, extending the symbol size to $N + N_G$ samples. After parallel-to-serial conversion, the peak cancellation procedure is applied to reduce the PAP ratio. It is also possible to do peak cancellation immediately after the IFFT and before the cyclic prefix and windowing. Except for the peak cancellation block, there is further no difference with a standard OFDM transmitter. For the receiver, there is no difference at all, so any standard OFDM receiver can be used.

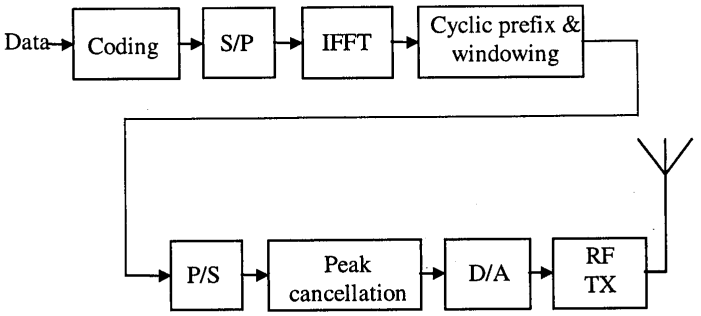

Figure 6.15 OFDM transmitter with peak cancellation.

In the previous figures, the peak cancellation was done after parallel-to-serial conversion of the signal. It is also possible to do the cancellation immediately after the IFFT, as depicted in Figure 6.16. In this case, the cancellation is done on a symbol-by-symbol basis. An efficient way to generate the cancellation signal without using a stored reference function is to use a lowpass filter in the frequency domain. In Figure 6.16, for each OFDM symbol, it is detected which samples exceed some predefined amplitude. Then, for each signal peak, an impulse is generated whose phase is equal to the peak phase and whose amplitude is equal to the peak amplitude minus the desired maximum amplitude. The impulses are then lowpass filtered on a symbol-by-symbol basis. Lowpass filtering is achieved in the frequency domain by taking the FFT, setting all outputs to zero whose frequencies exceed the frequency of the highest subcarrier, and then transforming the signal back by an IFFT.

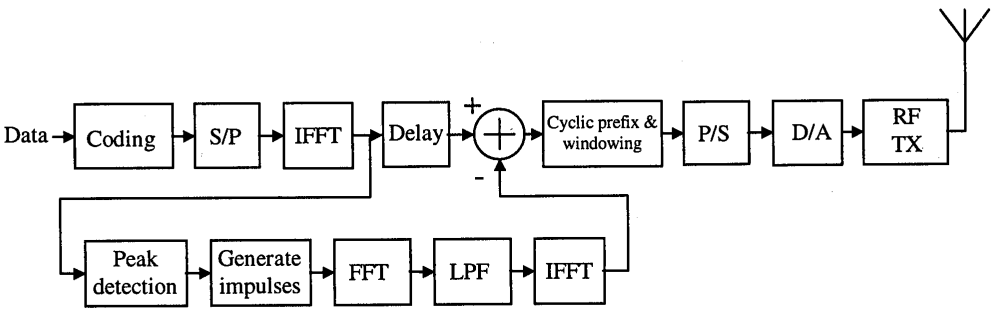

Figure 6.16 Peak Cancellation using FFT/IFFT to generate cancellation signal.

Figure 6.17 shows an example of the cyclic reference function that is used in all methods that apply cancellation *before* adding the cyclic prefix and windowing. In fact, this reference signal itself is a valid OFDM signal, which is obtained in the case of an all-ones input to the IFFT.

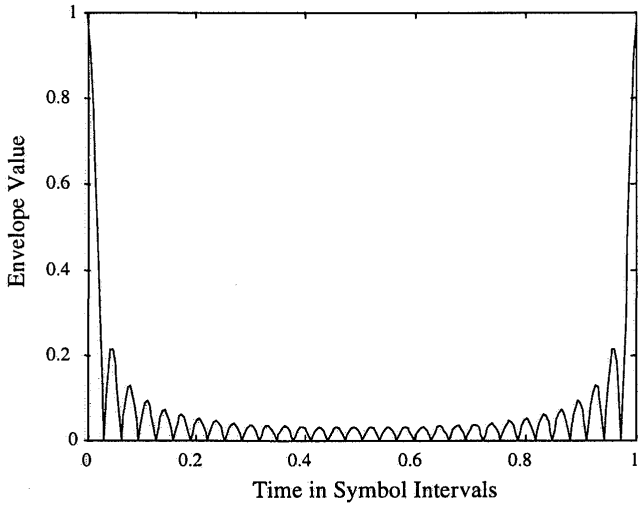

Figure 6.17 Envelope of cyclic reference function.

Figure 6.18 shows an example of the signal envelopes of one arbitrary OFDM symbol and the corresponding cancellation signal. In this particular case, the cancellation signal actually consists of two separate sinc functions, because one sinc function is not wide enough to reduce the peak in this example. After subtraction, the peak amplitude is reduced to a maximum of 3 dB above the rms value; see Figure 6.19.

As an example of the peak cancellation technique, Figure 6.20 shows simulated power spectral densities for an OFDM system with 32 carriers. Without clipping or peak cancellation, the worst case PAP ratio of this system is 15 dB, and the undistorted spectrum is depicted by curve (a). If the signal is clipped such that the PAP ratio reduces to 4 dB, a significant spectral distortion is visible; see curve (c). When peak cancellation is applied (b), a negligible distortion is present for the same PAP ratio of 4 dB.

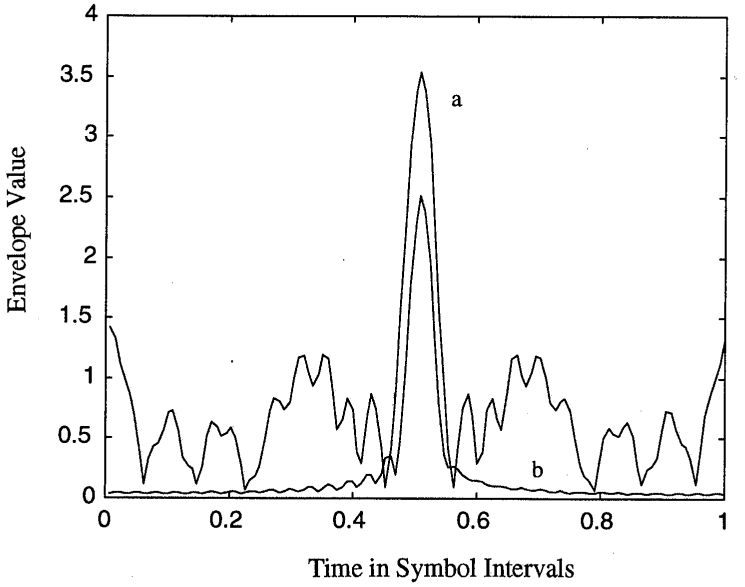

Figure 6.18 (a) OFDM symbol envelope, (b) cancellation signal envelope.

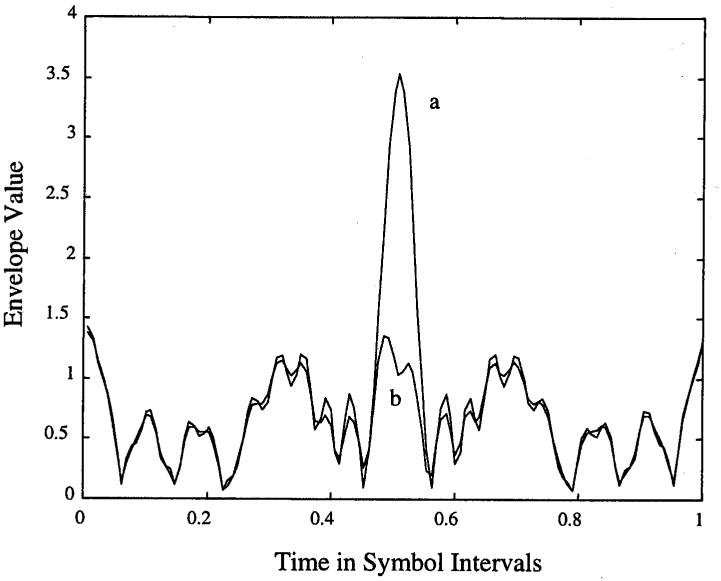

Figure 6.19 (a) OFDM symbol envelope, (b) signal envelope after peak cancellation.

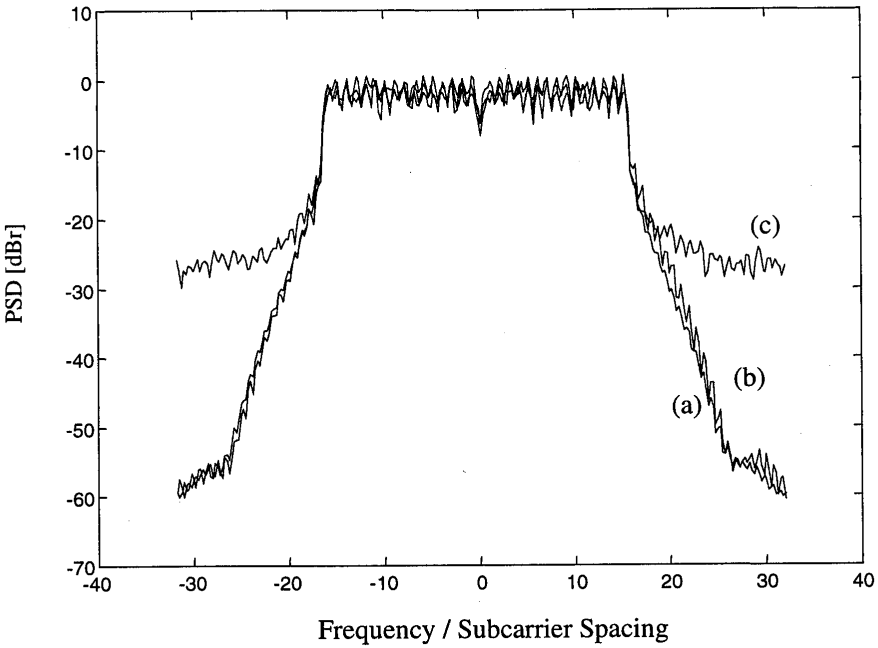

Figure 6.20 Power spectral density for (a) undistorted spectrum with 32 subcarriers, PAP = 15dB, (b) spectrum after peak cancellation to PAP = 4 dB, and (c) clipping to PAP = 4 dB. Reference cancellation function has a length equal to ¼ of the length of an OFDM symbol.

The effect of the peak cancellation on the PER is depicted in Figure 6.21. A rate 1/2, constraint length 7 convolutional code is used to encode the input bits. The coded bits are then modulated onto 48 OFDM subcarriers using 16-QAM. The curves show an SNR degradation of about 0.6 dB in AWGN when peak cancellation is used to reduce the PAP ratio to 6 dB.

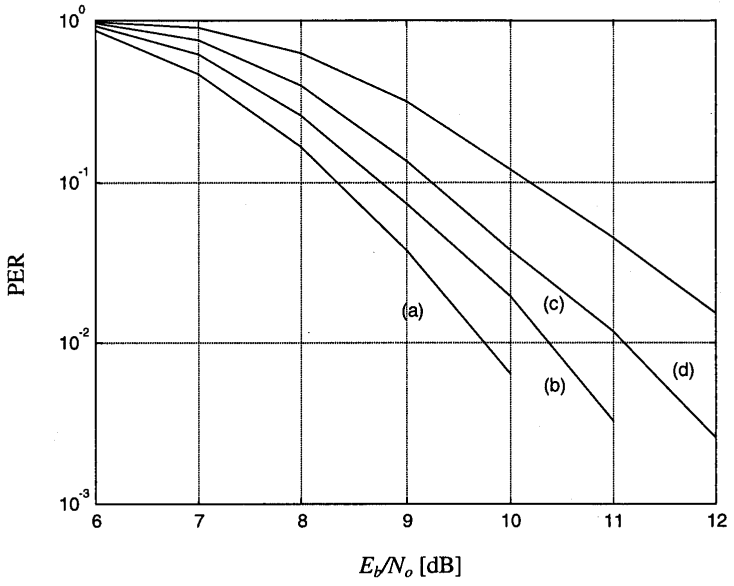

Figure 6.21 PER versus E_b/N_o for 64-byte packets in AWGN. Peak cancellation is applied to reduce the PAP ratio to (a) 16 (= no distortion), (b) 6, (c) 5, and (d) 4 dB.

At first sight, peak cancellation seems to be a fundamentally different approach than clipping or peak windowing. It can be shown, however, that peak cancellation is in fact almost identical to clipping followed by filtering. If a sampled OFDM signal *x(n)* is clipped to reduce the PAP ratio, the output signal *r(n)* can be written as

$$r(n) = x(n) - \sum_i a_i e^{j\varphi_i} \delta(n - \tau_i) \tag{6.6}$$

Here, a_i, φ_i, and τ_i are the amplitude, phase, and delay of the correction that is applied to the *i*th sample in order to reach the desired clipping level. Hence, it is possible to describe clipping as a linear process, even though this is not the way clipping is performed in practice. Now suppose the clipped signal is filtered by an ideal lowpass filter with an impulse response of $\text{sinc}(\pi nT)$, where T is chosen such that the filter bandwidth is equal or larger than the bandwidth of the OFDM signal. The filtered output is given by

$$r'(n) = x'(n) - \sum_i a_i e^{j\varphi_i} \cdot \text{sinc}(\pi T(n - \tau_i)) \tag{6.7}$$

This expression is identical to a peak cancellation operation, with the only exception that with peak cancellation, a sum of sinc functions is subtracted from the unfiltered OFDM signal *x(n)*, while in (6.7) we see a filtered signal *x'(n)*. In practice, however, also for peak cancellation, the OFDM signal needs to be filtered anyway to

remove aliasing after the digital-to-analog conversion. Hence, for practical purposes, it may be concluded that peak cancellation has the same effect as clipping followed by filtering, which was proposed as a PAP reduction technique in [5].

As a final comparison of the three described signal distortion techniques, Figure 6.22 shows the PERs for an OFDM system with 48 subcarriers for which the PAP ratio is reduced to 5 dB. In addition to the three PAP reduction technique, the nonlinear amplifier model described in section 6.3.1 was applied such that the output backoff of the transmitted OFDM signal was 6 dB. We can see from the figure that clipping (without filtering) performs slightly better than peak cancellation, and that peak windowing is slightly worse than peak cancellation.

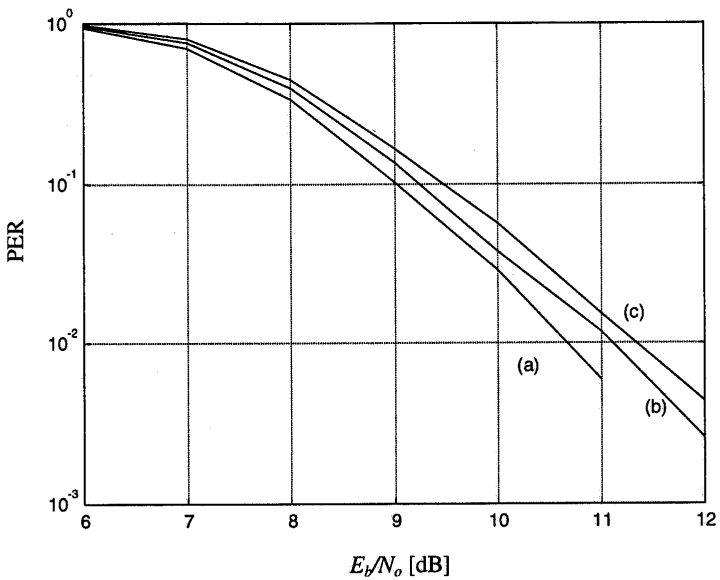

Figure 6.22 Packet error ratio versus E_b/N_o for 64-byte packets in AWGN. PAP ratio is reduced to 5 dB by (a) clipping, (b) peak cancellation, and (c) peak windowing.

6.5 PAP REDUCTION CODES

As Section 6.2 shows, only a small fraction of all possible OFDM symbols has a bad peak-to-average power ratio. This suggests another solution to the PAP problem, based on coding. The PAP ratio can be reduced by using a code which only produces OFDM symbols for which the PAP ratio is below some desirable level. Of course, the smaller the desired PAP level, the smaller the achievable code rate is. Section 6.2, however, already demonstrated that for a large number of subcarriers, a reasonable coding rate larger than 3/4 can be achieved for a PAP level of 4 dB. In [6], it was found that for eight channels, a rate 3/4 code exists that provides a maximum PAP ratio of 3 dB. The results in [6] are based on an exhaustive search through all possible (QPSK)

codewords. Unfortunately, these results only tell us that there exists a large number of code words; it does not say if there exists a structured way of encoding and decoding to generate a large part of these code words, nor what the minimum distance properties of the code are. However, [6] did mention the interesting fact that a large part of the codes found are *Golay complementary sequences*, which opened the way to a structured way of generating PAP-reduction codes. Golay complementary sequences are sequence pairs for which the sum of autocorrelation functions is zero for all delay shifts unequal to zero [7–9]. It was already mentioned in [10] that the correlation properties of complementary sequences translate into a relatively small PAP-ratio of 3 dB when the codes are used to modulate an OFDM signal. Based on all these hints towards Golay sequences, [11] presented a specific subset of Golay codes together with decoding techniques that combined peak-to-average power reduction with good forward-error correction capabilities. Based on this work, Golay codes were actually implemented in a prototype 20-Mbps OFDM modem for the European Magic WAND project [12]. Fundamental studies on the coding properties of Golay sequences appeared in [13–16], proving code set sizes, distance properties, the relation to Reed-Muller codes, and many more interesting details.

A sequence x of length N is said to be complementary to another sequence y if the following condition holds on the sum of both autocorrelation functions:

$$\sum_{k=0}^{N-1}(x_k x_{k+i} + y_k y_{k+i}) = 2N, \quad i = 0$$
$$= 0, \quad i \neq 0 \tag{6.8}$$

By taking the Fourier transforms of both sides of (6.8), the above condition is translated into

$$|X(f)|^2 + |Y(f)|^2 = 2N \tag{6.9}$$

Here, $|X(f)|^2$ is the power spectrum of x, which is the Fourier transform of its autocorrelation function. The discrete Fourier transform $X(f)$ is defined as

$$X(f) = \sum_{k=0}^{N-1} x_k e^{-j2\pi k f T_s} \tag{6.10}$$

Here, T_s is the sampling interval of the sequence x. From the spectral condition (6.9), it follows that the maximum value of the power spectrum is bounded by $2N$:

$$|X(f)|^2 \leq 2N \tag{6.11}$$

Because the average power of $X(f)$ (6.10) is equal to N, assuming that the power of the sequence x is equal to 1, the PAP ratio of $X(f)$ is bounded as

$$\text{PAP ratio} \leq \frac{2N}{N} = 2 \tag{6.12}$$

In an OFDM transmission, normally the IFFT is applied to the input sequence x. However, because the IFFT is equal to the conjugated FFT scaled by $1/N$, the conclusion that the PAP ratio is upper bounded by 2 is also valid when $X(f)$ is replaced by the inverse Fourier transform of the sequence x. Hence, by using a complementary code as input to generate an OFDM signal, it is guaranteed that the PAP ratio does not exceed 3 dB. Figure 6.23 shows a typical example of an OFDM signal envelope when using a complementary sequence. For this case of 16 channels, the PAP ratio is reduced by approximately 9 dB in comparison with the uncoded case of Figure 6.1.

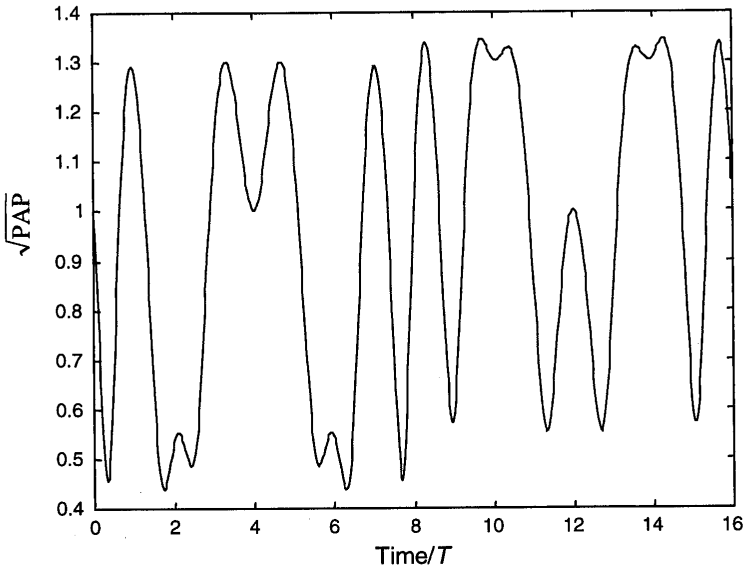

Figure 6.23 Square root of peak-to-average power ratio for a 16-channel OFDM signal, modulated with a complementary code.

6.5.1 Generating Complementary Codes

In [7–9], several coding rules are given for generating a set of complementary sequences, based upon some starting complementary pair, the *kernel*. For complementary sequences of length 2, for instance, a possible kernel is the pair 1, 1 and 1, –1. The basic coding rules for generating complementary codes from this kernel are [7, 9]:

1. Interchanging both codes,
2. Reversing and conjugating second code,
3. Phase-rotating second code,
4. Phase-rotating elements of even order in both codes,
5. Phase-rotating first code, and
6. Reversing and conjugating first code.

When rules 1 to 4 are applied, the following 16 different length 4 codes can be obtained for the case of 4 phase modulation (see Table 6.1):

Table 6.1
Length 4 complementary codes

1	1	1	-1
1	1	-1	1
1	-1	1	1
1	-1	-1	-1
1	j	1	-j
1	j	-1	j
1	-j	1	j
1	-j	-1	-j

1	1	j	-j
1	1	-j	j
1	-1	j	j
1	-1	-j	-j
1	j	j	1
1	j	-j	-1
1	-j	-j	1
1	-j	j	-1

The number of codes can be extended to 64 by applying the fifth and sixth rules, which gives the same result as applying 4 different phase shifts to the 16 codes. Hence, these 4-symbol codes can easily be generated by using a 16-word-long lookup table to encode 4 bits, followed by a phase rotation to map a total of 6 bits onto all possible complementary codes.

Unfortunately, as the previous example already indicated, the six coding rules do not unambiguously produce all complementary sequences. This makes it difficult to find the size of the code set and to find a systematic way to produce complementary sequences. Thus, some other algorithm has to be found to generate complementary codes.

[9] showed that from one set of complementary sequences, others can be generated by multiplying the original sequences with columns of the discrete Fourier transform matrix. Although [9] only mentions this method to generate sets with longer

code length by using the *Kronecker product*, it can also be used to generate different sequences with the same length, by multiplying an original sequence elementwise with columns of the DFT matrix. It is easy to show that such multiplications do not change the correlation properties. Each DFT column is a delta function in the frequency domain. Because multiplication in the time domain is equivalent to a convolution in the frequency domain, the power spectrum of a complementary sequence multiplied by a DFT column remains the same. Hence, also its correlation function, which is the Fourier transform of the power spectrum, remains the same, so that the outcome again is a complementary sequence.

Another interesting remark in [9] is that complementary sequences can be multiplied by columns of the binary *Walsh-Hadamard matrix*, without losing their complementary characteristics. Further, it is stated in [9] that "if the code is an expansion of shorter lengths, an arbitrary phase angle can be added to all elements in any orthogonal subset." These operations turn out to be very useful in generating distinct codes.

The coding algorithm for generating complementary sequences is now given by the following steps:

1. **Make a kernel**; that is, one complementary pair from which all other complementary sequences can be derived. For lengths equal to a power of two, kernels can easily be formed by using Golay's rule for length expansion. Starting with the length 2 sequence $A_1 B_1$, where $A_1 = 1$ and $B_1 = 1$, longer length codes can be formed by making $A_n B_n$ with $A_n = A_{n-1} B_{n-1}$ and $B_n = A_{n-1} - B_{n-1}$. In this way, codes of length 2^{n+1} are formed from the codes of length 2^n. For example, the following codes up to length 16 can be obtained:

$$\begin{aligned}
&\text{length 2} \;:\; A_1 B_1 = 1\ 1 \\
&\text{length 4} \;:\; A_2 B_2 = 1\ 1\ 1\ -1 \\
&\text{length 8} \;:\; A_3 B_3 = 1\ 1\ 1\ -1\ \ 1\ 1\ -1\ 1 \\
&\text{length 16} : A_4 B_4 = 1\ 1\ 1\ -1\ \ 1\ 1\ -1\ 1\ \ 1\ 1\ 1\ -1\ \ -1\ -1\ 1\ -1
\end{aligned} \tag{6.13}$$

2. **Determine the number of orthogonal subsets**. For length N codes, formed by the length expansion method described above, there are $\log_2 N$ orthogonal subsets, all of which can be given an arbitrary phase offset. The orthogonal subsets within a code are formed by all single elements, pairs, quads, and so forth, which are of even order. Thus, a length 16 code has 4 orthogonal subsets, being all even elements, pairs, quads, and one octet. All of these can be given a different phase without changing the complementary characteristics of the code. Further, it is also possible to apply an arbitrary phase shift to the entire code. Hence, a complementary code set based upon the kernel of (6.13) can be written as:

$$c = \{e^{j(\varphi_1+\varphi_2+\varphi_3+\varphi_4)}, e^{j(\varphi_1+\varphi_3+\varphi_4)}, e^{j(\varphi_1+\varphi_2+\varphi_4)}, -e^{j(\varphi_1+\varphi_4)}, e^{j(\varphi_1+\varphi_2+\varphi_3)}, e^{j(\varphi_1+\varphi_3)}, -e^{j(\varphi_1+\varphi_2)}, e^{j\varphi_1}\} \tag{6.14}$$

Notice that this code is actually implemented in a 20-Mbps OFDM modem for the Magic WAND project [12]. It is also used in the 11-Mbps IEEE 802.11 wireless LAN standard [17]. The latter is not an OFDM system, but here the benefit from using complementary sequences is in its good aperiodic autocorrelation properties, which makes it easier to build a receiver with sufficient robustness to multipath.

An alternative code description is to write the code phases as

$$\begin{bmatrix}\theta_1\\ \theta_2\\ \theta_3\\ \theta_4\\ \theta_5\\ \theta_6\\ \theta_7\\ \theta_8\end{bmatrix} = \begin{bmatrix}1&1&1&1&0\\ 1&0&1&1&0\\ 1&1&0&1&0\\ 1&0&0&1&1\\ 1&1&1&0&0\\ 1&0&1&0&0\\ 1&1&0&0&1\\ 1&0&0&0&0\end{bmatrix}\begin{bmatrix}\varphi_1\\ \varphi_2\\ \varphi_3\\ \varphi_4\\ \pi\end{bmatrix} \tag{6.15}$$

The output code is given by $\exp(j\cdot 2\pi\theta_i/M)$, where θ_i is the coded phase and M is the size of the phase constellation. For BPSK (M=2), the code set is equal to the Walsh-Hadamard codes, which is offset by the kernel—defined by the fourth column in (6.15).

3. **Finally, a transformation can be applied** that unfortunately cannot be described by simple multiplications or phase rotations. Instead, it can be described as an interleaving operation on the underlying shorter length codes that are used to make a longer length code [14]. For a length 8 sequence, for instance, two new length 8 codes can be generated by interleaving the first and second half of the original code. Interleaving the code three times reproduces the original code. In general, a code with a length of 2^n can be interleaved n–1 times before reproducing itself. The following example shows three different codes out of a length 8 code produced by interleaving:

$$\begin{aligned}&0:\ 1\ 1\ 1\ -1\ \ 1\ \ 1\ -1\ \ 1\\ &1:\ 1\ 1\ 1\ \ 1\ \ 1\ -1\ -1\ \ 1\\ &2:\ 1\ 1\ 1\ -1\ \ 1\ -1\ \ 1\ \ 1\end{aligned} \tag{6.16}$$

For a length 16 code, it turns out that except for four different codes that can be produced by interleaving the first and second half of the code, more codes can be made by simultaneously interleaving the quarters of the code, giving a total of $3 \cdot 4 = 12$ different codes. The described coding rules can now be used to determine the size of

complementary code sets. For an N-length code with M possible phases, the kernel can be multiplied by $1 + \log_2 N$ modified Walsh-Hadamard rows with M different phases. This gives a code set size of $M^{1+\log N}$. The amount of bits per codeword can be expressed as $(1 + \log_2 N)\log_2 M$. For instance, a length 8 code with four possible phases gives 8 bits per code word. The above numbers did not yet take into account the interleaving rule, which adds another $\log_2([(\log_2 N)!]/2)$ bits to the total number of bits per symbol (for $N > 4$ and N being a power of 2). Notice that the interleaving rule does not necessarily produce an integer number of bits per encoded symbol.

6.5.2 Minimum Distance of Complementary Codes

In OFDM systems, the effects of multipath are mitigated by error correction coding over the various subchannels. Thus, when using a PAP-reduction code, it would be very desirable if you could use this code also for forward-error correction. Otherwise, a separate code would be required, with the disadvantage of additional complexity and a reduction in the overall coding rate and spectral efficiency.

Therefore, the question arises as to what minimum distance the above mentioned complementary sequences have. Looking at (6.15), we can state that if this is the only generating rule used, then $N/2 + 1$ correctly received symbols are always sufficient to calculate the $1 + \log_2 N$ phases used to generate the complementary sequence. This is because with $1 + N/2$ phase observations, it is always possible to form $1 + \log_2 N$ independent equations which can be used to solve for the $1 + \log_2 N$ unknown phases. In fact, there are a certain number of combinations of $1 + \log_2 N$ independent equations. The equations are independent only if each phase—except φ_1—is present in at least one and at most $\log_2 N$ Equations. Since each phase—except φ_1—is present in exactly $N/2$ observations, $1 + N/2$ observations are sufficient to obtain at least one set of $1 + \log_2 N$ independent phase equations. Therefore, we can conclude that the minimum distance between 2 different complementary codes of length N is $N/2$ symbols, so it is possible to correct $N/4 - 1$ symbol errors or $N/2 - 1$ erasures.

The *minimum Euclidean distance*, which determines the performance in flat fading with additive noise, can be found by observing that a minimum distance between two code words is obtained if $N/2$ symbols have a minimum phase rotation of $2\pi/M$, where M is the number of phases. Thus, the minimum Euclidean distance d_{min} is

$$d_{\min} = \sqrt{\frac{N}{2}} \left\| 1 - \exp(j\frac{2\pi}{M}) \right\| \tag{6.17}$$

For instance, for 8-PSK and 8 channels, the minimum distance becomes 1.53, which is 6 dB larger than the distance of uncoded 8-PSK (= 0.765). Because the rate of the length-8 complementary codes is ½, a maximum coding gain of 3 dB can be achieved compared with uncoded 8-PSK.

The above distance calculations are only valid for complementary codes generated without using the interleaving rule. Two codes formed by interleaving generally have a distance that is less than $N/2$ symbols. For N=8, for instance, the interleaved codes (6.16) have a distance of only two symbols instead of four.

6.5.3 Maximum Likelihood Decoding of Complementary Codes

This section describes an optimal decoding technique for specific subsets of complementary codes, based on generalized Walsh-Hadamard encoding. With generalized Walsh-Hadamard coding, we mean that for a length $N = 2^n$ code, $n + 1$ phases are encoded into 2^n output phases by adding the first phase to all code phases, the second to all odd code phases, the third to all odd pairs of code phases, and so on. For a length 8 code, for instance, the phase encoding is given by (6.15). For BPSK ($M = 2$), the coding reduces to normal Walsh-Hadamard coding. For this case, the efficient fast Walsh transform can be used to realize maximum likelihood decoding. For larger constellation sizes, maximum likelihood decoding seems less trivial. In the worst case, it would require M^{n+1} Euclidean distance calculations or correlations, giving a total number of operations of NM^{n+1} (complex multiplications and additions). There is, however, quite some redundancy in the calculation of all possible correlations, just as for the binary case. This means it is possible to reduce the complexity of the maximum likelihood decoder by generalizing the fast Walsh transform to general phase constellations, as was first described in [18].

Figure 6.24 shows a butterfly that is used to calculate a 2-point binary fast Walsh transform. Using these butterflies, an N-point fast Walsh transform can be calculated with $N\log_2 N$ additions and subtractions.

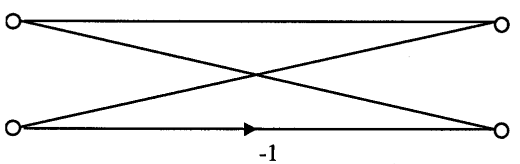

Figure 6.24 Butterfly of binary fast Walsh transform.

Now consider a 4-PSK generalized Walsh-Hadamard code. For length 2, the transform can be depicted as a butterfly with two inputs and four outputs (see Figure 6.25).

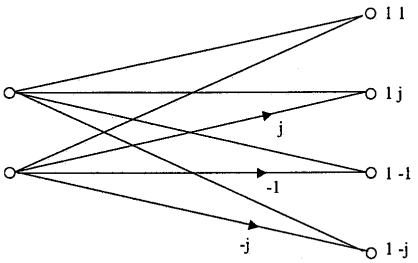

Figure 6.25 Butterfly of 4-PSK fast Walsh transform.

The right side of the butterfly shows the sequences used to correlate with the input sequence.

Using this butterfly, a transform of double length N can be constructed by doing two transforms on half of the code length, plus an additional stage of 4^{n-1} butterflies. A length 4 transform, for instance, can be constructed as depicted in the Figure 6.26. The four input points at the left are transformed into 16 output points by correlations with the complex sequences listed on the right.

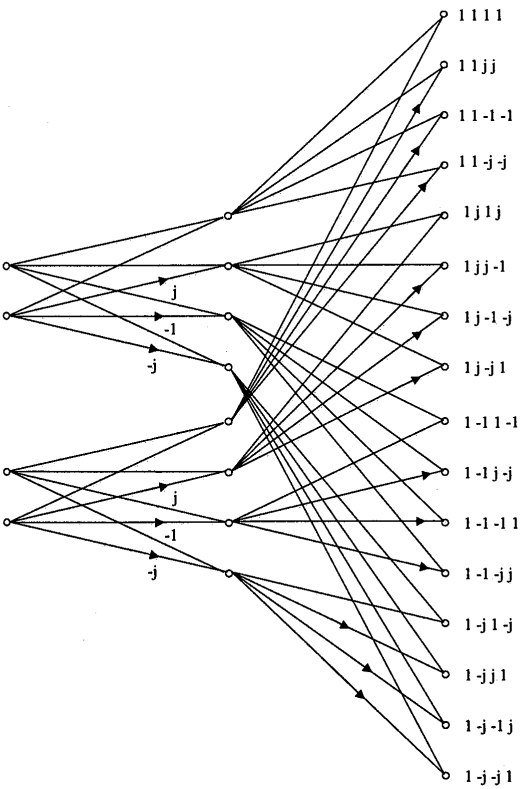

Figure 6.26 Length 4 4-PSK fast Walsh transform.

The 4-point transform can be extended to an 8-point transform by performing two length 4 transforms on two groups of 4 samples, and adding an additional stage of 16 butterflies to produce the length 8 results. Figure 6.27 shows this 8-point transform, where the first two 4-point transforms are drawn as a line to simplify the picture. In reality, each 4-point transform has 16 outputs, which are combined with the 16 outputs of the other 4-point transform in 4 different ways. Hence, the total number of outputs is 64.

There are 28 butterflies needed for a length 8 transform. Each butterfly requires four additions (the phase rotations are trivial for 4-PSK), so the total number of operations is 112 complex additions. The direct calculation method with 64 separate correlators requires 512 complex additions, so the fast transform reduces the complexity by almost a factor of 5.

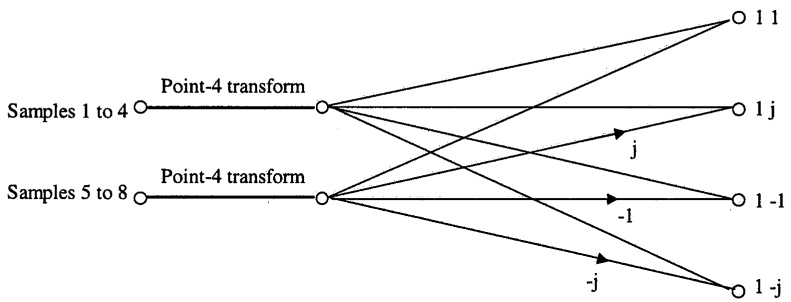

Figure 6.27 Length-8 4-PSK fast Walsh transform using length-4 transforms.

6.5.4 Suboptimal Decoding of Complementary Codes

For any coding technique to be successful, there have to be decoding techniques that are not too complex and with a performance not too far from that of optimal maximum likelihood decoding. For a complementary code for which the number of phases M is larger than 2 and the code length is larger than about 8, maximum likelihood decoding quickly becomes too complex for practical implementation. Hence, we want to find *suboptimal* decoding techniques that are less complex to implement. One way to decode the phase that is applied to all alternating elements of a complementary code is to multiply the complex odd samples with the complex conjugate of the even samples. By summing the results, we obtain a vector that has the desired phase value. The same procedure can be followed for even and odd pairs, quads, and so on. The phase that is applied to the entire code has to be found by correcting the complex samples for all other phases. For the length 8 code with complex samples x_i, the phase equations are given by

$$\begin{aligned}
\varphi_2 &= \arg\{x_1 x_2^* + x_3 x_4^* + x_5 x_6^* + x_7 x_8^*\} \\
\varphi_3 &= \arg\{x_1 x_3^* + x_2 x_4^* + x_5 x_7^* + x_6 x_8^*\} \\
\varphi_4 &= \arg\{x_1 x_5^* + x_2 x_6^* + x_3 x_7^* + x_4 x_8^*\} \\
\varphi_1 &= \arg\{x_1 e^{-j(\varphi_2+\varphi_3+\varphi_4)} + x_2 e^{-j(\varphi_3+\varphi_4)} + x_3 e^{-j(\varphi_2+\varphi_4)} + \\
&\quad x_4 e^{-j(\varphi_4)} + x_5 e^{-j(\varphi_2+\varphi_3)} + x_6 e^{-j(\varphi_3)} + x_7 e^{-j(\varphi_2)} + x_8\}
\end{aligned} \tag{6.18}$$

Here, *arg{}* means the calculation of the phase of a complex vector, and * denotes the complex conjugate. To convert the phases to bits, we have to make decisions for those constellation points that are closest to the phases found, just as we do in normal phase shift keying.

There are some alternative ways to estimate the phase of the entire code word. In (6.18), the estimated phases were used to eliminate the phase rotations caused by all phases except for φ_1. The same effect can be achieved by multiplying the received code samples with complex conjugates of y_i, where y_i is the term within the arg{} expression of φ_i in (6.18):

$$\begin{aligned}
\varphi_1 &= \arg\{x_1 y_2^* y_3^* y_4^* + x_2 y_3^* y_4^* + x_3 y_2^* y_4^* + x_4 y_4^* \\
&+ x_5 y_2^* y_3^* + x_6 y_3^* + x_7 y_2^* + x_8\}
\end{aligned} \tag{6.19}$$

The disadvantage of this method is that there is a certain noise enhancement because of the double and triple products of noisy phasors. A better estimate can be found by using only those terms that have no more than one phasor multiplication:

$$\varphi_1 = \arg\{x_4 y_4^* + x_6 y_3^* + x_7 y_2^* + x_8\} \tag{6.20}$$

Following the same argument, it is also possible to simplify (6.19) by using only terms with one or zero phase rotations:

$$\varphi_1 = \arg\{x_4 e^{-j\varphi_4} + x_6 e^{-j\varphi_3} + x_7 e^{-j\varphi_2} + x_8\} \tag{6.21}$$

The advantage of the above-described decoding technique is that it provides automatic weighting of the subchannels; erroneous channels with low amplitudes will only give a minor contribution to the phase estimates. In additive white Gaussian noise (AWGN), the described technique performs 3 dB worse than optimal maximum likelihood decoding, which can be argued as follows: the performance of maximum likelihood decoding is determined by the minimum Euclidean distance, which is four times the distance of uncoded 8-PSK for the length 8 complementary code with 8-PSK.

Looking at the decoding structure of (6.18), we can see that for each phase estimate, four or more vectors are added, which gives a 6-dB SNR improvement. Each of the added vectors, however, consists of a multiplication of two separate vectors with independent noise contributions. Hence, the detection SNR is improved by 3 dB only, as compared with 6 dB for a maximum likelihood decoding technique. Note that the difference with maximum likelihood decoding decreases in the case of frequency-selective channels. In the extreme case that four out of eight subchannels are completely lost, both will have the same symbol error probability.

Except for the soft-decision technique described above, it is also possible to do hard-decision erasure decoding. In this case, four out of eight subchannels are erased, based upon amplitude measurements obtained during training. Three subchannels can be erased arbitrarily; the fourth must be chosen such that all phase estimates in (6.18) have at least one element. Erasure decoding will fail if one of the unerased subchannels is in error. Thus, in AWGN, the bit-error probability is equal to that of uncoded 8-PSK, so there is a 6-dB loss compared with that of maximum likelihood decoding. Again, this loss is less in the case of frequency-selective channels.

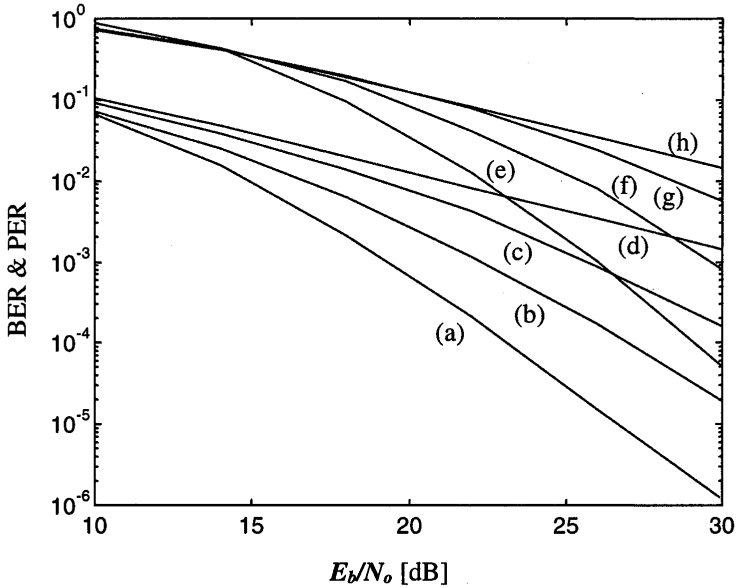

Figure 6.28 BER (a-d) and PER (e-h) versus mean E_b/N_o for delay spreads of (a) and (e) 50 ns, (b) and (f) 20 ns, (c) and (g) 10 ns, (d) and (h) 0.

Figure 6.28 shows BER and PER for single ATM cell packet versus mean E_b/N_o, averaged over a large (10^4) number of Rayleigh fading channels with an exponentially decaying power-delay profile. The results clearly show that the combination of OFDM and complementary coding can efficiently exploit the frequency diversity of the channel for delay spreads of 10 ns or more. In this simulation, the use

of 8-PSK length 8 complementary codes is assumed. Two independent codes together encode 24 bits into 16 OFDM channels. For a symbol duration of 1.2 μs, including a guard time of 400 ns, this gives a data rate of 20 Mbps. These parameters are used in the OFDM modem of Magic WAND.

6.5.5 Large Code Lengths

For OFDM systems with a large number of subcarriers, it may not be feasible to generate a sufficient number of complementary codes with a length equal to the number of channels. To avoid this problem, the total number of channels can be split into groups of channels; applying a complementary code to each group of subchannels increases the coding rate, at the cost of reduced error correction capability and PAP ratio. For 32 channels, for instance, 18 bits per symbol could be encoded using 8-PSK complementary codes. These codes would have a PAP ratio of 3 dB and a distance of 16 channel symbols, so 7 erroneous channels or 15 erased channels could be corrected. Instead of 32-channel codes, it is also possible to use four 8-channel codes or some other combination of shorter length codes. The sum of four 8-channel codes give a total of 48 bits per symbol and a PAP ratio of 9 dB (6-dB reduction), while it is possible to correct one error or three erasures per group of eight channels.

6.6 SYMBOL SCRAMBLING

Symbol scrambling techniques to reduce the PAP ratio of a transmitted OFDM signal can be seen as a special case of PAP reduction codes. The difference is that symbol scrambling does not try to combine forward-error correction and PAP reduction such as is done by the complementary codes. The basic idea of symbol scrambling is that for each OFDM symbol, the input sequence is scrambled by a certain number of scrambling sequences. The output signal with the smallest PAP ratio is transmitted. For uncorrelated scrambling sequences, the resulting OFDM signals and corresponding PAP ratios will be uncorrelated, so if the PAP ratio for one OFDM symbol has a probability p of exceeding a certain level without scrambling, the probability is decreased to p^k by using k scrambling codes. Hence, symbol scrambling does not guarantee a PAP ratio below some low level; rather, it decreases the probability that high PAP ratios occur. Scrambling techniques were first proposed in [19, 20] under the names *selected mapping* and *partial transmit sequences*. The difference between the two is that the first applies independent scrambling rotations to all subcarriers, while the latter only applies scrambling rotations to groups of subcarriers.

Figure 6.29 shows OFDM spectra for 64 subcarriers where the backoff is adjusted to maintain a –30 dB bandwidth that is twice the –3-dB bandwidth. A perfect linear power amplifier model is used, which clips the signal when the output power exceeds the saturation power level. The effect of scrambling has been simulated by scrambling the IFFT input data for each OFDM symbol with a certain number of

independent complementary sequences and selecting the output symbol that gives the smallest PAP ratio. We can see from Figure 6.29 that scrambling with 1 and 10 codes gives rather small improvements of 0.25 and 0.75 dB in the required backoff, respectively, compared with the no scrambling case.

Figure 6.30 shows similar spectra as in Figure 6.29, but now for a more strict requirement of a –50-dB bandwidth that is twice the –3-dB bandwidth. In this case, scrambling gives more gain in the required backoff, up to 2 dB for 10 scrambling codes. This is caused by the fact that with scrambling, the probability of exceeding a PAP ratio of 7 dB is much less than the probability of exceeding 4 dB (whose probability is close to 1). As a result of this, for a backoff value of 4 or 5 dB, the amount of clipping interference is not much different from that without scrambling.

Figures 6.29 and 6.30 assume a perfectly linear power amplifier. In reality, however, the amplifier has a certain nonlinear transfer function. Figure 6.31 shows simulated spectra using Rapp's power amplifier model with nonlinearity parameter $p = 2$, which closely resembles practical RF power amplifiers. We can see that the amplifier model changes the shape of the spectrum, but the relative gain of scrambling does not change significantly. Because for wireless systems the –30-dB bandwidth requirement of Figure 6.29 and 6.31 is more realistic than the –50-dB requirement of Figure 6.30, we can conclude that the benefits of scrambling are rather limited.

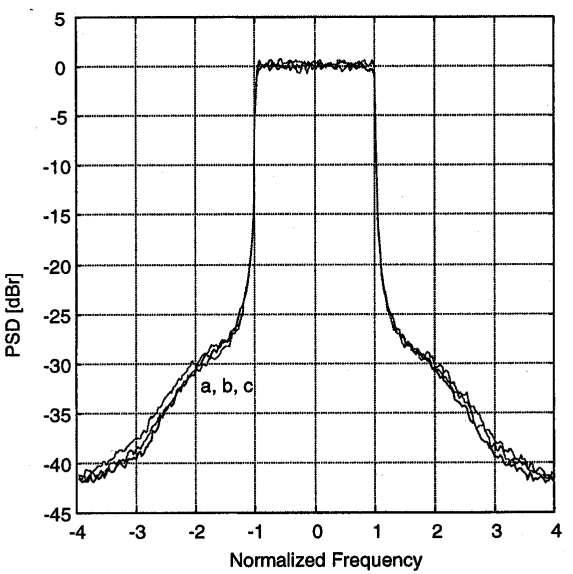

Figure 6.29 OFDM spectra for 64 subcarriers and p=100 using (a) no scrambling with 5.0-dB backoff, (b) 1 scrambling code with 4.7-dB backoff, and (c) 10 scrambling codes with 4.25-dB backoff.

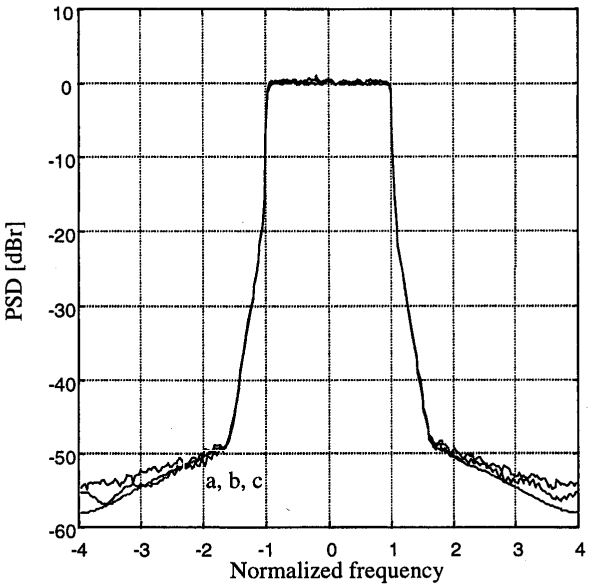

Figure 6.30 OFDM spectra for (a) no scrambling with a 8.5-dB backoff, (b) 1 scrambling code with a 7.2 dB backoff and (c) 10 scrambling codes with a 6.5-dB backoff.

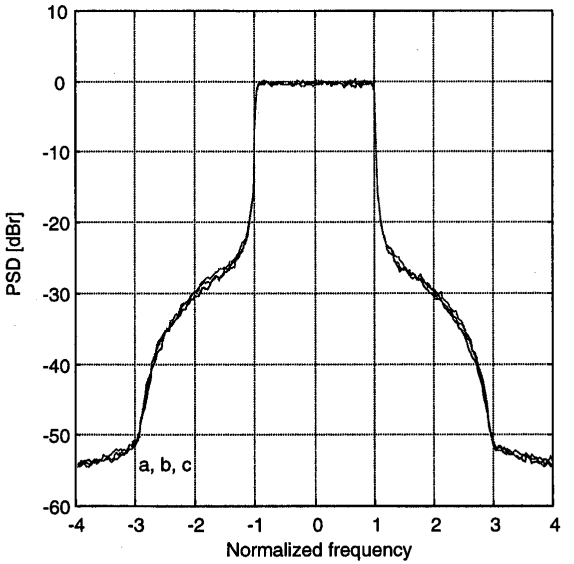

Figure 6.31 OFDM spectra for 64 subcarriers and Rapp's amplifier model with $p = 2$ using (a) no scrambling with 5.8-dB backoff, (b) 1 scrambling code with 5.3-dB backoff, and (c) 10 scrambling codes with 5.2-dB backoff.

REFERENCES

[1] Pauli, M., and H. P. Kuchenbecker, "Minimization of the Intermodulation Distortion of a Nonlinearly Amplified OFDM Signal," *Wireless Personal Communications*, Vol. 4, No. 1, pp. 93–101, Jan. 1997.

[2] Rapp, C., "Effects of HPA-Nonlinearity on a 4-DPSK/OFDM Signal for a Digital Sound Broadcasting System," *Proceedings of the Second European Conference on Satellite Communications*, Liège, Belgium, pp.179–184, Oct. 22–24, 1991.

[3] De Wild, A., "The Peak-to-Average Power Ratio of OFDM," M.Sc. thesis, Delft University of Technology, Delft, The Netherlands, Sept. 1997.

[4] May, T., and H. Rohling, "Reducing the Peak-to-Average Power Ratio in OFDM Radio Transmission Systems," *Proceedings of IEEE VTC '98*, Ottawa, Canada, pp. 2774–2778, May 18–21, 1998.

[5] Li, X., and L.J. Cimini, "Effects of Clipping and Filtering on the Performance of OFDM," *Proceedings of IEEE VTC'97*, pp.1634–1638, 1997.

[6] Wilkinson, T. A., and A. E. Jones, "Minimisation of the Peak-to-Mean Envelope Power Ratio of Multicarrier Transmission Schemes by Block Coding," *Proceedings of IEEE Vehicular Technology Conference*, Chicago, pp. 825–829, July 1995.

[7] Golay, M. J. E., "Complementary Series," *IRE Transactions on Information Theory*, Vol. IT-7, pp. 82–87, April 1961.

[8] Sivaswamy, R., "Multiphase Complementary Codes," *IEEE Transactions on Information Theory*, Vol. IT-24, No. 5, Sept. 1978.

[9] Frank, R. L., "Polyphase Complementary Codes," *IEEE Transactions on Infomation Theory*, Vol. IT-26, No. 6, Nov. 1980.

[10] Popovic, B. M., "Synthesis of Power Efficient Multitone Signals with Flat Amplitude Spectrum," *IEEE Transactions on Communications*, Vol. 39, No. 7, July 1991.

[11] Van Nee, R. D. J., "OFDM Codes for Peak-to-Average Power Reduction and Error Correction," *IEEE Global Telecommunications Conference*, London, pp. 740–744, Nov. 18–22, 1996.

[12] Van Nee, R. D. J., "An OFDM Modem for Wireless ATM," *IEEE Symposium on Communications and Vehicular Technology*, Gent, Belgium, October 7-8, 1996.

[13] Davis, J. A., and J. Jedwab, "Peak-to-Mean Power Control and Error Correction for OFDM Transmission Using Golay Sequences and Reed-Muller Codes," *Electronics Letters*, Vol. 33, pp. 267–268, 1997.

[14] Urbanke, R., and A. S. Krishnakumar, "Compact Description of Golay Sequences and their Extensions," *Proceedings of the Thirty-Fourth Annual Allerton*

Conference on Communication, Control and Computing Pagination, Urbana, IL, pp. 693–702, Oct. 2–4, 1996.

[15] Urbanke, R., and A. S. Krishnakumar, "Compact Description of Golay Sequences and their Extensions," Lucent Technologies Technical Memorandum, Doc. No. BL011217-961204-28TM, Dec. 20, 1996.

[16] Davis, J. A., and J. Jedwab, "Peak-to-Mean Power Control in OFDM, Golay Complementary Sequences and Reed-Muller Codes," HP Laboratories Technical Report, HPL-97-158, Dec. 1997.

[17] IEEE, 'Draft Supplement to Standard Part 11: Wireless LAN MAC and PHY Specifications: Higher Speed PHY Extension in the 2.4 GHz Band', P802.11B/D6.0, May 1999.

[18] Grant, A., and R. van Nee, "Efficient Maximum Likelihood Decoding of Q-ary Modulated Reed-Muller Codes," *IEEE Communications Letters*, Vol. 2, No. 5, pp. 134–136, May 1998.

[19] Müller, S. H., R. W. Bäuml, R. F. H. Fischer, and J. B. Huber, "OFDM with Reduced Peak-to-Average Power Ratio by Multiple Signal Representation," *Annals of Telecommunications*, Vol. 52, No. 1–2, pp. 58–67, Feb. 1997.

[20] Müller, S. H., and J. B. Huber, "OFDM with Reduced Peak-to-Average Power Ratio by Optimum Combination of Partial Transmit Sequences," *Electronics Letters*, Vol. 33, No. 5, pp. 368–369, Feb. 1997.

Chapter 7

BASICS OF CDMA

7.1 INTRODUCTION

This chapter illustrates the basic principles of CDMA to obtain a better understanding of combinations of CDMA with OFDM, as discussed in Chapters 8 and 9. The scope of the chapter is to give generic understanding of CDMA without overwhelming mathematical details. Readers should refer to Chapters 5 and 6 of [1] for a more extensive discussion on direct-sequence CDMA air interface design aspects and wideband CDMA air interface proposals, respectively. Furthermore, [1–15] provide details of spread-spectrum (SS) and CDMA technologies.

This chapter is divided into three sections. Section 7.2 presents a brief state-of-the-art of CDMA. Section 7.3 introduces the CDMA concept in general. It explains those criteria the transmitted signal has to fulfill to constitute a spread-spectrum modulation. Processing gain is defined. The fundamental properties of CDMA signals, namely multiple access capability, protection against multipath interference, privacy, interference rejection, antijamming capability, and low probability of interception are introduced. Different modulation methods for CDMA are treated in detail. These are direct-sequence spread-spectrum, frequency-hopping spread-spectrum, time-hopping spread-spectrum, and hybrid modulation. Each modulation scheme is described with the help of block diagrams for the transmitter and the receiver. In addition, how each spread-spectrum modulation scheme achieves the above-listed six properties of CDMA signals is discussed.

In Section 7.4, we review the fundamental elements of direct-sequence CDMA and its application into third-generation systems, namely RAKE receiver, power control, soft handover, interfrequency handover, and multiuser detection.

7.2 CDMA: PAST, PRESENT, AND FUTURE

The origins of spread-spectrum are in the military field and navigation systems. Techniques developed to counteract intentional jamming have also proved suitable for communication through dispersive channels in cellular applications. In this section we highlight the milestones for CDMA development starting from the 1950s after the formulation of the Shannon theorem [16]. An extensive overview of spread-spectrum history is given in [17].

In 1949, John Pierce wrote a technical memorandum in which he described a multiplexing system in which a common medium carries coded signals that need not be synchronized. This system can be classified as a time-hopping spread-spectrum multiple access system [17]. Claude Shannon and Robert Pierce introduced the basic ideas of CDMA in 1949 by describing the interference averaging effect and the graceful degradation of CDMA [18]. In 1950, De Rosa-Rogoff proposed a direct-sequence spread-spectrum system and introduced the processing gain equation and noise multiplexing idea [17]. In 1956, Price and Green filed for the antimultipath "RAKE" patent [17]. Signals arriving over different propagation paths can be resolved by a wideband spread-spectrum signal and combined by the RAKE receiver. The near-far problem (i.e., a high interference overwhelming a weaker spread-spectrum signal) was first mentioned in 1961 by Magnuski [17].

The cellular application of spread-spectrum was suggested by Cooper and Nettleton in 1978 [19]. During the 1980s, Qualcomm investigated DS-CDMA techniques, which finally led to the commercialization of cellular spread-spectrum communications in the form of the narrowband CDMA IS-95 standard in July 1993. Commercial operation of IS-95 systems started in 1996. In 1984, direct-sequence CDMA and hybrid CDMA/Frequency-Division Multiple Access (FDMA) were proposed among several proposals for the Group Special Mobile (the origin of the term GSM, which now stands for the Global System for Mobile Communications) multiple access schemes. They were investigated during 1984–86. Multiuser detection (MUD) has been subject to extensive research since 1986 when Verdu formulated an optimal multiuser detection for the AWGN channel, maximum likelihood sequence estimator (MLSE) [20].

During the 1990s, wideband CDMA techniques with a bandwidth of 5 MHz or more have been studied intensively throughout the world, and several trial systems have been built and tested [21]. These include FRAMES FMA2 (FRAMES Multiple Access) in Europe, Core-A in Japan, the European/Japanese harmonized WCDMA scheme, cdma2000 in the United States, and the TTA I and TTA II (Telecommunication Technology Association) schemes in Korea. Introduction of third-generation wireless communications systems using wideband CDMA is expected around the year 2000.

Wideband CDMA has a bandwidth of 5 MHz or more. The nominal bandwidth for all third-generation proposals is 5-MHz. There are several reasons for choosing this bandwidth. First, data rates of 144 and 384 Kbps, the main target of third-generation systems, are achievable within the 5-MHz bandwidth with a reasonable capacity. Even

a 2-Mbps peak rate can be provided under limited conditions. Second, lack of spectrum calls for reasonably small minimum spectrum allocation, especially if the system has to be deployed within the existing frequency bands occupied already by second-generation systems. Third, the 5-MHz bandwidth can resolve (separate) more multipaths than narrower bandwidths, increasing diversity and thus improving performance. Larger bandwidths of 10, 15, and 20-MHz have been proposed to support higher data rates more effectively.

Based on the above description, the CDMA era is divided in to three periods: (1) pioneer CDMA era, (2) narrowband CDMA era, and (3) wideband CDMA era, as shown in Table 7.1.

Table 7.1
CDMA Era

Pioneer Era

1949	John Pierce: time-hopping spread-spectrum
1949	Claude Shannon and Robert Pierce: basic ideas of CDMA
1950	De Rosa-Rogoff: direct-sequence spread-spectrum
1956	Price and Green: antimultipath RAKE patent
1961	Magnuski: near-far problem
1970s	Several developments for military field and navigation systems

Narrowband CDMA Era

1978	Cooper and Nettleton: cellular application of spread-spectrum
1980s	Investigation of narrowband CDMA techniques for cellular applications
1984	DS-CDMA and Hybrid CDMA/FDMA proposal for the Group Special Mobile in Europe
1986	Formulation of optimal multiuser detection by Verdu
1993	IS-95 standard

Wideband CDMA Era

1995	Europe: FRAMES FMA2 Japan : Core-A USA : cdma2000 Korea : TTA I, TTA II	} WCDMA
2000	Commercialization of wideband CDMA systems	

7.3 CDMA CONCEPTS

In CDMA, each user is assigned a unique code sequence (spreading code) it uses to encode its information-bearing signal. The receiver, knowing the code sequences of the user, decodes a received signal after reception and recovers the original data. This is possible because the cross-correlations between the code of the desired user and the codes of the other users are small. Because the bandwidth of the code signal is chosen to be much larger than the bandwidth of the information-bearing signal, the encoding process enlarges (spreads) the spectrum of the signal and is therefore also known as

spread-spectrum modulation. The resulting signal is also called a spread-spectrum signal, and CDMA is often denoted as spread-spectrum multiple access (SSMA).

The spectral spreading of the transmitted signal gives to CDMA its multiple access capability. It is therefore important to know the techniques necessary to generate spread-spectrum signals and the properties of these signals. A spread-spectrum modulation technique must fulfill two criteria:

1. The transmission bandwidth must be much larger than the information bandwidth.
2. The resulting radio-frequency bandwidth is determined by a function other than the information being sent (so the bandwidth is statistically independent of the information signal). This excludes modulation techniques like frequency modulation (FM) and phase modulation (PM).

The ratio of transmitted bandwidth to information bandwidth is called the *processing gain* G_p of the spread-spectrum system:

$$G_p = \frac{B_t}{B_i} \tag{7.1}$$

where B_t is the transmission bandwidth and B_i is the bandwidth of the information-bearing signal.

The receiver correlates the received signal with a synchronously generated replica of the spreading code to recover the original information-bearing signal. This implies that the receiver must know the code used to modulate the data.

Because of the coding and the resulting enlarged bandwidth, spread-spectrum (SS) signals have a number of properties that differ from the properties of narrowband signals. The most interesting from the communications systems point of view are discussed below. To have a clear understanding, each property has been briefly explained with the help of illustrations, if necessary, by applying direct-sequence spread-spectrum techniques.

Multiple access capability. If multiple users transmit a spread-spectrum signal at the same time, the receiver will still be able to distinguish among the users provided each user has a unique code that has a sufficiently low cross-correlation with the other codes. Correlating the received signal with a code signal from a certain user will then only despread the signal of this user, while the other spread-spectrum signals will remain spread over a large bandwidth. Thus, within the information bandwidth the power of the desired user will be larger than the interfering power provided there are not too many interferers, and the desired signal can be extracted. The multiple access capability is illustrated in Figure 7.1. In Figure 7.1(a), two users generate a spread-spectrum signal from their narrowband data signals. In Figure 7.1(b) both users transmit their spread-spectrum signals at the same time. At receiver 1, only the signal of user 1 is coherently summed by user 1, despreader and the user 1 data recovered.

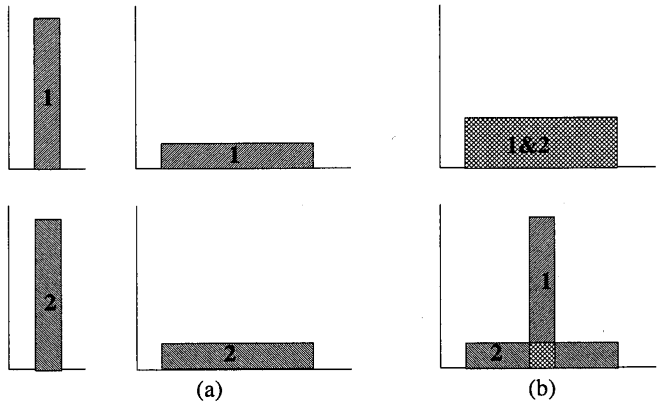

Figure 7.1 Principle of spread-spectrum multiple access.

Protection against multipath interference. In a radio channel there is not just one path between a transmitter and receiver. Because of reflections (and refractions), a signal is received from a number of different paths. The signals of the different paths are all copies of the same transmitted signal but with different amplitudes, phases, delays, and arrival angles. Adding these signals at the receiver will be constructive at some of the frequencies and destructive at others. In the time domain, this results in a dispersed signal. Spread-spectrum modulation can combat this multipath interference; however, the way in which this is achieved depends very much on the type of modulation used. In the next section, where CDMA schemes based on different modulation methods are discussed, we show for each scheme how multipath interference rejection is obtained.

Privacy. The transmitted signal can only be despread and the data recovered if the code is known to the receiver.

Interference rejection. Cross-correlating the code signal with a narrowband signal spreads the power of the narrowband signal thereby reducing the interfering power in the information bandwidth. Figure 7.2 illustrates this. The receiver observes spread-spectrum signal s summed with a narrowband interference i. At the receiver, the spread-spectrum signal is despread while the interference signal is spread, making it appear as background noise compared with the despread signal. Demodulation will be successful if the resulting background is of sufficiently weak energy in the despread information bandwidth.

Antijamming capability, especially narrowband jamming. This is more or less the same as interference rejection except the interference is now willfully inflicted on the system. It is this property, together with the next one, that makes spread-spectrum modulation attractive for military applications.

Low probability of interception (LPI). Because of its low power density, the spread-spectrum signal is difficult to detect and intercept by a hostile listener.

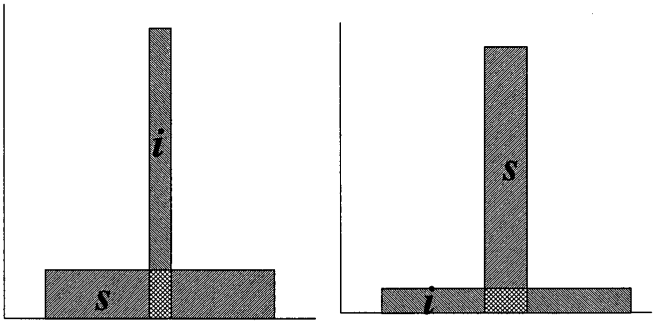

Figure 7.2 Interference rejection.

Figure 7.3 gives general classification of CDMA showing pure and hybrid CDMA.

Pure CDMA. There are three modulation techniques that generate spread-spectrum signals, known as Pure CDMA. These three techniques are as follows:

- *Direct-sequence (DS) CDMA.* The information-bearing signal is multiplied directly by a high-chip-rate spreading code.
- *Frequency-hopping (FH) CDMA.* The carrier frequency at which the information-bearing signal is transmitted is rapidly changed according to the spreading code.
- *Time-hopping (TH) CDMA.* The information-bearing signal is not transmitted continuously. Instead the signal is transmitted in short bursts where the times of the bursts are decided by the spreading code.

Hybrid CDMA. Two or more of the pure CDMA techniques can be used together to combine (known as *hybrid pure CDMA*) the advantages and, it is hoped, to combat their disadvantages. Further, it is possible to combine CDMA with other multiple access methods: contentionless (scheduling) access schemes (FDMA, TDMA), known as hybrid contentionless CDMA (e.g., TDMA/CDMA) [2], contention (random) access scheme (ISMA), known as hybrid contention CDMA (e.g., CDMA/ISMA) [2, 3], and orthogonal frequency division multiplexing (OFDM), known as hybrid OFDM/CDMA (e.g., MC-CDMA) [2]. Multicarrier (MC)-CDMA and multitone (MT)-CDMA are introduced in Chapter 8.

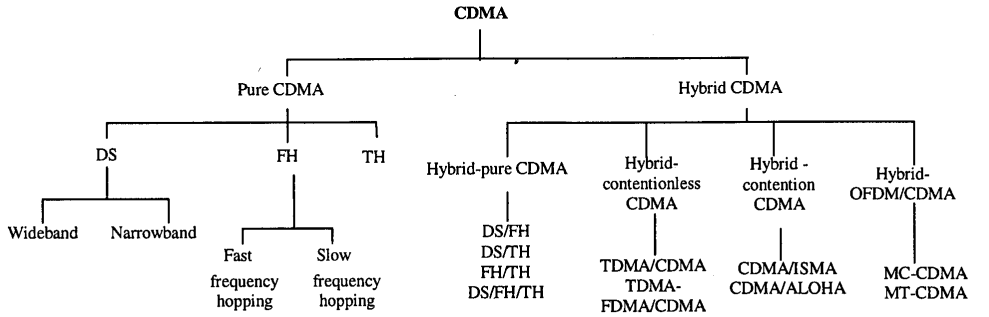

Figure 7.3 Classification of CDMA.

In the next section, the above-mentioned pure CDMA modulation techniques are used to show the multiple access capability of CDMA. The remainder of the chapters, however, mainly concentrate on direct-sequence (DS)-CDMA and its related subjects.

7.3.1 Pure CDMA

We can classify CDMA protocols in two different ways: by *concept* or by *modulation* method. The first classification gives us two protocol groups: *averaging systems* and *avoidance systems*. The averaging systems reduce the interference by averaging the interference over a wide time interval. The avoidance systems reduce the interference by avoiding it for a large part of the time.

Classifying by modulation gives us five protocols: direct-sequence (or pseudo-noise), frequency- and time-hopping protocols based on chirp modulation and hybrid methods. Of these, the first (DS) is an averaging CDMA protocol while the hybrid protocols can be averaging protocols depending on whether DS is used as part of the hybrid method. All the other protocols are of the avoidance type. Table 7.2 summarizes both ways of classification.

Table 7.2

Classifying CDMA protocols.

	DS	TH	FH	Chirp	Hybrid
Averaging	x				x
Avoidance		x	x	x	x

Direct-sequence. In DS-CDMA, the modulated information-bearing signal (the data signal) is directly modulated by a digital, discrete-time, discrete-valued code signal. The data signal can be either an analog signal or a digital one. In most cases it is a digital signal. In the case of a digital signal, the data modulation is often omitted and the data signal is directly multiplied by the code signal and the resulting signal modulates the wideband carrier. It is from this direct multiplication that the DS-CDMA gets its name.

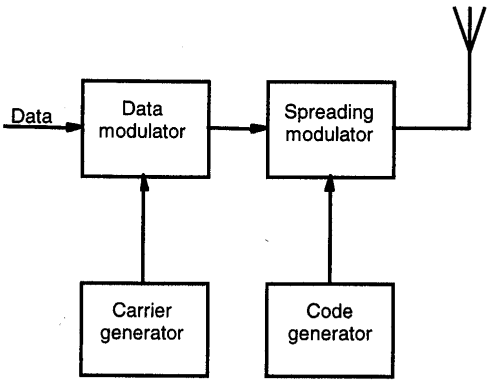

Figure 7.4 Block diagram of a DS-SS transmitter.

Figure 7.4 gives a block diagram of a DS-CDMA transmitter. The binary data signal modulates an RF carrier. The modulated carrier is then modulated by the code signal. This code signal consists of a number of code bits called "chips" that can be either +1 or −1. To obtain the desired spreading of the signal, the chip rate of the code signal must be much higher than the chip rate of the information signal. For the spreading modulation, various modulation techniques can be used, but usually some form of phase-shift keying (PSK) like binary phase-shift keying (BPSK), differential binary phase-shift keying (D-BPSK), quadrature phase-shift keying (QPSK), or minimum-shift keying (MSK) is employed.

If we omit the data modulation and use BPSK for the code modulation, we attain the block diagram given in Figure 7.5. The DS-SS signal resulting from this transmitter is shown in Figure 7.6. The rate of the code signal is called the *chip rate*; one chip denotes one symbol when referring to spreading code signals. In this figure, 10 code chips per information symbol are transmitted (i.e., the code chip rate is 10 times the data rate), so the processing gain is equal to 10.

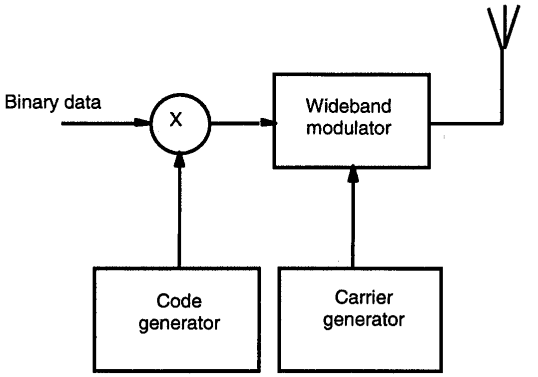

Figure 7.5 Modified block diagram of a DS-SS transmitter.

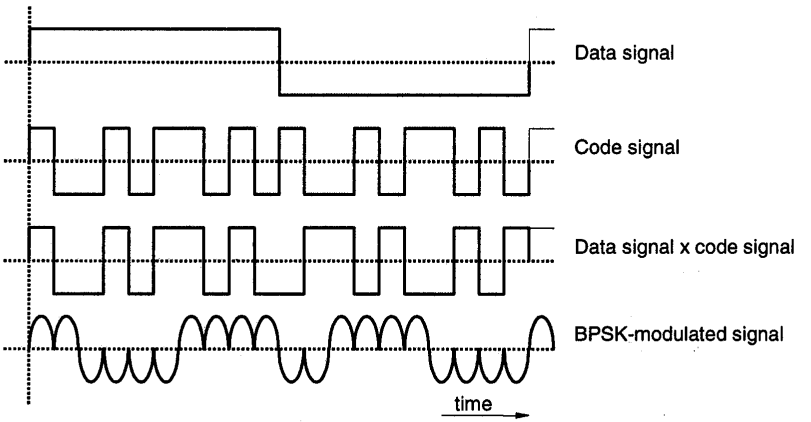

Figure 7.6 Generation of a BPSK-modulated spread-spectrum signal.

After transmission of the signal, the receiver (shown in Figure 7.7) despreads the spread-spectrum signal using a locally generated code sequence. To be able to perform the despreading operation, the receiver must not only know the code sequence used to spread the signal, but the codes of the received signal and the locally generated code must also be synchronized. This synchronization must be accomplished at the beginning of the reception and maintained until the whole signal has been received. The code synchronization/tracking block performs this operation. After despreading, a data-modulated signal results, and after demodulation, the original data can be recovered.

The previous section mentioned a number of advantages of spread-spectrum signals. The most important of those properties from the viewpoint of CDMA is the multiple access capability, the multipath interference rejection, the narrowband interference rejection, and with respect to secure/private communication, the LPI. We explain these four properties for the case of DS-CDMA.

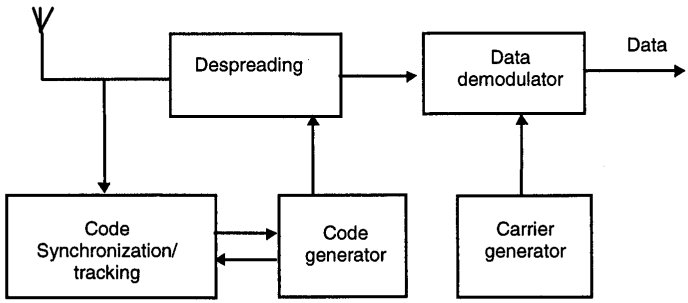

Figure 7.7 Receiver of a DS-SS signal.

Multiple access. If multiple users use the channel at the same time, multiple DS signal will overlap in time and frequency. At the receiver, despreading is used to remove the spreading code. This operation concentrates the power of the desired user in the information bandwidth. If the cross-correlations between the code of the desired user and the codes of the interfering users are small, coherent detection will only put a small part of the power of the interfering signals into the information bandwidth.

Multipath interference. If the code sequence has an ideal autocorrelation function, then the autocorrelation function is zero outside the interval $[-T_c, T_c]$, where T_c is the chip duration. This means that if the desired signal and a version that is delayed for more than $2T_c$ are received, despreading will treat the delayed version as an interfering signal, putting only a small part of the power in the information bandwidth.

Narrowband interference. The coherent detection at the receiver involves a multiplication of the received signal by a locally generated code sequence. As we saw at the transmitter, however, multiplying a narrowband signal with a wideband code sequence spreads the spectrum of the narrowband signal so that its power in the information bandwidth decreases by a factor equal to the processing gain.

LPI. Because the DS signal uses the whole signal spectrum all the time, it will have a very low transmitted power per hertz. This makes it very difficult to detect a DS signal.

Apart from the above-mentioned properties, DS-CDMA has a number of other specific properties that we can divide into advantageous (+) and disadvantageous (–) behavior:

+ The generation of the coded signal is easy to implement. It can be performed by a simple multiplication.
+ Because only one carrier frequency has to be generated, the frequency synthesizer (carrier generator) is simple.
+ No synchronization among the users is necessary.
– It is difficult to acquire and maintain the synchronization of the locally generated code signal and the received signal. Synchronization has to be kept within a fraction of the chip time.

- For correct reception, the synchronization error of locally generated code sequence and the received code sequence must be very small, a fraction of the chip time. This, combined with the nonavailability of large contiguous frequency bands, practically limits the bandwidth to 10 to 20 MHz.
- The power received from users close to the base station is much higher than that received from users further away. Because a user continuously transmits over the whole bandwidth, a user close to the base constantly creates a lot of interference for users far from the base station, making their reception impossible. This near-far effect can be solved by applying a power control algorithm so that all users are received by the base station with the same average power. This control, however, proves to be quite difficult because of feedback delays, imperfect power estimates, errors in the feedback channel, and traffic conditions.

Frequency-hopping. In frequency-hopping CDMA, the carrier frequency of the modulated information signal is not constant but changes periodically. During time intervals T, the carrier frequency remains the same, but after each time interval, the carrier hops to another (or possibly the same) frequency. The hopping pattern is decided by the spreading code. The set of available frequencies the carrier can attain is called the *hop-set.*

The frequency occupation of an FH-SS system differs considerably from a DS-SS system. A DS system occupies the whole frequency band when it transmits, whereas an FH system uses only a small part of the bandwidth when it transmits, but the location of this part differs in time.

Figure 7.8 illustrates the difference between the FH-SS and the DS-SS frequency usage. Suppose an FH system is transmitting in frequency band 2 during the first time period. A DS system transmitting in the same time period spreads its signal power over the whole frequency band so the power transmitted in frequency band 2 will be much less than that of the FH system. The DS system transmits in frequency band 2 during all time periods, however, while the FH system only uses this band part of the time. On average, both systems transmit the same power in the frequency band.

Figure 7.9 gives the block diagram for an FH-CDMA system. The data signal is baseband modulated. Using a fast frequency synthesizer that is controlled by the code signal, the carrier frequency is converted up to the transmission frequency.

The inverse process takes place at the receiver. Using a locally generated code sequence, the received signal is converted down to the baseband. The data are recovered after (baseband) demodulation. The synchronization/tracking circuit ensures that the hopping of the locally generated carrier synchronizes to the hopping pattern of the received carrier so that correct despreading of the signal is possible.

Within frequency-hopping CDMA, a distinction is made based on the hopping rate of the carrier. If the hopping rate is (much) greater than the symbol rate, the modulation is considered to be *fast frequency-hopping* (*F-FH*). In this case, the carrier frequency changes a number of times during the transmission of one symbol, so that

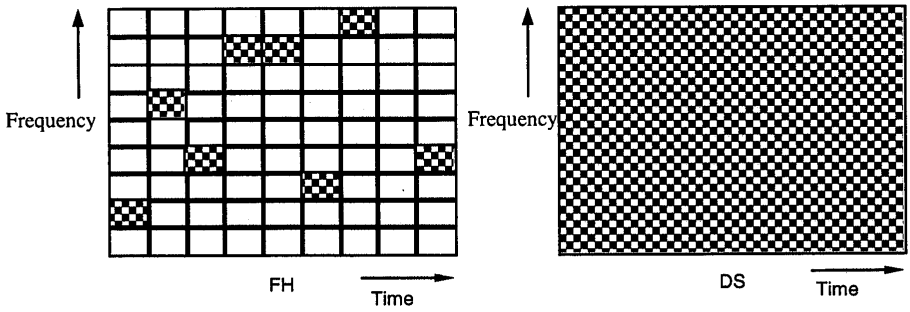

Figure 7.8 Time/frequency occupancy of FH and DS signals.

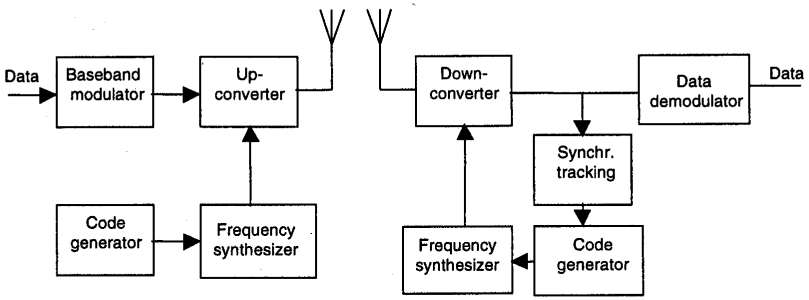

Figure 7.9 Block diagram of an FH-CDMA transmitter and receiver.

one bit is transmitted at different frequencies. If the hopping rate is (much) smaller than the symbol rate, it is *slow frequency-hopping* (*S-FH*). In this case, multiple symbols are transmitted at the same frequency.

The occupied bandwidth of the signal on one of the hopping frequencies depends not only on the bandwidth of the information signal, but also on the shape of the hopping signal and the hopping frequency. If the hopping frequency is much smaller than the information bandwidth (which is the case in slow frequency-hopping), then the information bandwidth is the main factor that decides the occupied bandwidth. If, however, the hopping frequency is much greater than the information bandwidth, the pulse shape of the hopping signal decides the occupied bandwidth at one hopping frequency. If this pulse shape is very abrupt (resulting in very abrupt frequency changes), the frequency band is very broad, limiting the number of hop frequencies. If we make sure that the frequency changes are smooth, the frequency band at each hopping frequency is about $1/T_h$ times the frequency bandwidth, where T_h is equal to the hopping frequency. We can make the frequency changes smooth by decreasing the transmitted power before a frequency hop and increasing it again when the hopping frequency has changed.

As has been done for DS-CDMA, we discuss the properties of FH-CDMA with respect to multiple access capability, multipath interference rejection, narrowband interference rejection, and probability of interception.

Multiple access. It is easy to visualize how the F-FH and S-FH CDMA obtain their multiple access capability. In the F-FH, one symbol is transmitted in different frequency bands. If the desired user is the only one to transmit in most of the frequency bands, the received power of the desired signal is much higher than the interfering power and the signal will be received correctly.

In the S-FH, multiple symbols are transmitted at one frequency. If the probability of other users transmitting in the same frequency band is low enough, the desired user is received correctly most of the time. For those times that interfering users transmit in the same frequency band, error-correcting codes are used to recover the data transmitted during that period.

Multipath interference. In the F-FH CDMA the carrier frequency changes a number of times during the transmission of one symbol. Thus, a particular signal frequency is modulated and transmitted on a number of carrier frequencies. The multipath effect is different at the different carrier frequencies. As a result, signal frequencies that are amplified at one carrier frequency are attenuated at another carrier frequency and vice versa. At the receiver, the responses at the different hopping frequencies are averaged, thus reducing the multipath interference. Because usually noncoherent combining is used, this is not as effective as the multipath interference rejection in a DS-CDMA system, but it still gives quite an improvement.

Narrowband interference. Suppose a narrowband signal is interfering on one of the hopping frequencies. If there are G_p hopping frequencies (where G_p is the processing gain), the desired user (on average) uses the hopping frequency where the interferer is located $1/G_p$ percent of the time. The interference is therefore reduced by a factor G_p.

LPI. The difficulty in intercepting an FH signal lies not in its low transmission power. During a transmission, it uses as much power per hertz as a continuous transmission. But the frequency at which the signal is going to be transmitted is unknown, and the duration of the transmission at a particular frequency is quite small. Therefore, although the signal is more readily intercepted than a DS signal, it is still a difficult task to perform.

Apart from the above-mentioned properties, the FH-CDMA has a number of other specific properties that we can divide into advantageous (+) and disadvantageous (–) behavior:

+ Time synchronization is much easier with FH-CDMA than with DS-CDMA. FH-CDMA synchronization has to be within a fraction of the hop time. Because spectral spreading is not obtained by using a very high hopping frequency but by using a large hop-set, the hop time will be much longer than the chip time of a DS-CDMA system. Thus, an FH-CDMA system allows a larger synchronization error.

+ The different frequency bands that an FH signal can occupy do not have to be contiguous because we can make the frequency synthesizer easily skip over certain parts of the spectrum. Combined with the easier synchronization, this allows much higher spread-spectrum bandwidths.
+ The probability of multiple users transmitting in the same frequency band at the same time is small. A user transmitting far from the base station is received by it even if users close to the base station are transmitting, as those users are probably transmitting at different frequencies. Thus, the near-far performance is much better than that of DS.
+ Because of the larger possible bandwidth a FH system can employ, it offers a higher possible reduction of narrowband interference than a DS system.
– A sophisticated frequency synthesizer is necessary.
– An abrupt change of the signal when changing frequency bands leads to an increase in the occupied spectrum. To avoid this, the signal has to be ramped up and down when changing frequency.
– Coherent demodulation is difficult because of the problems in maintaining a coherent reference phase between hops.

Time-hopping. In time-hopping CDMA, the data signal is transmitted in rapid bursts at time intervals determined by the code assigned to the user. The time axis is divided into frames, and each frame is divided into M timeslots. During each frame, the user transmits in one of the M timeslots. Which of the M timeslots is transmitted depends on the code signal assigned to the user. Because a user transmits all of its data in one, instead of M timeslots, the frequency it needs for its transmission has increased by a factor M. A block diagram of a TH-CDMA system is given in Figure 7.10.

Figure 7.11 shows the time-frequency plot of the TH-CDMA systems. Comparing Figure 7.11 with Figure 7.10, we see that the TH-CDMA uses the whole wideband spectrum for short periods instead of parts of the spectrum all of the time.

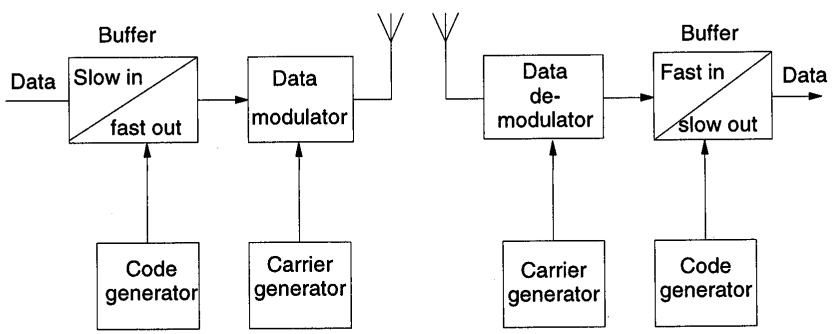

Figure 7.10 Block diagram of a TH-CDMA transmitter and receiver.

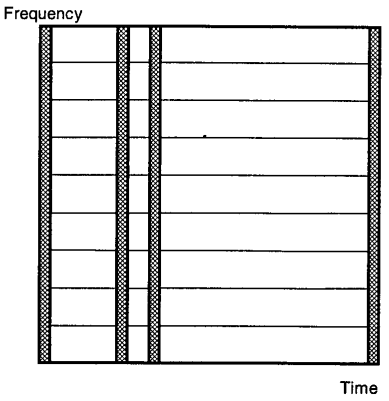

Figure 7.11 Time-frequency plot of TH-CDMA.

Following the same procedure as for the previous CDMA schemes, we discuss the properties of TH-CDMA with respect to multiple access capability, multipath interference rejection, narrowband interference rejection, and probability of interception.

Multiple access. The multiple access capability of TH-SS signals is acquired in the same manner as that of the FH-SS signals; namely, by making the probability of users' transmissions in the same frequency band at the same time small. In the case of time-hopping, all transmissions are in the same frequency band, so the probability of more than one transmission at the same time must be small. This is again achieved by assigning different codes to different users. If multiple transmissions do occur, error-correcting codes ensure that the desired signal can still be recovered.

If there is synchronization among the users, and the assigned codes are such that no more than one user transmits at a particular slot, then the TH-CDMA reduces to a TDMA scheme where the slot in which a user transmits is not fixed but changes from frame to frame.

Multipath interference. In the TH-CDMA, a signal is transmitted in reduced time. The signaling rate, therefore, increases, and dispersion of the signal now leads to overlap of adjacent bits. Therefore, no advantage is gained with respect to multipath interference rejection.

Narrowband interference. A TH-CDMA signal is transmitted in reduced time. This reduction is equal to $1/G_p$, where G_p is the processing gain. At the receiver we receive only an interfering signal during the reception of the desired signal. Thus, we receive only the interfering signal $1/G_p$ percent of the time, reducing the interfering power by a factor G_p.

LPI. With TH-CDMA, the frequency at which a user transmits is constant but the times at which a user transmits are unknown, and the durations of the transmissions are very short. Particularly when multiple users are transmitting, this makes it difficult for an

intercepting receiver to distinguish the beginning and end of a transmission and to decide which transmissions belong to which user.

Apart from the above-mentioned properties, the TH-CDMA has a number of other specific properties that we can divide into advantageous (+) and disadvantageous (–) behavior:

+ Implementation is simpler than that of FH-CDMA, as no relatively complex hopping frequency synthesizer is required.
+ TH-CDMA is a very useful method when the transmitter is average-power limited but not peak-power limited because the data are transmitted is short bursts at high power.
+ As with the FH-CDMA, the near-far problem is much less of a problem as most of the time a terminal far from the base station transmits alone and is not hindered by transmissions from stations close by.
– It takes a long time before the code is synchronized, and the time in which the receiver has to perform the synchronization is short.
– If multiple transmissions occur, a large number of data bits are lost, so a good error-correcting code and data interleaving are necessary.

Hybrid-pure-CDMA. The hybrid-pure-CDMA systems include all CDMA systems that employ a combination of two or more of the above-mentioned spread-spectrum modulation techniques or a combination of CDMA with some other multiple access technique. By combining the basic spread-spectrum modulation techniques, we have four possible hybrid systems: DS/FH, DS/TH, FH/TH, and DS/FH/TH; and by combining CDMA with TDMA or multicarrier modulation we have two more: CDMA/TDMA and MC-CDMA.

The idea of the hybrid system is to combine the specific advantages of each of the modulation techniques. If we take, for example, the combined DS/FH system, we have the advantage of the anti-multipath property of the DS system combined with the favorable near-far operation of the FH system. Of course, the disadvantage lies in the increased complexity of the transmitter and receiver. For illustration purposes, we give a block diagram of a combined DS/FH CDMA transmitter in Figure 7.12.

The data signal is first spread using a DS code signal. The spread signal is then modulated on a carrier whose frequency hops according to another code sequence. A code clock ensures a fixed relation between the two codes.

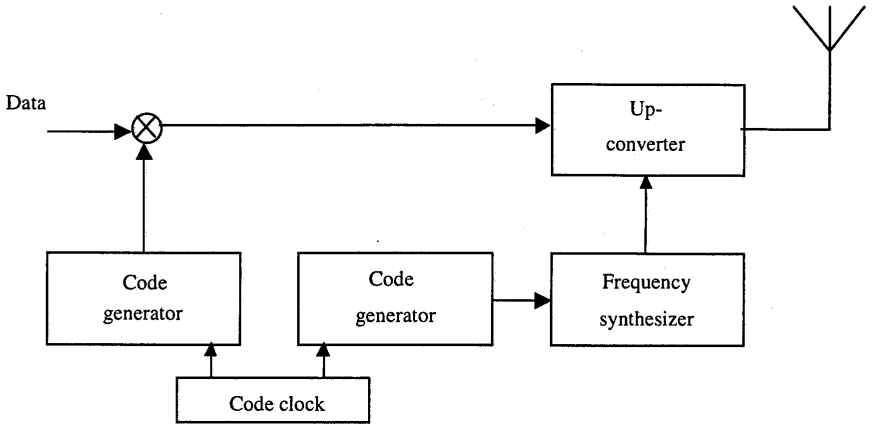

Figure 7.12 Hybrid DS-FH transmitter.

7.4 BASIC DS-CDMA ELEMENTS

In this section, we review the fundamental elements for understanding DS-CDMA and its application into third-generation systems; namely, RAKE receiver, power control, soft handover, interfrequency handover, and multiuser detection.

7.4.1 RAKE Receiver

A DS spread-spectrum signal waveform is well matched to the multipath channel. In a multipath channel, the original transmitted signal reflects from obstacles such as buildings and mountains, and the receiver receives several copies of the signal with different delays. If the signals arrive more than one chip apart from each other, the receiver can resolve them. Actually, from each multipath signal's point of view, other multipath signals can be regarded as interference and are suppressed by the processing gain. A further benefit is obtained, however, if the resolved multipath signals are combined using a *RAKE receiver*. Thus, the signal waveform of CDMA signals facilitates use of multipath diversity. Expressing the same phenomenon in the frequency domain means that the bandwidth of the transmitted signal is larger than the coherence bandwidth of the channel and the channel is frequency selective (i.e., only part of the signal is affected by the fading).

A RAKE receiver consists of correlators, each receiving a multipath signal. After despreading by correlators, the signals are combined using, for example, maximal ratio combining. Because the received multipath signals are fading independently, diversity order and thus performance are improved. Figure 7.13 illustrates the principle

of a RAKE receiver. After spreading and modulation, the signal is transmitted and it passes through a multipath channel, which can be modeled by a tapped delay line (i.e., the reflected signals are delayed and attenuated in the channel). In Figure 7.13 we have three multipath components with different delays (τ_1, τ_2, and τ_3) and attenuation factors (a_1, a_2, and a_3), each corresponding to a different propagation path. The RAKE receiver has a receiver finger for each multipath component. In each finger, the received signal is correlated by the spreading code, which is time-aligned with the delay of the multipath signal. After despreading, the signals are weighted and combined. In Figure 7.13, maximal ratio combining is used; that is, each signal is weighted by the (conjugated) path gain (or path attenuation factor). Because of transmitter or receiver movements, the scattering environment will change, and thus, the delays and attenuation factors change as well. Therefore, it is necessary to measure the tapped-delay-line profile and to reallocate RAKE fingers whenever the delays have changed by a significant amount. Small-scale changes, less than one chip, are taken care of by a code tracking loop, which tracks the time delay of each multipath signal.

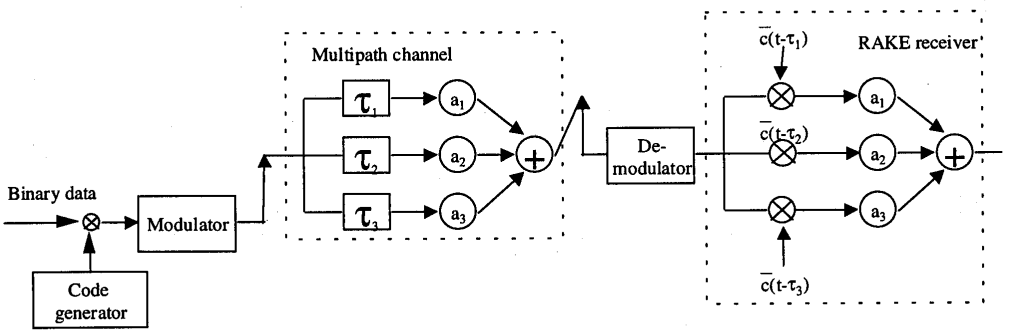

Figure 7.13 Principle of RAKE receiver.

7.4.2 Power Control

In the uplink of a DS-CDMA system, the requirement for power control is the most serious negative point. The power control problem arises because of the multiple access interference. All users in a DS-CDMA system transmit the messages by using the same bandwidth at the same time, and therefore users interfere with one another. Because of the propagation mechanism, the signal received by the base station from a user terminal close to the base station is stronger than the signal received from another terminal located at the cell boundary. Hence, the distant users are dominated by the close user. This is called the *near-far effect*. To achieve a considerable capacity, all signals, irrespective of distance, should arrive at the base station with the same mean power. A solution to this problem is power control, which attempts to achieve a constant received mean power for each user. Therefore, the performance of the transmitter power control (TPC) is one of the several dependent factors when deciding on the capacity of a DS-CDMA system.

In contrast to the uplink, in the downlink all signals propagate through the same channel and thus are received by a mobile station with equal power. Therefore, no power control is required to eliminate the near-far problem. Power control is still desirable, however, to minimize the interference to other cells. Ideally, you want to transmit just enough power to each user so that all users experience the same signal-to-interference ratio at the minimum required level. Unfortunately, power control in the DS-CDMA downlink actually creates a near-far problem. Therefore, the power for all users cannot be much smaller than that for the most remote user, resulting in more interference to other cells than in the case of ideal power control.

In addition to being useful against interfering users, power control improves the performance of DS-CDMA against fading channel by compensating the fading dips. If it followed the channel fading perfectly, power control would turn a fading channel into an AWGN channel by eliminating the fading dips completely.

Two types of power control principles exist: *open loop* and *closed loop*. In open-loop power control, the transmitter measures the interference conditions from the channel and adjusts the transmission power accordingly to meet the desired frame error rate (FER) target. Because the fast fading does not correlate between uplink and downlink, however, open loop power control will achieve the right power target only on average. Therefore, closed-loop power control is required. In closed-loop power control, the receiver measures the signal-to-interference ratio (SIR) and sends commands to the transmitter on the other end to adjust the transmission power.

7.4.3 Soft Handover

In soft handover, a mobile station is connected to more than one base station simultaneously. Soft handover is used in CDMA to reduce the interference into other cells and to improve performance through macrodiversity. Softer handover is a soft handover between two sectors of a cell.

Neighboring cells of a cellular system using either FDMA or TDMA do not use the same frequencies. The spatial separation between cells using the same frequencies is determined by the *frequency reuse factor*, which is the ratio of the total number of cells and the number of cells that use one particular frequency. Because of the processing gain, such spatial separation is not needed in CDMA, and a frequency reuse factor of one can be used. Usually, a mobile station performs a handover when the signal strength of a neighboring cell exceeds the signal strength of the current cell with a given threshold. This is called *hard handover*. To avoid excessive interference, an instantaneous handover from the current cell to the new cell is required when the signal strength of the new cell exceeds the signal strength of the current cell. This is not, however, feasible in practice because of rapid fluctuations of the signal strength. The handover mechanism should always allow the mobile station to connect into a cell, which it receives with the highest power (i.e., with the lowest path loss). Because in soft handover the mobile station is connected to either two or more base stations, its

transmission power can be controlled according to the cell, which the mobile station receives with the highest signal strength. A mobile station enters the soft handover state when the signal strength of a neighboring cell exceeds a certain threshold but is still below the current base station's signal strength.

Fortunately, the signal structure of CDMA is well suited for the implementation of soft handover. This is because in the uplink, two or more base stations can receive the same signal because of the reuse factor of one; and in the downlink, the mobile station can coherently combine the signals from different base stations since it sees them as just additional multipath components—provided that the base stations are time-synchronized to within a few chip intervals. This provides an additional benefit called macro diversity (i.e., the diversity gain provided by the reception of one or more additional signals). A separate pilot channel is usually used for the signal strength measurements for handover purposes.

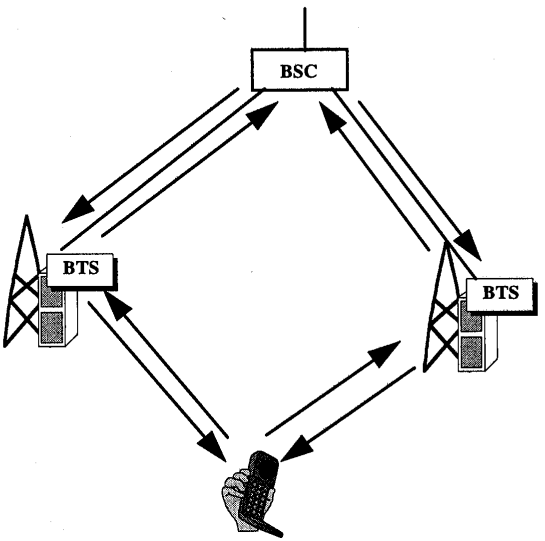

Figure 7.14 Principle of soft handover with two base station transceivers (BTS).

In the downlink, however, soft handover creates more interference to the system because the new base station now transmits an additional signal for the mobile station. It is possible that the mobile station cannot collect all of the energy that the base station transmits because of a limited number of RAKE fingers. Thus, the gain of soft handover in the downlink depends on the gain of macrodiversity and the loss of performance due to increased interference.

Figure 7.14 illustrates the soft handover principle with two base stations involved. In the uplink the mobile station signal is received by the two base stations, which, after demodulation and combining, pass the signal forward to the combining

point, typically to the base station controller (BSC). In the downlink, the same information is transmitted through both base stations, and the mobile station receives the information from two base stations as separate multipath signals and can therefore combine them.

7.4.4 Interfrequency Handover

The third-generation CDMA networks will have multiple frequency carriers in each cell, and a hot-spot cell could have a larger number of frequencies than neighboring cells. Further, in hierarchical cell structures, microcells will have a different frequency than the macrocell overlaying the microcells. Therefore, an efficient procedure is needed for a handover between different frequencies. A blind handover used by second generation CDMA does not result in an adequate call quality. Instead, the mobile station has to be able to measure the signal strength and quality of another carrier frequency, while still maintaining the connection in the current carrier frequency. Because a CDMA transmission is continuous, there are no idle slots for the interfrequency measurements as in the TDMA-based systems. Therefore, compressed mode and dual receiver have been proposed as a solution to interfrequency handover [22]. In the compressed mode, measurement slots are created by transmitting the data of a frame, for example, with a lower spreading ratio during a shorter period, and the rest of the frame is used for the measurements on other carriers. The dual receiver can measure other frequencies without affecting the reception of the current frequency.

7.4.5 Multiuser Detection

The current CDMA receivers are based on the RAKE receiver principle, which considers other users' signals as interference. In an optimal receiver, however, all signals would be detected jointly or interference from other signals would be removed by subtracting them from the desired signal. This is possible because the interference is deterministic and not random.

The capacity of a DS-CDMA system using RAKE receiver is interference limited. In practice this means that when a new user, or interferer, enters the network, other users' service quality degrades. The more the network can resist interference the more users can be served. Multiple access interference that disturbs a base or mobile station is a sum of both intra- and intercell interference.

Multiuser detection (MUD), also called joint detection and interference cancellation (IC), can reduce the effect of multiple access interference, and hence increases the system capacity. In the first place, MUD is considered to cancel only the intracell interference, meaning that in a practical system the capacity will be limited by the efficiency of the algorithm and the intercell interference.

In addition to capacity improvement, MUD alleviates the near-far problem typical to DS-CDMA systems. A mobile station close to a base station may block the whole cell traffic by using too high a transmission power. If this user is detected first and subtracted from the input signal, the other users do not see the interference.

Because optimal multiuser detection is very complex and difficult to implement in practice for any reasonable number of users, a number of suboptimal multiuser and interference cancellation receivers have been developed. The suboptimal receivers can be divided into two main categories: *linear detectors* and *interference cancellation*. Linear detectors apply a linear transform to the outputs of the matched filters that are trying to remove the multiple access interference (i.e., the interference due to correlations among user codes). Examples of linear detectors are decorrelator and linear minimum mean square error (LMMSE) detectors. In interference cancellation, multiple access interference is first estimated and then subtracted from the received signal. Parallel interference cancellation (PIC) and successive (serial) interference cancellation (SIC) are examples of interference cancellation.

REFERENCES

[1] Ojanperä, T., and R. Prasad, "*Wideband CDMA for Third Generation Mobile Communications*," Norwood, MA: Artech House, 1998.

[2] Prasad, R., "*Universal Wireless Personal Communications*," Norwood, MA: Artech House, 1998.

[3] Prasad, R., "*CDMA for Wireless Personal Communications*," Norwood, MA: Artech House, 1996.

[4] "Special Issue on Spread-Spectrum Communication," *IEEE Transactions on Communications*, Vol. COM-30, May 1982.

[5] Simon, M. K., J. K. Omura, R. A. Scholtz, and B. K. Levitt, *Spread-Spectrum Communications*, Vol. I, II, III, *Comp. Sci.*, 1985.

[6] Scholtz, R. A., "The Spread-Spectrum Concept," *IEEE Transactions on Communications*, Vol. COM-25, pp. 74 – 55, Aug. 1977.

[7] Torrieri, D. J., "*Principles of Secure Communication Systems*," Artech House, Norwood, Mass., 1985.

[8] Cooper, G. R., and C. D. McGillem, "*Modern Communication and Spread-Spectrum*," McGraw-Hill Book Company, New York 1986.

[9] Glisic, S. G., and P. A. Leppanen (eds.), "*Code Divison Multiple Access Communications*," Kluwer Academic Publishers, Boston, MA, 1995.

[10] Viterbi, A. J., "*CDMA Principles of Spread-Spectrum Communications*," Addison-Wesley Publishing Company, Reading, Mass., 1995.

[11] Dixon, R. C., "*Spread-Spectrum Systems*," John Wiley & Sons, New York, 1984.

[12] Glisic, S., and B. Vucetic, "*Spread-spectrum CDMA Systems for Wireless Communications*," Norwood, MA: Artech House, 1997.

[13] Glisic, S., and P. Leppänen, "*Wireless Communications: TDMA versus CDMA*," Boston, MA: Kluwer Academic Publishers, 1997.

[14] Ojanperä, T., and R. Prasad, "Overview of Air Interface Multiple Access for IMT-2000/UMTS," *IEEE Communications Magazine*, Vol. 36, pp. 82 - 95, Sep. 1998.

[15] Ojanperä, T., and R. Prasad, "An Overview of Third Generation Wireless Personal Communications: A European Perspective," *IEEE Personal Communications*, Vol. 5, pp. 59 – 65, Dec. 1998.

[16] Shannon, C. E., "A Mathematical Theory of Communication," *Bell System Technical Journal*, Vol. 27, pp. 379 – 423 and 623 – 656, 1948.

[17] Scholtz, R. A., "The Evolution of Spread-Spectrum Multiple-Access Communications," *in Code Division Multiple Access Communications* (eds.), Kluwer Academic Publishers, Boston, MA, 1995.

[18] Glisic, S. G., and P. A. Leppänen, "A conversation with Claude Shannon," *IEEE Communications Magazine*, Vol. 22, No. 5, pp.123 – 126, May 1984.

[19] Cooper, G. R., and R. W. Nettleton, "A spread-spectrum technique for high-capacity mobile communications," *IEEE Trans. Veh. Tech.*, Vol. 27, No. 4, pp. 264 – 275, Nov. 1978.

[20] Verdu, S., "Minimum Probability of Error for Asynchronous Gaussian Multiple Access," *IEEE Trans. on IT.*, Vol. IT-32, No. 1, pp. 85 – 96, Jan. 1986.

[21] Ojanperä, T., "Overview of Research Activities for Third Generation Mobile Communication," *Wireless Communications TDMA vs. CDMA* (eds.), Kluwer Academic Publishers, Dordrecht, Netherlands, pp. 415 – 446, 1997.

[22] Gustafsson, M., K. Jamal, and E. Dahlman, "Compressed Mode Techniques for Interfrequency Measurements in a Wide-band DS-CDMA System," *Proceedings of PIMRC'97*, Helsinki, Finland, pp. 23 – 35, Sep. 1997.

CHAPTER 8

MULTI - CARRIER CDMA

8.1 INTRODUCTION

Chapter 7 presented an overview of code division multiple access (CDMA). CDMA has been considered a candidate to support multimedia services in mobile communications because it has its own capabilities to cope with the asynchronous nature of multimedia data traffic, to provide higher capacity over conventional access schemes such as TDMA and FDMA, and to combat hostile channel frequency selectivity. Direct sequence (DS-) and Frequency hopping (FH-) CDMA systems have been subject to extensive research [1]. The development of a third generation mobile communications system has already been taking place using the wideband CDMA systems [2, 3].

Recently, a new CDMA system based on a combination of CDMA and orthogonal frequency division multiplexing (OFDM) signaling, which is called *Multi-Carrier (MC-) CDMA system*, has been reported in [4–6]. It has gained much attention, because the signal can be easily transmitted and received using the fast fourier transform (FFT) device without increasing the transmitter and receiver complexities and is potentially robust to channel frequency selectivity with a good frequency use efficiency.

So far, many reports have been dedicated for the bit-error ratio (BER) analysis of MC-CDMA system and the BER comparison between MC-CDMA and DS-CDMA systems in frequency selective Rayleigh fading channels [7–14]. In these works, "independent fading characteristic at each received path" has been often assumed for the BER analysis of DS-CDMA system, whereas "independent fading characteristic at each received subcarrier" is likewise for the BER analysis of MC-CDMA system. In general, however, fading characteristics among subcarriers are highly correlated, and the subcarrier correlation is uniquely determined by the multipath delay profile of the channel. Therefore, when we discuss BER performance of MC-CDMA systems and compare it with that of other multiple access systems such as DS-CDMA, it is essential

to make a fair assumption for all the systems compared, such as the same channel frequency selectivity and channel time selectivity as well as the same modulation/demodulation format, transmission rate, and processing gain. Further, when we design a MC-CDMA system and discuss the BER performance, it is essential to carefully determine two transmission parameters: the length of guard interval and the number of subcarriers. These significantly affect BER performance.

In Chapter 8, we discuss the advantages and disadvantages of the MC-CDMA system. To focus more attention on the MC-CDMA concept, we introduce a conventional DS-CDMA system for a comparison. The MC-CDMA system inevitably requires linear amplification because it is very sensitive to nonlinear amplification. This requirement could be realizable for base stations, so in this sense, we can say that the MC-CDMA system is well suited for a downlink channel. Therefore, in the BER investigation, we further discuss the downlink performance, although the uplink performance is shown as well. We show the BER performance with four different combining strategies such as orthogonality restoring combining (ORC), equal gain combining (EGC), maximum ratio combining (MRC), and minimum mean square error combining (MMSEC). They are all categorized into *single-user detection scheme* applicable for downlink and uplink channels, however, as shown later, the MC-CDMA uplink performance is still poor even with quasisynchronous scenario.

The chapter is organized as follows. Section 8.2 explains a frequency-selective fast Rayleigh fading channel to carry out the MC-CDMA system design and the BER evaluation. Section 8.3 shows the DS-CDMA and MC-CDMA systems and outlines the four different combining strategies for the MC-CDMA system. Section 8.4 discusses a MC-CDMA design method, namely, how to determine the number of subcarriers and the length of guard interval to minimize the BER for a given channel condition. Section 8.5 shows the theoretical BER lower bounds for both systems and proves their equivalence. Section 8.6 demonstrates the BER performance of MC-CDMA and DS-CDMA schemes in (synchronous) downlink and quasisynchronous uplink channels and discusses the advantages and disadvantages in terms of "bandwidth of transmitted signal spectrum" and "attainable BER performance." And finally, Section 8.7 draws our conclusions.

8.2 CHANNEL MODEL

As a frequency selective fast Rayleigh fading channel, we assume a wide sense stationary uncorrelated scattering (WSSUS) channel [15] with L received paths in the complex equivalent low-pass time-variant impulse response:

$$h^j(\tau;t)=\sum_{l=1}^{L} g_l^j(t)\delta(\tau-\tau_l) \tag{8.1}$$

where j is the user index, t and τ are the time and the delay, respectively, $\delta(\cdot)$ is the Dirac delta function, $g_l^j(t)$ is the l^{th} path gain for user j which is a mutually independent complex Gaussian random process with zero mean and variance σ_l^2 for different l, and τ_l is the propagation delay for the l-th path. Figure 8.1 shows the corresponding multipath power delay profile given by (we assume that there is no signal whose propagation delay exceeds the symbol duration)

$$\phi_c^j(\tau)=\frac{1}{2}E\left[h^{j*}(\tau;t)\cdot h^j(\tau;t)\right]=\sum_{l=1}^{L}\sigma_l^2\delta(\tau-\tau_l) \tag{8.2}$$

where $E(\cdot)$ is the expectation and * is the complex conjugate. With (8.2), the RMS (root mean square) delay spread (τ_{RMS}) can be calculated [16].

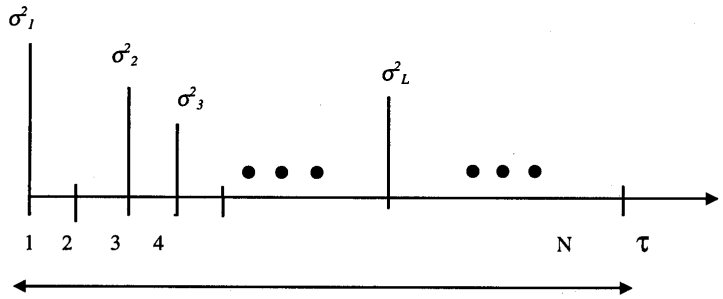

Figure 8.1 Multipath power delay profile.

On the other hand, the channel time selectivity is characterized by the normalized time autocorrelation function [15]:

$$\rho_l^j(\Delta t)=\frac{1}{2\sigma_l^2}E\left[g_l^j(t+\Delta t)\cdot g_l^{j*}(t)\right] \tag{8.3}$$

Assuming that an omnidirectional antenna is used at the receiver and the angular distribution of wave arrivals on each path is uniform, the autocorrelation is given by [17]

$$\rho_l^j(\Delta t)=J_0(2\pi f_D\Delta t)\approx 1-(\pi f_D\Delta t)^2 \quad (f_D\Delta t)<<1, \tag{8.4}$$

where $J_0(.)$ and f_D are the zero-order Bessel function of the first kind and the maximum Doppler frequency, respectively. Note that, for different j, the path gains $\{g_l^j(\cdot)\}$ are independent, identically distributed (i.i.d.) in an uplink channel and identically distributed in a downlink channel.

8.3 DS-CDMA AND MC-CDMA SYSTEMS

The OFDM scheme is robust to frequency-selective fading; however, it has some disadvantages such as difficulty in subcarrier synchronization and sensitivity to frequency offset and nonlinear amplification, which result from the fact that it is composed of many subcarriers with their overlapping power spectra and exhibits a non-constant nature in its envelope, see Chapters 4 and 6, respectively. In contrast to this, DS-CDMA is quite robust to frequency offsets and nonlinear distortion. The combination of OFDM signaling and CDMA scheme has one major advantage, however, in that it can lower the symbol rate in each subcarrier so that a longer symbol duration makes it easier to quasisynchronize the transmissions [18]. For instance, in [19], a multicarrier-based DS-CDMA scheme is proposed for a quasisynchronous system. In this chapter, we assume a quasisynchronous uplink channel, in addition to a (synchronous) downlink channel. We discuss the BER performance of MC-CDMA and DS-CDMA systems in multipath fading channels. To focus attention on the BER variations by different combining strategies, we assume a perfect subcarrier synchronization with no frequency offset and no nonlinear distortion and perfect subcarrier amplitude/phase estimation for MC-CDMA system. On the other hand, for the DS-CDMA system, we assume a perfect carrier synchronization and perfect path gain estimation.

8.3.1 DS-CDMA System

Figure 8.2(a) shows the DS-CDMA transmitter for the j^{th} user with binary PSK modulation/coherent (CBPSK) format. The complex equivalent lowpass transmitted signal is written as

$$s_{DS}^{j}(t) = \sum_{i=-\infty}^{+\infty} \sum_{k=0}^{K_{DS}-1} b_j(i) c_j(k) p_c(t - kT_c - iT_s) \tag{8.5}$$

where, $b_j(i)$ and $c_j(k)$ are the i^{th} information bit and the k^{th} chip of the spreading code with length K_{DS} and chip duration T_c, respectively, T_s (= $1/R$) is the symbol duration (R is the symbol rate), and $p_c(t)$ is the chip pulse waveform. For instance, when a rectangular pulse is used, $p_c(t)$ is given by

$$p_c(t) = \begin{cases} 1 & (0 \le t \le T_c) \\ 0 & (\text{otherwise}) \end{cases} \tag{8.6}$$

The mainlobe bandwidth of the transmitted signal spectrum for a rectangular pulse waveform is given by

$$B_{DS} = 2K_{DS}/T_s \tag{8.7}$$

and for the Nyquist pulse waveform with rolloff factor of α (see Figure 8.2(b)),

$$B_{DS} = (1+\alpha)K_{DS}/T_s \qquad (0 \le \alpha \le 1.0). \tag{8.8}$$

Figure 8.2(c) shows the I-finger DS-CDMA RAKE receiver for the j^{th} user. The received signal through the channel given by (8.1) is written as

$$r_{DS}(t) = \sum_{j=1}^{J} \int_{-\infty}^{+\infty} s_{DS}^{j}(t-\tau) \otimes h^{j}(\tau;t) d\tau + n(t)$$

$$= \sum_{l=1}^{L} \sum_{j=1}^{J} s_{DS}^{j}(t-\tau_l) g_l^{j}(t) + n(t) \tag{8.9}$$

where J is the number of total active users, $\otimes$ is the convolution operation, and $n(t)$ is the complex additive Gaussian noise (AWGN) with zero mean and variance σ_n^2. The decision variable at $t = iT_s$ is written as

$$D_{DS}^{j'} = \sum_{v=1}^{I} g_v^{*}(iT_s) \cdot \frac{1}{T_s} \int_{iT_s+\tau_v}^{iT_s+\tau_v+T_s} \sum_{k=0}^{K_{DS}-1} c_{j'}(k) p_c(t-kT_c-iT_s-\tau_v) r_{DS}(t) dt \tag{8.10}$$

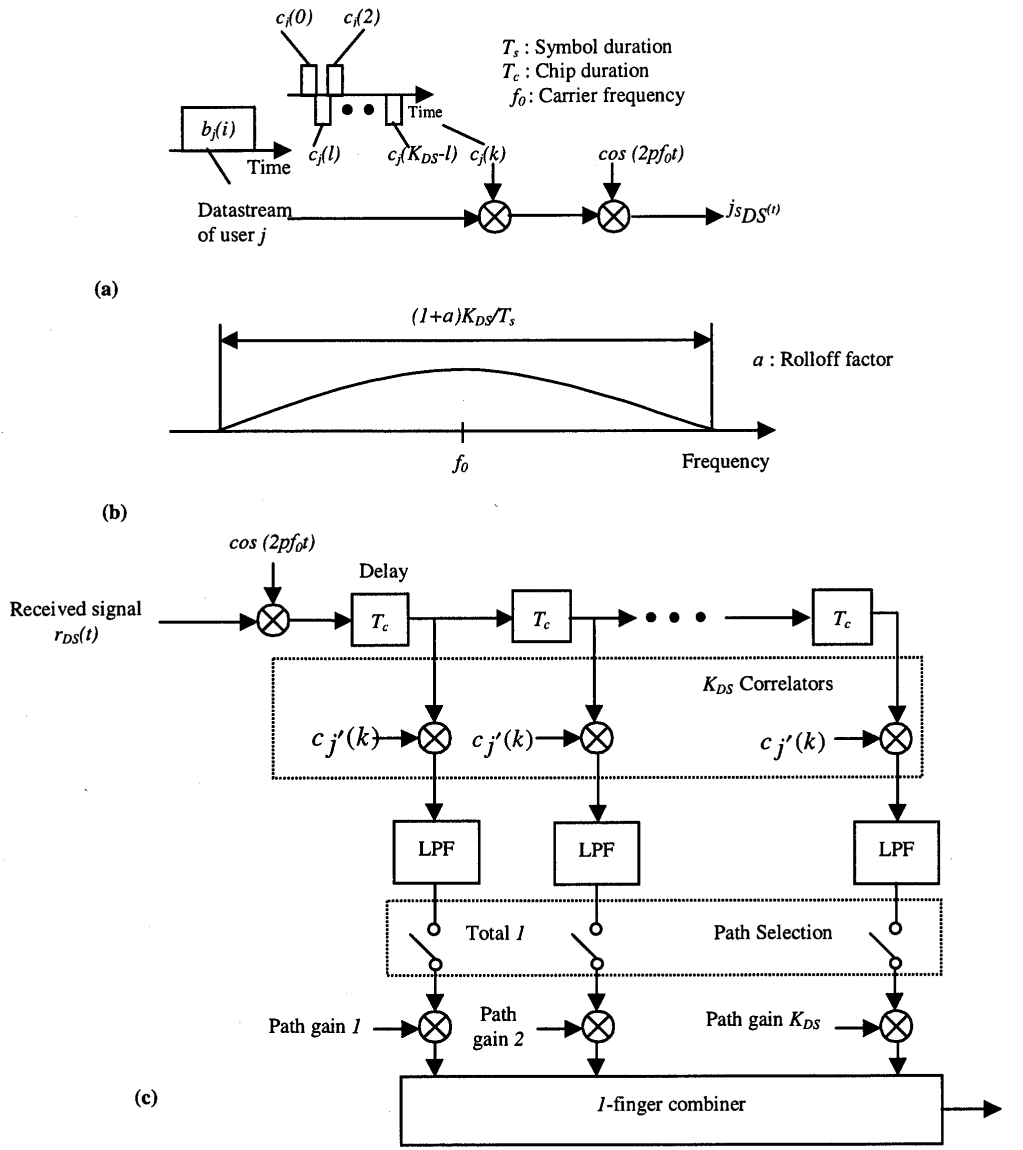

Figure 8.2 DS-CDMA system: (a) transmitter, (b) power spectrum of its transmitted signal, and (c) RAKE receiver.

8.3.2 MC-CDMA System

The MC-CDMA transmitter spreads the original signal using a given spreading code in the frequency domain. In other words, a fraction of the symbol corresponding to a chip of the spreading code is transmitted through a different subcarrier. For Multi-Carrier transmission, it is essential to have frequency nonselective fading over each subcarrier. Therefore, if the original symbol rate is high enough to become subject to frequency-selective fading, the signal needs to be serial-to-parallel converted first before being spread over the frequency domain. The basic transmitter structure of MC-CDMA scheme is similar to that of a normal OFDM scheme as described in Chapter 2. The main difference is that the MC-CDMA scheme transmits the same symbol in parallel through many subcarriers, whereas the OFDM scheme transmits different symbols.

Figure 8.3(a) shows the MC-CDMA transmitter for the j^{th} user with CBPSK format. The input information sequence is first converted into P parallel data sequences $(a_{j,0}(i), a_{j,1}(i), \ldots, a_{j,P-1}(i))$ and then each serial/parallel converter output is multiplied with the spreading code with length K_{MC}. All the data in total $N = P \times K_{MC}$ (corresponding to the total number of subcarriers) are modulated in baseband by the inverse discrete fourier transform (IDFT) and converted back into serial data. The guard interval Δ is inserted between symbols to avoid intersymbol interference caused by multipath fading, and finally the signal is transmitted after RF up-conversion. The complex equivalent lowpass transmitted signal is written as

$$s_{MC}^{j}(t) = \sum_{i=-\infty}^{+\infty} \sum_{p=0}^{P-1} \sum_{m=0}^{K_{MC}-1} a_{j,p}(i) d_j(m) p_s(t - iT_s') e^{j2\pi(Pm+p)\Delta f'(t-iT_s')} \tag{8.11}$$

$$T_s' = PT_s, \tag{8.12}$$

$$\Delta f' = 1/(T_s' - \Delta) \tag{8.13}$$

where $\{d_j(0), d_j(1), \ldots, d_j(K_{MC}-1)\}$ is the spreading code with length K_{MC}, T'_s is the symbol duration at subcarrier, $\Delta f'$ is the minimum subcarrier separation, and $p_s(t)$ is the rectangular symbol pulse waveform defined as

$$p_s(t) = \begin{cases} 1 & (-\Delta \le t \le T_s' - \Delta) \\ 0 & (\text{otherwise}) \end{cases} \tag{8.14}$$

The bandwidth of the transmitted signal spectrum is written as (see Figure 8.3(b))

$$\begin{aligned} B_{MC} &= (P \cdot K_{MC} - 1)/(T_s' - \Delta) + 2/T_s' \\ &\approx K_{MC}/T_s/(1 - \Delta/P) \\ &= (1+\beta)K_{MC}/T_s, \end{aligned} \tag{8.15}$$

$$\beta = \Delta / P \qquad (0 \le \beta \le 1.0), \tag{8.16}$$

where β is the bandwidth expansion factor associated with the guard interval insertion.

Note that, in (8.11), no spreading operation is done in the time domain. (8.12) shows that the symbol duration at subcarrier level is P times as long as the original symbol duration because of serial/parallel conversion. Although the minimum subcarrier separation is given by (8.13), the subcarrier separation for $a_{j,p}(i)$ is $\Delta f = P/(T'_s - \Delta)$ (see the hatched subcarrier power spectra in Figure 8.3(b)). Therefore, when setting K_{MC} to 1, the transmitted waveform given by (8.11) becomes all the same as an OFDM waveform with P subcarriers.

On the other hand, the received signal is written as

$$\begin{aligned} r_{MC}(t) &= \sum_{j=1}^{J} \int_{-\infty}^{+\infty} s_{MC}^{j}(t-\tau) \otimes h^{j}(\tau;t) d\tau + n(t) \\ &= \sum_{i=-\infty}^{+\infty} \sum_{p=0}^{P-1} \sum_{m=0}^{K_{MC}-1} \sum_{j=1}^{J} z_{m,p}^{j}(t) a_{j,p}(i) d_m^j p_s(t - iT'_s) e^{j2\pi(Pm+p)\Delta f' t} + n(t) \end{aligned} \tag{8.17}$$

where $z_{m,p}^{j}(t)$ is the received complex envelope at the $(mP+p)^{\text{th}}$ subcarrier of the j^{th} user.

The MC-CDMA receiver requires coherent detection for successful despreading operation. Figure 8.3(c) shows the MC-CDMA receiver for the j^{th} user. After down-conversion, the m-subcarrier components (m = 0,1, ..., K_{MC} - 1) corresponding to the received data $a_{j',p}(i)$ is first coherently detected with DFT and then multiplied with the gain $G_{j'}(m)$ to combine the energy of the received signal scattered in the frequency domain. The decision variable is the sum of the weighted baseband components given by (we can omit the subscription p without loss of generality)

$$D_{MC}^{j'}(t = iT_s) = \sum_{m=0}^{K_{MC}-1} G_{j'}(m) y(m) \tag{8.18}$$

$$y(m) = \sum_{j=1}^{J} z_m^j(iT_s) a_j d_m^j + n_m(iT_s) \tag{8.19}$$

where $y(m)$ and $nm(iTs)$ are the complex baseband component of the received signal after down-conversion and the complex additive Gaussian noise at the m^{th} subcarrier at $t = iTs$, respectively. Now, we discuss the following four combining strategies.

Orthogonality Restoring Combining

Choosing the gain in the down-link channel ($z_m^{\,1} = z_m^{\,2} = ... = z_m^{\,J} = z_m^{\,1}$) as

$$G_{j'}(m) = d_{j'}(m) z_m^* / |z_m|^2 \tag{8.20}$$

the receiver can eliminate the multiple access interference (MAI) perfectly [6]:

$$\hat{a}^{j'} = a^{j'} + \sum_{m=1}^{K_{MC}} d_{j'}(m) z_m^* / |z_m|^2 n_m \tag{8.21}$$

In (8.21), however, low-level subcarriers tend to be multiplied by the high gains, and the noise components are amplified at weaker subcarriers. This noise amplification effect degrades BER performance. Note that ORC is applicable only for the downlink channel.

Equal Gain Combining

The gain for EGC is given by [4]

$$G_{j'}(m) = d_{j'}(m) z_m^{j'*} / |z_m^{j'}| \tag{8.22}$$

Maximal Ratio Combining

The gain for MRC is given by [4]

$$G_{j'}(m) = d_{j'}(m) z_m^{j'*} \tag{8.23}$$

In the case of a single user, the MRC method minimizes the BER.

Minimum Mean Square Error Combining

The MMSEC criterion states that the error in the estimated data symbols must be orthogonal to the baseband components of the received subcarriers:

$$E\left[\left(a^{j'} - \hat{a}^{j'}\right) y(m')^*\right] = 0 \qquad \left(m' = 1,\ 2, \ldots, K_{MC}\right) \tag{8.24}$$

$G_{j'}(m)$ is given by [6]

$$G_{j'}(m) = d_{j'}(m) z_m^{j'*} / \left(\sum_{j=1}^{J} |z_m^j|^2 + \sigma_n^2 \right) \tag{8.25}$$

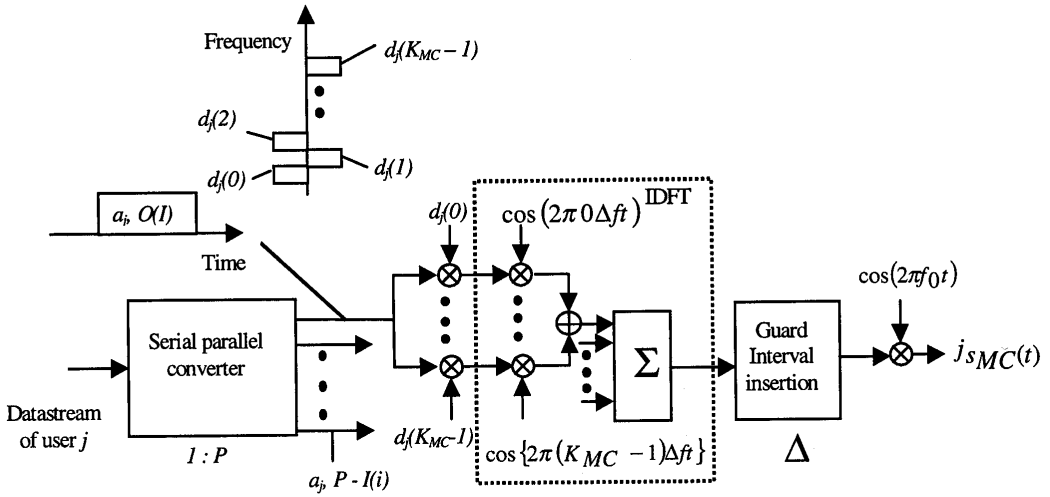

(a) Transmitter

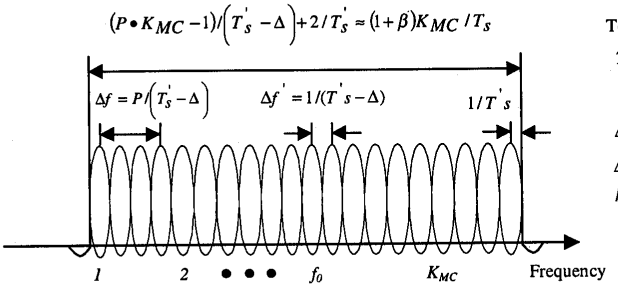

Total P• K_{MC} subcarriers
T_s' : Symbol duration
f_o : Carrier frequency
Δ : Guard interval
Δf : Subcarrier separation
$\Delta f'$: Minimum subcarrier separation
β : Bandwidth expansion factor

(b) Power spectrum of transmitted signal

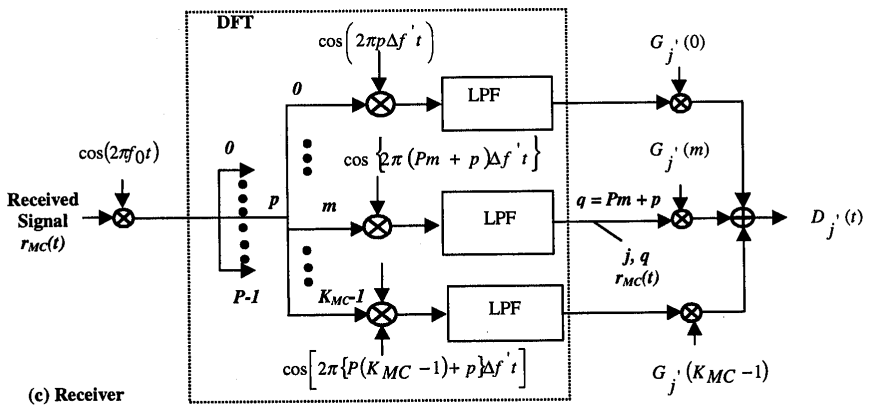

(c) Receiver

Figure 8.3 MC-CDMA system.

Note that, in the downlink application, for small $|z_m|$, the gain becomes small to avoid excessive noise amplification, while for large $|z_m|$, it becomes proportional to the inverse of the subcarrier envelope $z_m^*/|z_m|^2$ to recover orthogonality among users [6].

8.4 MC-CDMA SYSTEM DESIGN

To determine the number of subcarriers and the length of guard interval, we derive the autocorrelation function of the received signal. The received signal for the j^{th} user is given by

$$r_{MC}^{j}(t) = \int_{-\infty}^{+\infty} s_{MC}^{j}(t-\tau) \otimes h(\tau;t) d\tau + n(t) \tag{8.26}$$

where $h^j(\tau;t)$ is given by (8.1) and $\{\tau_l\}$ is classified as follows:

$$\begin{aligned} &0 \le \tau_l \le \Delta && (l = 1,\ldots,L_1) \\ &\Delta < \tau_l < T_s && (l = L_1+1,\ldots,L_1+L_2(=L)) \end{aligned} \tag{8.27}$$

The Fourier coefficient of the q^{th} $(q = mP + p)$ subcarrier at $t = iT_s'$ is given by (see Figure 8.3(c))

$$r_{MC}^{j,q}(iT_s') = \frac{1}{T_s' - \Delta} \int_{iT_s'}^{iT_s'+T_s'-\Delta} r_{MC}^{j}(t) e^{-j2\pi q \Delta f'(t-iT_s')} dt \tag{8.28}$$

The normalized autocorrelation function of the q^{th} subcarrier between $t = iT_s'$ and $t = (i-1)T_s'$ for the j^{th} user is written as (see Appendix 8A)

$$\begin{aligned} R_{MC}^{j,q}(\Delta, N, R', f_D, \tau_{\text{RMS}}) &= \frac{E\left[r_{MC}^{j,q}(iT_s') \cdot r_{MC}^{*j,q}((i-1)T_s')\right]}{E\left[r_{MC}^{j,q}(iT_s') r_{MC}^{*j,q}(iT_s')\right]} \\ &= \frac{\sigma_{S1}^2}{\sigma_{S2}^2 + \sigma_I^2 + \sigma_n^2} \end{aligned} \tag{8.29}$$

$$\sigma_{S1}^2 = \sum_{l=1}^{L_1} \sigma_l^2 \left\{ 1 - \left(\frac{\pi f_D}{R'} \right)^2 \left(\frac{(N-\Delta R')^2}{6} + N^2 \right) \right\}$$

$$+ \sum_{l=L_1+1}^{L_1+L_2} \sigma_l^2 \frac{(N-\tau_l R')^2}{(N-\Delta R')^2} \left\{ 1 - \left(\frac{\pi f_D}{R'} \right)^2 \left(\frac{(N-\tau_l R')^2}{6} + N^2 \right) \right\} \tag{8.30}$$

$$\sigma_{S2}^2 = \sum_{l=1}^{L_1} \sigma_l^2 \left\{ 1 - \left(\frac{\pi \quad f_D}{R'} \right)^2 \frac{(N-\Delta R')^2}{6} \right\}$$

$$+ \sum_{l=L_1+1}^{L_1+L_2} \sigma_l^2 \frac{(N-\tau_l R')^2}{(N-\Delta R')^2} \left\{ 1 - \left(\frac{\pi \quad f_D}{R'} \right)^2 \frac{(N-\tau_l R')^2}{6} \right\}$$

$$+ \sum_{l=L_1+1}^{L_1+L_2} \sigma_l^2 \frac{(-\Delta R'+\tau_l R')^2}{(N-\Delta R')^2} \left\{ 1 - \left(\frac{\pi \quad f_D}{R'} \right)^2 \frac{(-\Delta R'+\tau_l R')^2}{6} \right\} \qquad (8.31)$$

$$\sigma_I^2 = \sum_{l=1}^{L_1} \sum_{k=0,k\neq q}^{N-1} \sigma_l^2 \frac{\left(\frac{\pi \quad f_D}{R'} \right)^2 (N-\Delta R')^2}{2\pi^2 (k-q)^2}$$

$$+ \sum_{l=L_1+1}^{L_1+L_2} \sum_{k=0,k\neq q}^{N-1} \sigma_l^2 \left\{ \frac{\left(\frac{\pi \quad f_D}{R'} \right)^2 (N-\tau_l R')^2}{2\pi^2 (k-q)^2} \cos\left(\frac{2\pi(k-q)(N-\tau_l R')}{N-\Delta R'} \right) \right\}$$

$$+ \frac{\left(\frac{\pi \quad f_D}{R'} \right)^2 (N-\Delta R')(N-\tau_l R')}{\pi^3 (k-q)^3} \sin\left(\frac{2\pi(k-q)(N-\tau_l R')}{N-\Delta R'} \right)$$

$$+ \left(\frac{1}{2\pi^2 (k-q)^2} + \frac{3\left(\frac{\pi f_D}{R'} \right)^2 (N-\Delta R')^2}{4\pi^4 (k-q)^4} \right) \cdot \left(1 - \cos\left(\frac{2\pi(k-q)(N-\tau_l R')}{N-\Delta R'} \right) \right)$$

$$+\frac{\left(\frac{\pi f_D}{R'}\right)^2(-\Delta R'+\tau_l R')^2}{2\pi^2(k-q)^2}\cos\left(\frac{2\pi(k-q)(-\Delta R'+\tau_l R')}{N-\Delta R'}\right)$$

$$+\frac{\left(\frac{\pi f_D}{R'}\right)^2(N-\Delta R')(-\Delta R'+\tau_l R')}{\pi^3(k-q)^3}\sin\left(\frac{2\pi(k-q)(-\Delta R'+\tau_l R')}{N-\Delta R'}\right)$$

$$+\left(\frac{1}{2\pi^2(k-q)^2}+\frac{3\left(\frac{\pi f_D}{R'}\right)^2(N-\Delta R')^2}{4\pi^4(k-q)^4}\right)\cdot\left(1-\cos\left(\frac{2\pi(k-q)(-\Delta R'+\tau_l R')}{N-\Delta R'}\right)\right) \tag{8.32}$$

where R' ($= K_{MC}R$) is the chip rate.

In an OFDM scheme, generally, when the transmission rate, R', in the case of MC-CDMA scheme) is given, the transmission performance becomes more sensitive to time selective fading as the number of subcarriers N increases, because the longer symbol duration means an increase in the amplitude and phase variation during a symbol, causing an increased level of ICI. As N decreases, the modulation becomes more robust to fading in time, but it becomes more vulnerable to delay spread, as the ratio of delay spread and symbol time increases, see Figure 8.4. The latter is not necessarily true if the guard time is kept at a fixed value, but as the symbol duration decreases, a fixed guard interval (Δ) means an increased loss of power, see Figure 8.5. Therefore, for given R (R'), f_D and τ_{RMS}, there exists an optimum that minimizes the BER in both N and Δ [21].

In the MC-CDMA scheme, N_{opt} and Δ_{opt} maximizes the ACF given by (8.29) to (8.32), because it means a measure to show how much the received signal is distorted in the time frequency, selective fading channel (i.e., how we can place the signal on the time-frequency plane, so that it suffers from minimum distortion):

$$\left[N_{opt},\Delta_{opt}\right]=\arg\left\{\max R_j\left(N,\Delta|R',f_D,\tau_{RMS}\right)\right\} \tag{8.33}$$

Therefore, with (8.33), we determine two parameters, N_{opt} and Δ_{opt}.

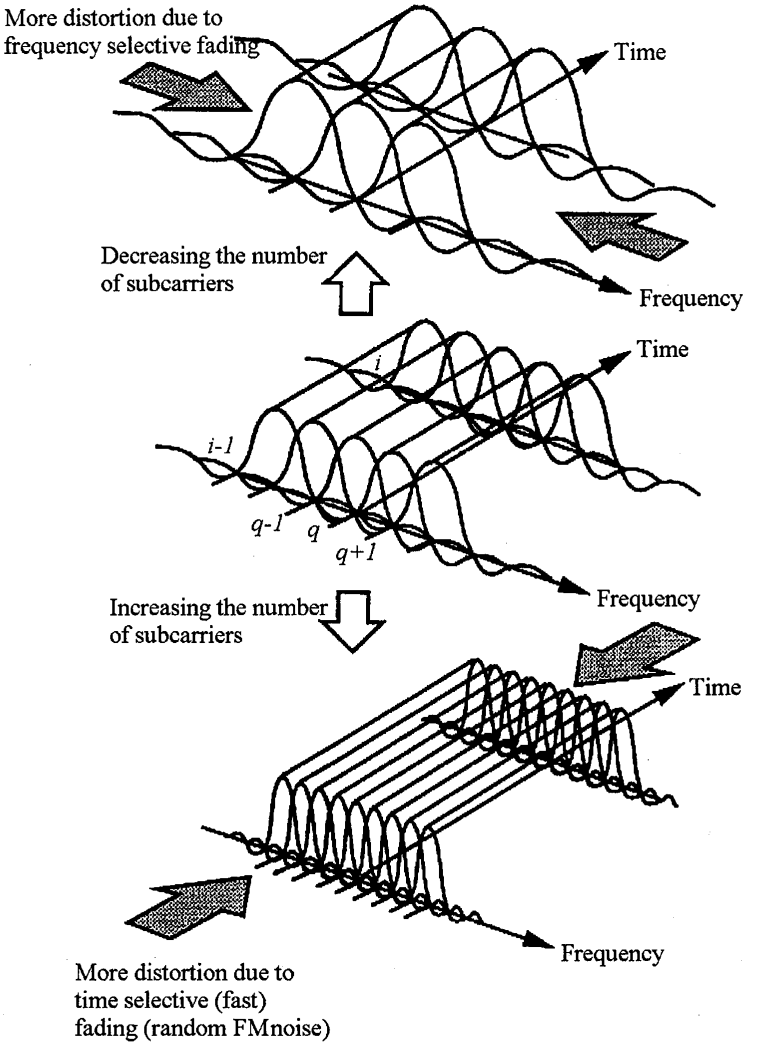

Figure 8.4 Optimum in the number of subcarriers.

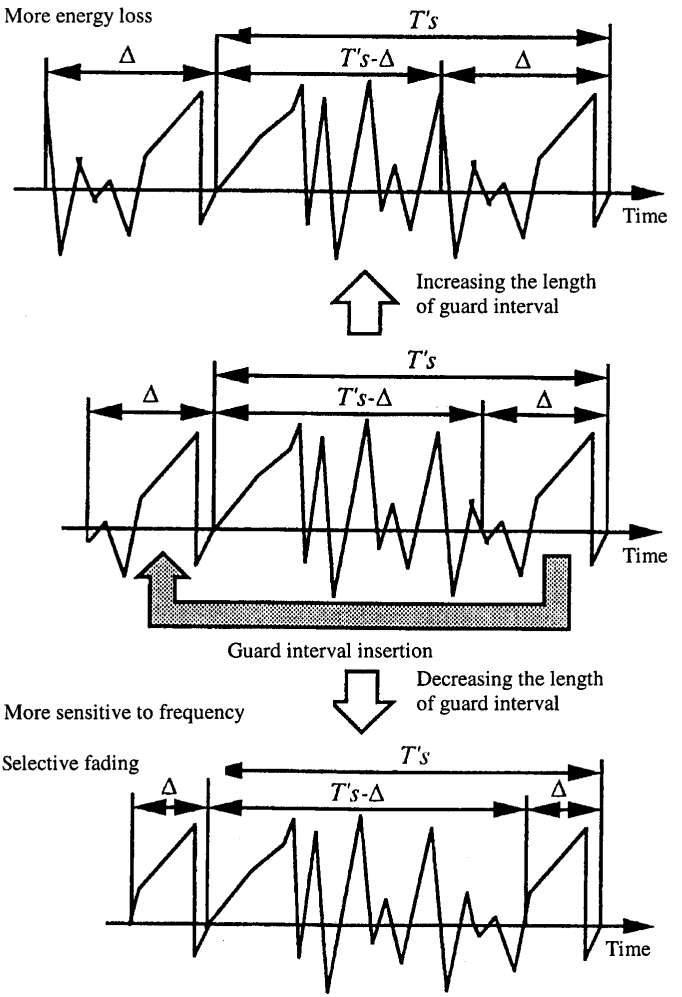

Figure 8.5 Optimum in the length of guard interval.

8.5 BER LOWER BOUND

8.5.1 DS-CDMA System

Defining $\mathbf{r_t}$ as the received signal vector, the time domain covariance matrix $\mathbf{M_t}$ is given by

$$\mathbf{r_t} = [r_1, r_2, \ldots r_L]^T, \tag{8.34}$$

$$\mathbf{M_t} = \frac{1}{2} E[\mathbf{r_t} \cdot \mathbf{r_t}^T]$$

$$= \begin{bmatrix} \sigma_1^2 & 0 & \cdots & 0 \\ 0 & \sigma_2^2 & & \vdots \\ \vdots & & \ddots & \vdots \\ \vdots & & & 0 \\ 0 & \cdots & 0 & \sigma_L^2 \end{bmatrix}, \tag{8.35}$$

In the above equation, we assume a perfect auto-correlation characteristic for the spreading codes.

The BER of time domain I-finger DS-CDMA RAKE receiver in the case of a single user is uniquely determined by the eigenvalues of $\mathbf{M_t}$ (in this case, the eigenvalues are $\sigma_1^2, \sigma_2^2, \ldots, \sigma_L^2$) [22]. For example, when $\sigma_l^2 (l = 1, \ldots, L)$ are different from each other, BER is given by

$$\mathrm{BER}_{\mathrm{DS}} = \sum_{l=1}^{I} w_l \frac{1}{2} \left\{ 1 - \sqrt{\frac{\sigma_l^2 / \sigma_n^2}{1 + \sigma_l^2 / \sigma_n^2}} \right\} \tag{8.36}$$

$$w_l = \frac{1}{\prod_{v=1, v \neq l}^{I} \left(1 - \frac{\sigma_v^2}{\sigma_l^2} \right)} \tag{8.37}$$

$$\sigma_t^2 = \sum_{l=1}^{L} \sigma_l^2 \tag{8.38}$$

where σ_t^2 is the total power of the received signal. If all multipath signals have equal power, so $\sigma_l^2 (l = 1, \ldots, L)$ are all the same $\left(= \sigma_s^2 \right)$ [15], then the BER is given as

$$\mathrm{BER}_{\mathrm{DS}} = \left(\frac{1-\mu_{\mathrm{DS}}}{2}\right)^{I} \sum_{l=0}^{I-1} \binom{I-1+l}{l} \left(\frac{1+\mu_{\mathrm{DS}}}{2}\right)^{l},$$

(8.39)

$$\mu_{\mathrm{DS}} = \sqrt{\frac{\sigma_s^2/\sigma_n^2}{1+\sigma_s^2/\sigma_n^2}}, \tag{8.40}$$

Note that the L-finger RAKE receiver achieves the minimum BER (the BER lower bound) [15].

8.5.2 MC-CDMA System

For the case of a single user, the frequency domain MC-CDMA RAKE receiver based on the MRC method achieves the minimum BER (the BER lower bound) [15].

Defining $\mathbf{r_f}$ as the received signal vector, the frequency domain covariance matrix $\mathbf{M_f}$ is given by

$$\mathbf{r_f} = \left[z_1, z_2, \ldots, z_{K_{MC}}\right]^T, \tag{8.41}$$

$$\mathbf{M_f} = \frac{1}{2} E\left[\mathbf{r_f} \cdot \mathbf{r_f}^T\right] = \{m_f^{a,b}\},$$

$$m_f^{a,b} = \Phi_C\left((a-b)\Delta f\right), \tag{8.42}$$

where $\{m_f^{a,b}\}$ is the a-b element of $\mathbf{M_f}$, and $\Phi_C(\Delta f)$ is the spaced frequency correlation function defined as the Fourier transform of the multipath delay profile:

$$\Phi_C(\Delta f) = \int_{-\infty}^{+\infty} \phi_c(\tau) e^{-j2\pi\Delta f\tau} d\tau. \tag{8.43}$$

Defining $\lambda_1, \lambda_2, \ldots, \lambda_{K_{MC}}$ as the nonzero eigenvalues of $\mathbf{M_f}$, BER is given by a form similar to (8.36) or (8.40) [22]. For example, when $\lambda_m\left(m = 1, \ldots, K_{\mathrm{MC}}\right)$ are different from each other,

$$\mathrm{BER}_{\mathrm{MC}} = \sum_{m=1}^{K_{\mathrm{MC}}} v_m \frac{1}{2}\left\{1 - \sqrt{\frac{\lambda_m/N_0}{1+\lambda_m/N_0}}\right\} \tag{8.44}$$

$$v_m = \frac{1}{\prod_{u=1, u\neq m}^{K_{MC}} \left(1-\frac{\lambda_u}{\lambda_m}\right)} \tag{8.45}$$

Also, when $\lambda_m\left(m = 1, \ldots, K_{MC}\right)$ are all the same (= λ):

$$\mathrm{BER}_{\mathrm{MC}} = \left(\frac{1-\mu_{\mathrm{MC}}}{2}\right)^{K_{\mathrm{MC}}} \sum_{m=0}^{K_{\mathrm{MC}}-1} \binom{M-1+m}{m} \left(\frac{1+\mu_{\mathrm{MC}}}{2}\right)^{m}$$

$$\mu_{\mathrm{MC}} = \sqrt{\frac{\lambda / N_0}{1+\lambda / N_0}} \tag{8.46}$$

8.5.3 BER Lower Bound Equivalence

When there are L paths in the symbol duration at subcarrier T_s' in the multipath delay profile shown in Figure 8.1, we obtain the following $N \times N$ time-domain covariance matrix with time resolution of T_s'/N:

$$\mathbf{M}_t' = \begin{bmatrix} \sigma_1^2 & 0 & \cdots & \cdots & \cdots & 0 \\ 0 & 0 & & & & \cdots \\ \cdots & & \sigma_1^2 & & & \cdots \\ \cdots & & & \sigma_3^2 & & \cdots \\ \cdots & & & & \cdots & 0 \\ 0 & \cdots & \cdots & \cdots & 0 & \cdots \end{bmatrix}, \tag{8.47}$$

where the nonzero eigenvalues of $\mathbf{M}_t'$ are $\sigma_1^2, \sigma_2^2, \sigma_3^2, \ldots, \sigma_L^2$.

The corresponding $N \times N$ frequency domain covariance matrix with frequency resolution of $1/T_s$ is given by

$$\mathbf{M}_f' = \mathbf{W}\mathbf{M}_t'\mathbf{W}^*, \tag{8.48}$$

where $\mathbf{W}$ is the $N \times N$ DFT matrix given by

$$\mathbf{W} = \left\{w^{i,j}\right\}$$

$$w^{i,j} = e^{j2\pi\frac{ij}{N}} \tag{8.49}$$

We define $\mathbf{r}_1$ as the eigenvector corresponding to the eigenvalue σ_l^2:

$$\mathbf{M}_t' r_1 = \sigma_l^2 \mathbf{r}_1 \qquad (l = 1, 2, \ldots, L) \tag{8.50}$$

Also, we define $\mathbf{z}_1$ as

$$\mathbf{z}_1 = \mathbf{W}\,\mathbf{r}_1 \qquad (l = 1, 2, \ldots, L) \tag{8.51}$$

Now we can theoretically prove that the frequency domain covariance matrix has all the same eigenvalues as the time domain covariance matrix as follows:

$$\begin{aligned}\mathbf{M}'_f \mathbf{z}_1 &= \mathbf{W}\mathbf{M}'_t\mathbf{W}^*.\mathbf{W}\mathbf{r}_1 \\ &= \mathbf{W}\mathbf{M}'_t\mathbf{r}_1 \\ &= \mathbf{W}\sigma_l^2\mathbf{r}_1 \\ &= \sigma_l^2\mathbf{W}\mathbf{r}_1 \\ &= \sigma_l^2\mathbf{z}_1 \end{aligned} \tag{8.52}$$

The above equation shows that the nonzero eigenvalues of $\mathbf{M}'_f$ are $\sigma_1^2,\sigma_2^2,\sigma_3^2,...,\sigma_L^2$. Therefore, as long as we use the same frequency-selective fading channel, the BER lower bound of the MC-CDMA system is the same as that of the DS-CDMA system. Also, the assumption of independent fading characteristic at each subcarrier implies a frequency selective fading at each subcarrier, because it requires independent N paths uniformly scattered in the symbol duration at subcarrier.

8.6 NUMERICAL RESULTS

To demonstrate the numerical results, we assume

- RMS delay spread τ_{RMS} = 20 ns,
- Doppler power spectrum with maximum Doppler frequency f_D = 10 Hz,
- Transmission rate R = 3 Msymbols/s (BPSK format),
- Walsh Hadamard codes with K_{MC} = 32 for the MC-CDMA system,
- Gold codes with K_{DS} = 31 for the DS-CDMA system ($K_{MC} \approx K_{DS}$).

First, to design the MC-CDMA system and to select one best suited combining strategy in the MC-CDMA system, we assume a simple 2-path multipath delay profile often encountered in urban and hilly areas [23, 24], where the first and second paths have the same power (2-path i.i.d. delay profile) [25].

8.6.1 MC-CDMA System Design

Figure 8.6 shows the optimal values in the number of subcarriers N and the length of guard interval Δ versus the normalized RMS delay spread σ_{RMS} as a function of the Doppler frequency f_D, where Δ, σ_{RMS} and f_D are normalized by R'. This figure is obtained from the maximization of (8.33). For given f_D and R', both N_{opt} and Δ_{opt} increases as σ_{RMS} increases. For the above parameters, we obtain $f_D / R' \approx 10^{-7}$ and $\tau_{\text{RMS}} R' = 1.92$, so we choose $\left[N_{\text{opt}}, \Delta_{\text{opt}} / T_s'\right] = [256, 0.015]$ as an optimal set. It means

that the original data sequence is first converted into eight parallel sequences (P = 8), and then each sequence is mapped onto 32 subcarriers, and the length of the guard interval is negligibly short, as compared with the symbol duration at subcarrier.

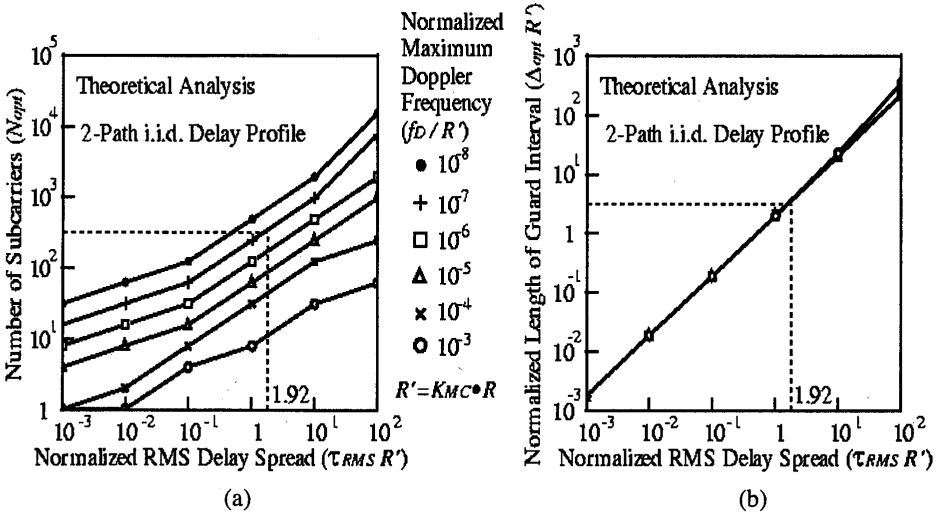

Figure 8.6 (a) Optimum number of subcarriers, and (b) optimum length of guard interval.

From (8.7) and (8.16), B_{MC} and B_{DS} are calculated as 97.8 MHz and 186 MHz, respectively, so the bandwidth of the DS-CDMA signal is 1.9 times as wide as that of the MC-CDMA signal as long as the same rectangular pulse format is employed. From (8.8), however, if a Nyquist pulse is employed in the DS-CDMA system, the difference in the signal bandwidth diminishes as the roll-off factor becomes small (there is no difference when α = 0.05). Therefore, we can conclude that MC-CDMA system has no major advantage in terms of signal bandwidth, as compared with the DS-CDMA system. Note, however, that when Nyquist filters are introduced in the transmitter and receiver for base bandpulse shaping in a DS-CDMA system, the RAKE receiver may wrongly combine paths. This is because noise-causing distortion in the autocorrelation characteristic often results in a wrong correlation [26].

How many users the system can accommodate depends on the attainable BER performance; in other words, the combining strategy employed in the MC-CDMA system and the number of fingers in the DS-CDMA system. We discuss BER performance in the following two subsections.

8.6.2 Down-Link BER Performance

Figures 8.7, 8.8, and 8.9 show the downlink BER performance of MC-CDMA scheme with EGC, MRC and MMSEC for the 2-path i.i.d. delay profile, respectively. Here, the theoretical BER lower bound is given by (8.39) with $I = 2$. In these figures, the BER for the ORC is shown, and further, the BER of MC-FDMA scheme is also shown, which supports 32 users at most, assigning a different set of eight subcarriers to each user. This scheme obtains no frequency diversity effect, so the theoretical BER is given by [15].

$$BER_{\text{MC-FDMA}} = \frac{1}{2}\left(1 - \sqrt{\frac{E_b / N_0}{1 + E_b / N_0}}\right) \tag{8.53}$$

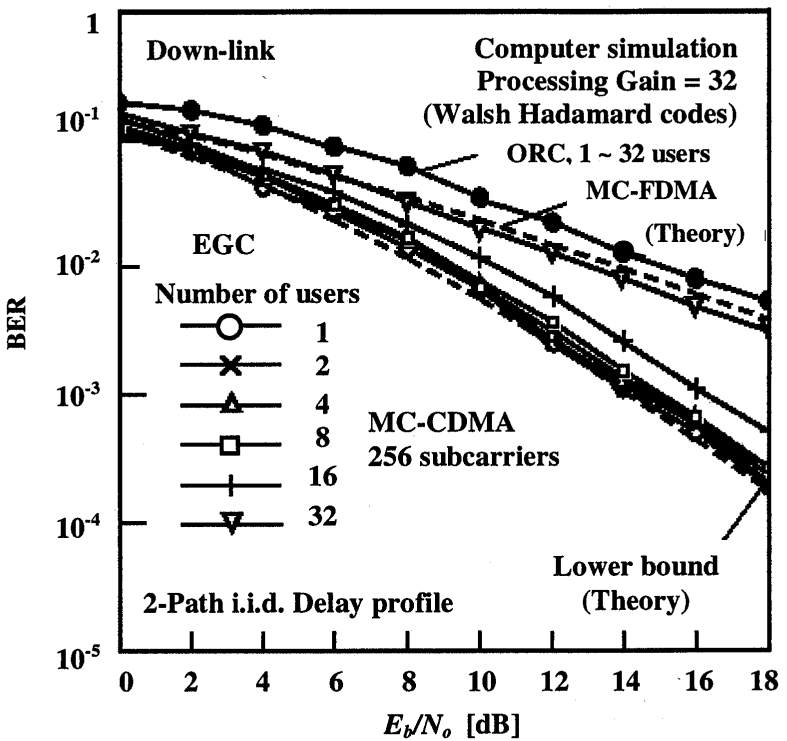

Figure 8.7 Down-link BER of MC-CDMA system with EGC.

BER performance of the ORC is independent of the number of users; however, it is worse than that of the MC-FDMA scheme. Therefore, we do not have to employ the ORC even when we can estimate the channel condition perfectly. The MRC can perform better when the number of users is less than eight. For the case of more users,

however, the performance abruptly becomes worse, because the interference resulting from distorted code orthogonality is multiplied in the combining process. On the other hand, as the interference is not multiplied in the EGC, it can perform better than the MRC for the cases of 16 and 32 users. The MMSEC can perform best among the four combining strategies, although it requires information on the number of total active users and the noise power, in addition to the channel condition. In the following downlink BER comparison, we select the MMSEC as the best combining strategy.

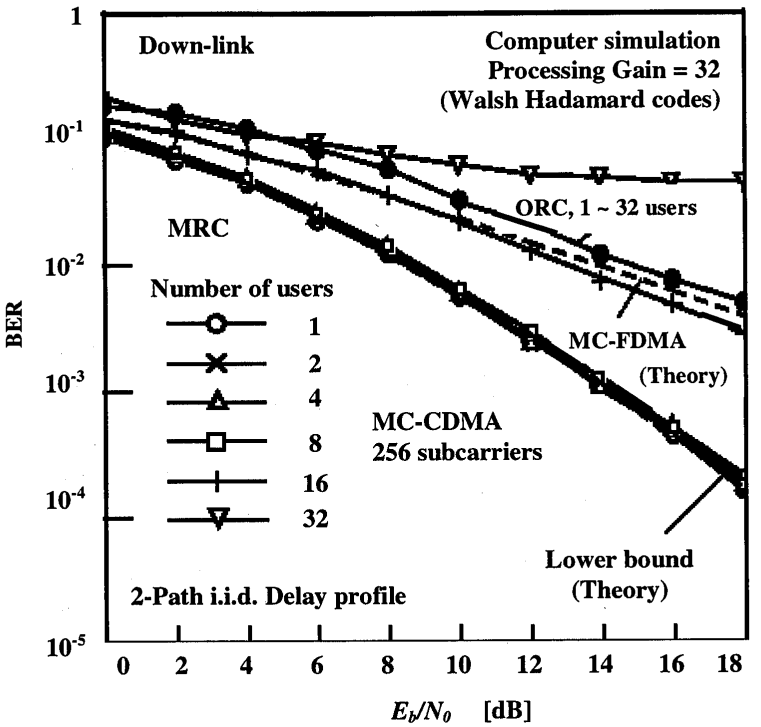

Figure 8.8 Downlink BER of MC-CDMA system with MRC.

Figure 8.10 shows the BER comparison between DS-CDMA and MC-CDMA schemes for the 2-path i.i.d. delay profile. For the DS-CDMA scheme, the BER of 2 (full)-finger RAKE combiner is a little worse than the lower bound even for the case of a single user because of the self-interference resulting from the imperfect auto-correlation characteristic of the Gold codes. Also, the BER of a 1-finger RAKE combiner, which selects the largest path, is worse than that of a 2-finger RAKE combiner, because it always misses a part of the received signal energy scattered in the time domain. On the other hand, for the MC-CDMA scheme, the MMSEC outperforms the full-finger DS-CDMA RAKE combiner. This is because the MMSEC-based MC-CDMA scheme can effectively combine all the received signal energy scattered in the frequency domain.

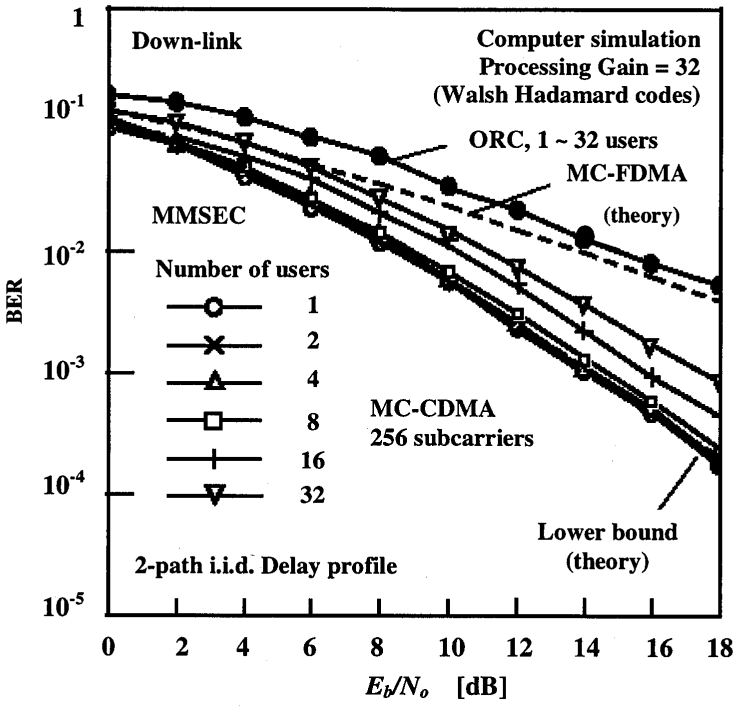

Figure 8.9 Downlink BER of MC-CDMA system with MMSEC.

Figure 8.11 shows the BER comparison for a 7-path exponential delay profile with a delay spread of 10 ns. We obtain $[N_{opt}, \Delta_{opt}/T'_s]=[1024, 0.018]$ as an optimal set for this particular channel, and the theoretical BER lower bound is given by (8.36) with $I = 7$.

For the DS-CDMA scheme, the BER performance depends on how many fingers the RAKE receiver employs. Usually, a 1-, 2-, 3- or 4-finger RAKE receiver is used, depending on hardware limitation. Therefore, if the received signal is composed of more paths than the number of RAKE fingers, the receiver misses a part of its energy. In these figures, the BERs of 1-finger, 2-finger, and 3-finger RAKE combiners are worse than that of seven (full)-finger RAKE combiners, because they always miss a larger part of the received signal energy scattered in the time domain. On the other hand, for the MC-CDMA scheme, the MMSEC outperforms the 3-finger DS-CDMA RAKE combiner, and for the case of eight users or more, it performs better than the full-finger DS-CDMA RAKE combiner.

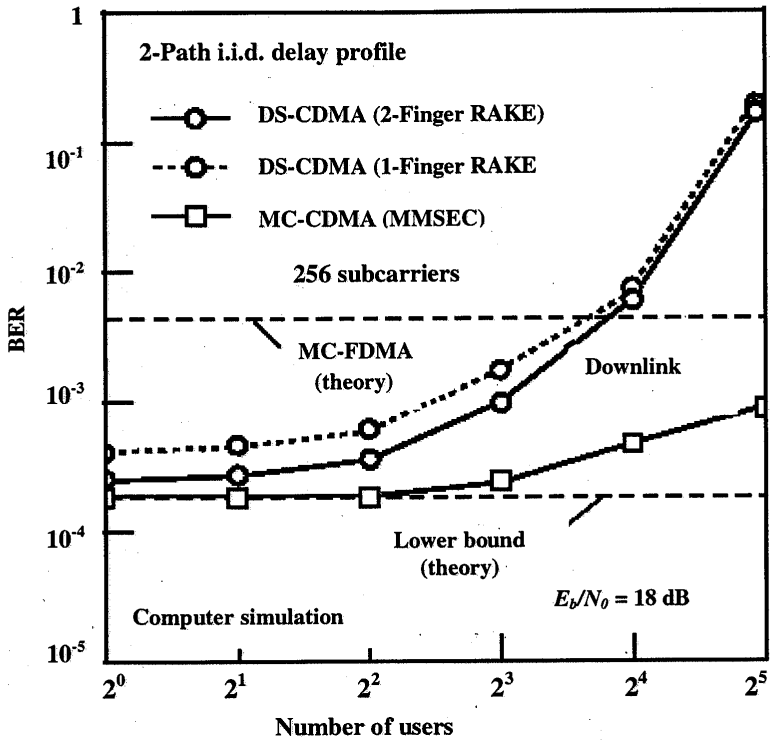

Figure 8.10 BER comparison in a downlink channel with 2-path i.i.d. multipath delay profile.

From all the results obtained in this subsection, we can conclude that it could be difficult for a DS-CDMA receiver to employ all the received signal energy scattered in the time domain, whereas an MC-CDMA receiver can effectively combine all the received signal energy scattered in the frequency domain. A DS-CDMA receiver needs to make efforts to select larger paths; on the other hand, MC-CDMA receiver does not care about where the received signal energy is. This is a significant advantage of the MC-CDMA scheme over a DS-CDMA scheme, and it makes the MMSEC-based MC-CDMA a promising access scheme in a downlink channel.

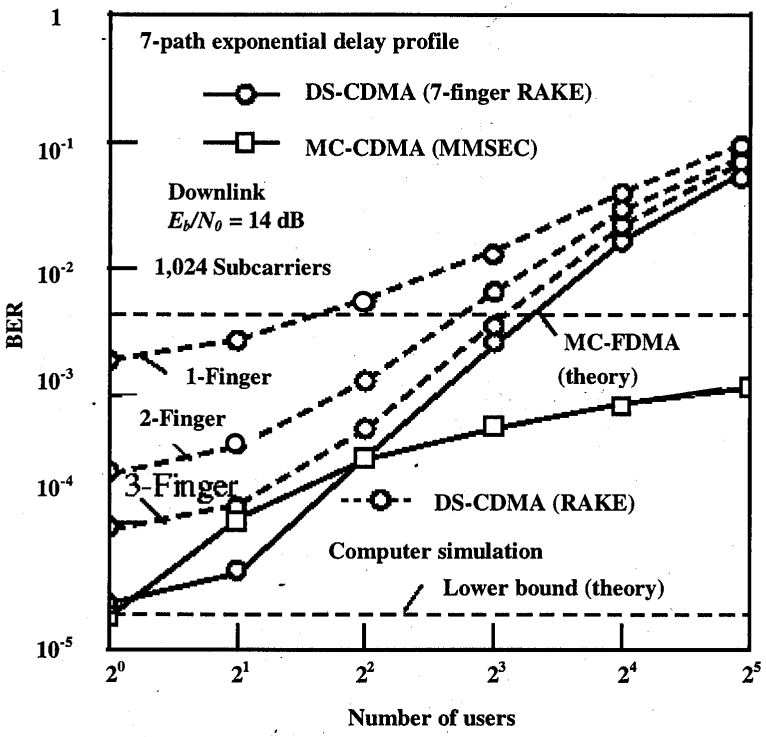

Figure 8.11 BER comparison in a downlink channel with 7-path exponential multipath delay profile.

8.6.3 Uplink BER Performance

Figures 8.12, 8.13, and 8.14 show the uplink BER performance of MC-CDMA system with EGC, MRC, and MMSEC for the 2-path i.i.d. delay profile, respectively. In these figures, the BER of an MC-FDMA scheme and the BER lower bound are also shown. The MMSEC can perform best among the three combining strategies, although there is no large difference in the attainable BER. Therefore, we select it as the best combining strategy.

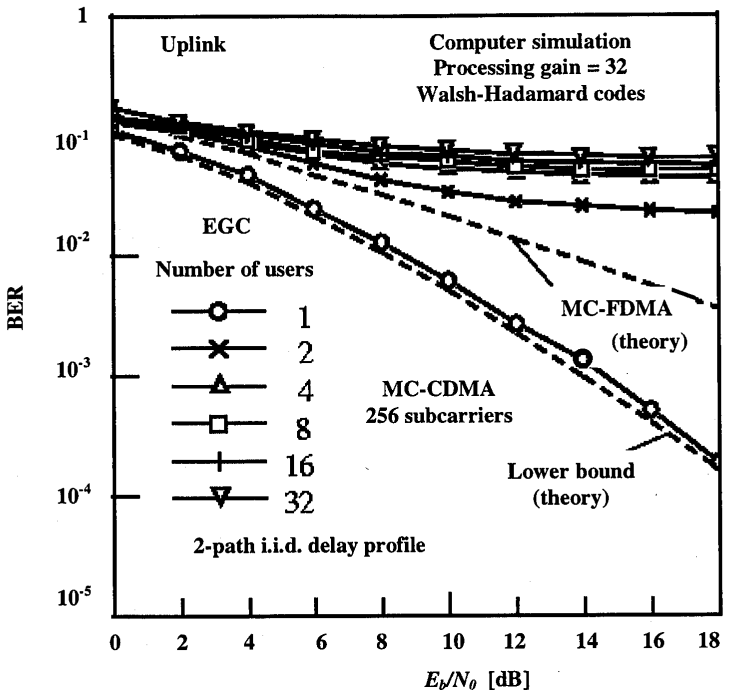

Figure 8.12 Uplink BER of MC-CDMA system with EGC.

Figures 8.15 and 8.16 show the BER comparison between DS-CDMA and MC-CDMA schemes for the 2-path i.i.d. and 7-path exponential delay profiles, respectively. As compared with the DS-CDMA scheme, the MMSEC performs well only for the case of a single user and otherwise performs poorly. This is because the code orthogonality among users is totally distorted by the instantaneous frequency response. Therefore, in the uplink application, a multiuser detection scheme is required, which jointly detects the signals to mitigate the nonorthogonal properties [27]. There are many other detectors reported in the literature [28, 29].

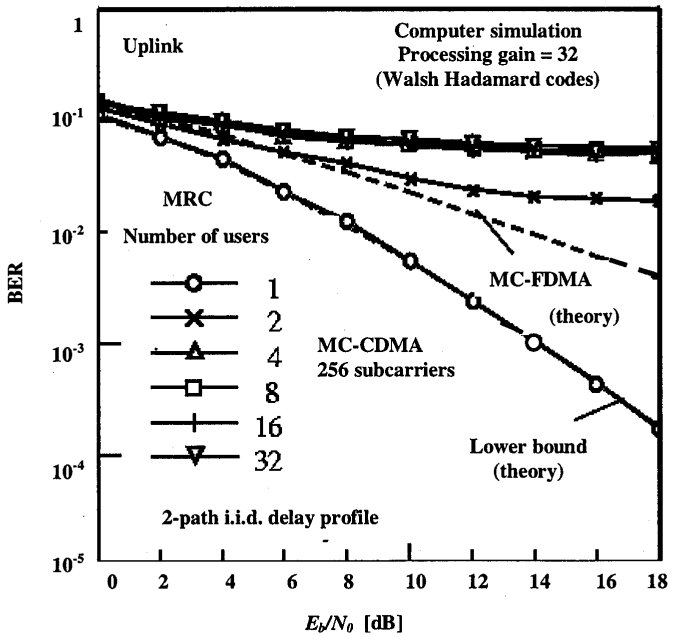

Figure 8.13 Uplink BER of MC-CDMA system with MRC.

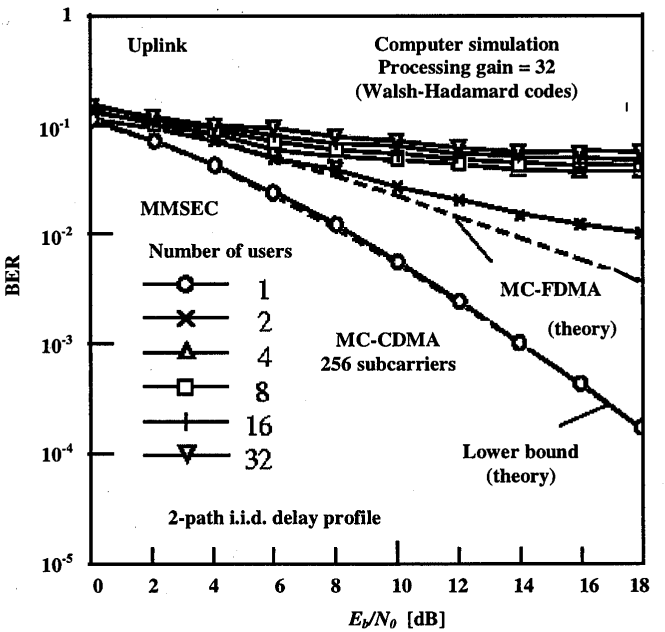

Figure 8.14 Uplink BER of MC-CDMA systems with MMSEC.

8.7 CONCLUSIONS

In this chapter, we discussed the advantages and disadvantages of the MC-CDMA system and have shown the BER performance by computer simulation.

An MC-CDMA system has no major advantage over a DS-CDMA system in terms of required bandwidth, because the bandwidth of the MC-CDMA signal spectrum is almost the same as that of a DS-CDMA signal spectrum. Also, in terms of transmission performance, the BER lower bound of an MC-CDMA system is the same as that of a DS-CDMA system. Therefore, if we make every effort to improve the BER in each system, there is no difference in the attainable BER as long as the same channel is used.

A DS-CDMA system cannot always employ all the received signal energy scattered in the time domain, whereas an MC-CDMA system can effectively combine all the received signal energy scattered in the frequency domain. The MMSEC-based MC-CDMA is a promising scheme in a downlink channel, although estimation of the noise power as well as the subcarrier reference values is required. On the other hand, in the uplink application, a multiuser detection is required because the code orthogonality among users is totally distorted by the channel frequency selectivity.

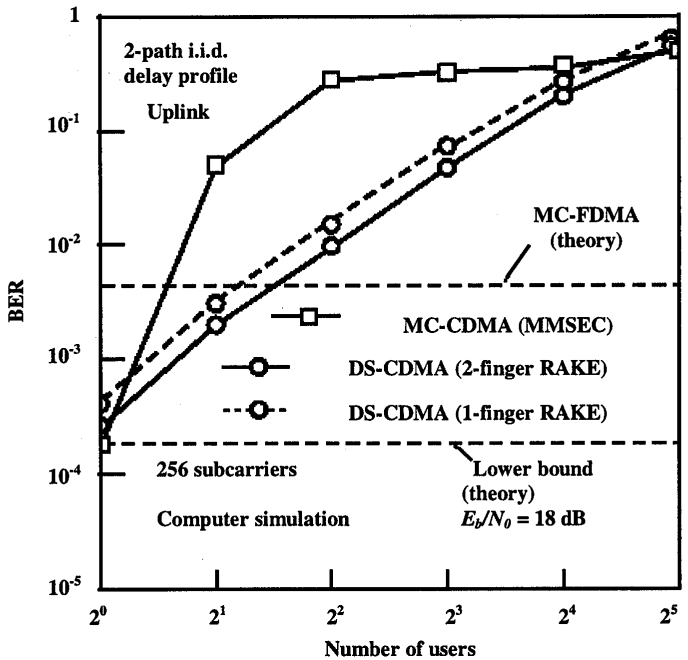

Figure 8.15 BER comparison in an uplink channel with 2-path i.i.d. multipath delay profile.

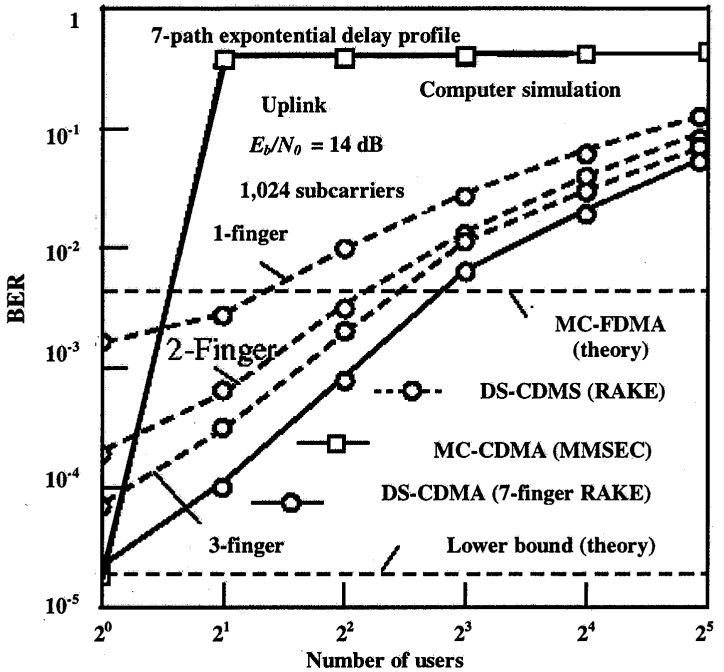

Figure 8.16 BER comparison in an uplink channel with 7-path exponential multipath delay profile.

APPENDIX 8A

(8.11) is written as

$$s_{MC}^{j}(t)=\sum_{i=-\infty}^{+\infty}\sum_{q=0}^{N-1}c_{j,q}(i)\,p_s\left(t-iT_s'\right)e^{j2\pi\Delta f\,/\,P.q(t-T_s')} \tag{8A.1}$$

$$c_{j,q=Pm+p}(i)=a_{j,p}(i)d_j(m) \tag{8A.2}$$

where $c_{j,q}(i)$ has the following property:

$$E\left[c_{j,q}(i)\cdot c_{j,q'}(i)\right]=\begin{cases}1 & (q=q')\\ 0 & (q\neq q')\end{cases} \tag{8A.3}$$

Substituting (8.1) and (8.26) into (8.28) leads to

$$\begin{aligned}r_{MC}^{j,q}(iT_s')=&\left\{\sum_{l=1}^{L_1}\frac{1}{T_s'-\Delta}\int_{iT_s'}^{iT_s'+T_s'-\Delta}g_l^j(t)dtc_{j,q}(i)e^{-j2\pi q\Delta f'\tau_l}\right.\\&\left.+\sum_{l=L_1+1}^{L_1+L_2}\frac{1}{T_s'-\Delta}\int_{iT_s-\Delta+\tau_l}^{iT_s+T_s'-\Delta}g_l^j(t)dt\cdot c_{j,q}(i)e^{-j2\pi q\Delta f'\tau_l}\right\}\\&+\left\{\sum_{l=1}^{L_1}\sum_{k=0,k\neq q}^{N-1}\frac{1}{T_s'-\Delta}\int_{iT_s'}^{iT_s'+T_s'-\Delta}g_l^j(t)e^{j2\pi(k-q)\Delta f'(t-iT_s')}dt\cdot c_{j,k}(i)e^{-j2\pi k\Delta f'\tau_l}\right.\\&+\sum_{l=L_1+1}^{L_1+L_2}\sum_{k=0,k\neq q}^{N-1}\frac{1}{T_s'-\Delta}\int_{iT_s'-\Delta+\tau_l}^{iT_s'+T_s'-\Delta}g_l^j(t)e^{j2\pi(k-q)\Delta f'(t-iT_s')}dt\cdot c_{j,k}(i)e^{-j2\pi k\Delta f'\tau_l}\\&\left.+\sum_{l=L_1+1}^{L_1+L_2}\sum_{k=0,k\neq q}^{N-1}\frac{1}{T_s'-\Delta}\int_{iT_s'}^{iT_s'-\Delta+\tau_l}g_l^j(t)e^{j2\pi(k-q)\Delta f'(t-iT_s')}dt\cdot c_{j,k}(i-1)e^{-j2\pi k\Delta f'(\tau_l-T_s')}\right\}\\&+\sum_{l=L_1+1}^{L_1+L_2}\frac{1}{T_s'-\Delta}\int_{iT_s'}^{iT_s'-\Delta+\tau_l}g_l^j(t)dt\cdot c_{j,q}(i-1)e^{-j2\pi q\Delta f'(\tau_l-T_s')}+n_q(i)\end{aligned} \tag{8A.4}$$

where the first term of (8A.4) represents the desired signal component, the second and third terms represent ICI and ISI components, respectively, and $n_q(i)$ is the Gaussian random noise component with zero mean and variance σ_n^2.

With (8A.4), $E\left[r_{j,q}(iT_s')r_{j,q}^{*}\left((i-1)T_s'\right)\right]$ and $E\left[r_{j,q}(iT_s')r_{j,q}^{*}(iT_s')\right]$ in (8.29) written as

$$E\left[r_{MC}^{j,q}(iT_s')\cdot r_{MC}^{*j,q}((i-1)T_s')\right]=\sum_{l=1}^{L_1}\frac{1}{(T_s'-\Delta)^2}\int_0^{T_s'-\Delta}\int_{-T_s'}^{-\Delta}\rho_l(x-y)dxdy$$

$$+\sum_{l=L_1+1}^{L_1+L_2}\frac{1}{(T_s'-\Delta)^2}\int_{-\Delta+\tau_l}^{T_s'-\Delta}\int_{-T_s'-\Delta+\tau_l}^{-\Delta}\rho_l(x-y)dxdy \quad (8A.5)$$

$$E\left[r_{MC}^{j,q}(iT_s')\cdot r_{MC}^{*j,q}(iT_s')\right]=\sum_{l=1}^{L_1}\frac{1}{(T_s'-\Delta)^2}\int_0^{T_s'-\Delta}\int_0^{T_s'-\Delta}\rho_l(x-y)dxdy$$

$$+\sum_{l=L_1+1}^{L_1+L_2}\frac{1}{(T_s'-\Delta)^2}\int_{-\Delta+\tau_l}^{T_s'-\Delta}\int_{-\Delta+\tau_l}^{T_s'-\Delta}\rho_l(x-y)dxdy$$

$$+\sum_{l=1}^{L_1}\sum_{k=0,k\neq q}^{N-1}\frac{1}{(T_s'-\Delta)^2}\int_0^{T_s'-\Delta}\int_0^{T_s'-\Delta}\rho_l(x-y)e^{j2\pi(k-q)\Delta f'(x-y)}dxdy$$

$$+\sum_{l=L_1+1}^{L_1+L_2}\sum_{k=0,k\neq q}^{N-1}\frac{1}{(T_s'-\Delta)^2}\int_{-\Delta+\tau_l}^{T_s'-\Delta}\int_{-\Delta+\tau_l}^{T_s'-\Delta}\rho_l(x-y)e^{j2\pi(k-q)\Delta f'(x-y)}dxdy$$

$$+\sum_{l=L_1+1}^{L_1+L_2}\sum_{k=0}^{N-1}\frac{1}{(T_s'-\Delta)^2}\int_0^{-\Delta+\tau_l}\int_0^{-\Delta+\tau_l}\rho_l(x-y)e^{j2\pi(k-q)\Delta f'(x-y)}dxdy+\sigma_n^2 \quad (8A.6)$$

Taking account of $N = T_s'K_{MC}R$, substituting (8.4) into (8A.5) and (8A.6) leads to (8.30), (8.31), and (8.32).

REFERENCES

[1] Prasad, R., *CDMA for Wireless Personal Communications*, Norwood, MA: Artech House, 1996.

[2] Prasad, R., *Universal Wireless Personal Communications*, Norwood, MA: Artech House, 1998.

[3] Ojanperä, T., and R. Prasad, *Wideband CDMA for Third Generation Wireless Personal Communications*, Norwood, MA: Artech House, 1998.

[4] Yee, N., J-P. Linnartz and G. Fettweis, "Multi-Carrier CDMA in Indoor Wireless Radio Networks," *Proc. of IEEE PIMRC'93*, pp.109–113, Sept. 1993.

[5] Fazel, K., and L. Papke, "On the performance of convolutionally-coded CDMA/OFDM for Mobile Communication System," *Proc. of IEEE PIMRC'93*, pp.468–472, Sept. 1993.

[6] Chouly, A., A. Brajal and S. Jourdan, "Orthogonal Multicarrier Techniques applied to Direct Sequence Spread Spectrum CDMA Systems,' *Proc. of IEEE GLOBECOM'93*, pp.1723–1728, Nov. 1993.

[7] Fazel, K., S. Kaiser and M. Schnell, "A Flexible and High Performance Cellular Mobile Communications System Based on Orthogonal Multi-Carrier SSMA," *Wireless Personal Communications*, Vol.2, No. 1 & 2, pp.121–144, Kluwer Academic Publishers, Nov. 1995.

[8] Möller, T., H. Rohling and R. Grönheid, "Comparison of Different Detection Algorithms for OFDM-CDMA in Broadband Rayleigh Fading," *Proc. of IEEE VTC'95*, pp.835–838, July 1995.

[9] Kaiser, S., "OFDM-CDMA versus DS-CDMA: Performance Evaluation for Fading Channels," *Proc. of IEEE ICC'95*, pp.1722–1726, June 1995.

[10] Kaiser, S., "On the Performance of Different Detection Techniques for OFDM-CDMA in fading channels," *Proc. of IEEE GLOBECOM'95*, pp.2059–1063, Nov. 1995.

[11] Hara, S., T-H. Lee and R. Prasad, "BER Comparison of DS-CDMA and MC-CDMA for Frequency Selective Fading Channels," *Proc. of 7th Tyrrhenian International Workshop on Digital Communications*, pp.3–14, Sept. 1995.

[12] Hara, S., and R. Prasad, "DS-CDMA, MC-CDMA and MT-CDMA For Mobile Multi-media Communications," *Proc. of IEEE VTC'96*, pp.1106–1110, April 1996.

[13] Prasad, R., and S. Hara, "An Overview of Multi-Carrier CDMA," *Proc. of the 4th IEEE International Symposium on Spread Spectrum Techniques and Applications (ISSSTA'96)*, pp.107–114, Sept. 1996.

[14] Kleer, F., S. Hara and R. Prasad, "Detection Strategies and Cancellation Schemes in a MC-CDMA System," in *CDMA Techniques For Third Generation Mobile Systems* edited by F. Swarts, P. van Rooyan, I. Oppermann and M. P. Lötter, Kluwer Academic Publishers, Boston/Dordrecht/London, 1999.

[15] Proakis, J. G., *Digital Communications, 3rd ed.* New York: Mc-Graw Hill, 1995, pp.758–785.

[16] Lee, W.C.Y., *Mobile Communications Engineering*, New York: Mc-Graw Hill, 1995, pp.40–44.

[17] Jakes Jr., W. C., *Microwave Mobile Communications*, New York: Wiley, 1974, pp.19–26.

[18] Chen, Q., E. S. Sousa and S. Pasupathy, "Performance of a Coded Multi-Carrier DS-CDMA System in Multi-path Fading Channels," *Wireless Personal Communications*, Vol.2, Nos.1 & 2, pp.167–187, 1995.

[19] Da Silva, V. M., and E. S. Sousa, "Multicarrier orthogonal CDMA signals for quasi-synchronous communication systems," *IEEE J. Select. Areas in Commun.*, Vol. JSAC-12, No. 5, June 1994.

[20] Dambacher, P., *Digital Broadcasting, The Institution of Electrical Engineers*, pp.97–114, 1996.

[21] Hara, S., M. Mouri, M. Okada and N. Morinaga, "Transmission performance analysis of multi-carrier modulation in frequency selective fast Rayleigh fading channel," *Wireless Personal Communications*, Vol. 2, No. 4, pp.335–356, 1995/1996.

[22] Monsen, P., "Digital transmission performance on fading dispersive diversity channels," *IEEE Trans. Commun.*, Vol. COM-21, pp.33–39, Jan. 1973.

[23] Rappaport, T. S., *Wireless Communications, Principles and Practice*, Upper Saddle River, NJ, Prentice-Hall, pp.188 – 189, 1996.

[24] Steele, R., *Mobile Radio Communications*, London: Prentech Press, pp. 727 – 729, 1992.

[25] Cimini, L. J., "Analysis and Simulation of a Digital Mobile Channel Using Orthogonal Frequency Division Multiplexing," *IEEE Trans. on Commun.*, Vol. COM-33, No. 6, pp. 665–675, June 1985.

[26] Sampei, S., *Applications of Digital Wireless Technologies to Global Wireless Communications*, Upper Saddle River, NJ: Prentice-Hall, pp. 315–332, 1997.

[27] A. Duel-Hallen, J. Holtzman and Z. Zvonar, "Multiuser detection for CDMA system," *IEEE Personal Communications*, Vol. 2, No. 2, pp. 46–58.

[28] Rohling, H., et al., "Performance comparison of different multiple access schemes for the downlink of an OFDM communication system," *VTC '97*, pp. 1365–1369, 1997.

[29] Chuang, J. C-I, "An OFDM-based System with Dynamic Packet Assignment and Interference Suppression for Advanced Cellular Internet Service," *Globecom'98*, Sydney, Australia, 1998.

CHAPTER 9

Orthogonal Frequency Division Multiple Access

9.1 INTRODUCTION

The previous chapter described some ways in which OFDM could be used both as a modulation scheme and as part of the multiple access technique, by applying a spreading code in the frequency domain. In this chapter, a variation on this theme is described, namely orthogonal frequency division multiple access (OFDMA). In OFDMA, multiple access is realized by providing each user with a fraction of the available number of subcarriers. In this way, it is equal to ordinary frequency division multiple access (FDMA); however, OFDMA avoids the relatively large guard bands that are necessary in FDMA to separate different users. An example of an OFDMA time-frequency grid is shown in Figure 9.1, where seven users *a* to *g* each use a certain fraction—which may be different for each user—of the available subcarriers. This particular example in fact is a mixture of OFDMA and Time Division Multiple Access (TDMA), because each user only transmits in one out of every four timeslots, which may contain one or several OFDM symbols.

9.2 FREQUENCY-HOPPING OFDMA

In the previous example of OFDMA, every user had a fixed set of subcarriers. It is a relatively easy change to allow hopping of the subcarriers per timeslot, as depicted in Figure 9.2. Allowing hopping with different hopping patterns for each user actually transforms the OFDMA system in a frequency-hopping CDMA system. This has the benefit of an increased frequency diversity, because each user uses all of the available bandwidth, as well as the interference averaging benefit that is common for all CDMA variants. By using forward-error correction coding over multiple hops, the system can correct for subcarriers in deep fades or subcarriers that are interfered by other users. Because the interference and fading characteristics change for every hop, the system

performance depends on the average received signal power and interference, rather than on the worst case fading and interference power.

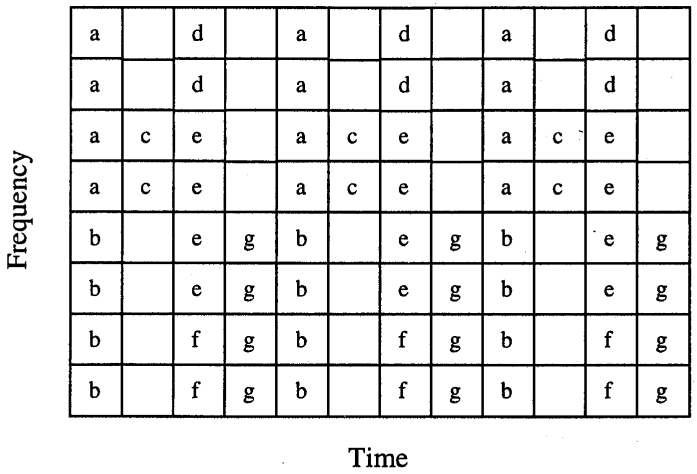

a		d		a		d		a		d	
a		d		a		d		a		d	
a	c	e		a	c	e		a	c	e	
a	c	e		a	c	e		a	c	e	
b		e	g	b		e	g	b		e	g
b		e	g	b		e	g	b		e	g
b		f	g	b		f	g	b		f	g
b		f	g	b		f	g	b		f	g

Figure 9.1 Example of the time-frequency grid with seven OFDMA users, a to g, which all have a fixed set of subcarriers every four timeslots.

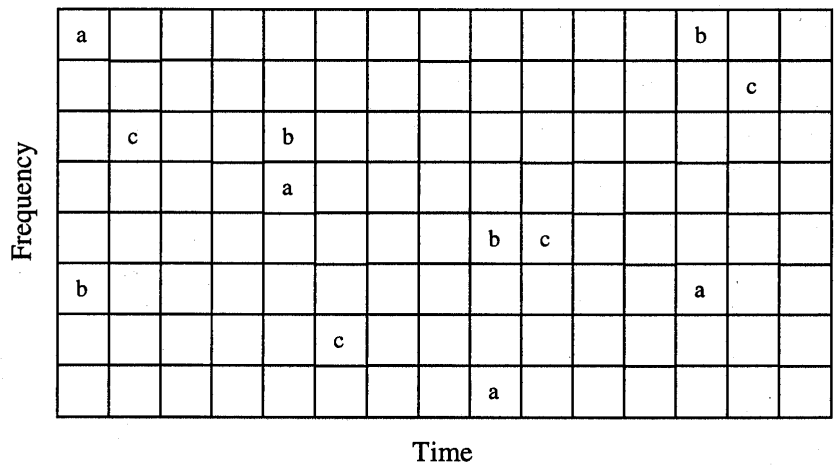

a												b		
													c	
	c			b										
				a										
								b	c					
b												a		
					c									
								a						

Figure 9.2 Example of the time-frequency grid with three hopping users, a, b and c, which all have one hop every four time slots.

A major advantage of frequency-hopping CDMA systems over direct-sequence or multicarrier CDMA systems is that it is relatively easy to eliminate intracell interference by using orthogonal hopping patterns within a cell. An example of such an orthogonal hopping set is depicted in Figure 9.3. For N subcarriers, it is always possible to construct N orthogonal-hopping patterns. Some useful construction rules for generating hopping patterns can be found in [1].

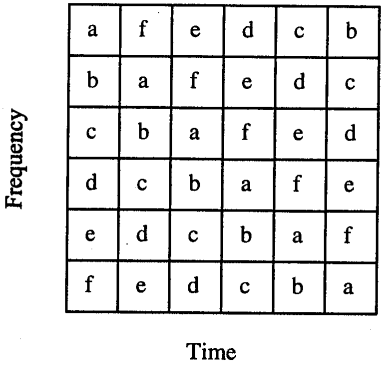

a	f	e	d	c	b
b	a	f	e	d	c
c	b	a	f	e	d
d	c	b	a	f	e
e	d	c	b	a	f
f	e	d	c	b	a

Figure 9.3 Example of six orthogonal hopping patterns with six different hopping frequencies.

9.3 DIFFERENCES BETWEEN OFDMA AND MC-CDMA

The main differences between OFDMA and the MC-CDMA techniques discussed in Chapter 8 is that users within the same cell use a distinct set of subcarriers, while in MC-CDMA, all users use all subcarriers simultaneously. To distinguish different users, orthogonal or near-orthogonal spreading codes are used in MC-CDMA. Because of code distortion by multipath fading channels, however, MC-CDMA loses its orthogonality in the uplink even for a single cell. This makes rather complicated equalization techniques necessary, which introduce a loss in SNR performance and diminish the complexity advantage of OFDM over single-carrier techniques. OFDMA does not have this disadvantage, because in a single cell, all users have different subcarriers, thereby eliminating the possibility of intersymbol or intercarrier interference. Hence, OFDMA does not suffer from intracell interference, provided that the effects of frequency and timing offsets between users are kept at a sufficiently low level. This is a major advantage of OFDMA compared with MC-CDMA and DS-CDMA, because in those systems, intracell interference is the main source of interference. A typical ratio of intracell and intercell interference is 0.55 [2]. Because the system capacity is inversely proportional to the total amount of interference power, a capacity gain of 2.8 can be achieved by eliminating all intracell interference, so that is the maximum capacity gain of OFDMA over DS-CDMA and MC-CDMA networks.

The main advantages of using CDMA in general or MC-CDMA in particular is interference averaging. In CDMA, the interference consists of a much larger number of interfering signals than the interference in a non-CDMA system. Each interfering signal is subject to independent fading, caused by shadowing and multipath effects. For both the CDMA and the non-CDMA system, an outage occurs when the total interference power (after despreading for the CDMA system) exceeds some maximum value. In a non-CDMA system, the interference usually consists of a single or a few cochannel interferers. Because of fading, the interference power is fluctuating over a large range,

so a large fading margin has to be taken into account, which reduces system capacity. In a CDMA system, the interference is a sum of a large number of interfering signals. Because all these signals fade independently, the fluctuation in the total interference power is much less than the power fluctuation of a single interfering signal. Hence, in a CDMA system the fading margin can be significantly smaller than the margin for a non-CDMA system. This improvement in margin largely determines the capacity gain of a CDMA system.

In OFDMA, interference averaging is obtained by having different hopping patterns within each cell. The hopping sequences are constructed in such a way that two users in different cells interfere with each other only during a small fraction of all hops. In a heavily loaded system, many hops will interfere, but the interference will be different for each hop. Hence, by forward-error correction across several hops, the OFDMA performance will be limited by the average amount of interference rather than the worst case interference. An additional advantage of OFDMA over DS-CDMA and MC-CDMA is that there are some relatively simple ways to reduce the amount of intercell interference. For instance, the receiver can estimate the signal quality of each hop and use this information to give heavily interfered hops a lower weight in the decoding process.

Another important feature of CDMA is the possibility to perform soft handover by transmitting two signals from different base stations simultaneously on the same channel to one mobile terminal. Combining the signals from different base stations gives a diversity gain that significantly reduces the fading margin, because the probability that two base stations are in a fade is much smaller than the probability that one base station is in a fade. Less fading means that less power has to be transmitted, and hence less interference is generated, which gives an improvement in the capacity of the system. A nice feature of CDMA soft handover is that it has no impact on the complexity of the mobile terminal; as far as the mobile terminal is concerned, the overlapping signals of different base stations have the same effect as overlapping signals caused by multipath propagation.

For OFDMA systems, two basic soft handover methods exist, applicable to both the uplink and the downlink. (base station-to-mobile, mobile-to-base station). A requirement for both methods is that the transmissions from and to the base stations are synchronized such that the delay differences at the two base stations are well within the guard time of the OFDM symbols.

The first technique is to use the same set of subcarriers and the same hopping sequence in two cells to connect to two base stations. Hence, in the downlink the mobile receives a sum of two signals with identical data content. The mobile is not able to distinguish between the two base stations; the effect of soft handover is similar to that of adding extra multipath components, increasing the diversity gain. This type of soft handover is similar to soft handover in DS-CDMA networks.

The second way for soft handoff is to use different sets of subcarriers in two cells. In contrast to the first method, in the downlink the mobile has to distinguish now

between the two base stations. It has to demodulate the signals from the two base stations separately, after which they can be combined, preferably by using maximal ratio combining. This type of soft handover is similar to the one that could be used in a non-CDMA network.

Advantages of the second method over the first—in the downlink—are an increased SNR gain because of receiver diversity, and more freedom for the base stations to allocate available subcarriers. In the first method, base stations are forced to use the same subcarriers. A main advantage of the first method is its simpler implementation; no additional hardware is needed, only some extra protocol features to connect to two base stations simultaneously. The second method does require extra hardware, because it has to demodulate an extra set of subcarriers. Further, it has to perform extra processing for the maximal ratio combining of the signals from the different base stations.

9.4 OFDMA SYSTEM DESCRIPTION

As an example of an OFDMA system, this section gives a description of a system that was proposed for the European UMTS [3, 4]. Table 9.1 summarizes the parameters and key technical characteristics of this OFDMA air interface.

Table 9.1
Parameters of the Proposed OFDMA system

No.	Parameter	Value
1	Subcarrier spacing	4.1666 kHz
2	Symbol time	288.46 μs
3	Number of subcarriers per bandslot of 100 kHz	24
4	Pre-guard time	38 μs
5	Post-guard time	8 μs
6	Modulation unit	1 bandslot and 1 time slot (= 1 symbol)
7	Modulation block	4 time slots and 1 bandslot

Figure 9.4 illustrates the time-frequency grid of the OFDMA system. The resources (time and frequency) are allocated based on the type of services and operational environment. The number of timeslots and bandslots per user is variable to realize variable data rates. The smallest data rate is obtained for one bandslot of 24 subcarriers per timeslot of 288.46 μs.

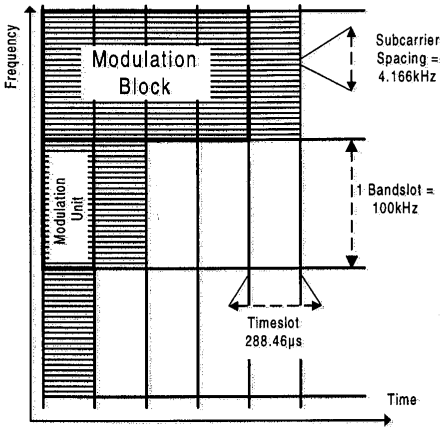

Figure 9.4 Time-frequency grid.

The following summary shows some advantages of the proposed OFDMA system:

- Use of frequency-hopping OFDMA for interference averaging and frequency diversity;
- Time-division duplex MAC with dynamic channel allocation used for unpaired spectrum allocations, asymmetrical services, and unlicensed usage;
- Straightforward and efficient high bit rate support by allocating more subcarriers and/or timeslots;
- Small guard band requirements at approximately 100 kHz;
- No frequency planning option available; effective re-use factor of 1;
- GSM backwards compatibility; and
- Minimum bandwidth requirements for system deployment only 1.6 MHz (or less) and deployment possible in steps of 100kHz.

Figure 9.5 shows the TDMA frame structure. Each frame is of length 4.615 ms, which is divided into 4 subframes of length 1.1534 ms. A sub-frame contains 4 time-slots of duration 288.46 µs. The timeslot contains a guard period, power control information and data. Every OFDM symbol is mapped onto one time-slot. The structure of an OFDMA symbol is depicted in Figure 9.6.

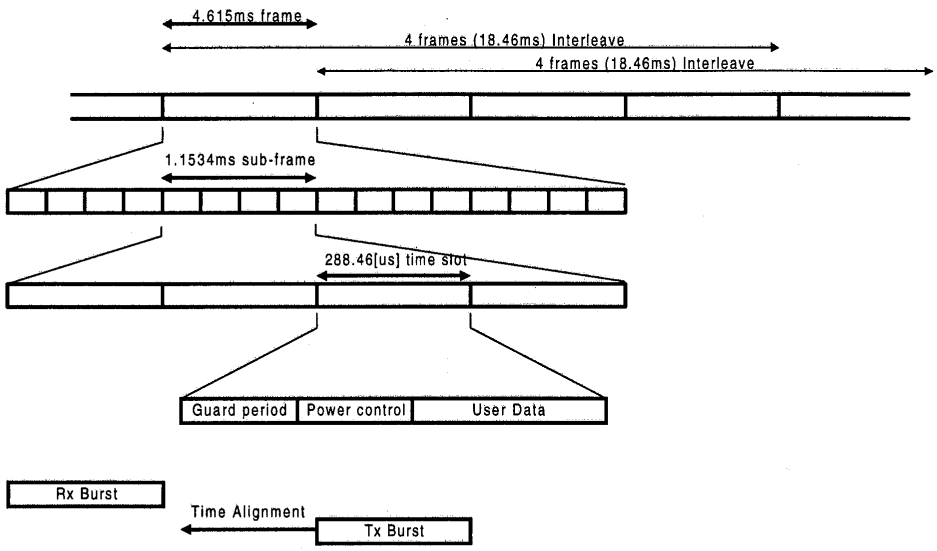

Figure 9.5 Frame (TDMA) Structure.

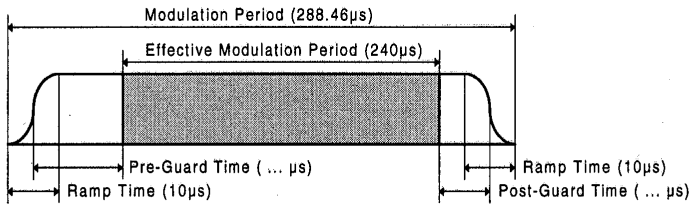

Figure 9.6 OFDM modulation burst.

The whole system frequency band is divided into small blocks (bandslots) with a fixed number of subcarriers. To maintain compatibility with GSM, a 100-kHz bandslot is chosen that consists of 24 subcarriers. Therefore, the subcarrier spacing is 100/24 = 4.167 kHz. Figure 9.7 shows the OFDMA frequency structure.

In each bandslot, the two subcarriers at the edge of the bandslot are left unmodulated to relax receiver blocking requirements. In addition, the interference of two adjacent blocks of subcarriers is reduced, which may occur when their orthogonality is compromised because of nonlinear PA effects. Adjacent bandslots can be concatenated to allow transmission of wideband services.

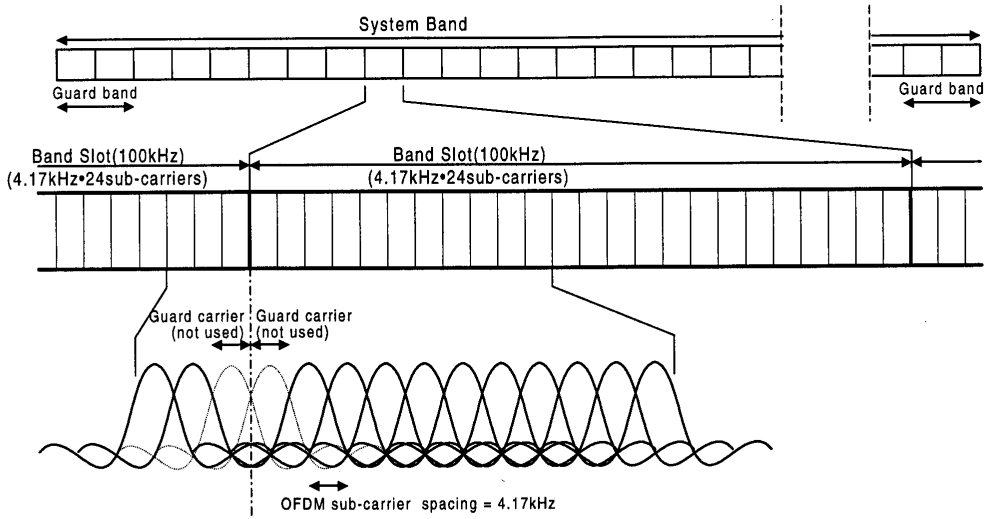

Figure 9.7 OFDMA frequency structure.

9.4.1 Channel Coding

Convolutional encoding and soft-decision Viterbi decoding is used for the basic data transmission. The objective of this coding is to achieve good quality in the tough mobile radio channel. A constraint length of seven is used together with variable coderates in the range of 1/4 to 3/4. To achieve very low bit-error rates (e.g. 10^{-6}) for video encoding or data transmission, a concatenated coding scheme is used with an inner convolutional code and an outer Reed-Solomon code.

9.4.2 Modulation

The modulation schemes of the OFDMA proposal are QPSK and 8-PSK with differential encoding in the frequency domain. An optional coherent mode with 16-QAM is available, which uses pilot subcarriers to obtain a channel estimate at the receiver. For differential encoding, each bandslot contains one known reference subcarrier value, as depicted in Figure 9.8.

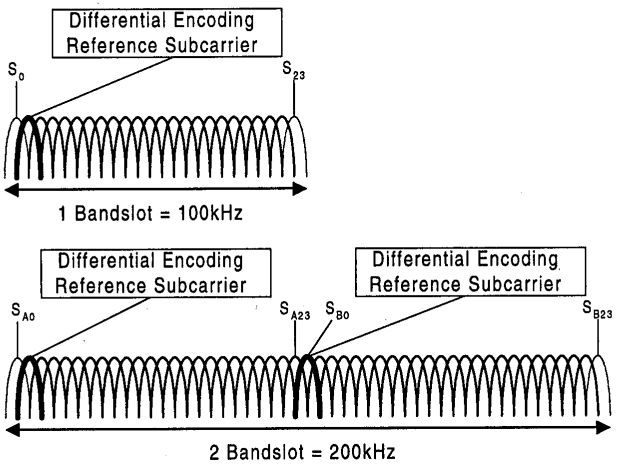

Figure 9.8 Reference subcarrier allocation.

9.4.3 Time and Frequency Synchronization

Synchronization is an essential issue for the OFDMA system. The following aspects are considered for uplink and downlink: initial modulation timing synchronization, modulation timing tracking, initial frequency offset synchronization, and frequency tracking.

9.4.4 Initial Modulation Timing Synchronization

Initial timing synchronization is required to adjust the mobile station's internal timing to the base station's timeframe. After switching on, the mobile station monitors the initial acquisition channel (IACH) and the broadcast channel (BCCH).

After the mobile has detected the base station's timing, it sends a random access channel (RACH) packet to the base station. The base station measures the time offset for the received RACH packet and sends back the necessary timing advance to the mobile (similar to GSM). In the frame structure of the OFDMA system, reserved slots for reception of RACH packets exist.

Because of the time and frequency structure of the OFDMA system, the timing tracking is less critical compared with other OFDM systems where users are interleaved in the frequency domain. The base station can measure the position of the received OFDM burst within the allocated slot for each mobile station individually and send the according timing alignment information back to the mobile station. In addition, timing information can be refined and tracked after the transformation in the subcarrier domain, where a time shift is observed as a phase rotation.

In the mobile station, the timing information is obtained and adjusted by the above-mentioned correlation algorithm. Accurate timing information is required to determine the position of the useful data samples within each burst so the FFT window can be placed correctly. The guard samples relax the requirement for accurate timing because the position of the FFT window can be shifted within the guard time without performance degradation. Additional timing offset correction can be performed to cope with the FFT window misplacements.

9.4.5 Initial Frequency Offset Synchronization

After initial timing synchronization of the mobile station, the frequency offset can be measured by phase comparison of the (ideally) equal time samples within each burst. Equal samples are placed in the guard interval of the OFDM burst. A phase rotation indicates a frequency offset. Using this technique, a frequency error up to half the subcarrier spacing can be detected. The initial offset, however, can be larger, so it has to be detected using the specially designed symbols in the IACH channel.

9.4.6 Synchronization Accuracy

The proposed synchronization, acquisition, and tracking algorithm is independent of the modulation scheme (coherent or noncoherent). For coherent 16-QAM reception, further processing in the frequency (subcarrier domain) is possible to improve the performance. Frequency domain time tracking (or combined time-domain/frequency-domain tracking algorithms) can be based on observing phase shifts of the known pilots within the time-frequency grid on the subcarrier domain.

In the downlink, only an IACH is multiplexed to allow fast and precise initial timing and frequency synchronization. In the actual communication mode, timing and frequency tracking can be performed using a correlation-based synchronization algorithm. In the uplink, the rough timing offset is detected by the base station by measuring the arrival time of the RACH burst. This gives an initial time-advance value that is reported back to the mobile. During communication, the arrival time of the burst is detected by the base station using the proposed tracking algorithm (same as in the downlink) or a tracking algorithm in the frequency (subcarrier) domain, based on the detected constellation rotation.

Both algorithms can also be combined. The alignment values are calculated regularly and reported to the mobile station. Accuracy requirements are relaxed because the design of the burst allows some overlapping arrival (another advancing feature of the raised cosine pulse-shaping besides the reduction of out-of-band emission). In addition, the guard time helps to compensate timing misalignments. The OFDMA burst design provides a guard interval at the front and an additional guard interval at the back

of the OFDM symbol—see Figure 9.9—which provides robustness against a timing inaccuracy of ±10 μs.

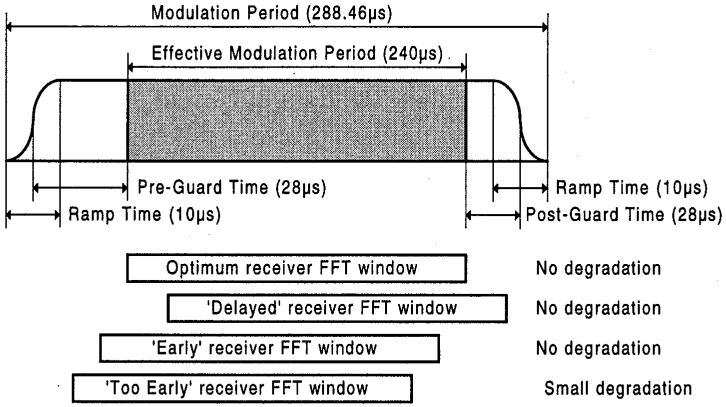

Figure 9.9 OFMDA burst and synchronization requirements.

9.4.7 Power Control

Power control in the uplink removes the unevenness of received signal strength at the base station side and decreases the total power to the minimum level required to support the specified quality of service (e.g. BER). The accuracy is less critical than CDMA because with OFDMA, orthogonality is always provided within one cell. A precise power control, however, not only improves the transmission performance but also minimizes the interference to other cells and therefore increases overall capacity.

The OFDMA concept uses both closed-loop and open-loop power control. Based on quality parameters, measured on a slot-by-slot basis, the power is adjusted in the mobile as well as in the base station transmitter. Each receiver measures the quality of the received burst (C/I ratio) and transmits in the next burst a request to the opposite transmitter to increase, keep, or decrease the power level in steps of 1 dB. For the fastest power control mode, one subcarrier is dedicated to carry power control information, and the power is then adjusted on a frame-by-frame basis (each 1.152 ms). Figure 9.10 depicts the power control operation.

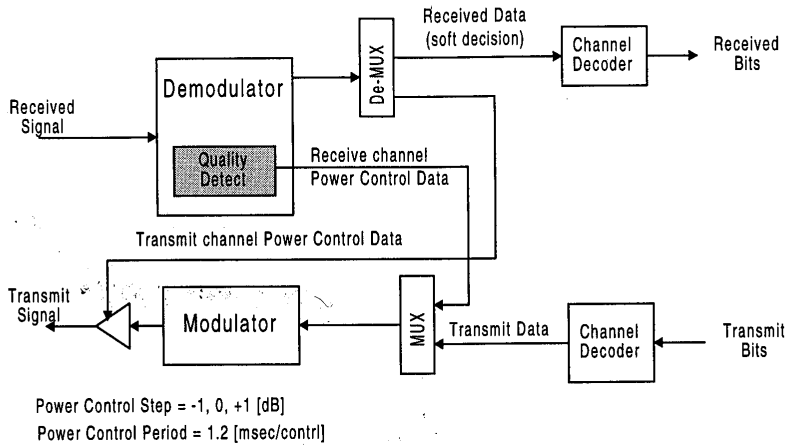

Figure 9.10 Operation of power control in a mobile station.

9.4.8 Random Frequency-Hopping Operation

Frequency hopping is very effective to achieve frequency diversity and interference diversity. Frequency diversity is useful to average the frequency-selective channel properties (fading dips). Interference diversity is one of the important techniques used in the OFDMA proposal and has been shown to improve capacity in slow frequency-hopping TDMA systems [8].

The random hopping pattern is designed to be orthogonal within one cell (no collisions in the time-frequency grid) and random between cells (this causes cochannel interference).

The frequency hopping pattern has to fulfill certain requirements:

- Orthogonality within one cell,
- Support of a variety of services by assigning different bandwidth (number of bandslots),
- Support of a variety of services by assigning timeslots (number of timeslots), and
- Support of a couple of timeslot structures (4-TDMA, 8-TDMA, 16-TDMA) within the pattern.

The hopping pattern is generated at the base station according to the expected service and traffic requirement and assigned to the cell. This assignment can be modified because of changes in the traffic characteristics. The base station can then support a set of services and a certain number of users for each service.

9.4.9 Dynamic Channel Allocation (Fast DCA)

Besides FH hopping mode, the system can also be operated in time division duplex (TDD) mode. Unlike the FH mode, the TDD mode does not separate the spectrum in an uplink and a downlink. Instead, it assigns bandslots individually to uplink or downlink connections. In TDD mode, a dynamic channel allocation algorithm is employed to avoid (rather than to average) excessive interference. The TDD mode is intended for pico-cellular, indoor use. The indoor environment is characterized by

- Short radio propagation delays (100m is traversed in 0.3 μs, or 0.1% of the symbol duration),
- Greater demand for high rate services, reducing the interference averaging advantage of frequency-hopping mode,
- High-speed data traffic is often asymmetric, prompting flexible division of bandwidth between uplink and downlink, and
- Less severe propagation conditions than those outdoor; mobility-induced Doppler spread and delay spread are both lower.

In the TDD mode, the transmissions of mobile users are scheduled by the base station, which regularly transmits a frame map containing:

- Bandslot allocations for the next frame. Bandslots can be allocated to
  - The base station for downlink transmission to a single terminal,
  - The base station for downlink transmission to all terminals (broadcast),
  - A single terminal for an uplink transmission, and
  - All (or a group of) terminals for contention based access,
- Transmit power assignments for MTs,
- Acknowledgements for contention traffic received in the previous frame,
- Slots are allocated on a connection basis, so that connection-dependent QoS can be provisioned (a mobile can have one or more connections), and
- Control data and user data are transmitted on different connections.

Terminals can transmit requests for bandslots in contention slots designated by the base station in the FM. They can also piggyback requests onto uplink transmissions, which provides contention free access, particularly under heavy traffic conditions. The base station performs interference measurements in all bandslots, except at the timeslots in which it is transmitting. This information is used by the bandslot allocation algorithm to assign uplink transmissions to slots with minimal interference. Note that an uplink transmission in an interference free slot (as measured by the base station) may interfere with a simultaneous uplink transmission at a neighboring base station. No simultaneous uplink and downlink transmissions may be scheduled within a cell. Therefore, the inability of the base station to measure interference in slots in which it is transmitting, does not reduce capacity.

The frame layout is entirely decided by the DCA algorithm. Like the FH algorithm, the DCA algorithm is distributed and does not rely on communication by

way of the infrastructure. Also, as the FH algorithm, it is not part of the system specification, the algorithm may be vendor specific, allowing competitive positioning within a standardized system.

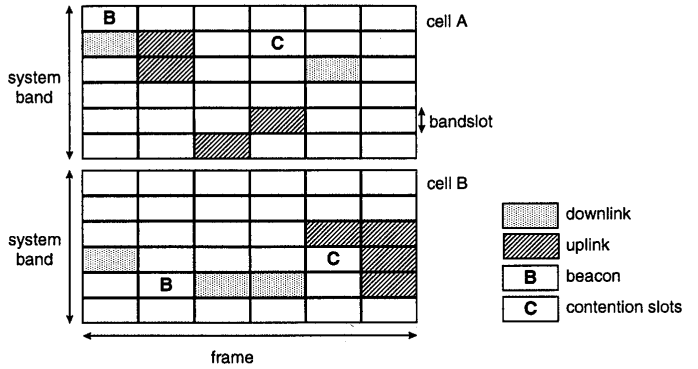

Figure 9.11 Example of frame layout.

An example of a frame layout is shown in Figure 9.11. The figure is purely illustrative. The frame duration and system bandwidth have unrealistically small values. Also, the packets, such as the frame map—that is transmitted in the beacon—and user data packets, occupy more than one bandslot in practice.

In general, the applied DCA algorithm must strive to reduce intracell and intercell interference. Constant bit-rate traffic causes long-term interference that is highly predictive of the interference in the next slot. If traffic is bursty, the predictive value of interference measurements is limited. Because a base station is not aware whether bandslots in neighboring cells are allocated to circuit mode or packet mode connections, base stations and mobiles average measurements over longer periods of time. As a rule, busy slots (high average interference level) are avoided for any transmission. Quiet slots (low average interference) are assigned to constant bit-rate connections, or to the guaranteed part of a variable bit-rate connection. Slots with medium average interference are assigned to connections with bursty traffic, which use contention mode access.

Initial association does not differ from the procedure in FH mode. When joining the base station, a mobile station first detects the location of the initial acquisition channel and the broadcast channel. The broadcast channel is used to convey the location of the frame map in the current frame to the mobile station. Once the frame map is located, it can be tracked because it advertises when it is moved to a different location.

9.4.10 Simple Dy

Simple DCA assi
during setup. This
This scheme is v
conditions compar
bandslot combinat
than the fast DCA
like cordless telepl

9.4.11 OFDMA C

System-level sim
environments. The
the simulated capa

Data 384 kb
Data 2048 kb
Speech 8 kb
Speech 8 kb
Speech 8 kb

9.5 CONCLU

OFDMA is a ver
hopping, it offers
systems, with the f

- OFDMA can a
interference, w
CDMA.
- OFDMA is fle
in a certain av
subcarriers. DS
of spectrum be

- OFDMA seems more suited than DS-CDMA and MC-CDMA for support of large data rates. When the data rates per user become larger, the spreading gain becomes lower, so the performance of a CDMA system converges to that of a nonspread system. In that case, OFDMA with dynamic channel allocation instead of frequency hopping makes more sense than multicode DS-CDMA or MC-CDMA.

REFERENCES

[1] Pottie, G. J., and A. R. Calderbank, "Channel Coding Strategies for Cellular Radio," *IEEE International Symposium on Information Theory*, San Antonio, TX, Jan. 1993.

[2] Viterbi, A. J., "The Orthogonal-Random. Waveform Dichotomy for Digital Mobile Communication," *IEEE Personal Communications*, pp.18–24, First Quarter 1994.

[3] OFDMA Evaluation Report, "The Multiple Access Scheme Proposal for the UMTS Terrestrial Radio Air Interface (UTRA) System, Part 1: System Description and Performance Evaluation," SMG2 Tdoc 362a/97, 1997.

[4] Suzuki, M., R. Boehnke, and K. Sakoda, "BDMA - Band Division Multiple Access. new Air-Interface for 3rd Generation Mobile System, UMTS, in Europe," *Proceedings ACTS Mobile Communications Summit*, Aalborg, Denmark, pp. 482–488, Oct. 1997.

[5] Rohling, H., and R. Grünheid, "Performance Comparison of Different Multiple Access Schemes for the Downlink of an OFDM Communication System," *Proceedings of IEEE VTC '97*, Phoenix, AZ, pp. 1365–1369, May 1997.

[6] Chuang, J., "An OFDM Based System with Dynamic Packet Assignment and Interference Suppression for Advanced Internet Service," *Globecom '98*, Sydney, Australia, May 1998.

[7] ETSI draft specification on the selection procedure for the choice of radio transmission technologies of the Universal Mobile Telecommunication System (UMTS), ETR/SMG-50402, Vers. 0.9.5.

[8] Olofsson, H., J. Naslund, and J. Sköld, "Interference Diversity Gain in Frequency Hopping GSM," *Proceedings IEEE Vehicular Technology Conference*, Chicago, pp. 102–106, June 1995.

CHAPTER 10

Applications of OFDM

10.1 INTRODUCTION

This chapter describes four applications of OFDM in wireless systems. The first two are broadcasting applications for both audio and television. The Digital Audio Broadcasting (DAB) standard was in fact the first OFDM-based standard. The main reasons to choose OFDM for this system, which also applies to Digital Video Broadcasting (DVB), are the possibility to make a single frequency network and the efficient handling of multipath delay spread.

After DAB and DVB, two wireless LAN applications are described. The first one is an OFDM-based wireless ATM network, which was developed in the European Magic WAND project. The last section describes the OFDM-based IEEE, ETSI and MMAC wireless LAN standard for the 5-GHz band, providing data rates of 6 up to 54 Mbps. This new standard is the first to use OFDM in packet-based wireless communication, after projects like Magic WAND demonstrated the viability of OFDM for this type of application.

10.2 DIGITAL AUDIO BROADCASTING

DAB is the successor of current analog audio broadcasting based on AM and FM. DAB offers improved sound quality, comparable to that of a compact disc, new data services, and a higher spectrum efficiency. DAB was standardized in 1995 by the European Telecommunications Standards Institute (ETSI) as the first standard to use OFDM [1, 2]. The basis for this standard was the specification developed by the European Eureka 147 DAB project, which started in 1988.

DAB has four transmission modes using different sets of OFDM parameters, which are listed in Table 10.1. The parameters for modes I to III are optimized for use

in specific frequency bands, while mode IV was introduced to provide a better coverage range at the cost of an increased vulnerability to Doppler shift.

Table 10.1
DAB OFDM Parameters.

	Mode I	**Mode II**	**Mode III**	**Mode IV**
Number of subcarriers	1,536	384	192	768
Subcarrier spacing	1 kHz	4 kHz	8 kHz	2 kHz
Symbol time	1.246 ms	311.5 μs	155.8 μs	623 μs
Guard time	246 μs	61.5 μs	30.8 μs	123 μs
Carrier frequency	<375 MHz	<1.5 GHz	<3 GHz	<1.5 GHz
Transmitter separation	<96 km	<24 km	<12 km	<48 km

One important reason to use OFDM for DAB is the possibility to use a single frequency network, which greatly enhances the spectrum efficiency. In a single-frequency network, a user receives the same signal from several transmitters simultaneously. Because of the propagation differences among transmitters, there is some delay between the arrival of the signals. This is illustrated in Figure 10.1, where two DAB signals arrive at the user with a delay difference that is equal to the distance difference (d_1–d_2) divided by the speed of light. Basically, to the user this situation is equivalent to a two-ray multipath channel. Hence, as long as the propagation differences between the two signals are smaller than the guard time of the OFDM symbols, no ISI or ICI will occur. The addition of the two time-shifted signals creates a diversity advantage for the user; the probability that the sum of both signals has an unacceptably low power because of shadowing or flat fading is much lower than the probability that one of the individual signals is too weak.

The DAB transmitted data consists of a number of audio signals, sampled at 48 kHz with an input resolution up to 22 bits. The digital audio signal is compressed to a rate in the range of 32 to 384 kbps, depending on the desired quality. The signal is divided into frames of 24 ms. The start of a frame is indicated by a null symbol, which is a silence period that is slightly larger than the duration of a normal OFDM symbol. Then, a reference OFDM symbol is sent which serves as the starting point for the differential decoding of the QPSK-modulated subcarriers. Differential encoding is applied in the time domain, so in the receiver, the phase of each subcarrier is compared with the phase of the same subcarriers from the previous OFDM symbol.

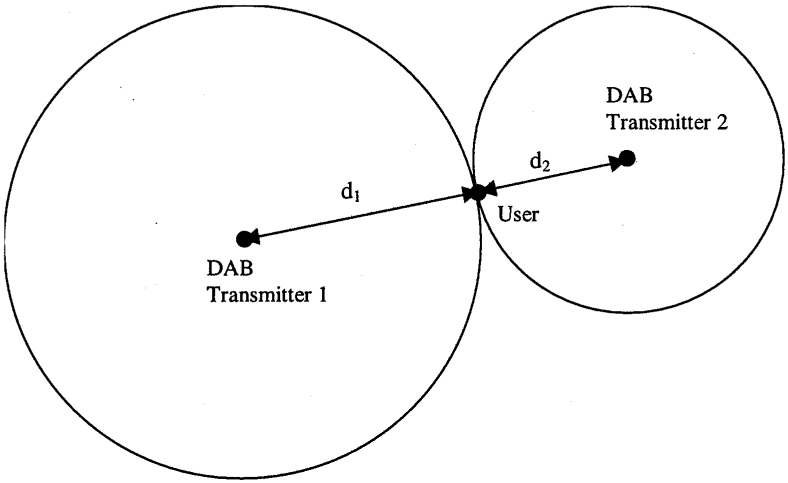

Figure 10.1 User receiving two DAB transmitters.

The digital input data is encoded by a rate 1/4 convolutional code with constraint length 7 to provide protection against fading subcarriers. The coding rate can be increased up to 8/9 by puncturing. This gives a maximum total data rate of $1{,}536*2*8/9*1/1.246 \cdot 10^{-3}$, which is approximately 2.2 Mbps. The coded data are interleaved to separate coded bits in the frequency domain as much as possible, which avoids large error bursts in case of a deep fade affecting a group of subcarriers.

10.3 TERRESTRIAL DIGITAL VIDEO BROADCASTING

Research on a digital system for television broadcasting has been carried out since the late 1980s. In 1993, a pan-broadcasting-industry group started the Digital Video Broadcasting (DVB) project. Within this project, a set of specifications was developed for the delivery of digital television over satellites, cable, and through terrestrial transmitters. This section describes the terrestrial DVB system, which was standardized in 1997 [3, 4].

Terrestrial DVB uses OFDM with two possible modes, using 1,705 and 6,817 subcarriers, respectively. These modes are referred to as 2k and 8k modes, respectively, as these are the sizes of the FFT/IFFT needed to generate and demodulate all subcarriers. The main reason to have two modes were doubts about the implementability of the 8k subcarrier system. Basically, the 2k system is a simplified version which requires an FFT/IFFT that is only a quarter of the size that is needed for the 8k system. Because the guard time is also four times smaller, the 2k system can handle less delay spread and less propagation delay differences among transmitters within a single-frequency network. The FFT interval duration for the 8k system is 896

μs, while the guard time can have four different values from 28 to 224 μs. The corresponding values for the 2k system are four times smaller.

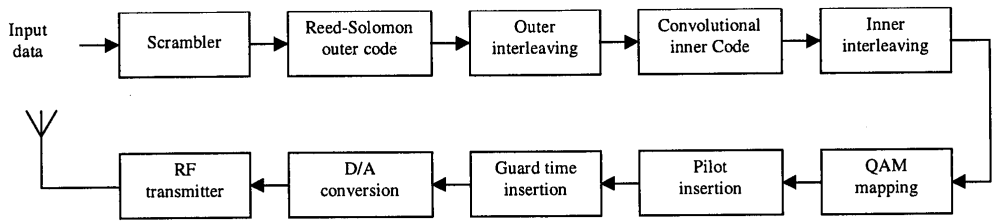

Figure 10.2 Block diagram of a DVB-T transmitter.

Figure 10.2 shows a block diagram of a DVB-T transmitter. The input data are divided into groups of 188 bytes, which are scrambled and coded by an outer shortened Reed-Solomon code (204,188, t=8). This code can correct up to eight erroneous bytes in a frame of 204 bytes. The coded bits are interleaved by a convolutional interleaver that interleaves byte-wise with a depth of 12 bytes and then again coded by a rate 1/2, constraint length 7 convolutional code with generator polynomials (171, 133 octal). The rate of this latter code can be increased by puncturing to 2/3, 3/4, 5/6, or 7/8. The convolutionally encoded bits are interleaved by an inner interleaver and then mapped onto QPSK, 16-QAM, or 64-QAM symbols.

For 16-QAM and 64-QAM, optional hierarchical coding can be applied. In this case, the constellation points are moved farther away from the origin so the quadrants can be detected more reliably than the position within each quadrant. This is illustrated in Figure 10.3 for a hierarchical 16-QAM constellation. For this constellation, the minimum distance between points from different quadrants is double the distance of a normal 16-QAM constellation, where the constellation points would have values of 1 and 3 instead of 2 and 4. Corrected for the increased power of the constellation, the detection of the quadrants has a 3-dB SNR advantage over the detection of points in a normal 16-QAM constellation. The advantage of this hierarchical coding is that users for which the SNR is just too low to decode all bits can at least decode the two most significant bits that determine the quadrant. These bits give them the same video signal, but at a lower resolution.

To obtain reference amplitudes and phases to perform coherent QAM demodulation, pilot subcarriers are transmitted. For the 8k mode, in each symbol there are 768 pilots, so 6,048 subcarriers remain for data. The 2k mode has 192 pilots and 1,512 data subcarriers. The position of the pilots varies from symbol to symbol with a pattern that repeats after four OFDM symbols. The pilots allow a receiver to estimate the channel both in frequency as well as in time, which is important as for mobile receivers there can be significant channel changes within a few OFDM symbols.

Techniques to do this type of two-dimensional channel estimation based on pilot subcarriers are described in Chapter 5.

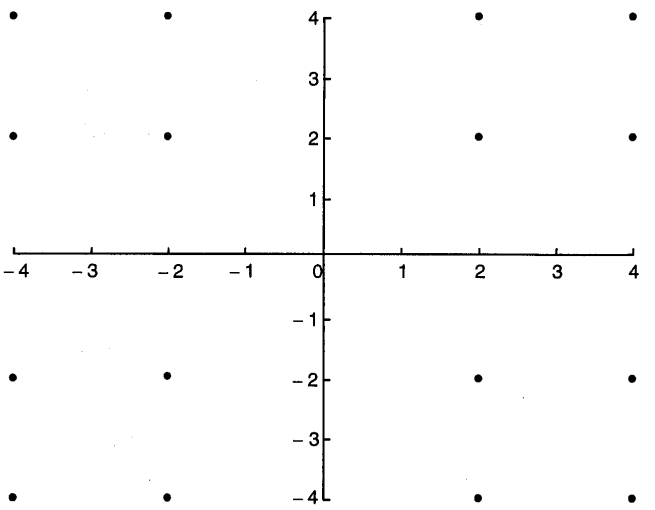

Figure 10.3 Hierarchical 16-QAM.

10.4 MAGIC WAND

The Magic WAND (Wireless ATM Network Demonstrator) project was part of the European ACTS (Advanced Communications Technology and Server) program [5]. The Magic WAND consortium members implemented a prototype wireless ATM network based on OFDM modulation. This prototype had a large impact on standardization activities in the 5-GHz band. First, by employing OFDM-based modems, Magic WAND helped to gain acceptance for OFDM as a viable modulation type for high-rate wireless communications. Second, the wireless ATM-based approach of Magic WAND forms the basis for the standardization of the HIPERLAN type 2 Data Link Layer.

Figure 10.4 shows one of the prototype Magic WAND 5-GHz modems demonstrating wireless video playback and Web browsing applications at the Demo '98 exhibition in Berlin [6].

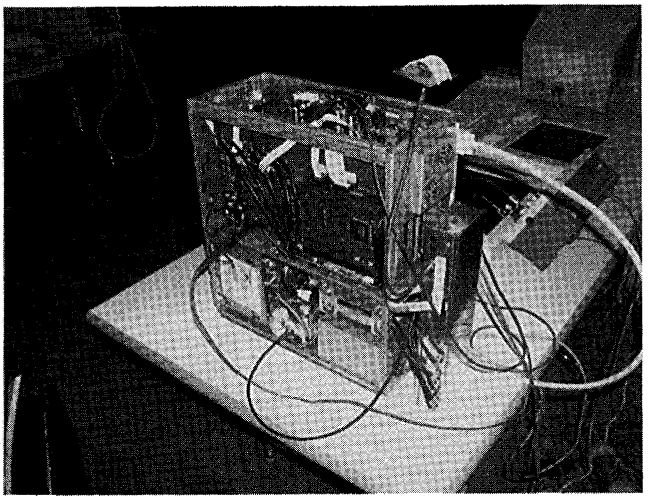

Figure 10.4 Magic WAND prototype 5-GHz modem.

10.4.1 Magic WAND Physical Layer

The main parameters of the WAND physical layer are listed in Table 10.2. OFDM with 16 subcarriers is used, the number of which was chosen to facilitate implementation. The 400-ns guard time provides a delay spread tolerance of about 50 ns. Because of a 240-ns rolloff time (see Chapter 2), the effective guard time is only 160 ns. While this is sufficient for most office buildings and the WAND trial site, a realistic product would require more delay spread robustness to also cover large office buildings and factory halls.

The OFDM subcarriers are 8-PSK modulated. At a symbol rate of 13.3 Msymbols/s, this gives a raw bit rate of 40 Mbps. The rate 1/2 complementary coding reduces the data rate to 20 Mbps. The subcarrier spacing is 1.25 MHz, which gives a total (3-dB) bandwidth of 20 MHz.

The packet preamble is 8.4 μs in duration and consists of one OFDM symbol, repeated seven times. This preamble is used for packet detection, automatic gain control, frequency offset estimation, symbol timing, and channel estimation.

The PHY payload holds an odd number of half-slots. Each half-slot consists of 9 symbols or 27 bytes. This number was chosen so that a full slot, of 54 bytes, can hold an ATM cell (which is 52 bytes long), and is also a multiple of 3 bytes, which is imposed by the PHY's modulation scheme.

Table 10.2
Main parameters of the WAND OFDM modem.

Number of subcarriers	16
Modulation	8-PSK
Coding	Two interleaved length 8 complementary codes, rate ½
Bit rate (after decoding)	20 Mbps (24 bits per symbol)
Symbol time	1.2 μs
Guard time	0.4 μs
Windowing	Raised cosine, rolloff factor = 0.2
Subcarrier spacing	1.25 MHz
Training length	7 symbols
Carrier frequency	5.2 GHz
Peak output power	1W

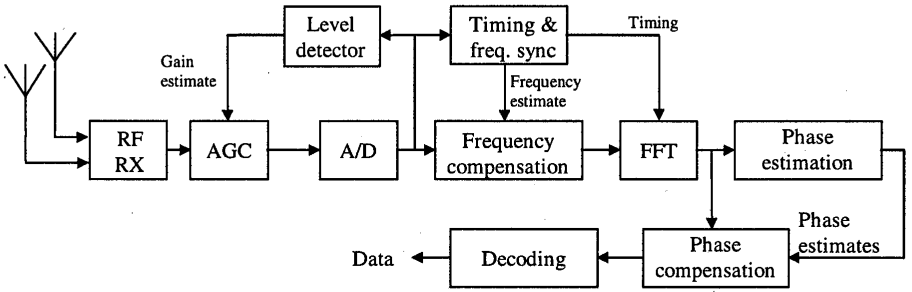

Figure 10.5 OFDM receiver.

Figure 10.5 shows a block diagram of the OFDM receiver. The RF receiver takes care of amplifying and down-converting the signal. The automatic gain control (AGC) is one of the most difficult parts in the receiver, since the gain has to settle within 3 μs after start of reception. After the analog-to-digital (A/D) conversion, the frequency of the signal has to be estimated and corrected for, because OFDM is sensitive to frequency errors (see Chapter 4).

By taking the FFT of groups of samples at the right time instants, the receiver obtains amplitude and phase estimates of the 16 subchannels. From the initial training sequence, the receiver has to acquire and track the reference phases for all subchannels. After phase compensation, finally the 24 information bits can be decoded from the 16 complex subcarrier values.

10.4.2 Coding

The WAND modem uses complementary codes for both forward-error correction coding and peak-to-average power (PAP) reduction. Length 8 complementary codes are used, with four input 8-PSK phases generating eight complex code outputs as described in Chapter 6. By taking the IFFT of these complex values, an OFDM signal with a low PAP ratio is obtained. To encode all 16 subcarriers, two length 8 codes are interleaved, which maximizes the benefits of frequency diversity. It is also possible to use length 16 complementary codes, but for that length, only five phases can be encoded into 16 subcarriers, reducing the coding rate from 1/2 to 5/16. The minimum distance of the length 8 code is four subsymbols. Hence, three arbitrary subchannels can be erased without causing errors, providing that the remaining subchannels are not in error.

10.4.3 Simulated Error Probabilities

Bit-error ratios (BER) and packet-error ratios (PER) for various delay spreads are depicted in Figure 10.6. For each mean E_b/N_o value, 40,000 ATM-cell transmissions have been simulated in Rayleigh fading channels, without antenna diversity. In all transmissions, a frequency offset of 40 kHz was simulated, which has to be estimated and compensated for by the receiver. Figure 10.6 clearly shows that the coded OFDM system is able to benefit from the frequency diversity, which is present for nonzero delay spreads.

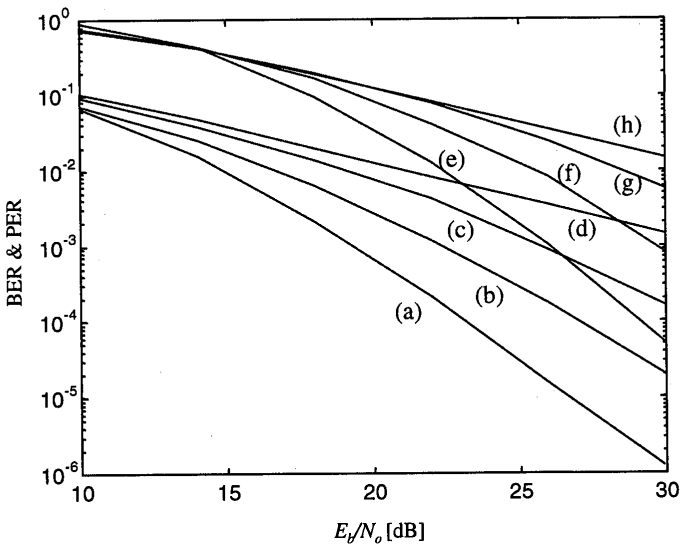

Figure 10.6 BER (a–d) and PER (e–h) versus mean E_b/N_o for delay spreads of (a,e) 50 ns, (b,f) 20 ns, (c,g) 10 ns, (d,h) 0.

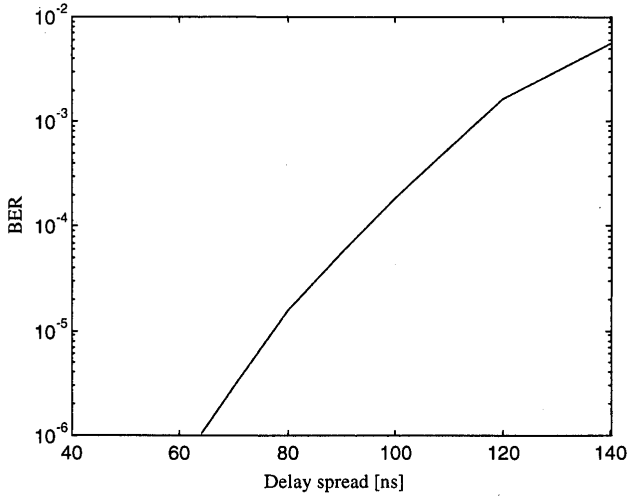

Figure 10.7 Irreducible BER versus delay spread for an exponential power delay profile.

For delay spreads larger than 50 ns, the error curves converge to some irreducible error floor, caused by intersymbol and intercarrier interference of multipath signals with excess delays larger than the guard time. In Figure 10.7, this irreducible BER is plotted versus the delay spread. Notice that an exponential power-delay profile is used in the simulations. For a two-ray model, for instance, the irreducible error floor arises only for delay spreads larger than half of the guard time (i.e., 200 ns for the prototype WAND modem). Thus, the exponential power delay profile gives much more pessimistic results in this respect. Conversely, the two-ray model is known to give less diversity gain, because there are only two independent fading paths.

10.4.4 Effects of Clipping

Despite the use of complementary coding in the WAND OFDM system, the transmitted signal still has a 6-dB PAP ratio. To make the efficiency of the transmitter power amplifier as high as possible, we have to accept a certain nonlinear distortion in the peaks of the OFDM signal. A crude analysis of this nonlinear distortion can be made by assuming a clipping transfer function. Figure 10.8 shows the BER in an AWGN channel for clipping levels of 0 to 4 dB below the maximum amplitude. It can be seen that significant degradation occurs only for a clipping level of more than 3 dB below the peak amplitude. Of course, such severe clipping is not allowed from a spectrum point of view, but the analysis at least shows that the OFDM transmission itself is relatively insensitive against clipping.

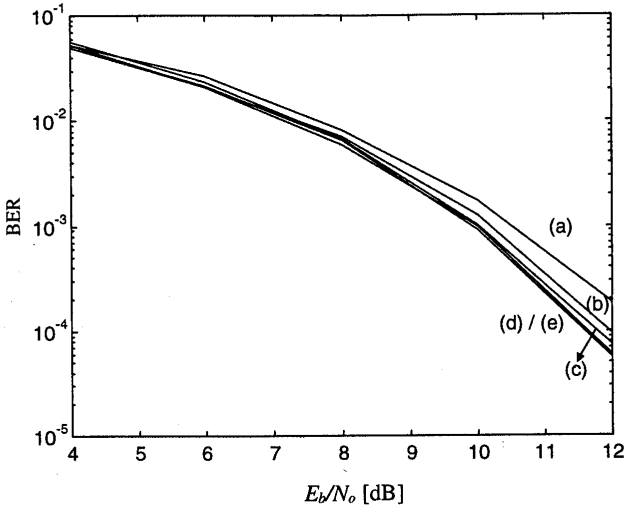

Figure 10.8 BER in AWGN with the transmitted OFDM signals clipped at (a) 4 dB, (b) 3 dB, (c) 2 dB, (d) 1 dB and (e) 0 dB below the maximum amplitude.

Clipping at the receiver is different from clipping at the transmitter, because the receiver does not know in advance what the peak amplitude is, contrary to the transmitter. Even after the initial training symbols, when the receiver freezes its AGC, the receiver does not know what the peak amplitude will be in the rest of the packet. Except for noise, this is caused by two effects: first, multipath fading channels change the peak-to-average power ratio of the OFDM signal and second, different symbols have different PAP ratios.

An OFDM receiver must freeze its AGC based on the observed amplitude level during training. The peak amplitude during training is most probably not the largest amplitude of the entire packet. Thus, the question is how to set the AGC level such that clipping effects are negligible. Based on the results from Chapter 6, the ideal AGC setting is such that the clipping level is about 6 to 10 dB above the average input power level. In this case, the interference caused by clipping is relatively small compared with the average signal power. If the clipping level is more than 10 dB above the average power level, then the risk exists that quantization noise starts dominating over clipping noise, as the most significant bits of the A/D converter are hardly used in this case.

10.4.5 Magic WAND Medium Access Control Layer

The MAC (Medium Access Control) and DLC (Data Link Control) layers of the WAND system have been combined in one layer, bearing the name MASCARA (Mobile Access Scheme based on Contention And Reservation for ATM). The underlying concept is based on the following set of ideas and requirements which are elaborated in the subsequent paragraphs.

- QoS-aware, reservation-based demand assigned protocol;
- Multiple virtual connections per terminal;
- Power efficiency;
- Cell transfer service for optimal interworking with ATM;
- Amortization of PHY overhead over multiple ATM cells;
- Contention-mode request and control channel; and
- ARQ (Automatic Repeat reQuest)-based cell loss recovery.

ATM is designed to offer service to wire-line users with a guaranteed quality of service. To extend ATM service to mobile terminals, the wireless access network needs to be QoS-aware as well. A centralized algorithm allotting transmission time to users on the basis of their explicit demands seems to be an obvious way to provide QoS and isolation among users' traffic streams. We note that the disadvantage over contention-based algorithms as used in wireless LANs and wireless PBXs is that they do not inherently support multicellular operation. To function correctly, they require a cellular frequency reuse topology, with perfect separation between radio cells with identical frequencies. As usual for wireless LANs, TDD between uplink and downlink is chosen, primarily to support traffic asymmetry.

As a multimedia terminal may have many simultaneous connections, most probably with different QoS requirements, the network must be able—besides addressing individual terminals—to distinguish separate connections of those terminals. Given the smaller number of users and the scarcity of bandwidth, the relatively large addressing overhead of ATM, being designed for large wire-line networks, must be avoided.

Mobile terminals draw power from batteries, and to extend battery-life the protocols need to be energy aware. A frame-based MAC, in which the access point notifies all associated terminals about their expected transmissions and receptions in the entire frame helps to conserve power: terminals switch on their radios only when necessary. From the energy perspective, the frame duration should be made as long as possible. QoS considerations, on the other hand, put a bound on the maximal frame length. For this scheme to work, a frame structure by itself is not sufficient. A common time base among terminals and access point is required as well. For practical reasons the granularity of time must be bounded. The unit of time in MASCARA is a timeslot, and all packet transmissions commence on a timeslot boundary.

To provide seamless interworking with the ATM backbone, and transparency to the user, packets must carry ATM cells. It makes sense to choose the slot duration equal to a cell's transmission time. The same length of time is imposed on the packet header (radio preamble and MAC header) as well. In the WAND system, the first half of the overhead slot is used for the preamble, the other half is used for the MAC header.

If each packet were to contain just one cell, the protocol efficiency would be merely 50%. To increase efficiency, a longer packet size can be adopted. On the other

hand, QoS-driven restrictions on cellization delay put an upper bound on packet length. In the case of 64 kbps speech traffic for instance, cellization delay is 6 ms per cell, which restricts the packet length to one or two cells. The logical decision is to allow packets of variable length, depending on the connection's delay requirements, with a payload of an integer number of cells.

Demand-assigned algorithms assign timeslots to terminals, based on terminal demand. Uplink packets contain fields in which a terminal can put its request. If a terminal cannot piggyback its request, because no timeslots were assigned to it (a deadlock situation), or because it cannot afford to wait for the next packet, the terminal can transmit its request in an unreserved timeslot. A contention period is scheduled at the end of every frame. Contention slots can be used for incidental control packets as well.

Adverse radio propagation conditions affect the cell loss ratio (CLR) QoS. By its nature, a radio network cannot provide the same QoS consistently. To sustain a negotiated CLR QoS as long as possible, the DLC layer adds ARQ capability to the system. ARQ can help to retain the agreed-on cell loss rate, at the cost of an increase in delay and data overhead.

Figure 10.9 depicts an example frame. Two mobile terminals (MT) and one access point (AP) are engaged in the exchange of packets. For instruction purposes, the frame duration is shorter than typically encountered in practice. The access point initiates every frame by broadcasting a frame header (FH), containing the slot map to all associated mobile terminals. The FH has a long preamble, allowing mobile terminals to synchronize to the access point. Subsequently, the access point sends its downlink data, one packet in this example. The channel remains idle for one slot to allow the access point to turn around its radio from transmitting to receiving. Then the mobile terminals are allowed to transmit their packets. In this example each mobile terminal transmits one. After the uplink period, a contention period is scheduled, which in this example is used by both terminals. Terminal 1 is transmitting two request packets and terminal 2 is transmitting a two-slot control packet. In the example, two packets collide, resulting in the loss of the control packet and one of the request packets. The second request packet is transmitted successfully in the third slot. After the contention period, and before the next frame, an idle slot is inserted to allow the mobile terminal radios to turn around.

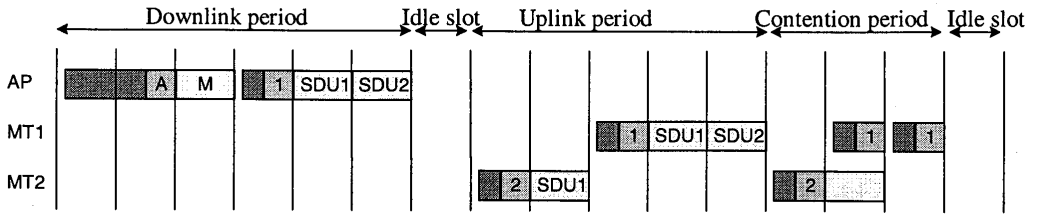

Figure 10.9 Magic WAND MAC frame.

The master scheduler, which must be able to schedule the transmissions of any mix of ATM traffic classes, employs a leaky-bucket-based scheme where the highest priority is given to constant bit-rate traffic, the second priority to variable bit rate, and so on. Tokens, which are generated at a constant rate, fill a bucket. The scheduler takes tokens from the bucket, and translates them in the allocation of slots in the slot map according to the connections' delay requirements. A traffic source can request slots (access points directly, mobile terminals use piggy-backed and contention requests) in excess of the mean rate. Depending on the negotiated burstiness of the source, which is reflected in a commensurate bucket depth, the scheduler grants the request. Effectively, the scheduler polices and shapes the traffic on the wireless link, to guarantee delay QoS compliance for all connections. See [7] for an extensive discussion of scheduling.

The second important measure of QoS, besides delay and delay jitter, is the connection's error performance over the wireless ATM link. In WAND, the radio physical layer provides a constant service that can meet typical real-time service requirements (e.g., for a voice service). TCP/IP-based data connections cannot tolerate high cell loss ($> 10^{-2}$) and these are protected by ARQ. Third, there are services such as video requiring real-time service with low error probability. The solution applied in WAND is to apply ARQ with a limited number of retransmissions.

10.5 IEEE 802.11, HIPERLAN/2 AND MMAC WIRELESS LAN STANDARDS

Since the beginning of the nineties, wireless local area networks (WLAN) for the 900-MHz, 2.4-GHz, and 5-GHz ISM (Industrial, Scientific, & Medical) bands have been available, based on a range of proprietary techniques. In June 1997, the Institute of Electrical and Electronics Engineers (IEEE) approved an international interoperability standard [8]. The standard specifies both medium access control (MAC) procedures and three different physical layers (PHY). There are two radio-based PHYs using the 2.4-GHz band. The third PHY uses infrared light. All PHYs support a data rate of 1 Mbps and optionally 2 Mbps. The 2.4-GHz frequency band is available for license-exempt use in Europe, the United States, and Japan. Table 10.3

lists the available frequency band and the restrictions to devices which use this band for communications.

Table 10.3
International 2.4-GHz ISM bands.

Location	Regulatory range	Maximum output power
North America	2.400–2.4835 GHz	1,000 mW
Europe	2.400–2.4835 GHz	100 mW (EIRP*)
Japan	2.471–2.497 GHz	10 mW

* EIRP = effective isotropic radiated power.

User demand for higher bit rates and the international availability of the 2.4-GHz band has spurred the development of a higher speed extension to the 802.11 standard. In July 1998, a proposal was selected for standardization, which describes a PHY providing a basic rate of 11 Mbps and a fall back rate of 5.5 Mbps. This PHY can be seen as a fourth option, to be used in conjunction with the MAC that is already standardized. Practical products, however, are expected to support both the high-speed 11- and 5.5-Mbit/s rates mode as well as the 1- and 2-Mbps modes.

A second IEEE 802.11 working group has moved on to standardize yet another PHY option, which offers higher bit rates in the 5.2-GHz band. This development was motivated by the adoption, in January 1997, by the U.S. Federal Communications Commission, of an amendment to Part 15 of its rules. The amendment makes available 300 MHz of spectrum in the 5.2-GHz band, intended for use by a new category of unlicensed equipment called Unlicensed National Information Infrastructure (UNII) devices [9]. Table 10.4 lists the frequency bands and the corresponding power restrictions. Notice that the maximum permitted output power depends on the emission bandwidth; for a bandwidth of 20 MHz, you are allowed to transmit at the maximum power levels listed in the middle column of Table 10.4. For a bandwidth smaller than 20 MHz the power limit reduces to the value specified in the right column.

Table 10.4
United States 5.2 GHz U-NII band.

Location	Maximum output power minimum of	
5.150–5.250 GHz	50 mW	4 dBm + $10\log_{10}B$*
5.250–5.350 GHz	250 mW	11 dBm + $10\log_{10}B$
5.725–5.825 GHz	1,000 mW	17 dBm + $10\log_{10}B$

* B is the –26-dB emission bandwidth in MHz.

Like the IEEE 802.11 standard, the European ETSI HIPERLAN type 1 standard [10] specifies both MAC and PHY. Unlike IEEE 802.11, however, no HIPERLAN type 1 compliant products are available in the market place. A newly formed ETSI working group called Broadband Radio Access Networks (BRAN) is now working on

extensions to the HIPERLAN standard. Three extensions are under development: HIPERLAN/2, a wireless indoor LAN with a QoS provision; HiperLink, a wireless indoor backbone; and HiperAccess, an outdoor, fixed wireless network providing access to a wired infrastructure.

In Japan, equipment manufacturers, service providers and the Ministry of Post and Telecommunications are cooperating in the Multimedia Mobile Access Communication (MMAC) project to define new wireless standards similar to those of IEEE 802.11 and ETSI BRAN. Additionally, MMAC is also looking into the possibility for ultra-high-speed wireless indoor LANs supporting large-volume data transmission at speeds up to 156 Mbps using frequencies in the 30– to 300– GHz band.

In July 1998, the IEEE 802.11 standardization group decided to select OFDM as the basis for their new 5-GHz standard, targeting a range of data rates from 6 up to 54 Mbps [12, 13]. This new standard is the first one to use OFDM in packet-based communications, while the use of OFDM until now was limited to continuous transmission systems like DAB and DVB. Following the IEEE 802.11 decision, ETSI BRAN and MMAC also adopted OFDM for their physical layer standards. The three bodies have worked in close cooperation since then to make sure that differences among the various standards are kept to a minimum, thereby enabling the manufacturing of equipment that can be used worldwide.

The focus of this section is on the physical layer side. In the case of the IEEE 802.11 standard, the MAC layer for the higher data rates remains the same as for the currently supported 1- and 2- Mbps rates. A description of this MAC can be found in [11].

10.5.1 OFDM Parameters

Table 10.5 lists the main parameters of the draft OFDM standard. A key parameter that largely determined the choice of the other parameters is the guard interval of 800 ns. This guard interval provides robustness to rms delay spreads up to several hundreds of nanoseconds, depending on the coding rate and modulation used. In practice, this means that the modulation is robust enough to be used in any indoor environment, including large factory buildings. It can also be used in outdoor environments, although directional antennas may be needed in this case to reduce the delay spread to an acceptable amount and increase the range.

Table 10.5
Main parameters of the OFDM standard.

Data rate	6, 9, 12, 18, 24, 36, 48, 54 Mbps
Modulation	BPSK, QPSK, 16-QAM, 64-QAM
Coding rate	1/2, 2/3, 3/4
Number of subcarriers	52
Number of pilots	4
OFDM symbol duration	4 μs
Guard interval	800 ns
Subcarrier spacing	312.5 kHz
–3-dB Bandwidth	16.56 MHz
Channel spacing	20 MHz

To limit the relative amount of power and time spent on the guard time to 1 dB, the symbol duration chosen is 4 μs. This also determines the subcarrier spacing at 312.5 kHz, which is the inverse of the symbol duration minus the guard time. By using 48 data subcarriers, uncoded data rates of 12 to 72 Mbps can be achieved by using variable modulation types from BPSK to 64-QAM. In addition to the 48 data subcarriers, each OFDM symbol contains an additional four pilot subcarriers, which can be used to track the residual carrier frequency offset that remains after an initial frequency correction during the training phase of the packet.

To correct for subcarriers in deep fades, forward-error correction across the subcarriers is used with variable coding rates, giving coded data rates from 6 up to 54 Mbps. Convolutional coding is used with the industry standard rate 1/2, constraint length 7 code with generator polynomials (133,171). Higher coding rates of 2/3 and 3/4 are obtained by puncturing the rate 1/2 code. The 2/3-rate is used together with 64-QAM only to obtain a data rate of 48 Mbps. The 1/2-rate is used with BPSK, QPSK, and 16-QAM to give rates of 6, 12, and 24 Mbps, respectively. Finally, the 3/4-rate is used with BPSK, QPSK, 16-QAM, and 64-QAM to give rates of 9, 18, 36, and 54 Mbps, respectively.

10.5.2 Channelization

Figure 10.10 shows the channelization for the lower and middle UNII bands. Eight channels are available with a channel spacing of 20 MHz and guard spacings of 30 MHz at the band edges in order to meet the stringent FCC-restricted band spectral density requirements. The FCC also defined an upper UNII band from 5.725 to 5.825 GHz, which carries another four OFDM channels. For this upper band, the guard spacing from the band edges is only 20 MHz, as the out-of-band spectral requirements for the upper band are less severe than those of the lower and middle UNII bands. In Europe, a total of 455 MHz is available in two bands, one from 5.15 to 5.35 GHz and

another from 5.470 to 5.725 GHz. In Japan, a 100 MHz wide band is available from 5.15 to 5.25 GHz, carrying four OFDM channels.

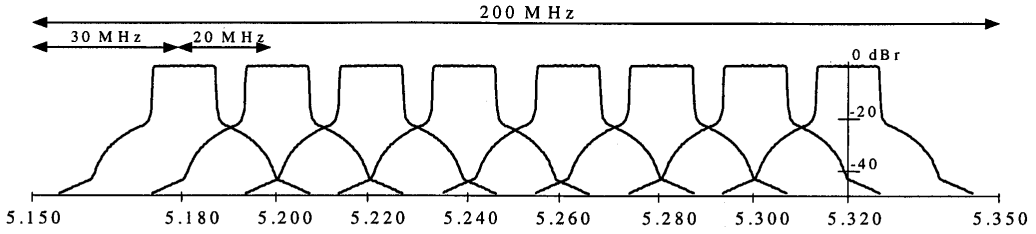

Figure 10.10 Channelization in lower and middle UNII band.

10.5.3 OFDM Signal Processing

The general block diagram of the baseband processing of an OFDM transceiver is shown in Figure 10.11. In the transmitter path, binary input data is encoded by a standard rate 1/2 convolutional encoder. The rate may be increased to 2/3 or 3/4 by puncturing the coded output bits. After interleaving, the binary values are converted into QAM values. To facilitate coherent reception, four pilot values are added to each 48 data values, so a total of 52-QAM values is reached per OFDM symbol, which are modulated onto 52 subcarriers by applying the IFFT. To make the system robust to multipath propagation, a cyclic prefix is added. Further, windowing is applied to attain a narrower output spectrum. After this step, the digital output signals can be converted to analog signals, which are then up-converted to the 5-GHz band, amplified and transmitted through an antenna.

The OFDM receiver basically performs the reverse operations of the transmitter, together with additional training tasks. First, the receiver has to estimate frequency offset and symbol timing, using special training symbols in the preamble. Then, it can do an FFT for every symbol to recover the 52-QAM values of all subcarriers. The training symbols and pilot subcarriers are used to correct for the channel response as well as remaining phase drift. The QAM values are then demapped into binary values, after which a Viterbi decoder can decode the information bits.

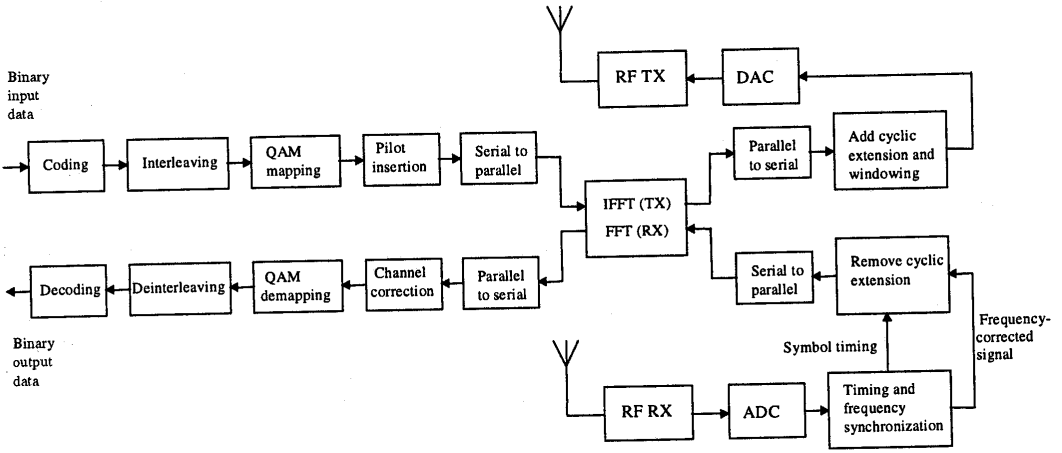

Figure 10.11 Block diagram of OFDM transceiver.

10.5.4 Training

Figure 10.12 shows the structure of the preamble that preceeds every OFDM packet. This preamble is essential to perform start-of-packet detection, automatic gain control, symbol timing, frequency estimation, and channel estimation. All of these training tasks have to be performed before the actual data bits can be successfully decoded.

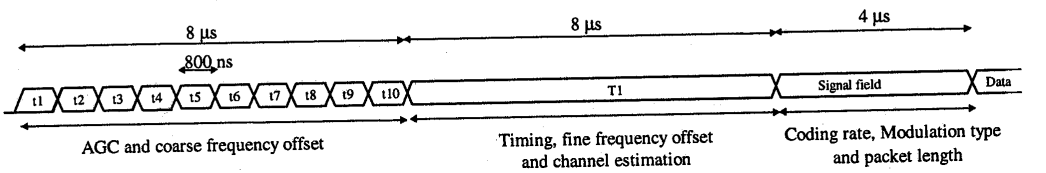

Figure 10.12 OFDM preamble.

The first part of the preamble consists of 10 repetitions of a training symbol with a duration of 800 ns each, which is only a quarter of the FFT duration of a normal data symbol. These short symbols are produced by using only nonzero subcarrier values for subcarrier numbers that are a multiple of 4. Hence, of all possible subcarrier numbers from –26 to +26, only the subset {–24, –20, –16, –12, –8, –4, 4, 8, 12, 16, 20, 24} is used. There are two reasons for using relatively short symbols in this part of the training; first, the short symbol period makes it possible to do a coarse frequency offset estimation with a large unambiguous range. For a repetitive signal with a duration of T, the maximum measurable unambiguous frequency offset is equal to $1/(2T)$, as higher frequency offsets result in a phase change exceeding π from one symbol to another. Hence, by measuring the phase drift between two consecutive short symbols with a

duration of 800 ns, frequency offsets up to 625 kHz can be estimated. If training symbols with a duration equal to the FFT interval of 3.2 μs were used, then the maximum frequency offset of only 156 kHz could be measured, corresponding to a relative frequency error of about 26 ppm at a carrier frequency of 5.8 GHz. The IEEE 802.11 standard specifies a maximum offset *per user* of 20 ppm, which means that the worst case offset as seen by a receiver can be up to 40 ppm, as it experiences the sum of the frequency offsets from both transmitter and receiver.

The second reason for using short symbols at the start of the training is that they provide a convenient way of performing AGC and frame detection. Detection of the presence of a packet can be done by correlating a short symbol with the next and detecting if the correlation magnitude exceeds some threshold. After each interval equal to two short symbol durations, the receiver gain can be adjusted after which detection and gain measuring can continue. Of course, this AGC algorithm could also be applied to long training symbols, but the advantage of short symbols is that we have more repetitions in the same amount of time, which makes it easier to do several measurements and gain adjustments during the training.

The short training symbols are followed by a long training symbol (T1) that contains 52 QPSK-modulated subcarriers like a normal data symbol. The length of this training symbol is twice that of a data symbol, however, which is done for two reasons. First, it makes it possible to do a precise frequency estimation on the long symbol. The long symbol is formed by cyclically extending the IFFT output signal to a length of 8 μs. Thus, it contains two and a half times the original IFFT duration. The first 1.6 μs serves as a guard interval, containing a copy of the last 1.6 μs of the IFFT output. The long training symbol makes it possible to do a fine frequency offset estimation by measuring the phase drift between samples that are 3.2 μs apart within the long training symbol. The second reason for having the long symbol is to obtain reference amplitudes and phases for doing coherent demodulation. By averaging the two identical parts of the long training symbol, coherent references can be obtained with a noise level that is 3 dB lower than the noise level of data symbols.

Both the long and short symbols are designed in such a way that the PAP ratio is approximately 3 dB, which is significantly lower than the PAP ratio of random OFDM data symbols. This guarantees the training degradation caused by nonlinear amplifier distortion to be smaller than the distortion of the data symbols. It also allows the use of a simple correlator implementation at the receiver as explained in Section 4.6.

After the preamble, there is still one training task left, which is tracking the reference phase. There will always be some remaining frequency offset that causes a common phase drift on all subcarriers. To track this phase drift, 4 of the 52 subcarriers contain known pilot values. The pilots are scrambled by a length 127 pseudonoise sequence to avoid spectral lines exceeding the average power density of the OFDM spectrum.

Figure 10.13 shows the time-fequency structure of an OFDM packet, where all known training values are marked in gray. It clearly illustrates how the packet starts with 10 short training symbols, using only 12 subcarriers, followed by the long training symbol and data symbols, with each data symbol containing four known pilot subcarriers.

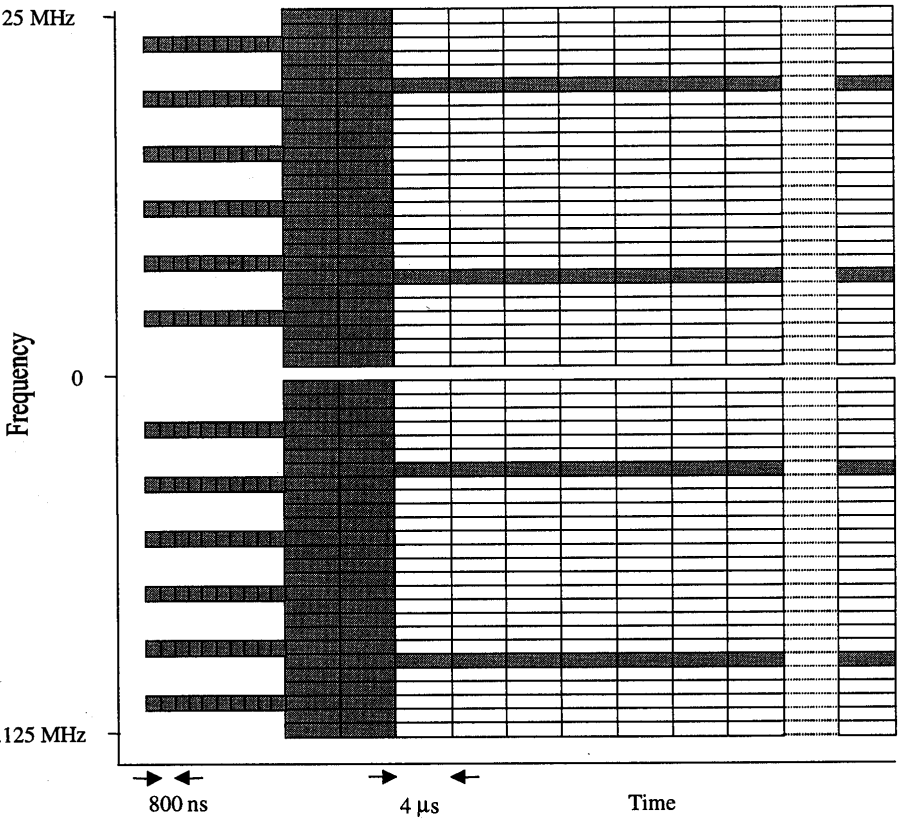

Figure 10.13 Time-frequency structure of an OFDM packet. Gray subcarriers contain known training values.

In the case of the IEEE 802.11 standard, at the end of the preamble a special OFDM data symbol at the lowest 6-Mbps rate is sent, which contains information about the length, modulation type, and coding rate of the rest of the packet. Sending this information at the lowest possible rate ensures that the dynamic rate selection is at least as reliable as the most reliable data rate of 6 Mbps. Further, it makes it possible for all users to decode the duration of a certain packet, even though they may not be able to decode the data content. This is important for the IEEE 802.11 MAC protocol, which specifies that a user has to wait until the end of any packet already in the air before trying to compete for the channel.

10.5.5 Differences Between IEEE 802.11, HIPERLAN/2 and MMAC

The main differences between IEEE 802.11 and HIPERLAN/2—which is standardized by ETSI BRAN [14]—are in the Medium Access Control (MAC). IEEE 802.11 uses a distributed MAC based on Carrier Sense Multiple Access with Collision Avoidance, (CSMA/CA), while HIPERLAN/2 uses a centralized and scheduled MAC, based on wireless ATM. MMAC supports both of these MACs. As far as the physical layer is concerned, there are a few relatively minor differences between IEEE 802.11 and HIPERLAN/2 which are summarized below:

- HIPERLAN uses different training sequences. The long training symbol is the same as for IEEE 802.11, but the preceding sequence of short training symbols is different. A downlink transmission starts with 10 short symbols as IEEE 802.11, but the first 5 symbols are different in order to detect the start of the downlink frame. The rest of the packets in the downlink frame do not use short symbols, only the long training symbol. Uplink packets may use 5 or 10 identical short symbols, with the last short symbol being inverted.
- HIPERLAN uses extra puncturing to accommodate the tail bits to keep an integer number of OFDM symbols in 54 byte packets. This extra puncturing operation punctures 12 bits out of the first 156 bits of a packet.
- In the case of 16-QAM, HIPERLAN uses a coding rate of 9/16 instead of 1/2—giving a bit rate of 27 instead of 24 Mbps—to get an integer number of OFDM symbols for packets of 54 bytes. The rate 9/16 is made by puncturing 2 out of every 18 encoded bits.
- Both IEEE 802.11 and HIPERLAN scramble the input data with a length 127 pseudo random sequence, but the initialization is different. IEEE 802.11 initializes with 7 random bits which are inserted as the first 7 bits of each packet. In HIPERLAN, the scrambler is initialized by {1, 1, 1} plus the first 4 bits of the Broadcast Channel at the beginning of a MAC frame. The initialization is identical for all packets in a MAC frame.
- HIPERLAN devices have to support power control in the range of -15 to 30 dBm with a step size of 3 dB.
- Dynamic frequency selection is mandatory in Europe over a range of at least 330 MHz for indoor products and 255 MHz (upper band only) for outdoor products. This means that indoor products have to support a frequency range from 5.15 to at least 5.6 GHz, covering the entire lower band and a part of the European upper band. Dynamic frequency selection was included to avoid the need for frequency planning and to provide coexistence with radar systems that operate in the upper part of the European 5 GHz band.

10.5.6 Simulation Results

Figure 10.14 shows the irreducible PER versus delay spread for a few different data rates. This is the minimum possible PER for a certain delay spread, for which all packet errors are caused by intersymbol interference because of path delays exceeding the guard time of the OFDM symbols. Hence, Figure 10.14 demonstrates the delay spread robustness for several data rates. For a 1% PER, the tolerable delay spread is close to 200 ns at 36 Mbps, while at 12 Mbps a delay spread of 450 ns can be tolerated. In practice, this means that the 36-Mbps rate can be used in most indoor environments, except some large factory buildings. The 54 Mbps rate can tolerate delay spreads up to about 120 ns, which is sufficient for most office buildings. The 12-Mbps rate can work in any indoor and even in outdoor environments. This is also true for the lowest rate of 6 Mbps, that is not included in Figure 10.14.

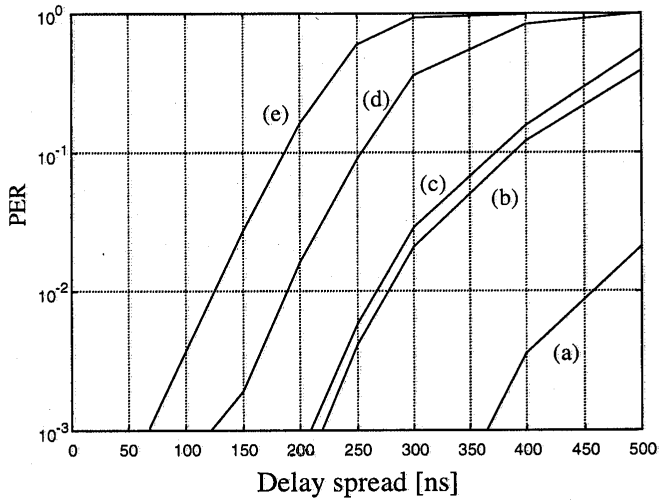

Figure 10.14 PER versus rms delay spread (no noise) for Rayleigh fading paths with an exponentially decaying power delay profile. Packet size is 64 bytes with data rates of (a) 12, (b) 18, (c) 24, (d) 36, and (e) 54 Mbps.

Figure 10.15 shows the PER versus E_b/N_o for a data rate of 24 Mbps in case of an AWGN channel and a Rayleigh fading channel with a delay spread of 100 ns. An E_b/N_o of about 18 dB is required to achieve a 1% PER in the fading channel, which is approximately 6 dB more than what is needed for an ideal Gaussian noise channel. Of course, other data rates have different requirements. Figure 10.16 shows the PER for various data rates as a function of the input power. We can see a difference of almost 18 dB in the signal power requirements of the lowest and highest data rates. This illustrates the importance of fallback rates; users who cannot use the highest rate because they are too far away or are in a bad multipath situation can at least obtain a data link at a lower rate.

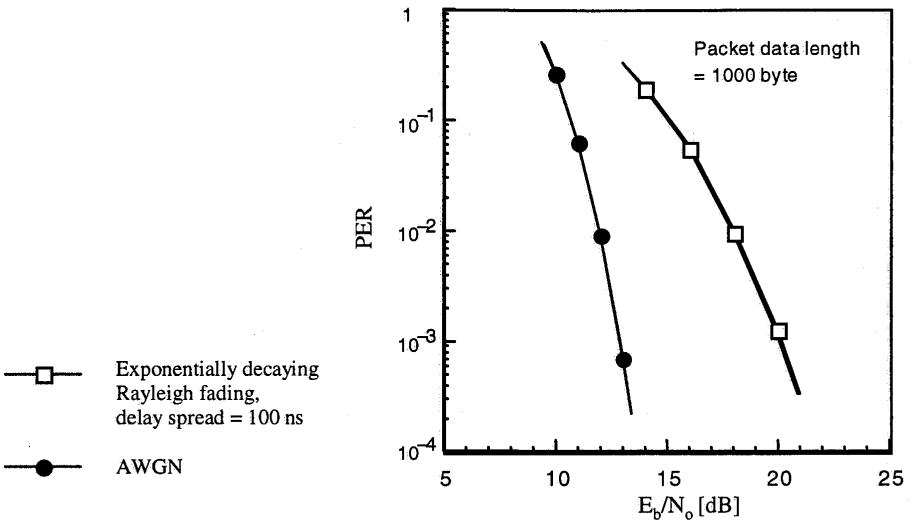

Figure 10.15 PER versus mean E_b/N_o for AWGN and Rayleigh fading with a 100-ns delay spread and a bit rate of 24 Mbps.

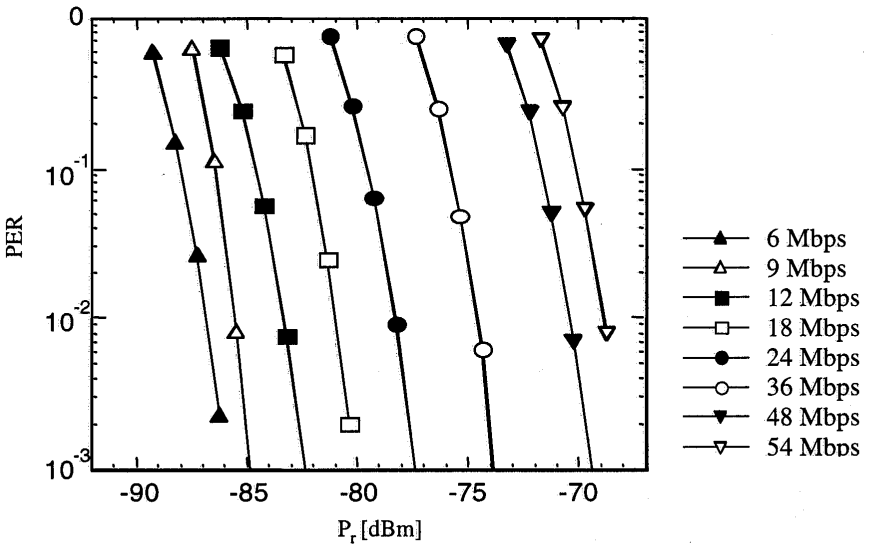

Figure 10.16 PER versus received power level for AWGN and various bit rates.

Figure 10.17 shows simulated spectra of an OFDM signal that is distorted by a nonlinear power amplifier with different backoff values. This is an important subject, because the susceptibility to nonlinear distortion and the need for large backoff values is often mentioned as a disadvantage of OFDM. As shown in [15], however, the effects of nonlinear distortion on the BER are negligible for backoff values of 6 dB or more, where the backoff is defined as the difference between the maximum (saturation) output power and the average output power in dB. The effects on the transmitted spectrum are illustrated in Figure 10.17. We can see that for a 7-dB backoff, the spectrum falls down very steeply after about 8 MHz, and only around 25 dB below the in-band density the spectrum starts to deviate significantly from an ideal undistorted OFDM signal. When the backoff is decreased to 5 dB, the out-of-band spectrum quickly grows toward the outer spectrum mask defined by IEEE 802.11.

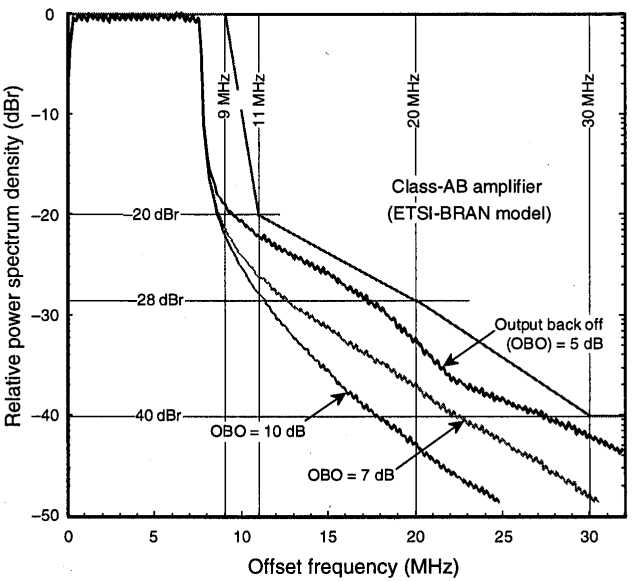

Figure 10.17 OFDM spectrum after a nonlinear power amplifier.

REFERENCES

[1] ETSI, "Radio Broadcasting Systems: Digital Audio Broadcasting to Mobile, Portable and Fixed Receivers," European Telecommunication Standard, ETS 300-401, Feb. 1995.

[2] Tuttlebee, W. H. W., and D. A. Hawkins, "Consumer Digital Radio: From Concept to Reality," *Electronics and Communication Engineering Journal*, Vol. 10, No. 6, pp. 263–276, Dec. 1998.

[3] ETSI, "Digital Video Broadcasting: Framing Structure, Channel Coding, and Modulation for Digital Terrestrial Television," European Telecommunication Standard, EN 300–744, Aug. 1997.

[4] Reimers, U., "DVB-T: The COFDM-Based System for Terrestrial Television," *Electronics and Communication Engineering Journal*, Vol. 9, No. 1, pp. 28–32, Feb. 1997.

[5] Mikkonen, J., J. P. Aldis, G. A. Awater, A. Lunn, and D. Hutchinson, "The Magic WAND—Functional Overview," *IEEE JSAC*, Vol. 16, No. 6, pp. 953–972, Aug. 1998.

[6] Awater, G. A., and J. Ala-Laurila, "Wireless ATM Network Demonstrator," Presentation and Demonstration, *Demo '98 conference*, Berlin, Germany, Oct. 15, 1998.

[7] Passas, N., S. Paskalis, D. Vali, L. Merakis, "Quality-of-Service-Oriented Medium Access Control for Wireless ATM Networks," *IEEE Communications Magazine*, Vol. 35, No. 11, Nov. 1997.

[8] IEEE. 802.11, IEEE Standard for Wireless LAN Medium Access Control (MAC) and Physical Layer (PHY) specifications, Nov. 1997.

[9] FCC, "Amendment of the Commission's Rules to Provide for Operation of Unlicensed NII Devices in the 5-GHz Frequency Range," Memorandum Opinion and Order, ET Docket No. 96–102, June 24, 1998.

[10] ETSI, "Radio Equipment and Systems, HIgh PErformance Radio Local Area Network (HIPERLAN) Type 1," European Telecommunication Standard, ETS 300–652, Oct. 1996.

[11] Crow, B. P., I. Widjada, J. G. Kim, and P. T. Sakai, "IEEE 802.11 Wireless Local Area Networks," *IEEE Communications Magazine*, pp. 116–126, Sept. 1997.

[12] Takanashi, H., and R. van Nee, "Merged Physical Layer Specification for the 5-GHz Band," IEEE P802.11-98/72-r1, Mar. 1998.

[13] IEEE, "Supplement to Standard for Telecommunications and Information Exchange Between Systems—LAN/MAN Specific Requirements—Part 11: Wireless MAC and PHY Specifications: High Speed Physical Layer in the 5-GHz Band," P802.11a/D7.0, July 1999.

[14] ETSI, "Broadband Radio Access Networks (BRAN); HIPERLAN Type 2 Technical Specification Part 1—Physical Layer," DTS/BRAN030003-1, Oct. 1999.

[15] Nee, R. van, "OFDM for High Speed Wireless Networks," IEEE P 802.11-97/123, Nov. 1997.

About the Authors

Richard D. J. van Nee was born in Schoonoord, the Netherlands, on January 17, 1967. He received an M.Sc. degree (cum laude) from Twente University of Technology, Enschede, the Netherlands, and a Ph.D. degree (cum laude) from Delft University of Technology, Delft, The Netherlands, in 1990 and 1995, respectively.

From December 1994, he worked as a private consultant to NovAtel Communications, Calgary, working on the design of multipath-robust GPS receivers, which were used in the reference stations of the United States Wide Area Augmentation System. In March 1995, he joined AT&T—now Lucent Technologies—Bell Labs in Utrecht, The Netherlands, where he is working in the area of high speed wireless communications. He was involved in the design of the OFDM modems for the European Magic WAND project. Together with NTT, he made the original OFDM-based proposal which lead to the IEEE 802.11 wireless LAN high-rate extension for the 5 GHz band. He was also one of the original proposers of the 11 Mbps IEEE 802.11 extension for the 2.4 GHz band. He holds several patents and published over 40 papers in the area of spread-spectrum tracking systems and OFDM.

Ramjee Prasad was born in Babhnaur (Gaya), Bihar, India, on July 1, 1946. He is now a Dutch Citizen. He received a B.Sc. (Eng) degree from Bihar Institute of Technology, Sindri, India and M.Sc. (Eng) and Ph. D. degrees from Birla Institute of Technology (BIT), Ranchi, India, in 1968, 1970 and 1979, respectively.

He joined BIT as a Senior Research Fellow in 1970 and became associate professor in 1980. While he was with BIT, he supervised a number of research projects in the areas of microwave communications and plasma engineering. During 1983 to 1988, he was with the University of Dar es Salaam (UDSM), Tanzania, where he rose to the level of professor of telecommunications at the Department of Electrical Engineering in 1986. At UDSM, he was responsible for the collaborative project "Satellite Communications for Rural Zones" with Eindhoven University of Technology, The Netherlands. From February 1988 to June 1999, he was with the Telecommunications and Traffic-Control Systems Group, Delft University of Technology (DUT), The Netherlands, where he was actively involved in the area of wireless personal and multimedia communications (WPMC). He was the Head of

the Transmission Research Section of IRCTR (International Research Center for Telecommunications - Transmission and Radar) and also Program Director of the Center for Wireless Personal Communications (CEWPC). Since June 1999, he has been with Aalborg University, Denmark as Co-director of Center for PersonKommunikation (CPK) and holds the Chair of Wireless Information and Multimedia Communications. He was involved in the European ACTS project FRAMES (Future Radio Wideband Multiple Access System) as a DUT Project Leader. He is Project leader of several international industrial funded projects. He has published over 300 technical papers, authored and co-authored three books "*CDMA for Wireless Personal Communications,*" "*Universal Wireless Personal Communications,*" and "*Wideband CDMA for Third Generation Mobile Communications*" published by Artech House, Boston. His current research interest lies in wireless networks, packet communications, multiple access protocols, adaptive equalizers, spread-spectrum CDMA systems, and multimedia communications.

He has served as a member of advisory and program committees of several IEEE international conferences. He has also presented keynote speeches, invited papers, and tutorials on WPMC at various universities, technical institutions, and IEEE conferences. He was the Organizer and Interim Chairman of the IEEE Vehicular Technology/Communications Society Joint Chapter, Benelux Section. He is now the Elected Chairman of the joint chapter. He is also founder of the IEEE Symposium on Communications and Vehicular Technology (SCVT) in the Benelux and he was the Symposium Chairman of SCVT'93.

He is the Co-ordinating Editor and Editor-in-chief of the Kluwer international journal on *Wireless Personal Communications* and also a member of the editorial board of other international journals, including the IEEE Communications Magazine and the IEE Electronics Communication Engineering Journal. He was the Technical Program Chairman of the PIMRC'94 International Symposium held in The Hague, The Netherlands, during September 19–23, 1994, and also of the Third Communication Theory Mini-Conference in conjunction with the GLOBECOM'94 held in San Francisco, CA, November 27–30, 1994. He was the Conference Chairman of IEEE Vehicular Technology Conference, VTC'99 (Fall), Amsterdam, The Netherlands held on September 19–22, 1999 and also the steering committee chairman of The Second International Symposium on Wireless Personal Multimedia Communications (WPMC), Amsterdam, The Netherlands held on September 21–23, 1999.

He is listed in the US Who's Who in the World. He is a fellow of the IEE, a fellow of the Institution of Electronics & Telecommunication engineers, a senior member of IEEE and a member of NERG (The Netherlands Electronics and Radio Society).

Index

The Artech House Universal Personal Communications Series

Ramjee Prasad, Series Editor

CDMA for Wireless Personal Communications, Ramjee Prasad

OFDM for Wireless Multimedia Communications, Richard van Nee and Ramjee Prasad

Third Generation Mobile Communication Systems, Ramjee Prasad, Werner Mohr, and Walter Konhäuser, editors

Universal Wireless Personal Communications, Ramjee Prasad

Wideband for Third Generation Mobile Communications, Tero Ojanperä and Ramjee Prasad, editors

For further information on these and other Artech House titles, including previously considered out-of-print books now available through our In-Print-Forever® (IPF®) program, contact:

Artech House
685 Canton Street
Norwood, MA 02062
Phone: 781-769-9750
Fax: 781-769-6334
e-mail: artech@artechhouse.com

Artech House
46 Gillingham Street
London SW1V 1AH UK
Phone: +44 (0)20 7596-8750
Fax: +44 (0)20 7630-0166
e-mail: artech-uk@artechhouse.com

Find us on the World Wide Web at:
www.artechhouse.com